Aix-Marseille University

Ph.D School 251 Environmental Sciences

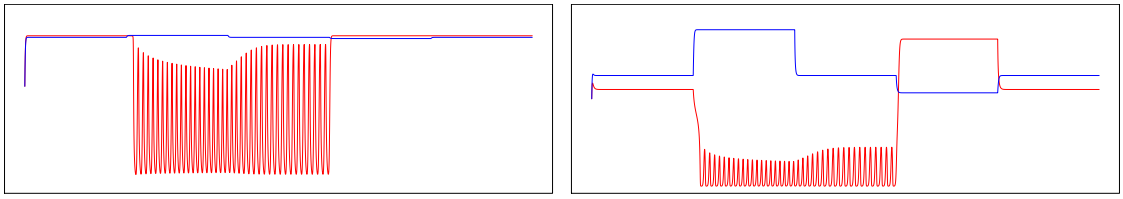

Uncertainty in predictive ecology: consequence of choices in model construction

Ph.D thesis defended by **Clément ALDEBERT**

the 29th November 2016

to obtain the degree of

Ph.D in Environmental Sciences

from Aix-Marseille University, France

speciality: **Oceanography**

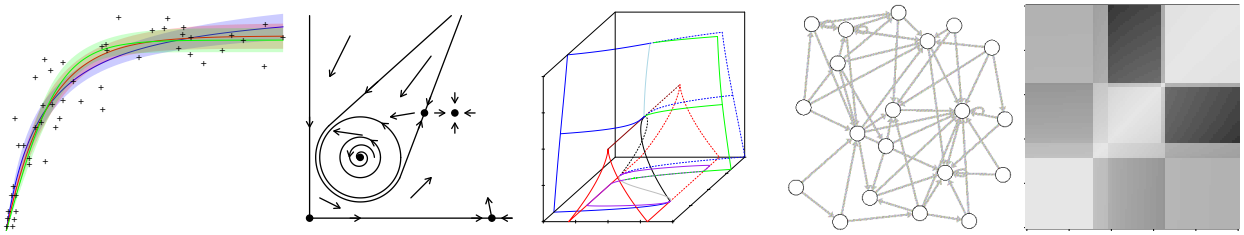

in front of the thesis committee composed by:

Stéphanie MAHEVAS	Senior Researcher, IFREMER	*Referee*
Jean-Luc GOUZÉ	Senior Researcher, INRIA	*Referee*
Mélika BAKLOUTI	Professor, Aix-Marseille University	*Jury member*
Antoine PERASSO	Assistant Professor, Université de Franche-Comté	*Jury member*
Jean-Christophe POGGIALE	Professor, Aix-Marseille University	*Ph.D advisor*
David NERINI	Assistant Professor, Aix-Marseille University	*Ph.D advisor*

Context

This Ph.D scholarship was funded by a grant from the French Ministry for Research and Education for research and teaching activities, from the 1^{st} October 2013 to the 30^{th} September 2016. This thesis was performed at Aix-Marseille University, through the Ph.D School 251 Environmental Sciences. The research work was performed at the Mediterranean Institute of Oceanography (UMR 110).

Ce travail de thèse a été financé par une bourse du Ministère de l'Enseignement Supérieur et de la Recherche pour mes activités de recherche et d'enseignement, du 1^{er} octobre 2013 au 30 septembre 2016. Cette thèse a été réalisée à l'Université d'Aix-Marseille, au sein de l'Ecole Doctorale 251 Sciences de l'Environnement. Le travail de recherche a été effectué au sein de l'Institut Méditerranéen d'Océanologie (UMR 110).

Structure and language of the manuscript

This manuscript is written as a monograph. For each chapter (except introduction and conclusion), a brief note mentions the current state of the corresponding work (published, to be adapted for publication, on going). For practical reasons (publications, international collaboration), I choose to write the whole manuscript in English. As I am not a native English-speaker, I apologize in advance for any language mistakes that may remain even after many revisions. This manuscript is made of eight main chapters organized in three parts. In addition, a last chapter written in French is a detailed summary of this thesis.

Ce manuscrit est écrit sous la forme d'un monographe. Pour chaque chapitre (hors introduction et conclusion), une note rapide précise l'état actuel du travail présenté (publié, à adapter pour publication, en cours). Pour des raisons pratiques (publications, collaboration internationale), j'ai choisi d'écrire l'intégralité du manuscrit en anglais. Comme l'anglais n'est pas ma langue maternelle, je m'excuse par avance pour toute erreur d'anglais qui subsisterait après de nombreuses révisions. Ce manuscrit est composé de huits chapitres principaux organisés en trois parties. Un neuvième chapitre écrit en français est un résumé détaillé de cette thèse.

Authorship

From design to writing through calculations and computing, all the original research work presented in this thesis was performed by myself. The only exception is the normal form derivation of the codimension-three bifurcation point in section 4.4, conducted by Bob Kooi from Vrije Universiteit (Amsterdam, Netherlands). At Aix-Marseille University (Marseille, France), Jean-Christophe Poggiale (PhD advisor), David Nerini (PhD advisor) and Mathias Gauduchon supervised and made valuable comments and suggestions on the entire thesis work. Bob Kooi supervised the work in chapters 4 and 7 and made valuable comments on chapters 3 and 6.

De la conception à la rédaction via les calculs analytiques et numériques, tout le travail de recherche original présenté dans cette thèse a été réalisé par moi-même. La seule exception est la réduction à la forme normale du point de bifurcation de codimension trois présentée dans la section 4.4, qui a été effectuée par Bob Kooi de Vrije Universiteit (Amsterdam, Netherlands). A l'Université d'Aix-Marseille (Marseille, France), Jean-Christophe Poggiale (directeur de thèse), David Nérini (directeur de thèse) et Mathias Gauduchon ont supervisé et fait d'importants commentaires et suggestions sur l'intégralité de ce travail de thèse. Bob Kooi a supervisé le travail présenté dans les chapitres 4 et 7 et fait d'importants conseils sur les chapitres 3 et 6.

Acknowledgments

First of all, I want to warmly thank Jean-Christophe and David for their constructive, efficient and friendly supervision during all this thesis. Thank you Jean-Christophe for your numerous advises on every aspects of research and life in research. Thank you David for the constructive discussions about almost every possible topics, from research to human life, and the challenging bets. I also warmly thank Mathias for his advises and ideas on many topics, always hidden behind a smile. My interest for mathematical modelling comes greatly from the interesting courses and internships I had with the three of you many years ago. Finally, I also want to warmly thank Bob, for his advises and his knowledge that he shared with me during the second half of my thesis.

I want to thank the members of the thesis committee for accepting to examine my work. I also acknowledge people who made this thesis possible. I want to thank Richard Sempéré (head of the MIO), Marc Pagano and François Carlotti (head of the Marine Ecology and Biology team), Dominique Estivale and people from the Ph.D school Environmental Sciences. For the technical aspects, I want to thank the staff of the "Cluster de calcul OSU Pytheas" for providing computing facilities that I used sometimes at the begining of this thesis. In addition, I want to thank the people who have developped all the free softwares and languages that I used along this thesis (Linux OS, Latex, R, C/C++, GNU Scientific Library, Matcont, ...) and researchers that made the current state of knowledge on ecology and mathematics.

At Zürich University, I want to thank Jordi Bascompte and his group for hosting me and also for various interesting discussions. Still in Zürich, I also want to acknowledge Owen Petchey and Frank Pennekamp for giving me the opportunity to continue my research activities as a postdoc in their group. Many thanks also to Anaïs for her "hurluberlutations" and to Aurélie for discussions about thesis life.

I am undebtful to Sergueï Petrovskii and two anonymous reviewers that make many valuable comments on my submitted manuscripts to Ecological Complexity. These comments helped me to greatly improve my writting skills and rose interesting questions on my initial work. I also want to thank the organizers and participants of the seminar "Doctoriales en Provence" (2014, Aix-Marseille University), the 8^{th} Summer school on Dynamic Energy Budget Theory (2015, Aix-Marseille University and VU Amsterdam) and the Summer School on Modelling Environmental Resilience (2016, Paris, Ecole Nationale Supérieure).

I want to thank the people from the lab, with special mention for Claude and the discussions about unexpected metrics and spaces, Gérald for the magic tricks and Phil' for the philosophical discussions. Special big-up for the team of the office during this final year of thesis writing:

Jonathan the binary copepod, elephant Morgan, knight Gwen, Benjamin "Darwin" Girardot, Marjorie the octopus and Lola the algae. Many thanks also to the office-mates from previous years: Chiara and her virtual fishes, Max, Dimitri the DEB co-learner, Starrlight, Etienne, Camille, and Anaïs. I also want to thank other Ph.D students in the lab: Mathilde, Yannick, Arnaud, Marion, and of course Marine and her diatoms near the printer. A special though to Marc and Louise for the years we shared as students in the same courses and irish pubs. I also want to thanks people from my second activity and way of life: all the scuba-diving friends, past and present. Both good and working moments we shared have helped me to remember that there is a life aside the thesis.

Finally, I want to thank my family, my parents and my sister who have always supported me. I have also a though for the missed ones that unfortunately left us during this thesis: Edmond, Maurice, Christian B. and Jean-Marc B. To conclude, many thanks to You, who have shared many aspects of my life during this thesis and supported me at various times.

All I want to say in these last
words is that I am
Glad that we met.
At the
Time I did not expect that, you brought
Happiness back into my life. I deeply
Enjoy all the time we share together.

Contents

Part I

Introduction

CHAPTER 1

Why using models in ecology?

"This is very much a personal view of what I think [...]
The only thing that is certain about this view [...]
is that much of it will surely turn out to be wrong"
Lord Robert May,
"Unanswered questions in ecology" (May, 1999).

Synopsis: everyone makes models

"Small wavelets grow at the East point of the island, so there is a Westward current and fishes are concentrated close to the South wall between 10 and 20 meters deep."[1] This statement is an example of the many others that we have all heard from "experienced people". By "experienced people", I mean people who (for any reasons) have learned from their environment, the sea, the mountain, or the woods in their neighborhood, during years or decades. Thanks to this long time of observation, they are able to make heuristic predictions about their environment or the weather. This ability is what we usually call "experience" or "intuition". Beyond this statistical approach, one can have some conceptual ideas on how things interact (*"Currents are important for fishes."*). These interactions can also be partly understood as a phenomenon (*"A stronger current means more fishes."*) or through their underlying mechanisms (*"The current carries food for organisms through advection."*). All these visions are based on models, i.e. on a simplified representation of a complex system. A complex system cannot be understood by simply disentangling it into smaller components like a clockwork. Thus, there is not a unique model to represent a complex system. For any situation, defining which model would be the most appropriate will always remain an open debate. But as we all have our own ideas on how the world is going on, **we all make models**.

1.1 Predicting the future: from intuition to mathematics

1.1.1 Personal experience as statistical and conceptual models

Personal experience is a way of learning based on the memory of repeated events. Thus, experience is a statistical model. A statistical model makes predictions based on previous observations. The replication of observations provides a frequency of events to estimate their probability of occurence. This estimate usually becomes more and more accurate as the number of observations increases. By observing the world around them during many years, "experienced people" are able to make heuristic predictions. Heuristic predictions can be correct, but sometimes they fail and we cannot explain why (Mouquet *et al.*, 2015). Indeed, there is no explanation of processes in a statistical model. This model is only based on correlations between multiple explanatory variables, but their interactions leading to these correlations are *a priori* unknown (Breiman, 2001).

A statistical approach can be useful to make operational predictions (for nice examples in oceanography, see Nerini & Ghattas, 2007, Nerini *et al.*, 2010, Bayle *et al.*, 2015). However, only

[1] I wrote this fictive citation (and the next ones in this paragraph) for the purpose of this introduction, based on similar sentences I heard from many "experienced people", sailors, fishermen, divers, and others.

situations that belong to the range of previously experienced ones can be predicted. Predicting events that are outside the scope of the model (extrapolation) is highly hazardous, as there is no constraint (data or assumptions on processes) on model predictions. This situation might be the rule rather than the exception, as unique events *stricto senso* are dominant. Indeed, only 75 events occurring independently one-after-one lead to $75! \approx 10^{106}$ possible sequences, which is more than the number of simple events that happened since the beginning ($\approx$ 15 billion years ago) of the known Universe (Elsasser, 1969 *in* Planque, 2015). Even if events are not independent to each other, all possible situations have not been realized in the past. A simple reason is that living organisms evolve, so unforseen genes and species can appear whereas other disappear.

Conceptual models go beyond statistical models in the sense that they specify interactions between compartments of interest (for an example in oceanography, see Legendre & Le Fèvre, 1989). This approach allows to make qualitative or semi-quantitative predictions like an expert judgement (again, we all make models). For example, assessing ecosystem state to help decision-making about environmental policies can be done by the mean of a conceptual model (Personnic *et al.*, 2014). Using this model, a semi-quantitative index of ecosystem state is derived from the state of each compartment. The later is estimated with more or less confidence depending on information availability (from no information to recent data, through experts judgement).

1.1.2 Describing processes: multiple approaches and complexity

The idea of describing processes with mathematics seems to start with Pythagoras (580-495 BC), and spread during the Renaissance with famous breakthroughs in astronomy (Israel, 1996). The astronomer Johannes Kepler (1571-1630) discovered the elliptic motion of planets and proposed a geometrical view of the Universe. Using a more quantitative approach based on numbers, Galileo Galilei (1564-1642) suggested that the world can be understood only if we know its language, the mathematics. A great step forward in mathematics was the invention of infinitesimal calculus (derivatives and integrals) by Pierre de Fermat (early 1600's-1665), Gottfried Leibniz (1646-1716) and Isaac Newton (1642-1727). Newton induced a stream of mechanistic view of sciences, later strengthened by Pierre-Simon Laplace (1749-1827) who argued that all phenomena follow an equation. This equation is a law that governs the phenomenon, according to the Newtonian approach.

The previous approach can succeed to describe a complicated system, like a clockwork. A complicated system can be simplified into smaller components and their understanding allows to understand the whole system. Conversely, a complex system cannot be simplified into subparts without loss of information, because of its emergent properties (Le Moigne, 1999). In addition, a complex system is made of so many components (e.g. 12 g of carbon ^{12}C corresponds to 6.022×10^{23}

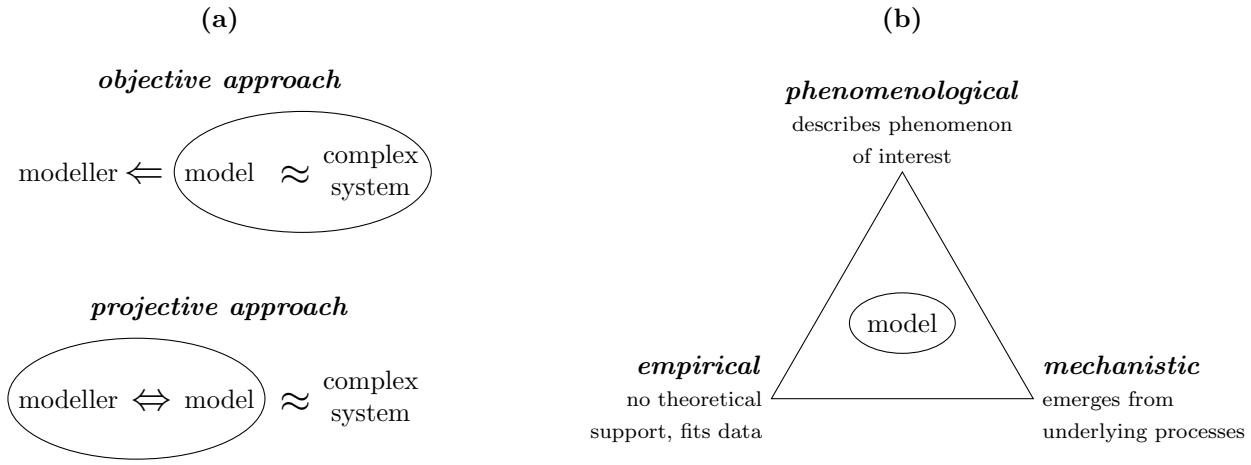

Figure 1.1. Modelling complex systems: objective vs. projective approach (a, redrawn from Le Moigne, 1999) and different types of models (b). In the objective approach, the model is attached to the system and is used by the modeller (the modeller is "outside" the couple model-system). In the projective approach, the modeller interacts with the model (choices in its design) in order to represent the system in the light of its interests (the system is "outside" the couple modeller-model). The different types of models are defined relatively to each other. Note that some parts of a model can be of one type, whereas some other parts are of another type.

atoms, the Avogadro's number) and interactions that it cannot be entirely described. So, it has to be modelled, the model being a simplified representation of the complex system. Research on complex systems in ecology started with the seminal work of von Bertalanffy (1968). Now, most sciences have to deal with the analysis of complex systems (Israel, 1996).

As a complex system will always be represented in an uncomplete way, the act of modelling requires to make choices. Choices in which system features (components, interactions) are taken into account depend on the scope of the study. Thus, modelling moves from an objective (Newtonian) approach to a projective approach (figure 1.1a). In this approach, there is not a single model of a given system, but a variety of models depending on modeller's interests. For example, an animal can be regarded as an emerging system made of numerous cells and molecules, or as the building block of a population made of numerous individuals.

The different models of a system can be classified relatively to each other into mechanistic, phenomenological and empirical models (figure 1.1b). In empirical models, the formulation of a phenomenon has no theoretical support, but this mathematical function fits empirical data. For example, data on the photosynthesis by phytoplankton P as a function of light irradiance L can be well-described by the hyperbolic tangent function (with parameters a and b):

$$P(L) = a \tanh(bL), \tag{1.1}$$

which has no known theoretical justification (Jassby & Platt, 1976).

In phenomenological models, the formulation of a phenomenon describes its emergent properties. For example, the logistic growth equation:

$$\frac{dx}{dt} = xR(x) = xr\left(1 - \frac{x}{K}\right), \tag{1.2}$$

is an ordinary differential equation that describes the growth of a population x through time t (Verhulst, 1838). The model assumes that the net growth rate of the population $R(x)$ is a decreasing function of x, given by $r(1 - x/K)$. This decrease is not explained by its underlying processes (e.g. competition between individuals, limited resources, diseases). It is only described using a maximum growth rate r and a maximum population size that can be supported by the environment K (carrying capacity).

Finally, mechanistic models represent a phenomenon from its underlying processes. If these processes satisfy some assumptions, these assumptions lead to the formulation of the phenomenon. For example, the functional response $f(x)$ (amount of prey x eaten per unit of predator per time unit) can be modelled by Holling's disc equation (Holling, 1959b):

$$f(x) = \frac{ax}{b + x}, \tag{1.3}$$

which is derived by assuming that (i) the spatial repartition of individuals is homogenous, and (ii) the predator split its time of activity between searching preys and handling a captured prey (and some additional assumptions). Note that mechanistic explanations of an empirical or a phenomenological model can be found after it was proposed (see Kooi *et al.*, 1998b, Poggiale, 1998, Loreau, 2010, for the logistic growth equation).

The logistic growth model (1.2) used as example is a determinic model. In deterministic models, one initial condition (e.g. population size) will always predict the same temporal dynamics of the system fixed parameter values. Conversely, stochastic models can predict different results from the same initial condition. It means that the model depends on some random variables (species productivity for example in Yachi & Loreau, 1999). These random variables can be viewed as a phenomenological representation of a phenomenon that emerges from numerous underlying processes that are not represented in the model.

Deterministic and stochastic models can be related through the theory of determinic chaos (for some examples, see chapter 2 in Guckenheimer & Holmes, 1983). Deterministic chaos emerges in systems with non-linear equations. Because of non-linearity, initially close trajectories of the system

diverge through time, a phenomenon coined sensitivity to initial conditions. This phenomenon was first described in an hydrodynamical model by Lorenz (1963), and then in simple ecological models by May (1974, 1976). Hastings *et al.* (1993) argued that there is no dichotomy between stochasticity and deterministic chaos. Indeed, deterministic chaos amplifies uncertainties in the initial state of a system into uncertainties in system dynamics. At a higher scale, these deterministic uncertainties can be viewed as stochasticity. For example, if everything was perfectly known, we will know the result of any roll of dice, despite it is sensitive to minor changes in our toss.

To conclude this first section entitled *Predicting the future*, let me emphasize that it concerns both operational forecasts of a given system (predictive modelling) and conceptual modelling (*sensu* Petrovskii & Petrovskaya, 2012). In conceptual modelling, the purpose of a model is to capture the qualitative features of a class of systems (e.g. a species growing on a limited resource) to test theoretical hypotheses, like the consequences of including a process or not. This leads us to an important property of a model, which is its capacity for abstraction and generality. Generality means that a single model can be used to represent different systems that share some common properties. These common properties are taken into account in an abstract way (e.g. not specific to a given organism). Thus, general hypotheses can be made about how this type of system works.

1.2 Ecology and complexity

1.2.1 A matter of scales, boundaries and approaches

Ecology[2] is the science that studies interactions of living organisms between themselves and their environment. Thus, even if ecology is often viewed as a part of biology, it interacts with physics (e.g. advection and diffusion in the water), chemistry (e.g. organic matter composition, contaminants), geology (e.g. soil composition, release of chemical compounds) and climate sciences. In addition, ecology investigates the levels of organisations of living systems. These levels are nested and span a large range of time and space scales (figure 1.2 and associated definitions). The scale of a single level like the individual can span numerous orders of magnitude (volume and lifetime of known organisms span more than 20 and 6 orders of magnitude respectively, Kooijman, 2010, chapter 8). This scaling implies that the number of components (molecules, cells, individuals) prohibits any description of the whole system even if all components and their interactions were known, which is a first aspect of the complexity of ecosystems.

Another aspect of the complexity in ecology is that all the levels of organisations have smooth

[2]The word *ecology* comes from the ancient greek words *oikos* and *logos* which mean *home* and *science*.

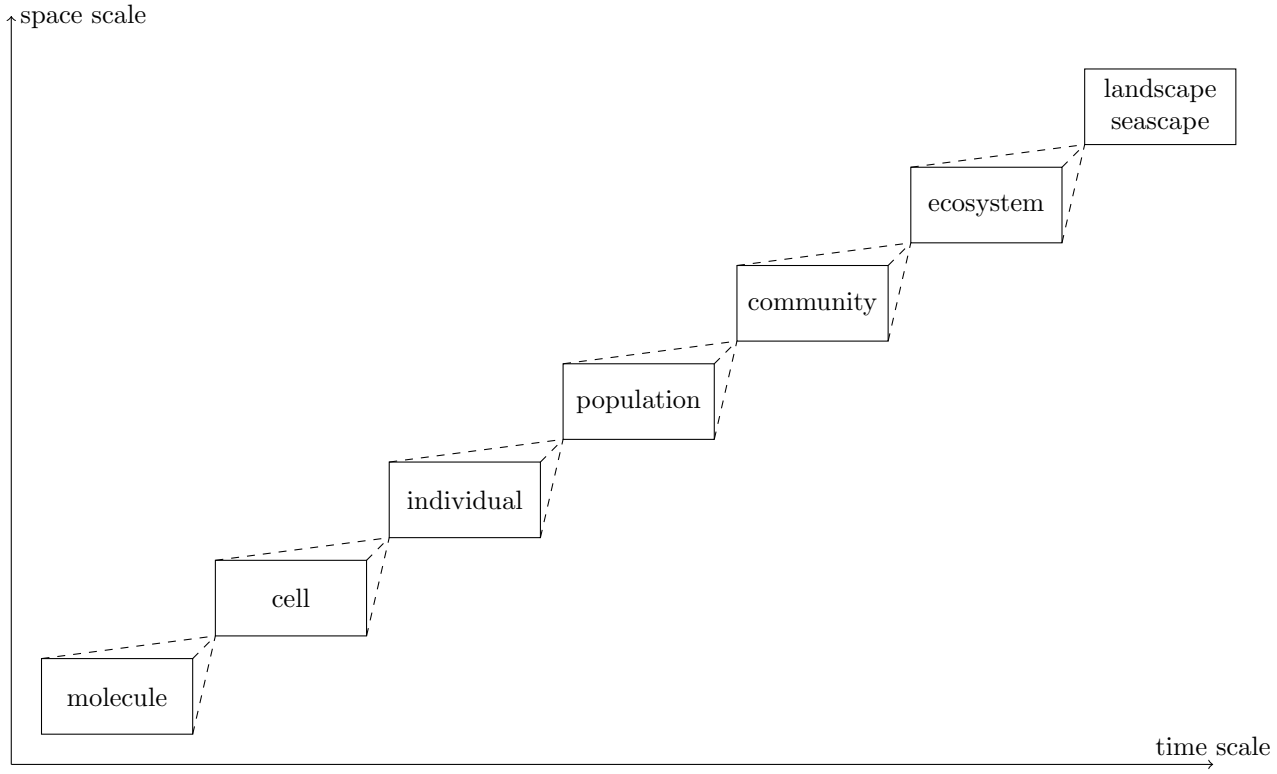

Figure 1.2. Nested levels of organisation of living systems, as a function of their relative scale. Molecules (and atoms) are the building blocks of matter, and so of cells. A cell can be an individual (unicellular organisms) or a part of an individual (multicellular organisms). A set of individuals of the same species is a population. Note that boundaries from cell to population can be vague and arbitrary (see Kooijman, 2010, section 1.1.2). A set of populations of different species is a community. This community is called biocenose if it gathers all the organisms present in a given ecosystem. The ecosystem is made of the biocenose, its biotic and abiotic environment (habitat), and all interactions between organisms and with the environment. Across the environment, the larger spatial organisation of multiple ecosystems (with their biotic and abiotic interactions) is called a landscape (or a seascape). From populations to landscapes, levels of organisations are defined at a given time and location, but also according to the scale and the scope of a study. For example, a landscape from the microbiologist point of view is only a tiny part of an ecosystem from the ichthyologist point of view. In addition, an individual (like a tree) can be a landscape for smaller organisms (micro-organisms, insects). Modified from Lévêque (2003).

boundaries (figure 1.2). Smooth boundaries also characterize systems of the same level. At all levels of organisation, living systems are open from the thermodynamic point of view, as energy and matter are exchanged. So, delimiting an ecosystem will be highly dependent of the scale and the scope of the study. Similarly, organisms themself are hard to classify (see Ragan, 2009, for an history of trees of life). Classifications are always evolving, the most common being the taxonomic classification (see Baldauf, 2003, 2008, for eucaryotes). Other classifications involve the functional role of organisms or their metabolism. Indeed, even strains of the same bacteria species can present many differences in phenotype (like the cyanobacterium *Crocosphaera watsonii*, Webb *et al.*, 2009).

Two main streams of research in ecology are population ecology and ecosystem ecology (Odum,

1964). The first one focuses on populations and their interactions, through changes in population abundances. Conversely, the second one focuses on the interactions between populations and their abiotic environment, through fluxes of matter and energy. These two approaches are not opposite, and more recent researches attempt to consider both (Loreau, 2010, and references therein).

Similarly, complex systems like living systems can be studied from two point of view, holism and reductionism. The holistic approach considers that due to its emergent properties, the complex system can only be considered as a whole by modelling these emergent properties. As an example in ecology, the integrative theory for ecosystems (Jørgensen *et al.*, 2007) attempts to model ecosystems from a thermodynamic point of view, through energy fluxes. Conversely, the reductionist approach focuses on some *a priori* important components of the system by the mean of mechanistic models. An example in ecology is the Dynamic Energy Budget theory (Kooijman, 2010) which focuses on individuals and offers a general framework to represent their metabolism (also through energy).

1.2.2 Interactions between organisms

Interactions between two organisms can be classified according to their respective impact on each organism (table 1.1). The three main interactions are exploitation, competition and mutualism. Exploitation concerns prey killed by their predator or eaten by a grazer (the prey survives), as well as a host infected by a parasite. Competition concerns organisms that share the same limiting factor. A limiting factor can be any form of resource (prey, nutrient, light), its pattern of spatio-temporal abundance (i.e. spikes, fluctuations, patchiness), a predator to escape from, space, and many others (Loreau, 2010). Mutualistic organisms are in a mutually beneficial interaction, like producting and sharing a limiting resource of the other (e.g. corals, Eynaud *et al.*, 2011, rhizobium, Akçay & Roughgarden, 2007). Finally, note that this classification of interactions is individual-based. At the population scale, exploitation can for example turn into indirect mutualism as the prey population is regulated (e.g. avoid excessive resource depletion by the prey, Loreau, 2010) by the predator population.

Interactions between multiple organisms are organized into networks, the most studied being food webs (predation, Cohen *et al.*, 1990) and mutualistic networks (Bascompte, 2008). Networks are usually characterized by their structural complexity (number of species[3] and interactions between them). The same structural complexity can be achieved by a huge number of networks. For example, consider 30 species that can all interact with each other (including themself through cannibalism). Assume 135 interactions between these species (15 % of the number of possible

[3]Except if it is stated otherwise, the word *species* is now used in its wide sense to refer to organisms that belong to the same taxa or functional group and that are lumped together for the purpose of the study.

Table 1.1. Different types of interactions between two organisms A and B, depending on their respective effect (positive, negative or neutral) on each other. From CF Boudouresque (pers. comm).

$A \rightarrow B$	$A \leftarrow B$	$A \leftrightarrow B$
+	−	exploitation
−	−	competition
+	+	mutualism
=	−	antagonism
=	+	commensalism
=	=	independance

interactions $30 \times 30 = 900$, a common value for food webs, Williams & Martinez, 2000), it leads to $C_{900}^{135} = 900!/(135!865!) \approx 6.2\ 10^{163}$ different networks. The square root of this number is higher then 10^{80}, the estimated number of atoms in the observable universe (Wikipedia Free Encyclopedia, 2016). This number does not take into account the fact that some interactions cannot occur due to physiological constraints (e.g. respective size of prey and predator, ability to produce a given chemical compound). But the idea behind this back-of-an-enveloppe calculation is that again, all the possible situations (here networks) cannot be explored due to their number.

1.3 Some current issues in ecological modelling

The four topics detailed in this section can be gathered within the following question: *how far choices in model construction can affect the predicted dynamics of ecological systems and the information they provide on their resilience?* This question is the guideline along this thesis (its scope is presented in the next section) that links the following issues in ecological modelling.

1.3.1 Computational ecology and the "unreasonable effectiveness of mathematics"

A feature of mathematical models that we have not already discussed is our ability to analyze and use this model. For example, a system of ordinary differential equations can be easily written. But solving this system (i.e. knowing the dynamics it predicts) or finding some of its general properties (i.e. equilibria, bifurcations) is mostly not possible analytically. Analytical results are generic as they are expressed as functions of parameters. Conversely, numerical results can be more easily obtained for specific parameter values and are mostly approximations. Their accuracy depends on methods used for numerical approximations. Numerical methods were initially used "by hand"

(e.g. Runge-Kutta methods to solve ordinary differential equations were proposed in 1901) and their use is rising since the development of computers.

The use of computers in modelling in ecology has reached the point where some authors talk about computational ecology as an emerging science (Petrovskii & Petrovskaya, 2012). The rise of computational ecology concerns both predictive and conceptual modelling. New ways of research in conceptual modelling have been opened thanks to numerical simulations. An example is the emergence of (stochastic) Individual-Based Models (DeAngelis & Grimm, 2014) that take into account many individuals in interaction (for an example on schooling fishes, see Accolla *et al.*, 2015). Another example is the possibility to explore a significant number (up to billions) of possible networks of interactions between tens of species (for food webs, see Gross *et al.*, 2009).

The increasing use of computer simulations rises the risk for the modeller to be lured by the "unreasonable effectiveness of mathematics" (Wigner, 1960, Anderson, 2005, 2010). The mathematical objects (e.g. models, functions) are not the objects (e.g. organisms, biological interactions) that they aimed to represent. This critical point has to be kept in mind everytime model results are related to the modelled system (interpretation, validation, figure 1.3). Indeed, a model can be an accurate description of a data set for purely statistical reasons, i.e. model complexity (number of state variables and parameters) makes it able to fit any data sets after parameter estimation. The risk is to think that the model is an appropriate description of the system (it captures most of the relevant processes) whereas we are just experiencing the statistical artifact of overparameterization. Thus, the choice of model complexity is a point still open to debate (Evans *et al.*, 2013). Another point of debate is also how researchers from different fields of science (biology and mathematics) and with different approaches (tendency toward detailed description vs. toward simplicity) should interact during model construction (Flynn, 2005).

The method for predictive modelling depicted in figure 1.3 highlights the importance of model verification and validation with empirical data. An additional step is the mathematical analysis of the model itself, to better understand why it succeeds or not to reproduce data and what would be its predictions outside its range of validation. However, a meta-analysis of 153 aquatic mechanistic models indicates that most of these operational models lack of validation, as well as a simple sensitivity analysis of their predictions (Arhonditsis & Brett, 2004). Indeed, a numerical sensitivity analysis (like robustness to changes in parameter values) can be computationally prohibitive in complex operational models. In addition, these models cannot be mathematically analyzed like simple models. This rises the interest of simple theoretical models. Knowing their mathematical properties and some generic biological results they provide can give clues to understand the predictions made by more complex models (Baklouti *et al.*, 2006b,a).

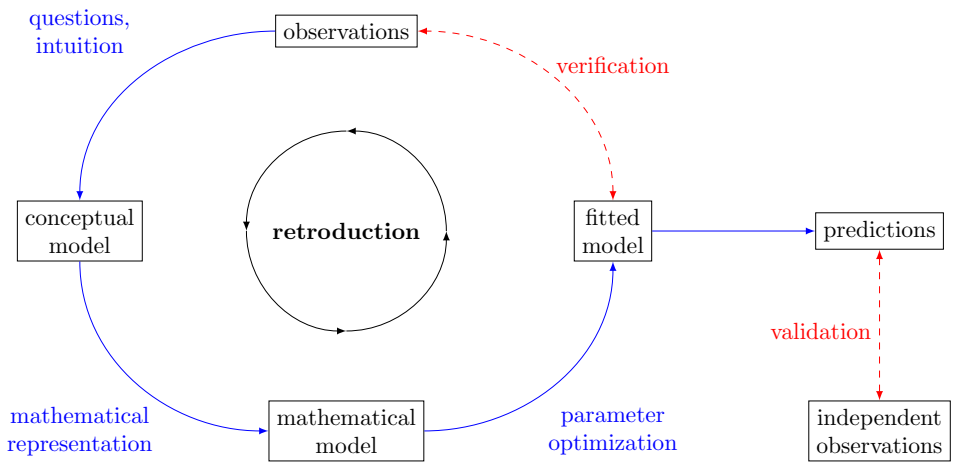

Figure 1.3. Method for predictive modelling according to Anderson (2010, modified). Blue steps are the classical way of model construction and model use. Red steps are model comparison to data.

1.3.2 The mathematical formulation of a process

As they are complex systems, even the physical and chemical environments are only represented in a simplified way in a model. However, as pointed out by Flynn (2005): *"The description of the physical environment is also simplistic, but physics and chemistry are sciences blessed with laws so at least implications can be more carefully considered."*. The notion of "laws" is used here in comparison to biology where there is nothing like the Newton laws of motion in classical mechanics. This means that the problem with physics and chemistry is mainly due to the number of components (atoms) of the system and to the resolution used for numerical simulations (like for weather forecasting). Conversely, biological systems at our scales of interest (individual, population) are already too complex to be described by such laws. Thus, multiple models can be built to describe one phenomenon.

Predation for instance can be modelled by multiple functional response formulations (for a review, see Jeschke *et al.*, 2002, Gentleman *et al.*, 2003). The concept of functional response was first introduced by Solomon (1949). Holling (1965) proposed a classification for functional responses that only depend on prey abundance, but predator-dependent and ratio-dependent functional responses also exist (Ivlev, 1955, Beddington, 1975, DeAngelis *et al.*, 1975, Arditi & Ginzburg, 1989, DeAngelis, 2013). These different types of functional responses correspond to different assumptions about the phenomenon of predation. So, it is not counter-intuitive that they lead to different model predictions (Oaten & Murdoch, 1975, Scheffer & de Boer, 1995, Cantrell & Cosner, 2001).

Surprisingly, different model predictions can also be obtained with functions that share common properties (e.g. for predation, they belong to the same type of functional response) and fit empirical

data with the same accuracy. This phenomenon is coined as structural sensitivity (Fussmann & Blasius, 2005, Cordoleani *et al.*, 2011). Structural sensitivity concerns both qualitative (structural stability, *sensu* Kuznetsov, 2004) and quantitative (e.g. equilibrium values) changes in model predictions. Structural sensitivity has been studied in small systems with a few state variables, mainly in the context of predator-prey interactions (Myerscough *et al.*, 1996, Wood & Thomas, 1999, Gross *et al.*, 2004, Fussmann & Blasius, 2005, Poggiale *et al.*, 2010, Cordoleani *et al.*, 2011, Adamson & Morozov, 2012, 2014). From an operational point of view, structural sensitivity is an issue as different model predictions are obtained from model formulations based on similar hypotheses (they share common properties) and that can be *a priori* considered as being close to each others (they fit the same data). In addition, structural sensitivity can have a greater impact than parameter values on model dynamics (Cordoleani *et al.*, 2011). However, parameter sensitivity is the more often investigated in model sensitivity analysis (Arhonditsis & Brett, 2004).

1.3.3 Diversity, networks of interaction and ecoystem functioning

The diversity of species and functional traits in an ecosystem affects the intensity of processes like carbon fixation, as well as the size and temporal variability of populations. To estimate these diversity-ecosystem functioning relationships, different diversity experiments were carried out on terrestrial plants (Hector *et al.*, 1999, Tilman *et al.*, 1997, 2001, 2006) or in controlled microcosms (Naeem *et al.*, 1994, Naeem & Li, 1997, McGrady-Steed *et al.*, 1997). Jiang & Pu (2009) made a review of recent empirical studies on the subject. In these studies, numerous biases (Huston, 1997) and confusing factors often alter the interpretation of the results (Hector, 1998, Loreau, 1998, Loreau & Hector, 2001). Bengtsson (1998) argued that these difficulties come from the fact that diversity is an abstract and aggregated property of the system.

In parallel to these empirical studies, theoretical researches have also been realized on the link between diversity and ecosystem functioning. The insurance hypothesis suggests that a higher diversity promotes a less variable ecosystem productivity by increasing the probability of having a performant species in every environmental condition (Yachi & Loreau, 1999). However, only up to n species can coexist on n limiting resources in an homogeneous environment (competitive exclusion principle, Loreau, 2010), which may prohibit an infinite increase of diversity.

Going beyond diversity, other studies investigated how ecosystem functioning is influenced by the complexity of the network of interactions (number of species and number of interactions). This complexity was initially though to promote the stability of ecological communities (MacArthur, 1955). The opposite was later argued by May (1972, 1973). May's seminal work led to a long-standing debate on whether a complex system would be more or less stable than a simple one.

This debate is still open (May, 1999, McCann, 2000, Loreau, 2010), mainly because there are many ways to define stability and complexity in ecology (Holling, 1973, Pimm, 1984, Grimm & Wissel, 1997). Another aspect of the complexity of interaction networks is the existence of clusters of highly interacting communities. These clusters are known to affect food web dynamics (Stouffer & Bascompte, 2010, 2011). However, the proper mathematical definition of these interacting communities and their detection are still the matter of ongoing researches (Fortunato, 2010).

The works mentioned in this subsection are motivated by questions on the role of diversity (complexity) in ecology. As a consequence, if diversity has a strong impact on system dynamics, this diversity should be taken into account in a model. Failing to do so would rise the risk to miss important properties of the ecological system that is studied. However, studying complex ecological models pose some problems highlighted in the previous subsections. In addition, the dynamics of complex ecological networks can be almost untractable as even simple models can predict complex dynamics (Kuznetsov & Rinaldi, 1996, Kooi & Boer, 2001), including deterministic chaos (Hastings & Powell, 1991, Rinaldi & De Feo, 1999).

1.3.4 System resilience and multiple stable states

Resilience was first defined by Holling (1973): *"Resilience determines the persistence of relationships within a system and is a measure of the ability of these systems to absorb changes of state variables, driving variables, and parameters, and still persist."*. This definition remains an abstract concept, as in an operational context most objects in the definition ("changes", "variables", "parameters", "persistence") can be defined and quantified in an almost infinite number of ways. However, the concept of resilience is used to refer to system ability to withstand and recover after external disturbances. The study of ecosystem resilience is growing, due to its importance for decision-making and environmental management policies (Scheffer *et al.*, 2009, 2012).

Some properties of a system that are related to the concept of resilience are well-defined from a mathematical point of view. A mathematical model can be caracterized by the asymptotic behaviour of the dynamics it predicts. These dynamics may converge on stable states (e.g. equilibrium, oscillations) that the system will maintain through time. A model can have different stable states, a situation called multiple (or alternative) stable states in ecology (Beisner *et al.*, 2003, Knowlton, 2004). The existence of these multiple stable states in a system facing a disturbance can lead to the phenomenon of hysteresis. Hysteresis occurs when the amount of changes required to put a system back in its original state is of higher absolute magnitude than the initial disturbance. This situation happens when the system has moved from one stable state to another due to the disturbance (e.g. Ludwig *et al.*, 1978).

1.4 Scope of this thesis

The research work presented in this thesis links the four topics detailed in the previous section. These different topics are gathered within the following question: *how far choices in model construction can affect the predicted dynamics of ecological systems and the information they provide on their resilience?*

The guideline along this thesis is the study of structural sensitivity using the example of predation formulation in various ecological models. Earlier studies on structural sensitivity focused for simplicity on models that: (i) have one stable state, (ii) have a few state variables, and (iii) make simple assumptions on individual metabolism (Myerscough *et al.*, 1996, Gross *et al.*, 2004, Fussmann & Blasius, 2005, Poggiale *et al.*, 2010, Cordoleani *et al.*, 2011, Adamson & Morozov, 2012). These three simplifications are relaxed during this thesis, in order to see if structural sensitivity is confined to simple theoretical models or if it can affect complex ecological models. The models studied in this thesis are more or less complex, which allows a more or less deep mathematical understanding of their behaviour. In addition, these models cover different aspects of complexity in ecology: the complexity of networks of interactions (holistic approach, tens of state variables) and the complexity of the intrinsic metabolism of organisms (reductionist approach, through Dynamic Energy Budget theory). Finally, these models can exhibit complex dynamics, including the coexistence of multiple stable states.

The next chapter introduces some mathematical tools to study population models through examples of applications (figure 1.4). It ends with an analysis of published data sets that shows why the formulation of a process like predation remains uncertain. The second part of this thesis presents a detailed study of structural sensitivity. This study starts with the impact of structural sensitivity on the predicted dynamics and resilience of a predator-prey model (chapter 3). Results are explained by a more detailed mathematical analysis using the framework of bifurcation theory (chapter 4). Then, the predator-prey model is extended to model complex food webs. Their dynamics are analyzed as a function of model formulation and the complexity of the interaction network (chapter 5). The third part of this thesis explores ways to deal with structural sensitivity. Chapter 6 suggests methods to quantify structural sensitivity in models with complex dynamics like multiple stable states and hysteresis. In addition to this mathematical approach, chapter 7 investigates if including some appropriate details in the metabolism representation of organisms can dampen the effect of structural sensitivity. Conclusions and implications of all chapters are summarized into the last chapter, which ends with perspectives for future researches and more personal comments on ecological modelling.

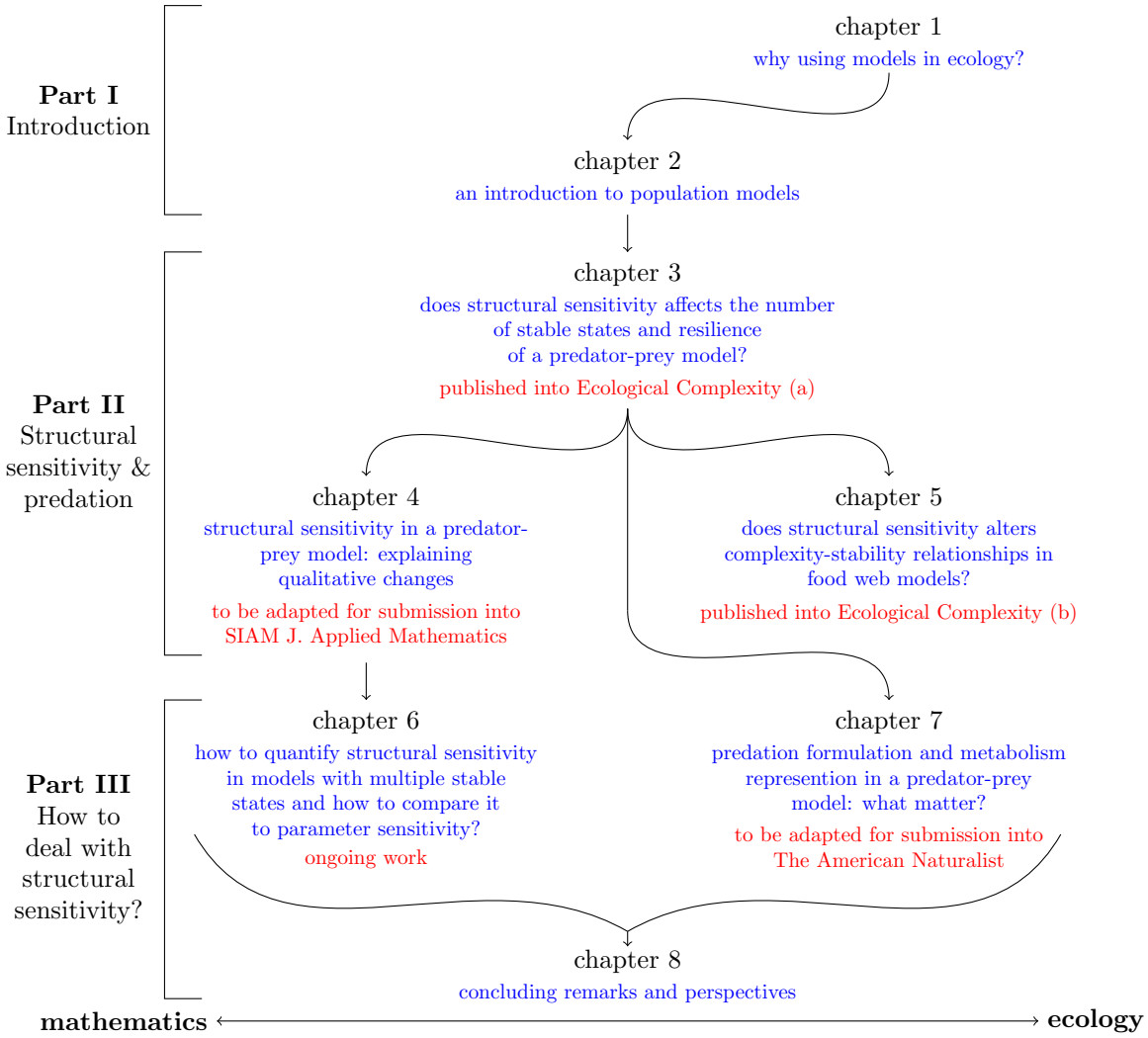

Figure 1.4. Scope of this thesis. For each chapter, the corresponding question (blue) and the current state of my research about it (red) are provided. Chapters are presented according to their relative location between the sciences of mathematics (left) and ecology (right). This location in purely subjective and personal: all chapters might be mathematics from an experimental biologist point of view, whereas they all might be ecology from the mathematician point of view. See section 1.4 for more detailed informations.
Advises to read this thesis (arrows): using examples in ecology, chapter 2 summarizes the required concepts of dynamical systems and bifurcations. The reader familiar with these notions can go quickly through this chapter. Conversely, the reader interested in the ecological applications of these notions can understand most of them by focusing on figures. Research presented in chapter 3 is the basis of all the topics investigated in the next chapters. Chapters 4 and 6 are oriented toward mathematical aspects and can be skipped by the reader most interested into ecological applications. In term of ecological applications, chapters 3 to 5 present a detailed analysis of structural sensitivity in models of varying complexity (part II), whereas chapters 6 and 7 explore ways to deal with this structural sensitivity in ecological modelling (part III). Conclusions and implications of all chapters are summarized into the last chapter, which ends with more personal comments and perspectives for future researches.

CHAPTER 2

An introduction to population models

"[...], mathematical modeling may be regarded as the most promising tool for predicting the reaction of natural ecosystems to external influences. However, scientists run into serious obstacles when taking this path, obstacles that are intrinsic to any attempt to apply mathematical methods to biology."

Alexander D. Bazykin,
"Nonlinear dynamics of interacting populations" (Bazykin, 1998)

This chapter introduces the main mathematical tools used in the remaining of this thesis. In this thesis, we focus on mathematical models that are dynamical systems, and more specifically on systems of ordinary differential equations (see for instance section 1.1 in Kuznetsov, 2004, for an overview of the different types of dynamical systems). These systems correspond to deterministic models that assume a continuous dynamics of the system through time (solutions are differentiable). Basics of differential systems are recalled in section 2.1 and illustrated by examples in population ecology in section 2.2. These examples are also used to introduce different notions of theoretical biology. These examples also highlight the qualitative changes in system dynamics that occur at thresholds on parameter values called bifurcations. The application of bifurcation theory to the study of living systems and the associated mathematical background are presented in section 2.3. Finally, the last two sections complete the informations given in the previous chapter on the modelling of complex networks of interaction and structural sensitivity. The mathematical backgound presented in sections 2.1 and 2.3 come from classical textbooks in applied mathematics, like Arnold (1974), Guckenheimer & Holmes (1983), Perko (1996) and Kuznetsov (2004).

2.1 Some basics of differential systems

Consider any system described by a finite number of state variables $x_i \in \mathbb{R}$ organized into a vector $\boldsymbol{x} \in \mathbb{R}^n$ (in fact, any compact subset of $\mathbb{R}^n$ can be considered). Consider that the evolution of these variables through time is given by the differential system:

$$\frac{d\boldsymbol{x}}{dt} = \boldsymbol{f}(\boldsymbol{x}, \boldsymbol{\alpha}), \tag{2.1}$$

where $\boldsymbol{f} : \mathbb{R}^n \times \mathbb{R}^p \to \mathbb{R}^n$ is a vector function made of n functions $f_i : \mathbb{R}^n \times \mathbb{R}^p \to \mathbb{R}$ parameterized by a vector of parameters $\boldsymbol{\alpha} \in \mathbb{R}^p$. For each $\boldsymbol{\alpha} \in \mathbb{R}^p$, system (2.1) defines a flow, i.e. an evolution operator $\varphi^t_{\boldsymbol{\alpha}} : \mathbb{R}^n \to \mathbb{R}^n$. This operator satisfies $\varphi^0_{\boldsymbol{\alpha}}\boldsymbol{x} = \boldsymbol{x}$ and $\varphi^{t+s}_{\boldsymbol{\alpha}}\boldsymbol{x} = \varphi^t_{\boldsymbol{\alpha}}(\varphi^s_{\boldsymbol{\alpha}}\boldsymbol{x})\ \forall s, t \in \mathbb{R}$, and it gives the state of the system $\boldsymbol{x}_{\boldsymbol{\alpha}}(t)$ at any time $t \in \mathbb{R}$:

$$\boldsymbol{x}_{\boldsymbol{\alpha}}(t) = \varphi^t_{\boldsymbol{\alpha}}\boldsymbol{x}(0),$$

knowing its initial state $\boldsymbol{x}(0)$. For a given initial state $\boldsymbol{x}(0)$, there is a unique system trajectory $\{\boldsymbol{x} \in \mathbb{R}^n / \boldsymbol{x} = \varphi^t_{\boldsymbol{\alpha}}\boldsymbol{x}(0), t \in \mathbb{R}\}$ according to Cauchy Theorem.

An invariant set $S \in \mathbb{R}^n$ satisfies $\varphi^t_{\boldsymbol{\alpha}}\boldsymbol{x} \in S\ \forall \boldsymbol{x} \in S,\ t > 0$. This means that any trajectories starting on the invariant set will remain on the invariant set while time is running. The simplest type of invariant set is an equilibrium $\boldsymbol{x}^*_{\boldsymbol{\alpha}}$, which satisfies $\varphi^t_{\boldsymbol{\alpha}}\boldsymbol{x}^*_{\boldsymbol{\alpha}} = \boldsymbol{x}^*_{\boldsymbol{\alpha}},\ t \in \mathbb{R} \Leftrightarrow \boldsymbol{f}(\boldsymbol{x}^*_{\boldsymbol{\alpha}}, \boldsymbol{\alpha}) = \boldsymbol{0}$.

An invariant set S is said to be Lyapunov stable if for any sufficiently small neighborhood $U \supset S$, there exists a neighborhood $V \supset S$ such that $\varphi^t_{\boldsymbol{\alpha}}\boldsymbol{x} \in U \ \forall \boldsymbol{x} \in V, \ \forall t > 0$. This means that every trajectory starting sufficiently close to the invariant set will remain inside any given bounded neighborhood of this invariant set. An invariant set S is said to be asymptotically stable if there exists a neighborhood $U \supset S$ such that $\varphi^t_{\boldsymbol{\alpha}}\boldsymbol{x} \to S, \ \forall \boldsymbol{x} \in U$ as $t \to +\infty$. This means that every trajectory starting sufficiently close to the invariant set will end up as close as we want of this invariant set after some time. Similarly, a closed invariant set S is called an attracting set if there is a neighborhood $U \supset S$ such that:

$$\varphi^t_{\boldsymbol{\alpha}}U \subset U, \ \forall t > 0 \text{ and } \bigcap_{t>0} \varphi^t_{\boldsymbol{\alpha}}U = S.$$

A closed set S is said to be topologically transitive if for all open subsets $U, V \subset S$, there is a t such that $\varphi^t_{\boldsymbol{\alpha}}U \cap V = \varnothing$. This means that every trajectory starting in the invariant set will cover almost all the invariant set. An attracting and topologically transitive set is called an attractor. The simplest attractor is an asymptotically stable equilibrium.

The remaining of this section focuses on the asymptotic stability analysis of an equilibrium $\boldsymbol{x}^*_{\boldsymbol{\alpha}}$ of system (2.1). Consider the following Taylor expansion of system (2.1) near $\boldsymbol{x}^*_{\boldsymbol{\alpha}}$:

$$\frac{d\boldsymbol{x}}{dt} = \boldsymbol{f}_{\boldsymbol{x}}(\boldsymbol{x}^*_{\boldsymbol{\alpha}}, \boldsymbol{\alpha})(\boldsymbol{x} - \boldsymbol{x}^*_{\boldsymbol{\alpha}}) + O(||\boldsymbol{x} - \boldsymbol{x}^*_{\boldsymbol{\alpha}}||^2),$$

where:

$$\boldsymbol{f}_{\boldsymbol{x}}(\boldsymbol{x}^*_{\boldsymbol{\alpha}}, \boldsymbol{\alpha}) = \begin{pmatrix} & \vdots & \\ \dots & \dfrac{\partial f_i(\boldsymbol{x}^*_{\boldsymbol{\alpha}}, \boldsymbol{\alpha})}{\partial x_j} & \dots \\ & \vdots & \end{pmatrix}, \tag{2.2}$$

is the Jacobian matrix of system (2.1) evaluated at equilibrium $\boldsymbol{x}^*_{\boldsymbol{\alpha}}$ (i and j are the row and column index respectively).

Jacobian matrix (2.2) has n eigenvalues $\lambda^{\boldsymbol{\alpha}}_1, ..., \lambda^{\boldsymbol{\alpha}}_n$. There are respectively n_s, n_u and n_c eigenvalues with negative ($\Re(\lambda^{\boldsymbol{\alpha}}_i) < 0$), positive ($\Re(\lambda^{\boldsymbol{\alpha}}_i) > 0$) and zero ($\Re(\lambda^{\boldsymbol{\alpha}}_i) = 0$) real part, with $n = n_s + n_u + n_c$. If all Jacobian's eigenvalues have non-zero real part ($n_c = 0$), the equilibrium is said to be hyperbolic. For a hyperbolic equilibrium $\boldsymbol{x}^*_{\boldsymbol{\alpha}}$, the term $O(||\boldsymbol{x} - \boldsymbol{x}^*_{\boldsymbol{\alpha}}||^2)$ is neglectible near equilibrium, where the Taylor expansion (2.1) can be approximated by the linear system:

$$\frac{d\boldsymbol{x}}{dt} = \boldsymbol{f}_{\boldsymbol{x}}(\boldsymbol{x}^*_{\boldsymbol{\alpha}}, \boldsymbol{\alpha})(\boldsymbol{x} - \boldsymbol{x}^*_{\boldsymbol{\alpha}}). \tag{2.3}$$

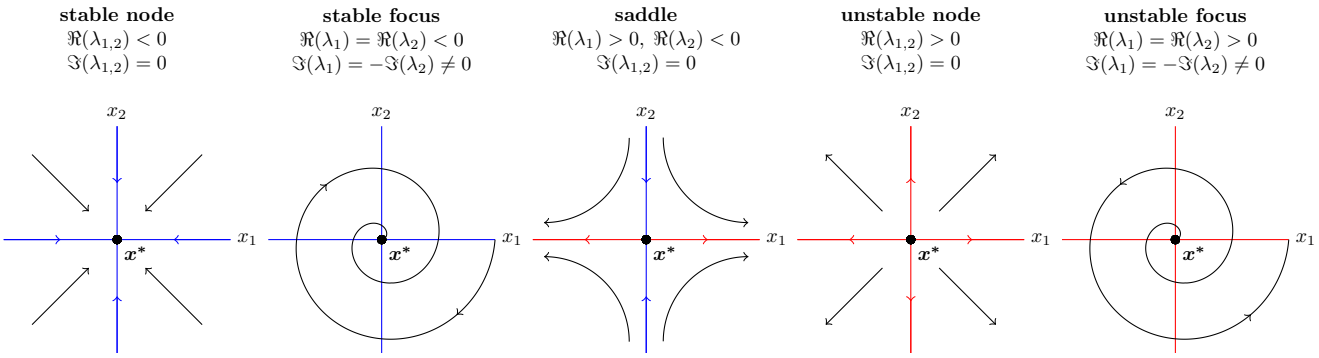

Figure 2.1. Topological classification of hyperbolic equilibria in $\mathbb{R}^2$. Blue (red) axes correspond to attractive (repulsive) directions. Arrows are examples of system trajectories.

This linear system is locally topologically equivalent to the non-linear system (2.1) (Hartman-Grobman Theorem). Two systems are said to be topologically equivalent if there is a smooth invertible map (homeomorphism) of one system's trajectories onto those of the other, i.e. systems are identical under a smooth invertible change of coordinates. Local topological equivalence of systems (2.1) and (2.3) implies that the local[1] asymptotic stability of equilibrium $\boldsymbol{x}^*_{\boldsymbol{\alpha}}$ in system (2.1) can be known from the analysis of the linear system (2.3).

Qualitative behaviour of the trajectories of linear system (2.3) are determined by eigenvalues of the Jacobian matrix (2.2). If all eigenvalues have negative real part ($n_s = n$), the equilibrium $\boldsymbol{x}^*_{\boldsymbol{\alpha}}$ is either a stable node (all eigenvalues are real) or a stable focus (there is at least one pair of complex conjugate eigenvalues). At the opposite, if all eigenvalues have positive real part ($n_u = n$), the equilibrium is either an unstable node or an unstable focus. Finally, if eigenvalues have real part of different signs ($n_s n_u \neq 0$), the equilibrium is a saddle. These conditions define five generic phase portraits (system dynamics in the state variables space) for equilibria in planar systems ($n = 2$, figure 2.1).

In every system (2.1), a linear analysis through the Jacobian matrix gives the local asymptotic stability (later called stability to ease reading) of hyperbolic equilibria. For non-hyperbolic equilibria, at least one eigenvalue has a zero real part ($n_c \geq 1$). Eigenvalue(s) with zero real part appear(s) for specific parameter values $\boldsymbol{\alpha}^*$. These thresholds are called bifurcations. A bifurcation is a qualitative change in the phase portrait of the system, like a change in equilibria existence and/or stability. Formally, the appearance of topologically non-equivalent phase portrait under variation of parameters is called a bifurcation (definition 2.11 in Kuznetsov, 2004). A bifurcation

[1]Here we are talking of local asymptotic stability as the linear approximation of the original (non-linear) system is only possible in a small neighborhood of the equilibrium. Thus, we can only know if trajectories starting close to the equilibrium will converge to it. Indeed, we have no information on dynamics far from equilibrium, where higher order terms in the Taylor expansion (2.1) are not neglectible.

can be understood from eigenvalues with zero real part (number, imaginary part) and by studying non-linear terms ($O(||\boldsymbol{x} - \boldsymbol{x}^*_{\boldsymbol{\alpha}}||^2)$ and higher order terms) that are no longer neglectible in the Taylor expansion (2.1). Most classical bifurcations will be presented in section 2.3.

2.2 Some examples of ecological models

As long as we are not explicitely studying bifurcations, model dependency to its parameters is not explicitely written for simplicity:

$$\frac{d\boldsymbol{x}}{dt} = \boldsymbol{f}(\boldsymbol{x}). \tag{2.4}$$

In addition, model (2.4) represents a biological system. Due to their biological meaning, parameters and state variables have to follow some constraints. For example, if state variables $\boldsymbol{x}$ are the size of different populations, we have $\boldsymbol{x} \in \mathbb{R}^n_+$ as a population density cannot be negative. Except if it is stated otherwise, all parameters are assumed to be positive.

2.2.1 Malthus' model of exponential growth

Malthus (1798) used the following linear model to describe the size of a population $x \in \mathbb{R}^+$:

$$\frac{dx}{dt} = rx \equiv f(x), \tag{2.5}$$

where parameter $r \neq 0$ is the growth rate of the population (birth rate minus death rate), which is assumed to be constant. Model (2.5) has one equilibrium $x^* = 0$ that satisfies $f(x^*) = 0$, which means that an extincted population remains extincted. Model (2.5) is one-dimensional, so its Jacobian matrix is a 1×1 matrix with one eigenvalue which is equal to its single element $f'(x)$. As $f'(x^*) = r$, this extinction equilibrium is stable if the growth rate is negative ($r < 0$), and unstable if it is positive ($r > 0$).

To complete the analysis on equilibrium and its stability, consider the solution of the linear differential equation (2.5):

$$x(t) = x(0)\exp(rt),$$

where $x(0) \in \mathbb{R}$ is the initial size of the population. Dynamics of population size for both $r > 0$ and $r < 0$ are qualitatively drawn and described in figure 2.2.

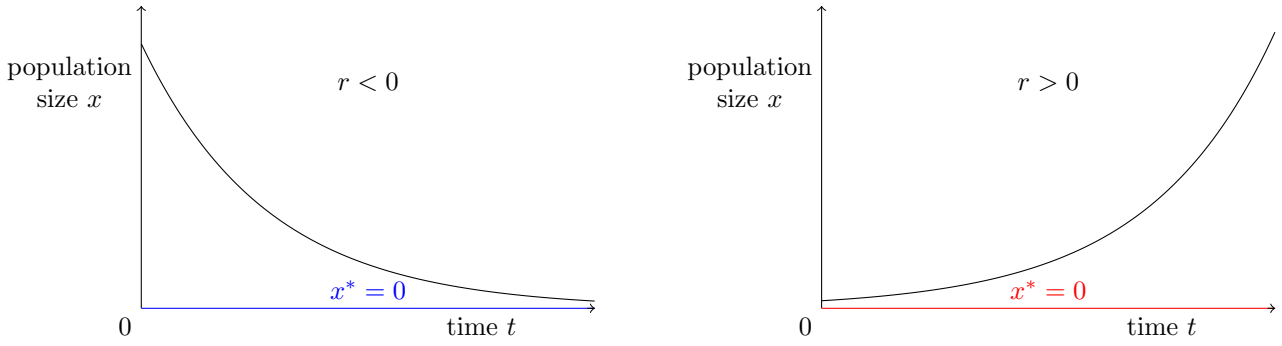

Figure 2.2. Qualitative dynamics of the exponential growth model. If the growth rate r is negative (left), population size decreases exponentially toward the extinction equilibrium which is stable (blue). If the growth rate r is positive (right), population size increases exponentially, even when it is initially close to the extinction equilibrium which is unstable (red).

2.2.2 Logistic growth model: from local to global stability

The logistic growth equation (Verhulst, 1838) is an extension of the exponential growth model (2.5) where the population growth rate $R(x)$ depends on population size $x \in \mathbb{R}^+$:

$$\frac{dx}{dt} = R(x)x.$$

The logistic growth model assumes that the growth rate is a linear and decreasing function $R(x) = r(1 - x/K)$. Parameter $r > 0$ is the intercept of $R(x)$ and the maximum growth rate of the population. Parameter $K > 0$ is the environmental carrying capacity, i.e. the maximum population size that the environment can support ($R(K) = 0$). If population size is above this maximum, then the growth rate is negative. The decrease of the growth rate with population size can be explain for example by intra-specific competition for a limiting resource or diseases. The logistic growth model is:

$$\frac{dx}{dt} = rx\left(1 - \frac{x}{K}\right) \equiv f(x). \tag{2.6}$$

Model (2.6) has two equilibria which are solutions of $f(x) = 0$, $x^{(0)} = 0$ and $x^{(1)} = K$. Their local stability is given by the derivative:

$$f'(x) = r\left(1 - \frac{2x}{K}\right).$$

Thus, the extinction equilibrium $x^{(0)}$ is unstable ($f'(0) = r > 0$), whereas the persistence equilib-

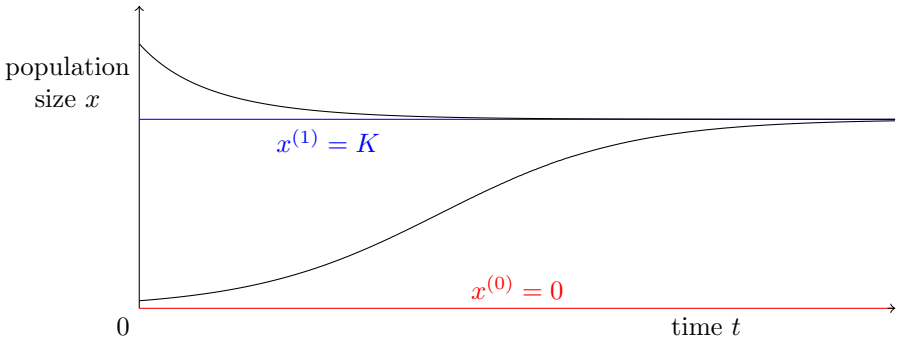

Figure 2.3. Qualitative dynamics of the logistic growth model. Dynamics correspond to different initial conditions above and below the environmental carrying capacity K. For both initial conditions, population size converges toward the stable persistence equilibrium (blue), even if it starts close to the unstable extinction equilibrium (red).

rium $x^{(1)}$ is stable ($f'(K) = -r < 0$).

To complete the previous analysis, consider the solution of the non-linear differential equation (2.6) obtained for instance through a change of state variable $y = 1/x$ (the differential equation in y is linear):

$$x(t) = \frac{Kx(0)}{x(0) + (K - x(0))\exp(-rt)}, \tag{2.7}$$

where $x(0) \in \mathbb{R}^+$ is the initial population size. Dynamics of population size are qualitatively drawn and described in figure 2.3. From solution (2.7), one can see that:

$$\lim_{t \to +\infty} x(t) = K, \ \forall x(0) \in \mathbb{R}_+^*,$$

i.e. that every trajectory of system (2.6) (except the one that starts at $x(0) = 0$ which is an equilibrium) converges asymptotically on $x^{(1)} = K$. This equilibrium is said to be globally stable (on $\mathbb{R}_+^*$). Note that the extinction equilibrium of the exponential growth model is also globally stable if the growth rate is negative.

2.2.3 Lotka-Volterra predator-prey model: neutral oscillations

Independently of each other, Lotka (1925) and Volterra (1926) proposed the following model to describe the dynamics of a predator population x_2 that feeds upon a prey population x_1

($\boldsymbol{x} = (x_1, x_2)^T \in \mathbb{R}^2_+$):

$$\frac{d\boldsymbol{x}}{dt} = \boldsymbol{f}(\boldsymbol{x}) \Leftrightarrow \left\{ \begin{array}{rcccl} \dfrac{dx_1}{dt} & = & rx_1 - ax_1x_2 & = & (r - ax_2)x_1 \\ \dfrac{dx_2}{dt} & = & bx_1x_2 - mx_2 & = & (bx_1 - m)x_2. \end{array} \right. \tag{2.8}$$

This model assumes that the prey grows exponentially in absence of predator (with growth rate r), and that the predator has a linear mortality rate m. The attack rate a defines a linear (type-I) functional response (amount of prey eaten per predator and unit of time) to model predation. Predation gives the growth rate of the predator population bx_1, where the ratio b/a is an efficiency (it may also include a unit conversion factor between x_1 and x_2 if necessary).

Model (2.8) has two equilibria corresponding respectively to extinction $\boldsymbol{x^{(0)}} = (0, 0)^T$ and coexistence $\boldsymbol{x^{(1)}} = (m/b, r/a)^T$ of populations. Their local stability can be studied by computing the Jacobian matrix:

$$\boldsymbol{f}_{\boldsymbol{x}}(\boldsymbol{x}) = \begin{pmatrix} r - ax_2 & -ax_1 \\ bx_2 & bx_1 - m \end{pmatrix}.$$

This matrix evaluated at the extinction equilibrium $\boldsymbol{x^{(0)}}$ is diagonal:

$$\boldsymbol{f}_{\boldsymbol{x}}(\boldsymbol{x^{(0)}}) = \begin{pmatrix} r & 0 \\ 0 & -m \end{pmatrix}.$$

Thus, its eigenvalues are $\lambda_1 = r > 0$ and $\lambda_2 = -m < 0$, which means that extinction equilibrium is unstable and is a saddle. Jacobian matrix evaluated at coexistence equilibrium:

$$\boldsymbol{f}_{\boldsymbol{x}}(\boldsymbol{x^{(1)}}) = \begin{pmatrix} 0 & -am/b \\ br/a & 0 \end{pmatrix},$$

has two conjugate pure imaginary eigenvalues $\lambda_{1,2} = \pm i\sqrt{rm}$. These eigenvalues have zero real part, which means that equilibrium $\boldsymbol{x^{(1)}}$ is non-hyperbolic. This non-hyperbolic equilibrium is locally neither attractive (asymptotically stable) or repulsive (unstable) and we cannot conclude on model dynamics. To better understand dynamics of model (2.8), consider the following Lyapunov function $H : \mathbb{R}^2_{+*} \to \mathbb{R}^+$:

$$H(\boldsymbol{x}) = bx_1 - m\ln(x_1) + ax_2 - r\ln(x_2), \tag{2.9}$$

which is definite positive $\mathcal{C}^1$ function (continuous and differentiable function with continuous first

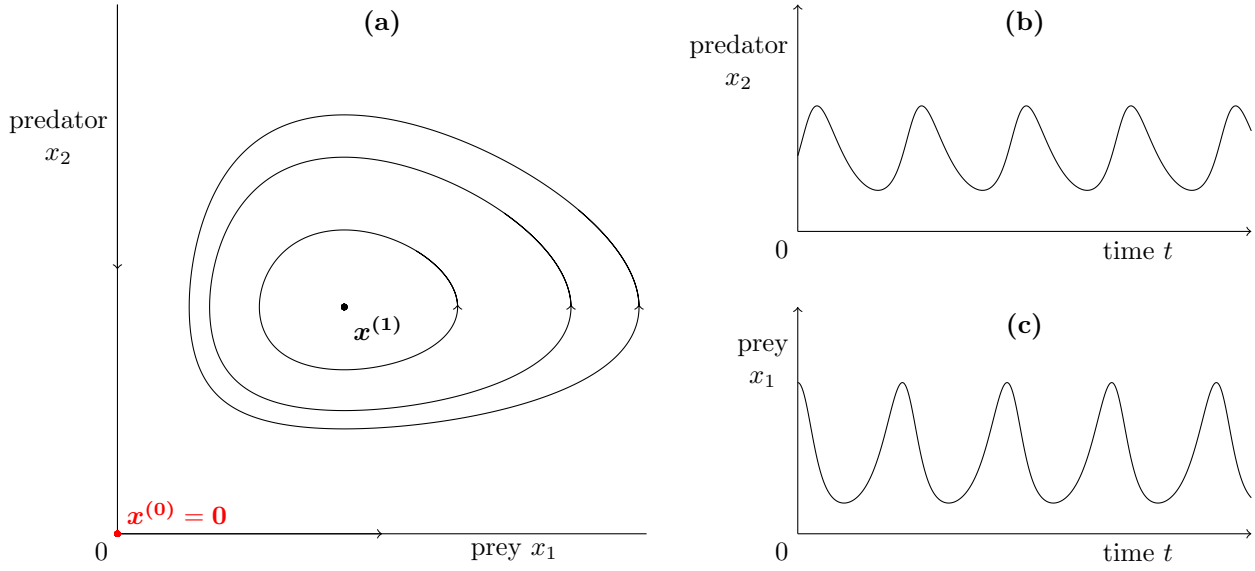

Figure 2.4. Qualitative dynamics of Lotka-Volterra predator-prey model. a: Phase portrait with three examples of trajectories, which are all closed curves defined by their initial condition. The extinction equilibrium $\boldsymbol{x^{(0)}}$ is unstable (red) and the coexistence equilibrium $\boldsymbol{x^{(1)}}$ is non-hyperbolic (black). b,c: Example of predator-prey dynamics through time.

order partial derivatives) with a global minimum at $\boldsymbol{x^{(1)}}$. Its time derivative is always zero:

$$\frac{dH(\boldsymbol{x})}{dt} = \frac{\partial H}{\partial x_1}\frac{dx_1}{dt} + \frac{\partial H}{\partial x_2}\frac{dx_2}{dt} = 0,\ \forall \boldsymbol{x} \in \mathbb{R}^2_{+*}.$$

Thus all trajectories of model (2.8) in $\mathbb{R}^2_{+*}$ are closed orbits defined by their initial condition, as presented in figure 2.4. Population oscillations are said to be neutral as each orbit is neither attractive or repulsive.

2.2.4 Model of insect outbreaks: bifurcations, multiple stable states and hysteresis

In order to understand the origin of insect outbreaks, Ludwig *et al.* (1978) proposed the following model of an insect population $N \in \mathbb{R}^+$:

$$\frac{dN}{dt} = RN\left(1 - \frac{N}{K}\right) - \frac{BN^2}{A^2 + N^2}P. \tag{2.10}$$

It assumes that the insect population follows a logistic growth (with maximum growth rate R and carrying capacity K) in absence of predator. The predator population P is assumed to be constant with respect to the time scale of the insect population dynamics. The predation flux is given by a type-III functional response, where A is a half-saturation constant of the predator and B its maximum feeding rate. Thus, five parameters define model (2.10), which can be simplified by the following changes of coordinates and parameters:

$$\tau = \frac{BP}{A}t,\ x = \frac{N}{A},\ r = \frac{AR}{BP},\ k = \frac{K}{A}, \tag{2.11}$$

leading to the new model with only two parameters:

$$\frac{dx}{d\tau} = x\left[r\left(1-\frac{x}{k}\right) - \frac{x}{1+x^2}\right] := f(x) = x(g_1(x) - g_2(x)), \tag{2.12}$$

where $g_1(x) := r(1-x/k)$ and $g_2(x) = x/(1+x^2)$.

Model (2.12) has one unstable trivial equilibrium $x^{(0)} = 0$ ($f'(0) = r > 0$) corresponding to population extinction. Positive equilibria satisfy $g_1(x) = g_2(x)$, where function $g_1(x)$ depends on parameters r and k. Depending on parameter values, there are one to three positive equilibria (figure 2.5). The stability of a positive equilibria $x^{(i)}$ is given the sign of:

$$\text{sign}\left(f'(x^{(i)})\right) = \text{sign}\left(g_1'(x^{(i)}) - g_2'(x^{(i)})\right),$$

which can be determined by a graphical analysis (figure 2.5). If one positive equilibrium denoted by $x^{(1)}$ exists, it is always stable. When there are three positive equilibria, two of them are stable ($x^{(1)}$ and $x^{(3)}$). Which one is reached depends on the location of the initial condition with respect to the unstable equilibrium $x^{(2)}$. This unstable equilibrium collides with one of the stable equilibria at the limit cases where there are two equilibria, one of them being a double equilibrium ($x^{(1,2)}$ or $x^{(2,3)}$), which is non-hyperbolic. The qualitative change from one to three positive equilibria that occurs when parameters r and K are changed corresponds to a fold bifurcation (presented in subsection 2.3.3).

The bifurcation occurs if there is an equilibrium x^* such that $f(x^*) = 0$ (equilibrium condition) and $f'(x^*) = 0$ (bifurcation condition). These conditions can be written as conditions on parameter values:

$$r = \frac{2x^{*3}}{(1+x^{*2})^2},\ k = \frac{2x^{*3}}{x^{*2}-1},$$

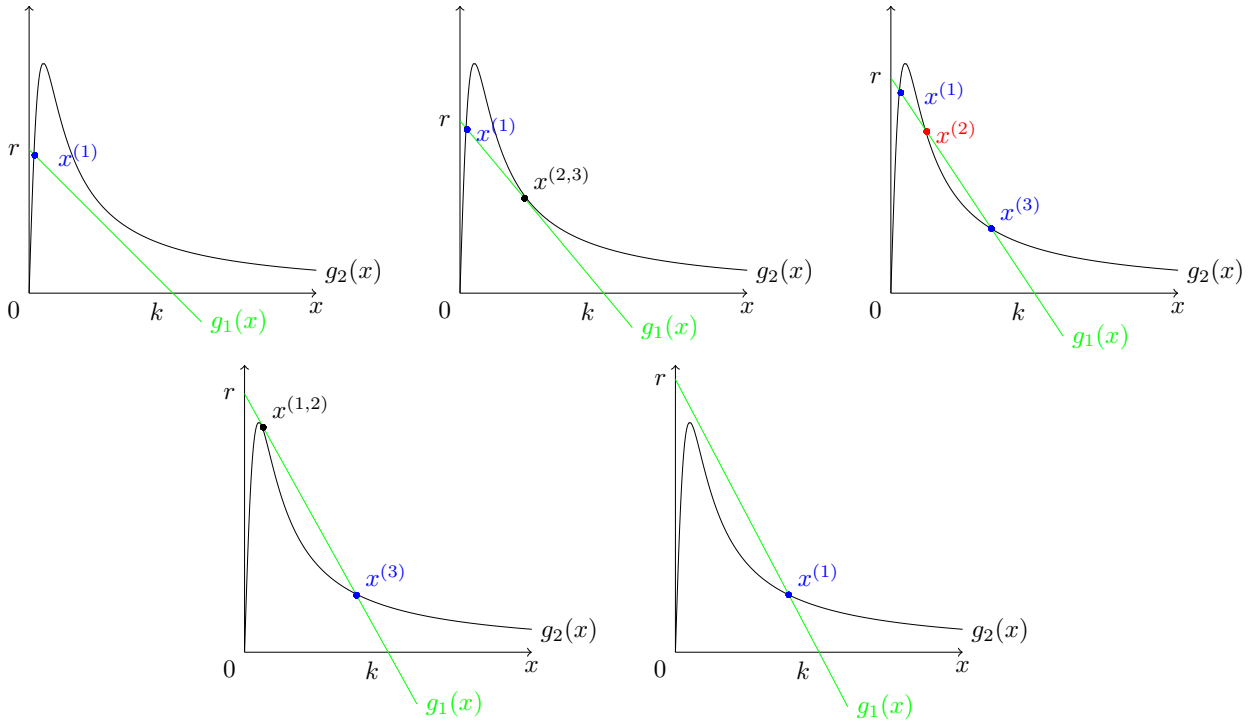

Figure 2.5. Graphical analysis of the model of insect outbreak: positive equilibria existence and stability. Existence and stability of positive equilibria depend on parameters r and k which affect function g_1 (green). Functions g_1 and g_2 intersect at positive equilibria. Their stability is given by the functions slope at equilibrium (blue: stable, red: unstable, black: non-hyperbolic equilibrium).

which are used to draw the bifurcation diagram in figure 2.6 that summarizes model dynamics.

An interesting feature of model (2.10) is the possibility for hysteresis phenomena. As an example, suppose that the insect population is at equilibrium $x^{(1)}$ and that there are three positive equilibria according to parameter values. Increasing parameter r (e.g. by hunting the predator population and decreasing P in (2.11)) above the bifurcation threshold and then decreasing it to its original value (e.g. by predator re-introduction) will put the insect population at the positive equilibrium $x^{(3)}$. Thus, population is at a different equilibrium than before disturbance, even if all environmental conditions (parameter values) are the same as initially. This hysteresis phenomenon may explain some of the observed insect outbreaks.

2.2.5 Rosenzweig & MacArthur's predator-prey model: invasibility, stable oscillations and enrichment paradox

Rosenzweig & MacArthur (1963) studied a family of models like model (2.13) to describe the

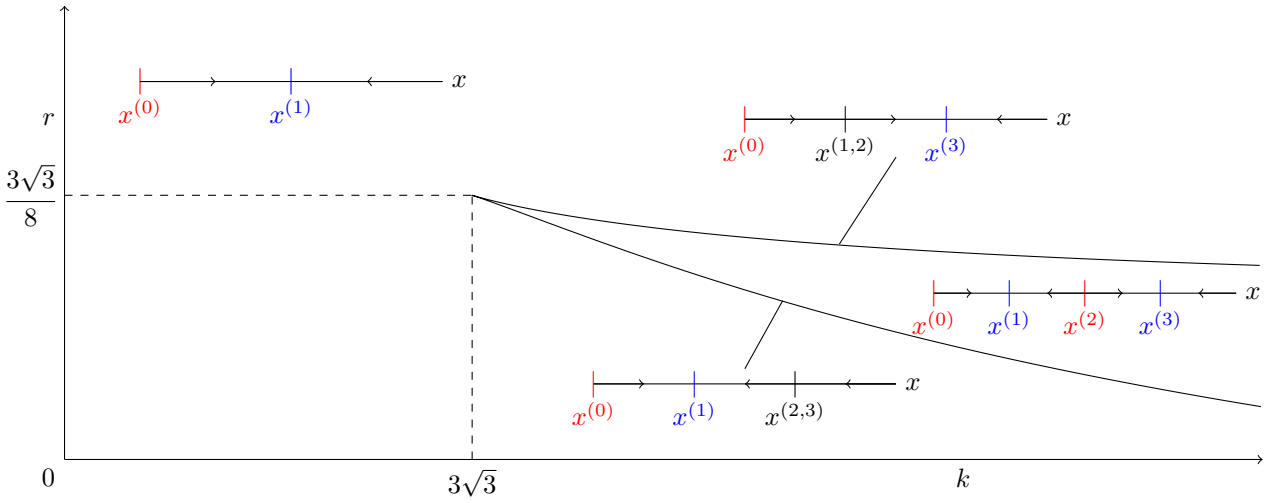

Figure 2.6. Bifurcation diagram and phase portraits of the model of insect outbreak. The curve is the fold bifurcation where there is a double equilibrium ($x^{(1,2)}$ or $x^{(2,3)}$). There are three positive equilibria within the region defined by this curve and one positive equilibrium outside (always denotes $x^{(1)}$ for simplicity). Their stability is indicated by their color (blue: stable, red: unstable, black: non-hyperbolic equilibrium).

dynamics of a predator population x_2 that feeds on a prey population x_1 ($\boldsymbol{x} = (x_1, x_2)^T \in \mathbb{R}^2_+$):

$$\frac{d\boldsymbol{x}}{dt} = \boldsymbol{f}(\boldsymbol{x}) \Leftrightarrow \begin{cases} \dfrac{dx_1}{dt} &= rx_1\left(1 - \dfrac{x_1}{K}\right) - G(x_1)x_2 \\ \dfrac{dx_2}{dt} &= eG(x_1)x_2 - mx_2. \end{cases} \tag{2.13}$$

This model assumes that the prey grows logistically in absence of predator (with maximum growth rate r and carrying capacity K) and that the predator has a linear mortality rate m. The predation flux is proportional to the prey-dependent functional response $G(x_1)$. For the sake of generality, this function is not specified and we only assume that (i) no prey is eaten in absence of prey ($G(0) = 0$), and that (ii) an increase of prey population implies an increase of prey consumption per unit of predator ($G'(x_1) > 0\ \forall x_1 \in \mathbb{R}^+$). Predator growth is the predation flux times parameter e, which is an efficiency (times a unit conversion factor if required).

Model (2.13) has up to three equilibria (with $G^{-1} \circ G = \mathrm{id}$, we assume that G^{-1} exists):

$$\boldsymbol{x^{(0)}} = (0,0)^T,\ \boldsymbol{x^{(1)}} = (K,0)^T,\ \boldsymbol{x^{(2)}} = \left(x_1^{(2)} := G^{-1}\left(\frac{m}{e}\right), x_2^{(2)} := \frac{rex_1^{(2)}}{m}\left(1 - \frac{x_1^{(2)}}{K}\right)\right)^T.$$

The coexistence equilibrium $\boldsymbol{x^{(2)}}$ exists if $\sup_{x_1 \in \mathbb{R}^+} G(x_1) > m/e$ and $x_1^{(2)}, x_2^{(2)} \in \mathbb{R}^+$. Prey popula-

tion $x_1^{(2)}$ is positive as $G(x_1)$ is a strictly increasing function. Predator population $x_2^{(2)}$ is positive only if $x_1^{(2)} < K$. Thus, having $K > G^{-1}(m/e)$ is a necessary condition for equilibrium $\boldsymbol{x^{(2)}}$ existence.

The local stability of equilibria can be studied using the Jacobian matrix:

$$\boldsymbol{f}_{\boldsymbol{x}}(\boldsymbol{x}) = \begin{pmatrix} r\left(1 - \dfrac{2x}{K}\right) - G'(x_1)x_2 & -G(x_1) \\ eG'(x_1)x_2 & eG(x_1) - m \end{pmatrix}. \tag{2.14}$$

By evaluating this matrix at equilibria $\boldsymbol{x^{(0)}}$ and $\boldsymbol{x^{(1)}}$, one can check that the trivial equilibrium $\boldsymbol{x^{(0)}}$ is always a saddle, whereas the prey equilibrium $\boldsymbol{x^{(1)}}$ is a stable node when $K < G^{-1}(m/e)$ (i.e. when $\boldsymbol{x^{(2)}}$ does not exist) and is a saddle otherwise. The transition $K = G^{-1}(m/e)$ between these two situations involves a non-hyperbolic double equilibrium ($\boldsymbol{x^{(1,2)}} := \boldsymbol{x^{(1)}} = \boldsymbol{x^{(2)}}$) and corresponds to a transcritical bifurcation (presented in subsection 2.3.4). This bifurcation implies that $\boldsymbol{x^{(2)}}$ is a stable node for $K \gtrapprox G^{-1}(m/e)$. So, this bifurcation is a threshold on carrying capacity K above which the predator population can survive and invade the system.

Jacobian matrix (2.14) evaluated at coexistence equilibrium $\boldsymbol{x^{(2)}}$:

$$\boldsymbol{f}_{\boldsymbol{x}}(\boldsymbol{x^{(2)}}) = \begin{pmatrix} r\left(1 - \dfrac{2x_1^{(2)}}{K}\right) - G'(x_1^{(2)})x_2^{(2)} & -\dfrac{m}{e} \\ eG'(x_1^{(2)})x_2^{(2)} & 0 \end{pmatrix},$$

has eigenvalues with real parts of the same sign ($\lambda_1\lambda_2 = \det(\boldsymbol{f}_{\boldsymbol{x}}(\boldsymbol{x^{(2)}})) = mG'(x_1^{(2)})x_2^{(2)} > 0$). These real parts are negative if $\lambda_1 + \lambda_2 = \mathrm{Tr}(\boldsymbol{f}_{\boldsymbol{x}}(\boldsymbol{x^{(2)}})) < 0$, which gives the following condition for the stability of the coexistence equilibrium when it exists:

$$G'(x_1^{(2)}) > \frac{r}{x_2^{(2)}}\left(1 - \frac{2x_1^{(2)}}{K}\right). \tag{2.15}$$

At, the limit case $\mathrm{Tr}(\boldsymbol{f}_{\boldsymbol{x}}(\boldsymbol{x^{(2)}})) = 0$, $\boldsymbol{f}_{\boldsymbol{x}}(\boldsymbol{x^{(2)}})$ has a pair of conjugate pure imaginary eigenvalues (as $\det(\boldsymbol{f}_{\boldsymbol{x}}(\boldsymbol{x^{(2)}})) > 0$). This means that the system exhibits a Hopf bifurcation (presented in subsection 2.3.5) which gives birth to a limit cycle under genericity conditions.

Whether condition (2.15) is satisfied or not depends on the exact formulation of the functional response. For a type-I functional response ($G(x_1) = ax_1$ with an attack rate a), one can check that equilibrium $\boldsymbol{x^{(2)}}$ is globally stable when it exists (using Dulac's criterion). Rosen-

zweig & MacArthur (1963) analyzed graphically model (2.13) for any type-II functional response ($\lim_{x_1\to\infty} G(x_1) < +\infty$, $G''(x_1) < 0\ \forall x_1 \in \mathbb{R}^+$). As an example of type-II functional response, we consider the classical Holling's disc equation (Holling, 1959b):

$$G(x_1) = \frac{ax_1}{b + x_1}, \tag{2.16}$$

where a is the attack rate and b the half-saturation constant of the predator. With functional response (2.16), the coexistence equilibrium writes:

$$\boldsymbol{x^{(2)}} = \left(x_1^{(2)} := \frac{mb}{ea - m}, x_2^{(2)} := \frac{rex_1^{(2)}}{m}\left(1 - \frac{x_1^{(2)}}{K}\right)\right)^T.$$

This equilibrium is stable if the condition:

$$K > K^{(H)} := \frac{2mb}{ea - m} + b,$$

is fulfilled (one can prove that it is globally stable, see Hsu, 1977). The threshold $K = K^{(H)}$ corresponds to a supercritical Hopf bifurcation (the proof that it is supercritical can be found in Kuznetsov, 2004, example 3.1), which gives birth to a stable limit cycle for $K > K^{(H)}$. If we summarize model dynamics, for low carrying capacity K the prey follows a logistic growth (figure 2.3) and the predator cannot invade. Predator can invade on a stable coexistence equilibrium for intermediate K (figure 2.7a,b). For higher K, i.e. in an environment where prey resources are abundant, the coexistence equilibrium is destabilized and there are stable predator-prey oscillations (figure 2.7c). This phenomenon is known as the enrichment paradox (Rosenzweig, 1971).

2.2.6 General expression for ecological models

Most ecological models can be written in the form:

$$\frac{d\boldsymbol{x}}{dt} = \boldsymbol{f}(\boldsymbol{x}) \Leftrightarrow \frac{dx_i}{dt} = g_i(\boldsymbol{x})x_i,\ i = 1, ..., n, \tag{2.17}$$

where the function $g_i(\boldsymbol{x}) := f_i(\boldsymbol{x})/x_i$ has a finite value at $x_i = 0$. One can check that all models presented in this section can be written in this way. They are sometimes called Kolmogorov's models for communities (Brauer & Castillo-Chávez, 2001, section 5.4 for instance). The factorisation

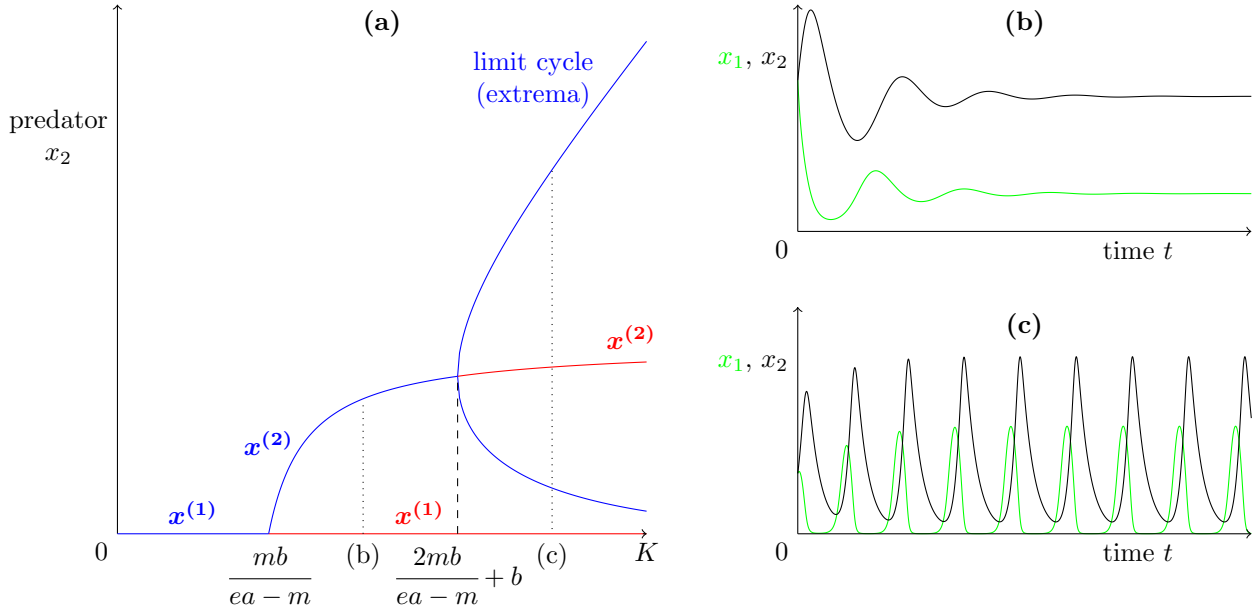

Figure 2.7. Bifurcation diagram and qualitative dynamics of Rosenzweig & MacArthur's model with Holling disc equation. a. Bifurcation diagram showing stable (blue) and unstable (red) equilibria as a function of prey carrying capacity K (the trivial equilibrim is not shown). Depending on carrying capacity, qualitatively different dynamics with a stable equilibrium (b) or a stable limit cycle (c) are obtained when the predator survives.

by x_i implies that the sets:

$$S_i = \{\boldsymbol{x} \in \mathbb{R}^n | x_i = 0, x_j > 0 \; \forall j \in [1,n] \backslash i\} \; , \; i = 1, .., n,$$

and $\mathbb{R}_+^{*\,n}$ are invariant sets.

From an ecological point of view, the factorisation by x_i means that the function $g_i(\boldsymbol{x})$ is the rate of change of x_i across time. This rate of change is (in general) something like a gross rate (which depends on resource and/or predation) minus a mortality rate, minus predation by other species, etc. The fact that a set S_i is an invariant set means that an extincted population $x_i = 0$ will remain extincted. In addition, it implies that a population size cannot move from a positive value (which has a biological interpretation) to a negative value (which has no biological meaning). Models that cannot be written like in (2.17) are models with a migration of individuals from another place for instance.

2.3 Bifurcation theory

Examples in previous section show that system dynamics qualitatively change at thresholds on parameter values called bifurcations. The next subsection links bifurcation theory and the study of biological systems. Then, subsection 2.3.2 introduces some concepts of bifurcations of equilibria. Some bifurcations and their analysis are presented in the last subsections. These subsections can be understood by the reader mostly interested by biological applications of bifurcation theory by having a look to figures. Figures explain the qualitative changes in system dynamics that occur when some parameters cross different types of bifurcation.

2.3.1 Bifurcations and chaos in living systems

Even if living systems are far more complex than a model, a four-dimensional model was enough to understand the qualitative dynamics of an experimental predator-prey system (Fussmann *et al.*, 2000). In this system, a prey (*Chlorella vulgaris*, a unicellular *Chlorophyceae*) grows on nitrogen and is eaten by a metazoan predator with an age-structured life cycle (*Brachionus calyciflorus*, a planktonic rotifer). These species are cultivated in a chemostat, with varying environmental parameters (dilution rate and resource concentration in the feed). These parameters have threshold values defining if a species can survive (transcritical bifurcations) and if they coexist at equilibrium or exhibit oscillations (supercritical Hopf bifurcation). These different dynamics are observed experimentally for parameter values that are consistent with the bifurcation analysis of the model. This model was parameterized using additional experiments. An important difference between experiments and model is that population concentrations can be infinitely small in a model. Conversely, infinitely small population concentrations in the real system means extinction, a point that can be taken into account in a model through an extinction threshold in results interpretation.

Similarly, mathematical tools developped in chaos theory are now used to analyze living systems (Bjørnstad, 2015). For example, microbial and planktonic communities were monitored during long-term experiments (Becks *et al.*, 2005, Benincà *et al.*, 2008). The obtained time series of species abundance exhibit a sensitivity to initial conditions (detected using Lyapunov exponents) highlighting the chaotic dynamics of these experimental communities. Recently, a rocky intertidal community located in a marine reserve was showed to sustain irregular species fluctuations, explained by an alternance between stabilizing periods and periods of chaos (Benincà *et al.*, 2015). This conclusion comes from the analysis of a 20-year time serie and a simple four-dimensional model. Even if this model cannot make precise quantitative predictions, it is sufficient to understand the pattern of observed dynamics.

2.3.2 General concepts on bifurcations of equilibria

Consider any differential system of the form:

$$\frac{d\boldsymbol{x}}{dt} = \boldsymbol{f}(\boldsymbol{x}, \boldsymbol{\alpha}), \tag{2.18}$$

with the same notation as in (2.1). This first paragraph introduces concepts of eigenspaces and invariant manifolds that help to understand the next paragraphs about local bifurcations. For fixed $\boldsymbol{\alpha}$ and any equilibrium $\boldsymbol{x}^*_{\boldsymbol{\alpha}}$, there is a stable (respectively center or unstable) eigenspace E^s (E^c or E^u) spanned by eigenvectors of Jacobian matrix (2.2) associated to eigenvalues with negative (zero or positive) real part. In the linearized system (2.3), trajectories from any initial conditions in the stable (unstable) eigenspace converge on $\boldsymbol{x}^*$ when t goes to infinity (minus infinity). Similarly to this property of eigenspaces, stable and unstable manifolds of the equilibrium $\boldsymbol{x}^*_{\boldsymbol{\alpha}}$ can be defined in the non-linear system (2.18):

$$W^s = \left\{ \boldsymbol{x} \in \mathbb{R}^n | \lim_{t \to +\infty} \varphi^t_{\boldsymbol{\alpha}} \boldsymbol{x} = \boldsymbol{x}^*_{\boldsymbol{\alpha}} \right\},$$

$$W^u = \left\{ \boldsymbol{x} \in \mathbb{R}^n | \lim_{t \to -\infty} \varphi^t_{\boldsymbol{\alpha}} \boldsymbol{x} = \boldsymbol{x}^*_{\boldsymbol{\alpha}} \right\}.$$

Eigenspaces and manifolds are invariant sets of the linear and non-linear systems respectively. Each eigenspace is tangent (linear approximation) to its corresponding manifold at $\boldsymbol{x}^*_{\boldsymbol{\alpha}}$. So, there is at least one local center manifold W^c_{loc} tangent to the center eigenspace E^c.

When a bifurcation occurs for specific parameter values $\boldsymbol{\alpha}^*$, system (2.18) has a non-hyperbolic equilibrium $\boldsymbol{x}^*$, i.e. the Jacobian matrix $\boldsymbol{f}_{\boldsymbol{x}}(\boldsymbol{x}^*, \boldsymbol{\alpha}^*)$ has at least one eigenvalue with zero real part. Thus, non-linear terms cannot be neglected in the Taylor expansion (2.1) of the system near equilibrium. Note that if not all eigenvalues have zero real part ($n_c < n$), a smaller differential system:

$$\frac{d\boldsymbol{x}^{\boldsymbol{c}}}{dt} = \boldsymbol{f}^{\boldsymbol{c}}(\boldsymbol{x}^{\boldsymbol{c}}, \boldsymbol{\alpha}), \tag{2.19}$$

can be built to approximate the dynamics of system (2.18) near $\boldsymbol{x}^*$ on a center manifold W^c_{loc}, with $\boldsymbol{x}^{\boldsymbol{c}} \in \mathbb{R}^{n_c}$ (Center Manifold Theory, chapter 5 in Kuznetsov, 2004). Indeed, qualitative dynamics in the $n_s + n_u$ other dimensions are given by the eigenvalues with non-zero real part.

The previous paragraph described how to obtain a local approximation of the system near equilibrium and near bifurcation. If this local approximation fulfills the genericity conditions of a bifurcation (see next paragraph), then system (2.18) is locally topologically equivalent to the

normal form of this bifurcation. A normal form of a bifurcation is a (not unique) simple system that exhibits all the qualitative characteristics (number of equilibria, their stability, etc.) of this bifurcation with a minimum number of state variables and parameters. This minimal number of parameters required to observe a bifurcation is called the codimension of the bifurcation.

From a practical point of view, a bifurcation in the n-dimensional non-linear system (2.18) is first characterized by the eigenvalues and sometimes higher order terms with zero real part (number and imaginary part), which give the type of bifurcation. This bifurcation occurs if the system satisfies the genericity conditions: (i) non-degeneracy conditions (higher order terms in the Taylor expansion are non-zero) and (ii) transversality conditions (the bifurcation is crossed). If one of these conditions is violated, the bifurcation is said to be degenerated. The degenerated bifurcation itself has its own genericity conditions. These concepts are illustrated in the next subsections, which present three codimension-one bifurcations. Two of them are generic (fold and Hopf) and one is degenerated (transcritical) in models like (2.18), but it is generic in most population models. Last subsection briefly introduces more complicated bifurcations that occur in some models studied in this thesis.

2.3.3 Fold bifurcation (from Guckenheimer & Holmes, 1983)

This bifurcation is also known as "tangent", "limit point" and "saddle-node" bifurcation. Consider that the following n-dimensional and one-parameter system:

$$\frac{d\boldsymbol{x}}{dt} = \boldsymbol{f}(\boldsymbol{x}, \alpha),\ \boldsymbol{x} \in \mathbb{R}^n,\ \alpha \in \mathbb{R}, \tag{2.20}$$

with smooth f, has for $\alpha = \alpha^*$ an equilibrium $\boldsymbol{x}^*_{\boldsymbol{\alpha}^*}$. Suppose that the Jacobian matrix $\boldsymbol{f}_{\boldsymbol{x}}(\boldsymbol{x}^*, \alpha^*)$ has $n-1$ eigenvalues with non-zero real part and a single zero eigenvalue with a right eigenvector $\boldsymbol{q}$ (which satisfies $\boldsymbol{f}_{\boldsymbol{x}}(\boldsymbol{x}^*_{\boldsymbol{\alpha}^*}, \alpha^*)\boldsymbol{q} = \boldsymbol{0}$) and a left eigenvector $\boldsymbol{p}$ (which satisfies $\boldsymbol{p}^T\boldsymbol{f}_{\boldsymbol{x}}(\boldsymbol{x}^*_{\boldsymbol{\alpha}^*}, \alpha^*) = \boldsymbol{0}^T$). If the following conditions are satisfied:

(non-degeneracy) $\boldsymbol{p}^T\boldsymbol{f}_{\boldsymbol{xx}}(\boldsymbol{x}^*_{\boldsymbol{\alpha}^*}, \alpha^*)(\boldsymbol{q}, \boldsymbol{q}) \neq 0$[2],

(transversality) $\boldsymbol{p}^T\boldsymbol{f}_{\alpha}(\boldsymbol{x}^*_{\boldsymbol{\alpha}^*}, \alpha^*) \neq 0$,

[2] The tensor $\boldsymbol{f}_{\boldsymbol{xx}}(\boldsymbol{x}^*_{\boldsymbol{\alpha}^*}, \alpha^*)$ applied to any vectors $\boldsymbol{u}, \boldsymbol{v} \in \mathbb{R}^n$ is the following vector of bilinear applications:

$$\boldsymbol{f}_{\boldsymbol{xx}}(\boldsymbol{x}^*_{\boldsymbol{\alpha}^*}, \alpha^*)(\boldsymbol{u}, \boldsymbol{v}) = \begin{pmatrix} \vdots \\ \sum_{j=1}^{n}\sum_{k=1}^{n} \dfrac{\partial^2 f_i(\boldsymbol{x}^*_{\boldsymbol{\alpha}^*}, \alpha^*)}{\partial x_j \partial x_k} u_j v_k \\ \vdots \end{pmatrix}.$$

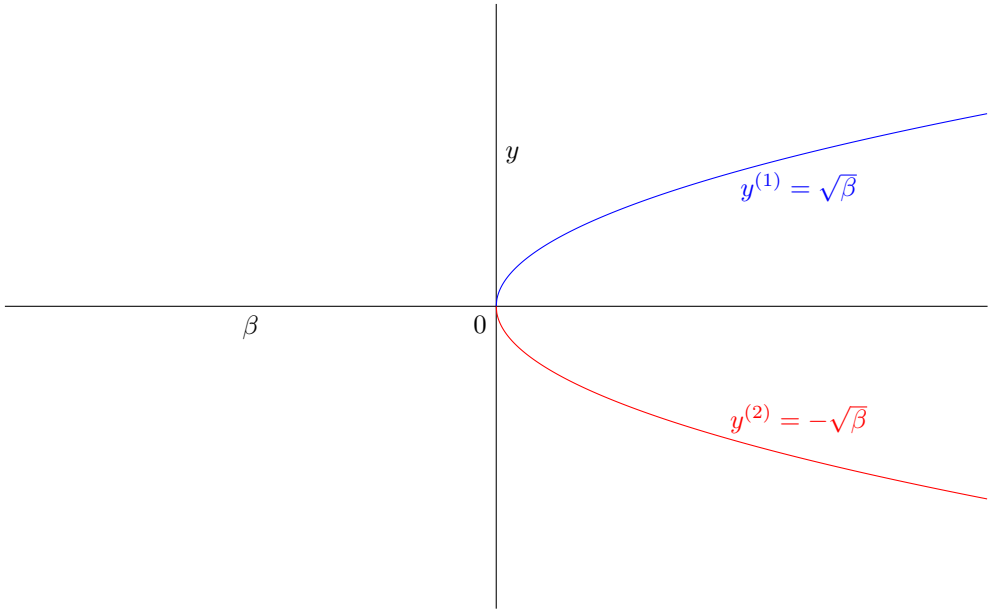

Figure 2.8. Bifurcation diagram of the normal form of the fold bifurcation. The blue (red) equilibrium is stable (unstable).

the reduction of system (2.20) on a center manifold is locally topologically equivalent near $\boldsymbol{x}^*_{\boldsymbol{\alpha}^*}$ to one of the following normal forms:

$$\frac{dy}{dt} = \beta \pm y^2, \ y \in \mathbb{R}, \ \beta \in \mathbb{R}.$$

The normal form:

$$\frac{dy}{dt} = \beta - y^2 \equiv g(y, \beta), \tag{2.21}$$

is a system with no equilibrium if $\beta < 0$ and two equilibria $y^{(1)} = -y^{(2)} = \sqrt{\beta}$ if $\beta > 0$. One equilibrium is stable ($\lambda = g_y(y^{(1)}, \beta) = -2\sqrt{\beta}$) and the other one is unstable ($\lambda = g_y(y^{(2)}, \beta) = 2\sqrt{\beta}$). When $\beta = 0$, these two equilibria collide an disappear in a double equilibrium $y^{(1,2)} = 0$ which is non-hyperbolic as $\lambda = 0$ (figure 2.8).

One can check that the non-hyperbolic equilibrium $y^{(1,2)} = 0$ of the normal form (2.21) satisfies the genericity conditions of the fold bifurcation. Indeed, we have:

$$g_{yy}(y^{(1,2)}, 0) = -2, \ q = p = 1, \ g_\beta(y^{(1,2)}, 0) = 1.$$

Thus, both non-degeneracy and transversality conditions are satisfied:

$$p^T g_{yy}(y^{(1,2)}, 0)(q, q) = -2 \neq 0,\ p^T g_\beta(y^{(1,2)}, 0) = 1 \neq 0.$$

2.3.4 Transcritical bifurcation (from Guckenheimer & Holmes, 1983)

Consider that the following n-dimensional and one-parameter system:

$$\frac{d\boldsymbol{x}}{dt} = \boldsymbol{f}(\boldsymbol{x}, \alpha),\ \boldsymbol{x} \in \mathbb{R}^n,\ \alpha \in \mathbb{R}, \tag{2.22}$$

with smooth f, has an equilibrium $\boldsymbol{x}^*_{\boldsymbol{\alpha}}\ \forall \alpha$ (thus, the transversality condition of the fold bifurcation is violated). Suppose that at $\alpha = \alpha^*$, the Jacobian matrix $\boldsymbol{f}_{\boldsymbol{x}}(\boldsymbol{x}^*_{\boldsymbol{\alpha}^*}, \alpha^*)$ has $n-1$ eigenvalues with non-zero real part and a single zero eigenvalue with a right eigenvector $\boldsymbol{q}$ and a left eigenvector $\boldsymbol{p}$. If the following conditions are satisfied:

(non-degeneracy) $\boldsymbol{p}^T \boldsymbol{f}_{\boldsymbol{xx}}(\boldsymbol{x}^*_{\boldsymbol{\alpha}^*}, \alpha^*)(\boldsymbol{q}, \boldsymbol{q}) \neq 0$,

(transversality) $\boldsymbol{p}^T \boldsymbol{f}_{\boldsymbol{x}\alpha}(\boldsymbol{x}^*_{\boldsymbol{\alpha}^*}, \alpha^*)\boldsymbol{q} \neq 0$,

the reduction of system (2.22) on a center manifold is locally topologically equivalent near $\boldsymbol{x}^*_{\boldsymbol{\alpha}^*}$ to one of the following normal forms:

$$\frac{dy}{dt} = y(\beta \pm y),\ y \in \mathbb{R},\ \beta \in \mathbb{R}.$$

The normal form:

$$\frac{dy}{dt} = y(\beta - y) \equiv g(y, \beta),$$

is a system with two equilibria $y^{(0)} = 0$ and $y^{(1)} = \beta$. Equilibrium $y^{(0)}$ is stable if $\beta < 0$ ($\lambda = g_y(0, \beta) = \beta$) whereas equilibrium $y^{(1)} = \beta$ is stable if $\beta > 0$ ($\lambda = g_y(\beta, \beta) = -\beta$). At $\beta = 0$, these two equilibria collide in one non-hyperbolic equilibrium $y^{(0,1)} = 0$ with $\lambda = 0$ and are said to exchange their stability (figure 2.9).

Transcritical bifurcation is a non-generic bifurcation, as it implies that the transversality condition of the fold bifurcation is violated. However, this condition is violated by equilibria associated to species extinction in ecological models that can be written in the form (2.17). In these models, the transcritical bifurcation delimits the cases where a population can invade or not (see section 2.2.5 for example). Thus, even if the transcritical bifurcation is non-generic in systems like 2.18 (it is not presented in Kuznetsov, 2004), it is a generic bifurcation in Kolmogorov systems.

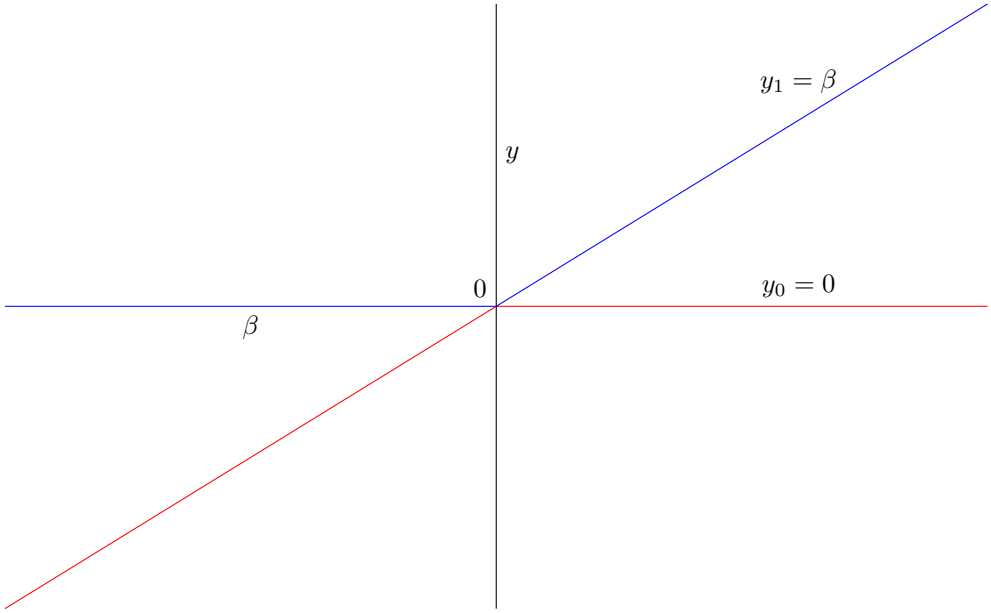

Figure 2.9. Bifurcation diagram of the normal form of the transcritical bifurcation. The blue (red) equilibrium is stable (unstable).

2.3.5 Hopf bifurcation (from Guckenheimer & Holmes, 1983, Kuznetsov, 2004)

Consider that the following n-dimensional ($n \geq 2$) and one-parameter system:

$$\frac{d\boldsymbol{x}}{dt} = \boldsymbol{f}(\boldsymbol{x}, \alpha), \ \boldsymbol{x} \in \mathbb{R}^n, \ \alpha \in \mathbb{R}, \tag{2.23}$$

with smooth $\boldsymbol{f}$, has for α sufficiently close to α^* an equilibrium $\boldsymbol{x}^*_{\boldsymbol{\alpha}}$ and that the Jacobian matrix $\boldsymbol{f}_{\boldsymbol{x}}(\boldsymbol{x}^*_{\boldsymbol{\alpha}}, \alpha)$ has a pair of complex conjugate eigenvalues $\lambda_{1,2}(\alpha) = \mu(\alpha) \pm i\omega(\alpha)$, where $\mu(\alpha^*) = 0$ and $\omega(\alpha^*) > 0$, and $n - 2$ eigenvalues with non-zero real part. If the following conditions are satisfied:

(non-degeneracy) $l_1(\alpha^*) \neq 0$, where the first Lyapunov coefficient $l_1(\alpha)$ is computed using second- and third-order terms in system (2.23) (see eq. 3.20 and 5.39 in Kuznetsov, 2004, for two-dimensional and n-dimensional systems respectively) and indicates if these terms make the vicinity of equilibrium attractive ($l_1(\alpha^*) < 0$, supercritical case) or repulsive ($l_1(\alpha^*) > 0$, subcritical case) near bifurcation,

(transversality) $\mu_\alpha(\alpha^*) \neq 0$,

the reduction of system (2.23) on a center manifold is locally topologically equivalent near $\boldsymbol{x}^*_{\boldsymbol{\alpha}^*}$ to one of the following normal forms:

$$\frac{d\boldsymbol{y}}{dt} = \begin{pmatrix} \beta & -1 \\ 1 & \beta \end{pmatrix} \boldsymbol{y} \pm \left(y_1^2 + y_2^2\right) \boldsymbol{y},\ \boldsymbol{y} = \begin{pmatrix} y_1 \\ y_2 \end{pmatrix} \in \mathbb{R}^2,\ \beta \in \mathbb{R}.$$

The normal form:

$$\frac{d\boldsymbol{y}}{dt} = \begin{pmatrix} \beta & -1 \\ 1 & \beta \end{pmatrix} \boldsymbol{y} - \left(y_1^2 + y_2^2\right) \boldsymbol{y} \equiv \boldsymbol{F}(\boldsymbol{y}, \beta), \tag{2.24}$$

is a system with one equilibrium $\boldsymbol{y}^* = \boldsymbol{0}\ \forall \beta$. At this equilibrium, Jacobian matrix:

$$\boldsymbol{F}_{\boldsymbol{y}}(\boldsymbol{0}, \beta) = \begin{pmatrix} \beta & -1 \\ 1 & \beta \end{pmatrix} \tag{2.25}$$

has eigenvalues $\lambda_{1,2} = \beta \pm i$. By defining the complex variable $z = \rho e^{i\theta} \equiv y_1 + iy_2$, system (2.24) can be written in polar coordinates:

$$\begin{cases} \dfrac{d\rho}{dt} &= \rho\left(\beta - \rho^2\right) \equiv g(\rho, \beta) \\ \dfrac{d\theta}{dt} &= 1, \end{cases} \tag{2.26}$$

where $\rho \in \mathbb{R}^+$ is the modulus of z and θ is its argument. The differential equation for θ in (2.26) describes a rotation counter-clockwise at constant speed. The differential equation for ρ has an equilibrium $\rho^{(0)} = 0\ \forall \beta$, which corresponds to the equilibrium $\boldsymbol{y}^* = \boldsymbol{0}$ in cartesian coordinates. This equilibrium is stable for $\beta < 0$ (as $g_\rho(0, 0) = \beta$), non-linearly stable for $\beta = 0$ (due to the $-\rho^3$ term in $g(\rho, \beta)$), and unstable for $\beta > 0$. For $\beta > 0$, $g(\rho, \beta)$ also vanishes for $\rho^{(1)} = \sqrt{\beta}$ which is a stable equilibrium (as $g_\rho(\sqrt{\beta}, \beta) = -2\beta$) of the differential equation for ρ. This equilibrium corresponds to the radius of a stable limit cycle of system (2.26) (figure 2.10, top).

System (2.24) is the normal form of the supercritical Hopf bifurcation. The subcritical Hopf bifurcation (figure 2.10, bottom) has the following normal form:

$$\frac{d\boldsymbol{y}}{dt} = \begin{pmatrix} \beta & -1 \\ 1 & \beta \end{pmatrix} \boldsymbol{y} + \left(y_1^2 + y_2^2\right) \boldsymbol{y}, \tag{2.27}$$

which can be analyzed in the same way as system (2.24). Differences with the supercritical case are: (i) the limit cycle is unstable and exists for $\beta < 0$, (ii) equilibrium $\boldsymbol{y}^* = \boldsymbol{0}$ is nonlinearly

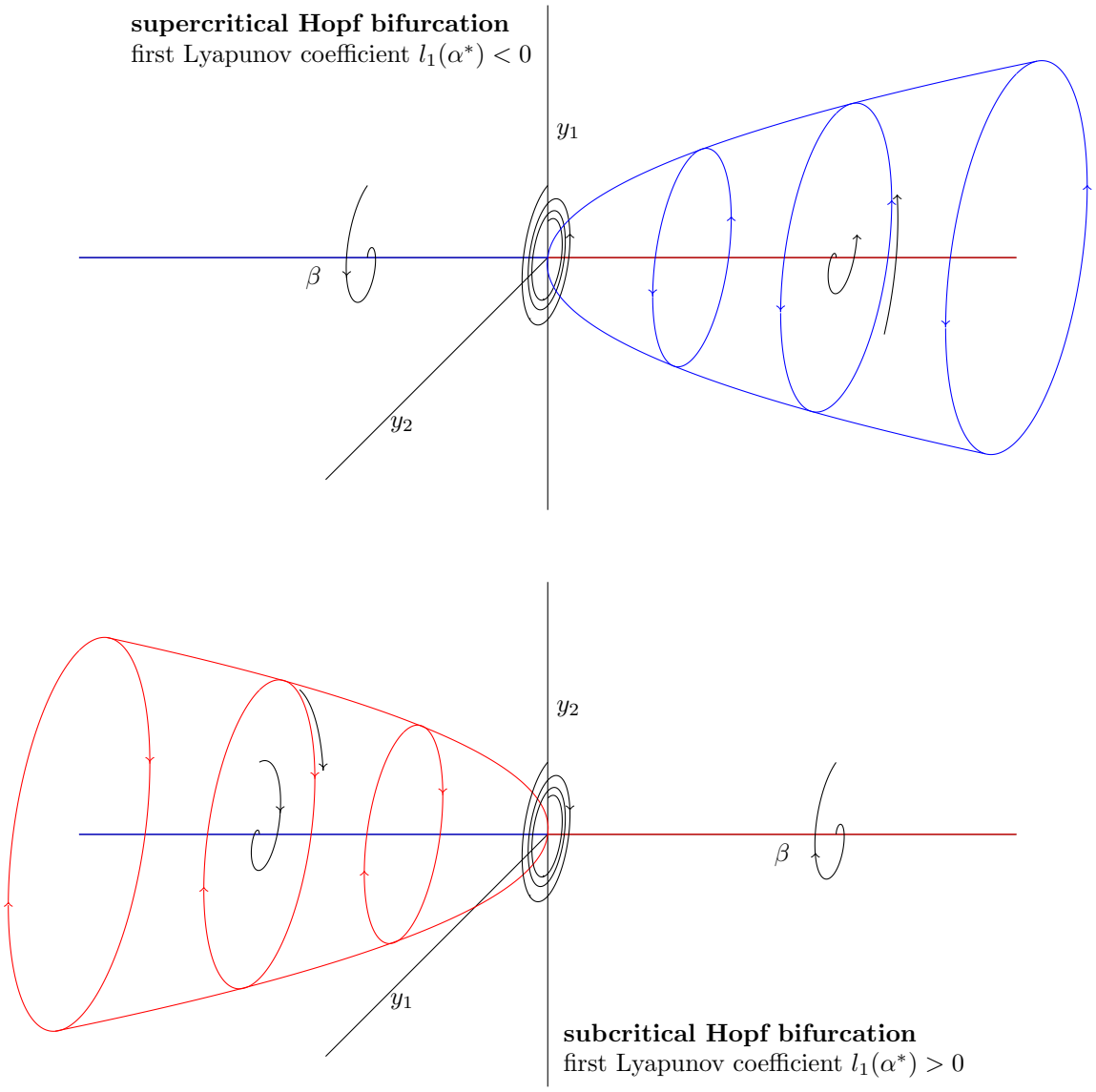

Figure 2.10. Bifurcation diagram of the normal form of the Hopf bifurcation in the supercritical and subcritical cases. The blue (red) equilibrium and cycle are stable (unstable).

unstable at $\beta = 0$. Subcritical versus supercritical Hopf bifurcations in any system (2.23) can be discriminated by computing the first Lyapunov coefficient of the system at the bifurcation $l_1(\alpha^*)$.

2.3.6 Other bifurcations and numerical analysis

Most of other bifurcations that are encountered in this thesis are either codimension-one bifurcations of cycles or codimension-two bifurcations of equilibria. The latters require generically that two parameter values are changed. Each bifurcation is presented graphically to help the reader to visualize some results presented in the next chapters.

The three codimension-two bifurcations of equilibria presented can occur in planar system. For each of them, I do not discuss the genericity conditions (the reader is refered to the mentionned references) and I present only the supercritical case (parameter $s = -1$ in the normal form). In the supercritical (resp. subcritical, $s = 1$) case, non-zero higher order terms in the Taylor expansion (2.1) make the vicinity of the equilibrium attractive (resp. repulsive) near bifurcation. One can remark that it extends the concept of subcritical and supercritical Hopf bifurcation discussed in the previous subsection.

The Cusp bifurcation (figure 2.11) is a fold bifurcation that violates the non-degeneracy condition. Two generic fold bifurcation curves meet tangentially at the Cusp bifurcation. At this point, there is a triple equilibrium. Up to three equilibria can coexist near bifurcation, with possibility for hysteresis phenomenon. For example, hysteresis in the model of insect outbreak (section 2.2.4) is due to this bifurcation (point of the horn in figure 2.6).

Similarly, the Bautin bifurcation (also called "Generalized Hopf", figure 2.12) is a Hopf bifurcation that violates the non-degeneracy condition. A Hopf bifurcation curve switches from subcritical to supercritical at a Bautin point. From this point, a codimension-one bifurcation of limit cycles emerges. This bifurcation is a limit point of cycles (also called "tangent bifurcation of cycles", figure 5.15, p171 in Kuznetsov, 2004) where two limit cycles collide and disappear similarly to equilibria at a fold bifurcation (transition from phase portait 3 to 1).

Finally, the Bogdanov-Takens bifurcation (figure 2.13) occurs when two real eigenvalues are equal to zero. This occurs when a fold bifurcation curve crosses a Hopf bifurcation curve. The Hopf bifurcation curve ends at the Bogdanov-Takens point. From this point, one branch of the fold bifurcation curve T_e^s gives birth to a stable equilibrium (the non-hyperbolic equilibrium at the fold bifurcation has a stable manifold) whereas the other branch T_e^u gives birth to an unstable equilibrium (the non-hyperbolic equilibrium has an unstable manifold). In both cases, a saddle is also created. This saddle collides with the limit cycle (coming from the Hopf bifurcation) at a homoclinic to saddle bifurcation (transition from phase portrait 3 to 4). This codimension-one

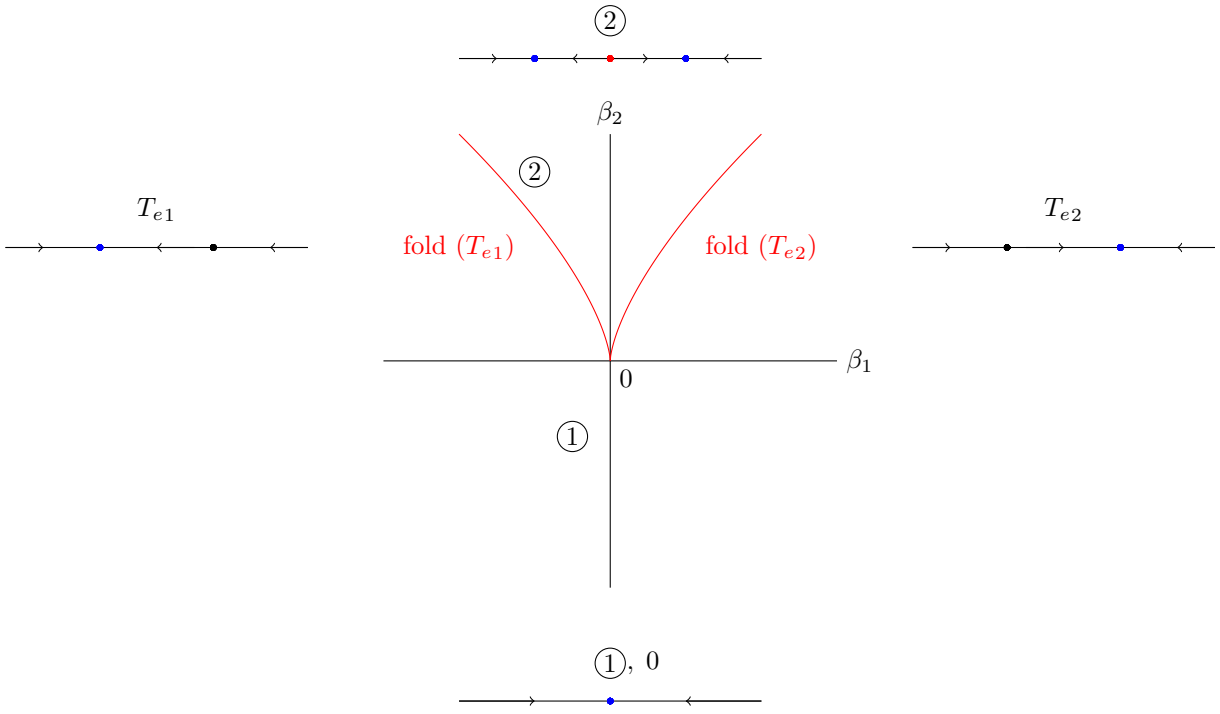

Figure 2.11. Bifurcation diagram of the normal form of the supercritical ($s = -1$) Cusp bifurcation. In the phase portaits, blue (red, black) equilibria are stable (unstable, non-hyperbolic). Equilibria stability of equilibria is reversed in the subcritical case. See section 8.2 in Kuznetsov (2004) for more informations.

global bifurcation involves a homoclinic orbit, which is a curve connecting the stable and unstable manifolds of a saddle (figures 6.7 and 6.8, p201 in Kuznetsov, 2004).

Other homoclinic orbits are involved in codimension-one global bifurcations. There are the "big" saddle homoclinic orbit (figure 6.16, p207 in Kuznetsov, 2004) and the homoclinic to saddle-node orbit (figure 7.2, p252 in Kuznetsov, 2004).

Bifurcations can be studied analytically (e.g. chapters 4 and 7). However, such analysis can be performed only for relatively simple models (a few state variables, equilibria conditions that can be determined) and bifurcations (mainly of equilibria, like the fold and transcritical bifurcations). In other situations, numerical methods have to be used for a specific set of parameters. For fixed parameters, equilibria and limit cycles are computed numerically. Then, their numerical values are continued as a function of a parameter using Newton-like methods (chapter 10 in Kuznetsov, 2004). During numerical continuation, suitable "test functions" that vanish at a given bifurcation (two examples are provided in chapter 3) are used to detect if this bifurcation occurs. This bifurcation can again be continued as a function of some parameters (in general two) using Newton-like methods. The limit of these methods is the specification of a system of equations to

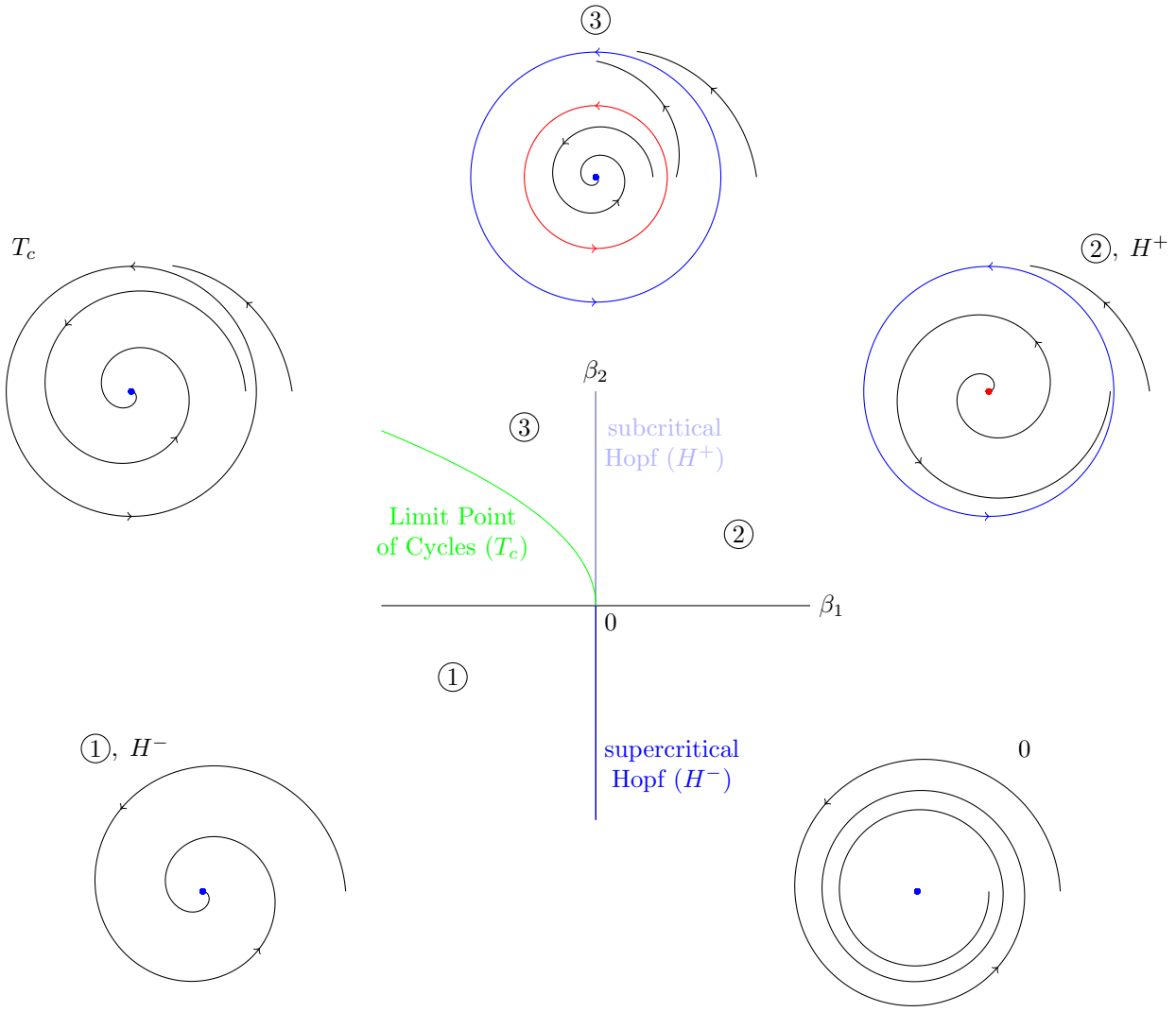

Figure 2.12. Bifurcation diagram of the normal form of the supercritical ($s = -1$) Bautin bifurcation. In the phase portaits, blue (red, black) equilibrium and limit cycles are stable (unstable, non-hyperbolic). Stability of both equilibrium and cycles is reversed in the subcritical case. See section 8.3 in Kuznetsov (2004) for more informations.

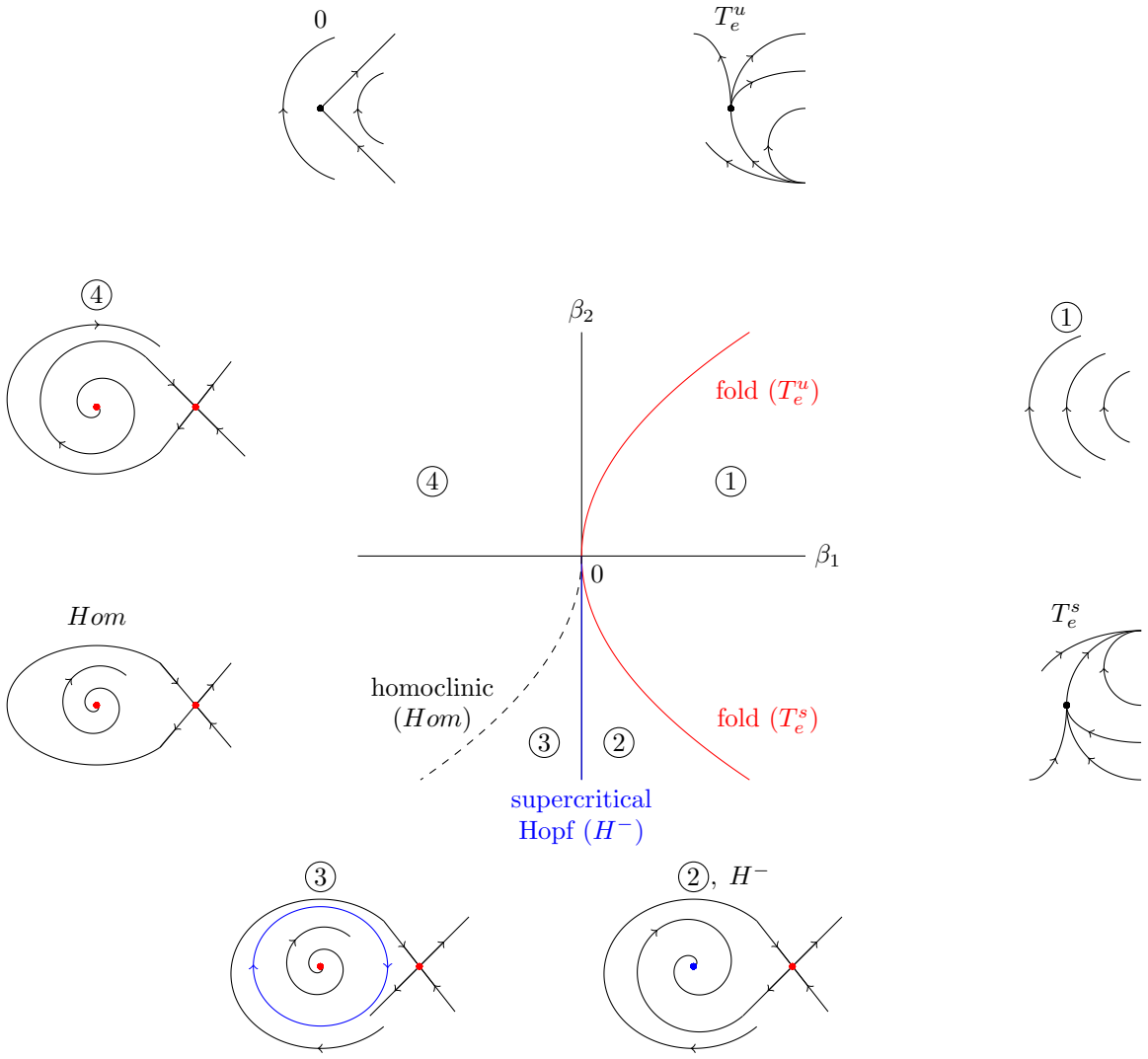

Figure 2.13. Bifurcation of the normal form of the supercritical ($s = -1$) Bogdanov-Takens bifurcation. In the phase portaits, blue (red, black) equilibria and limit cycles are stable (unstable, non-hyperbolic). Stability of equilibrium and cycles is reversed in the subcritical case. See section 8.4 in (Kuznetsov, 2004) for more informations.

solve. This system becomes more complex for bifurcations of higher codimension and bifurcations invoving cycles. Thus, bifurcation analysis can be limited by practical issues such as the number of state variables of the model, and the number of parameters with respect to which the analysis is conducted.

2.4 Modelling ecological networks

A network of interactions can be represented mathematically using a graph. A graph is an object made of nodes also called vertices (e.g. species) connected by edges (e.g. trophic interactions). Here, we do not go to the mathematical formalism of graphs as it is not required for the work presented in this thesis. However, we want to mention the existing mathematical background for the analysis of graphs (graph theory, Diestel, 2010) like food webs. An example of application performed during this thesis (but not presented in this manuscript as it was only preliminary tests) is the detection of clusters of highly interacting species within food webs (see Fortunato, 2010, for a review of existing methods).

The simplest way to see ecological networks is to consider that they have a static structure of interactions (for food webs, see Cohen *et al.*, 1990). This structure have many properties, like the connectance (different definitions) which is a scaled measure of the number of interactions between species. Other properties often considered in food webs are the length of trophic chains, proportion of cannibal species, proportion of basal species (species without prey) and top predators (species without predator). These properties can be highly dependent to the food web resolution (Martinez, 1991, Solow & Beet, 1998), i.e. the way data were processed to build the network of interactions. Indeed, similar species are often aggregated together into a trophic species, compartment or functional group for practical reasons (data availability, scope of the study).

To mimic the stucture of observed food webs, different stochastic models have been proposed to randomly build food webs with empirically consistent properties (Cohen & Newman, 1985, Williams & Martinez, 2000, 2004, Cattin *et al.*, 2004, Stouffer *et al.*, 2005, Allesina *et al.*, 2008). The purpose of most of these models was to identify a few simple rules that are enough to reproduce most of the diversity of food web structures that are observed. Another application is to use these models to build numerous (millions or billions) virtual food webs to do theoretical studies (like the work presented in chapter 5 and references therein). These modelling studies are based on statistical results across hypothetical food webs. Food web structures are used to build a dynamical system that describes the dynamics of populations constrained by the structure interactions.

Going beyond the static view of ecological networks, some studies focus on the origin of their

structure through species evolution (Drossel *et al.*, 2001, Loeuille & Loreau, 2005, Rossberg *et al.*, 2006, among others). Evolution emerges from constraints on population dynamics. In other words, evolutionary models take the reverse approach than dynamical systems built from static webs. In evolutionary models, population dynamics comes first and selects which species can coexist. Then, species evolve at a larger time scale, with the apparition of new species (random draws create new parameter values). New species will either survive or disappear due to population dynamics, leading to a constantly evolving network structure.

2.5 Structural sensitivity and functional response

The three most classical functional response formulations proposed by Holling (1965) are depicted in figure 2.14. Each function belongs to a given type corresponding to some general properties (e.g. pointwise properties, monotonicity, convexity, limits). These properties might be satisfied by an infinite number of mathematical functions. Some of these functions are built from a mechanistic explanation of the process of predation. To give an order of magnitude, a review by Jeschke *et al.* (2002) listed 47 functional responses, 18 of them being type-II functional responses and 24 others satisfying the type-II properties under some circumstances. In addition, a formulation can be extended to model a predator feeding on multiple preys using different assumptions (Gentleman *et al.*, 2003). Again, this increases the number of existing mathematical formulations (with a theoretical support in ecology) to represent a single process.

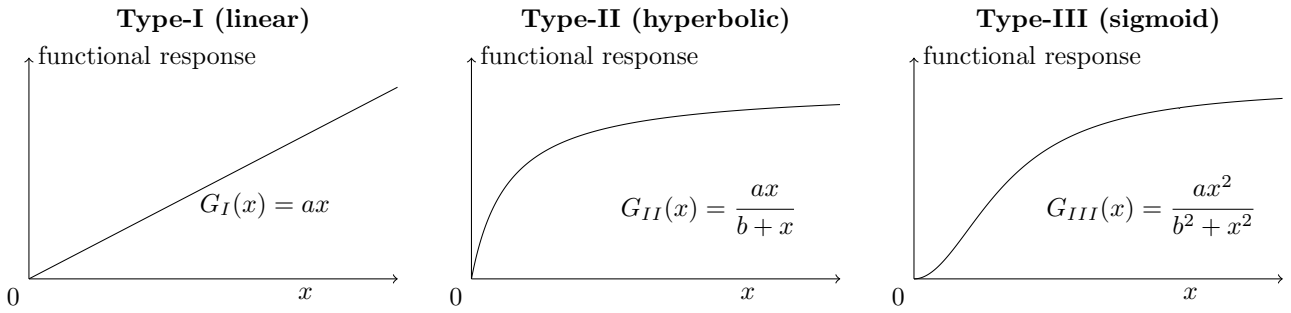

Figure 2.14. The three different types of functional responses proposed by Holling (1965).

When functional responses with the same number of parameters and that belong to the same type are fitted to data, they are all acceptable from a statistical point of view (figure 2.15, differences in the R^2 have an order of magnitude of 10^{-2}, data not shown). From a biological point of view, some functional responses might be more or less relevant depending on the existence of a mechanistic explanation for them. However, a "perfect" functional response cannot be built due

to the complexity of the process to model. Thus, even if a function without a mechanistic explanation (like the hyperbolic tangent in figure 2.15) would be less interesting for the theory behind the model, this function remains an appropriate description of the process from a quantitative point of view as it fits data (for the hyperbolic tangent, see Jassby & Platt, 1976).

Functions that belong to the same type and that are quantitatively close (like in figure 2.15) can predict different dynamics, like equilibrium vs. fluctuating dynamics (structural sensitivity). Earlier studies on structural sensitivity in predator-prey models focused for simplicity on models that: (i) have one stable state (equilibrium or limit cycle), (ii) have a few state variables, and (iii) make simple assumptions on individual metabolism[3] (Myerscough *et al.*, 1996, Gross *et al.*, 2004, Fussmann & Blasius, 2005, Cordoleani *et al.*, 2011, Adamson & Morozov, 2012). These three simplifications are relaxed in the next chapters to go toward the analysis of more complex models. A model with multiple stable states is considered in chapters 3 and 4, whereas chapter 5 deals with a model based on tens of state variables (food webs) and chapter 7 goes toward more metabolic details using the framework of Dynamic Energy Budget theory.

[3]Poggiale *et al.* (2010) explored structural sensitivity in models based on Dynamic Energy Budget theory, but they used model simulations and did not perform a bifurcation analysis of their models.

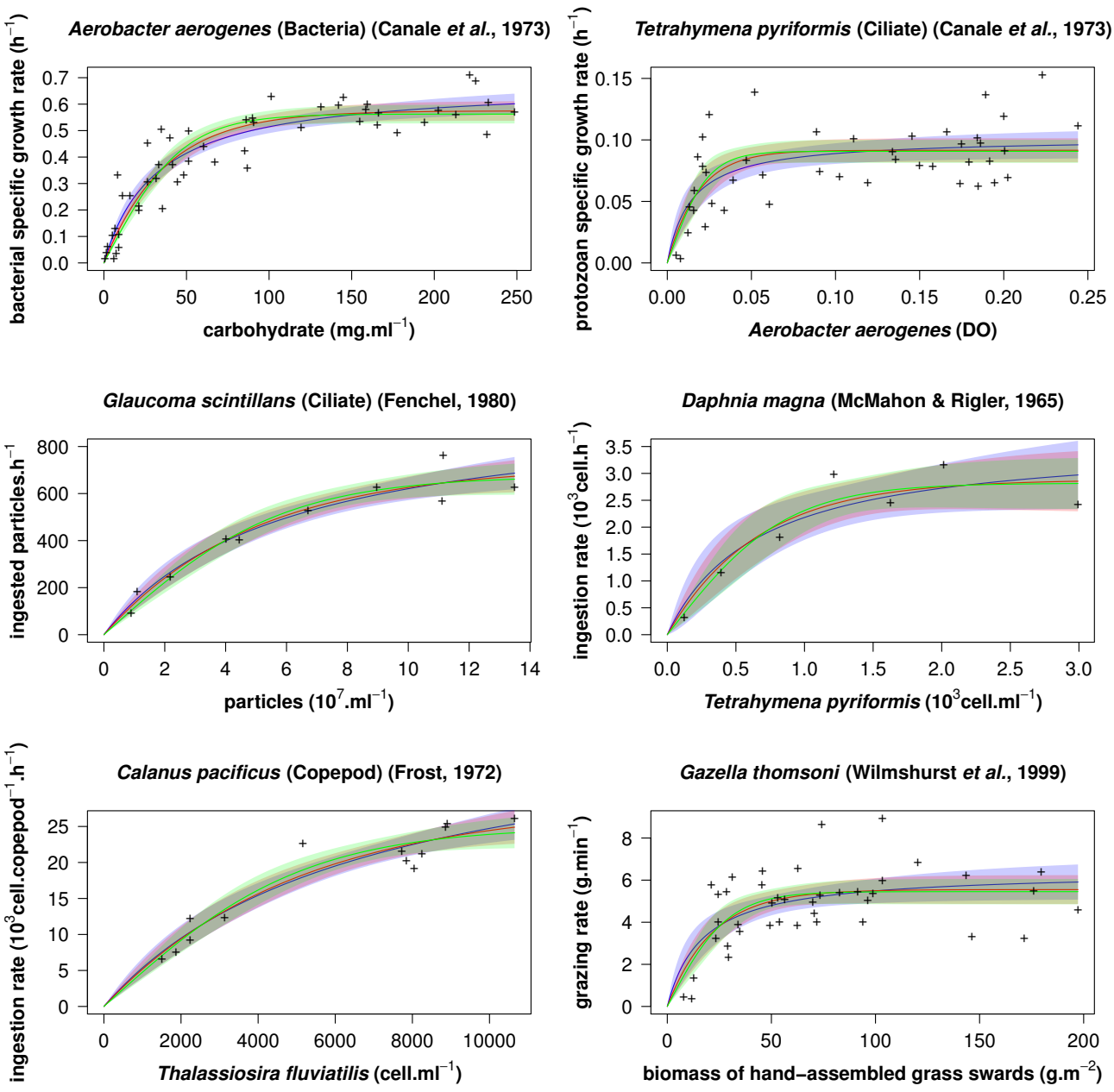

Figure 2.15. Estimation of the functional response (3 different formulations) to six empirical data sets. Original data (+) are extracted from figures in McMahon & Rigler (1965), Frost (1972), Canale *et al.* (1973), Fenchel (1980), Wilmshurst *et al.* (1999). For each data set, three functional responses are fitted to data (plain curves), the shaded ranges corresponding to the $[2.5\,\%, 97.5\,\%]$ confidence interval on parameters estimation. Functional response formulations are: Holling's disc equation ($ax/(b+x)$, x being the amount of prey available, blue), Ivlev's functional response ($a(1-\exp(-bx))$, red) and the hyperbolic tangent function ($a\tanh(bx)$, green).

Part II

Structural sensitivity and predation: from predator-prey systems to food webs, through multiple stable states and resilience

CHAPTER 3

Structural sensitivity and resilience in a predator-prey model

"A management approach based on resilience [...] would emphasize the need to [...] view events in a regional rather than a local context"

Crawford S. Holling,
"Resilience and stability of ecological systems" (Holling, 1973)

The work presented in this chapter has been published into Aldebert *et al.* (2016b):
Aldebert, C., Nerini, D., Gauduchon, M., Poggiale, JC. 2016. Structural sensitivity and resilience in a predator-prey model with density-dependant mortality. *Ecological Complexity*

3.1 Introduction

The choice of a model formulation in biology is often associated to uncertainties. Uncertainties arise from intrinsic data variability and simplified assumptions chosen to represent complex processes. Numerous mathematical formulations of a process are relevant in the sense that: (i) they fit empirical data, (ii) their properties and assumptions are consistent with the knowledge of the studied system (Mullin *et al.*, 1975, Cordoleani *et al.*, 2011). Even if these functions are quantitatively close, they can predict very different model dynamics (Myerscough *et al.*, 1996, Wood & Thomas, 1999, Gross *et al.*, 2004, Fussmann & Blasius, 2005, Poggiale *et al.*, 2010, Adamson & Morozov, 2012, 2014). This change in model dynamics can be both quantitative and qualitative, a phenomenon coined "*structural sensitivity*" (Cordoleani *et al.*, 2011).

Structural sensitivity has been mainly explored in models of predator-prey interactions. Predation emerges from the interplay between physiological, individual and collective processes. Depending on which processes are considered, predation can be modelled using numerous functional responses (amount of prey eaten per predator and per time unit, see Jeschke *et al.*, 2002, Gentleman *et al.*, 2003, for a review). Functional responses are classified by their main mathematical properties that define different types, such as Holling-types (1959a) or with vs. without predator interference (Beddington, 1975, DeAngelis *et al.*, 1975). Two functions of different type create different dynamics (Oaten & Murdoch, 1975, Scheffer & de Boer, 1995, Cantrell & Cosner, 2001). But different dynamics are also generated by functions that belong to the same type. Thus, a model is structurally sensitive to the functional response formulation. For example, different type-II functional responses predict either a stable equilibrium or oscillations in predator-prey and food chain models. These models are also more sensitive to functional response formulation than to parameter values (Myerscough *et al.*, 1996, Gross *et al.*, 2004, Fussmann & Blasius, 2005, Cordoleani *et al.*, 2011, Adamson & Morozov, 2012, 2014).

To overcome both parameter and structural sensitivity, Gross & Feudel (2006) proposed a method called generalized modelling. The local stability of positive equilibria is studied in a class of models without specifying their exact formulation and parameter values (see Yeakel *et al.*, 2011, for a review in ecology). New parameters are defined to describe system dynamics near an equilibrium. As a drawback, this method is local and cannot explore global situations as a whole, like multiple stable states.

Multiple stable states can be important to investigate how a system behaves when facing some disturbances. Thus, the study of multiple stable states is of growing interest in ecology (Beisner *et al.*, 2003, Knowlton, 2004, Scheffer *et al.*, 2009, 2012). Despite this interest, studies

on structural sensitivity focused on qualitative change (equilibrium vs. limit cycle) of a single stable state (except a short note in Fussmann & Blasius, 2005). The number of stable states can be modified by a quantitatively small change of model formulation in theory (as discussed by Adamson & Morozov, 2014), but such possibility has not been investigated so far. However, multiple stable states can coexist in predator-prey models like Bazykin's model (Bazykin *et al.* 1985, *in* Metzler & Wischniewsky, 1985, Bazykin, 1998, Kuznetsov, 2004).

Bazykin's model is equivalent to Rosenzweig & MacArthur's model (1963, section 2.2.5 of this thesis) with density-dependent mortality for the predator. The predator has no density-dependent mortality in previous studies on structural sensitivity and generalized predator-prey models (Kuehn & Gross, 2011, Yeakel *et al.*, 2011). However, density-dependent mortality represents the effects of diseases and/or competition and can be relevant for a wide range of predator species (Loreau, 2010). Furthermore, a density-dependent mortality is often used for the top-most predator in applied ecological models as a closure term to implicitely represent higher trophic levels (Fulton *et al.*, 2003a,b). Predator competition modelled with quadratic mortality implicitely involves other limiting resource than the prey. In case of predator interference, the functional response may be predator-dependent (Ivlev, 1955, Beddington, 1975, DeAngelis *et al.*, 1975, Arditi & Ginzburg, 1989, DeAngelis, 2013). However, different predator-dependent functional responses exist and structural sensitivity can also be studied in models based on this type of functions.

The question we want to address in this chapter is: what is the impact of structural sensitivity on the number of stable states? We focus on Bazykin's model which can exhibit multiple stable states. This predator-prey model can be a building block of some food web models (Plitzko *et al.*, 2012, chapter 5 of this thesis and references therein) and its study may help to understand those more complex models. The next section presents Bazykin's model and the functional response formulations that we test. Then a bifurcation analysis is conducted for two functional response formulations (section 3.3). In section 3.4, we derive a generalized predator-prey model in order to identify stabilizing factors independently of a specific formulation. This provides an additional understanding of the local stability of equilibria found in the previous section. Finally, results are discussed using examples where system resilience predicted by the model is tested using different functional response formulations.

3.2 Predator-prey model

We modelled predator-prey dynamics with Bazykin's model. We wrote the model in a form that can easily be extended to more complex food webs. Population dynamics are modelled using the

following differential system:

$$\begin{cases} \dfrac{dB_{prey}}{dt} &= \left[\lambda q^{\phi} - \alpha_{prey} - \omega\beta_{prey}B_{prey}\right] B_{prey} - G^{\phi}(B_{prey})B_{pred} \\ \dfrac{dB_{pred}}{dt} &= \left[\lambda G^{\phi}(B_{prey}) - \alpha_{pred} - \beta_{pred}B_{pred}\right] B_{pred}, \end{cases} \tag{3.1}$$

where $\boldsymbol{B} = (B_{prey}, B_{pred})^T$ is the vector made of the respective biomass of unstructured prey and predator populations. In model (3.1), the prey grows using an implicit constant resource with a rate q^{ϕ}. The predator feeds on the prey with a functional response $G^{\phi}(B_{prey})$. We assume that both populations have the same conversion efficiency λ. Each population has intrinsic losses due to (i) linear mortality with a mortality rate α_{prey} (resp. α_{pred}) and (ii) competition with a per-capita density-dependent mortality rate β_{prey} (resp. β_{pred}). Prey competition is proportional to an environmental parameter ω, so prey carrying capacity is proportional to $1/\omega$. Predation is modelled using a type-II functional response G^{ϕ} which does not depend on predator biomass and fulfills the following properties:

$$G^{\phi} \in \mathcal{C}^2,\ G^{\phi}(0) = 0,\ G^{\phi}(B_{prey}) \geq 0,\ G^{\phi\prime}(B_{prey}) > 0,\ G^{\phi\prime\prime}(B_{prey}) < 0,\ \lim_{B_{prey}\to+\infty} G^{\phi}(B_{prey}) < +\infty, \tag{3.2}$$

where $\mathcal{C}^2$ is the class of twice continuously differentiable functions. Other properties means that G^{ϕ} is null in absence of prey, increases with prey biomass, is concave and saturates at high prey biomass.

As examples of functions with properties (3.2), we consider Holling's disc equation (1959b, 1965) G^H and Ivlev's functional response (1955) G^I (figure 3.1):

$$G^H(B_{prey}) = \frac{a^H_{pred}B_{prey}}{1 + h^H_{pred}a^H_{pred}B_{prey}},\ G^I(B_{prey}) = \frac{1}{h^I_{pred}}\left(1 - \exp\left(-h^I_{pred}a^I_{pred}B_{prey}\right)\right).$$

For the first formulation, parameters a^H_{pred} and h^H_{pred} are respectively the attack rate and the handling time of the predator. For the second formulation, parameter $1/h^I_{pred}$ is the maximal consumption rate and $a^I_{pred}h^I_{pred}$ is the satiation coefficient of the predator. Parameters are defined in order to have a consistent mathematical meaning across formulations:

$$G^{\phi\prime}(0) = a^{\phi}_{pred},\ \lim_{B_{prey}\to+\infty} G^{\phi}(B_{prey}) = \frac{1}{h^{\phi}_{pred}}.$$

Thus, a^{ϕ}_{pred} gives the slope of the functional response at the origin, and $1/h^{\phi}_{pred}$ gives the asymptotic

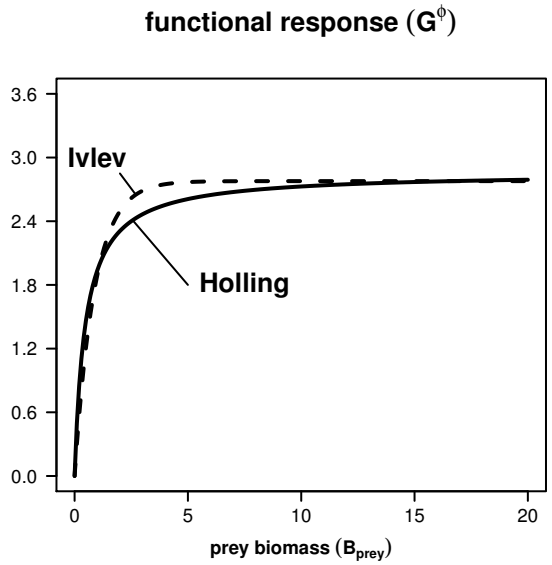

Figure 3.1. Functional responses used in the model: Holling's disc equation (solid) and best fitted Ivlev's functional response (dashed). The former is used as "data" to parameterize the latter (Appendix, section 3.7) Parameter values are given in table 3.1. For the sake of visibility, only a part of the fitting range ($[0, B_{res}] = [0, 500]$) is shown.

value of the functional response when it saturates at high prey biomass.

Resource consumption q^ϕ has the same equation as the functional response G^ϕ with a constant pool of resource B_{res}:

$$q^H = \frac{a^H_{prey} B_{res}}{1 + h^H_{prey} a^H_{prey} B_{res}},\ q^I = \frac{1}{h^I_{prey}} \left(1 - \exp\left(-h^I_{prey} a^I_{prey} B_{res}\right)\right),$$

so q^ϕ is a constant. Organism's metabolic rates are strongly influenced by body mass. We assume that some parameter values scale allometrically with species body mass M_{prey} and M_{pred} (Brown *et al.*, 2004, Kooijman, 2010):

$$a^\phi_i = a^\phi M_i^{-0.25},\ h^\phi_i = h^\phi M_i^{0.25},\ \alpha_i = \alpha M_i^{-0.25},\ \beta_i = \beta M_i^{-0.25} \text{ with } i = prey, pred.$$

These relationships imply an allometric scaling of resource consumption $q^\phi \propto M^{-0.25}_{prey}$ and predation $G^\phi \propto M^{-0.25}_{pred}$. So we define $\overline{q}^\phi := q^\phi M^{0.25}_{prey}$ and $\overline{G}^\phi := G^\phi M^{0.25}_{pred}$, which do not depend on

Table 3.1. Parameter values used in the predator-prey model. Parameter values from Heckmann *et al.* (2012) were estimated from empirical data sets (up to > 700 organisms from unicellular eukaryotes to plants and mammals, which span 20 orders of magnitude in body mass, Brown *et al.*, 2004, Brose *et al.*, 2006) using allometric scaling or set to values similar to other studies for comparison (like Kartascheff *et al.*, 2009, 2010).

biological meaning	parameter	value	source	unit
mortality rate	α	0.3	(Heckmann *et al.*, 2012)	time^{-1}
per-capita competition rate	β	0.5	(Heckmann *et al.*, 2012)	$\text{biomass}^{-1}\text{time}^{-1}$
assimilation efficiency	λ	0.65	(Heckmann *et al.*, 2012)	-
resource biomass	B_{res}	500	(Heckmann *et al.*, 2012)	biomass
Holling's disc equation:				
attack rate	a^H	6	(Heckmann *et al.*, 2012)	$\text{biomass}^{-1}\text{time}^{-1}$
handling time	h^H	0.35	(Heckmann *et al.*, 2012)	time
Ivlev's functional response:				
maximal consumption rate	$1/h^I$	$1/0.36$	section 3.7	time^{-1}
satiation coefficient	$a^I h^I$	3.17×0.36	section 3.7	biomass^{-1}

species body mass. Hence, model (3.1) can be written using body masses:

$$\frac{d\boldsymbol{B}}{dt} = \boldsymbol{F}(\boldsymbol{B}) \Leftrightarrow \begin{cases} \dfrac{dB_{prey}}{d\bar{t}} &= \left[\lambda \overline{q}^{\phi} - \alpha - \omega\beta B_{prey}\right] B_{prey} - \overline{G}^{\phi}(B_{prey}) B_{pred} (M_{pred}/M_{prey})^{-0.25} \\ \dfrac{dB_{pred}}{d\bar{t}} &= \left[\lambda \overline{G}^{\phi}(B_{prey}) - \alpha - \beta B_{pred}\right] B_{pred} (M_{pred}/M_{prey})^{-0.25}, \end{cases} \tag{3.3}$$

with a time re-scaling $\bar{t} = tM_{prey}^{-0.25}$ in order to have a model that does not depend on both species body mass but on their ratio M_{pred}/M_{prey}. When Holling's disc equation is used, model (3.3) can be written in the form of Bazykin's model (Bazykin *et al.* 1985, *in* Metzler & Wischniewsky, 1985, Bazykin, 1998, Kuznetsov, 2004) after appropriate re-scaling and parameter changes.

Parameter values are listed in table 3.1. To parameterize Ivlev's functional response, we consider Holling's disc equation as "data" and optimize Ivlev's parameters in order to minimize the weighted Euclidean distance between the two functional responses (Appendix, section 3.7 for details). This optimization is done to simulate a fit of both functional responses on empirical data (as done by Mullin *et al.*, 1975, Cordoleani *et al.*, 2011). To do this, the optimization step gives a better fit between functional responses (correlation coefficient $\rho = 0.93$) than using the same a^{ϕ} and h^{ϕ} values for both formulations ($\rho = 0.86$), as done for example by Anderson *et al.* (2010).

3.3 Bifurcation analysis for different functional responses

Model (3.3) has two trivial equilibria:

$$O = (0,0) \quad \text{and} \quad E_0 = \left(K := \frac{\lambda \overline{q}^{\phi} - \alpha}{\omega \beta}, 0 \right), \tag{3.4}$$

where K is prey carrying capacity. Equilibrium O always exists and is a saddle. Equilibrium E_0 exists if $\lambda \overline{q}^{\phi} > \alpha$. It is a stable node if $\alpha > \lambda \overline{G}^{\phi}(K)$ (figure 3.2, phase portrait #0) and a saddle otherwise (other phase portraits). The threshold $\alpha = \lambda \overline{G}^{\phi}(K)$ corresponds to a transcritical bifurcation where a stable positive equilibrium appears when $1/\omega$ is increasing. The twelve generic phase portraits found for this system are presented in figure 3.2. Briefly, the system exhibits up to three positive equilibria (phase portraits #3, #4 and #6 to #11) due to the density-dependent mortality of the predator, as well as up to two limit cycles (phase portraits #7 and #11). Multiple attractors co-exist in seven phase portraits (phase portraits #4 to #8, #10 and #11).

An analysis of model (3.1) with Holling's disc equation is presented in Bazykin (1998) and Kuznetsov (2004), based on a two-dimensional bifurcation diagram with respect to the saturation parameter of the functional response and the density-dependent mortality of the predator. Here we focus on two parameters that are expected to vary across ecosystems and species: (i) prey carrying capacity ($K \propto 1/\omega$) and (ii) species body mass ratio (M_{pred}/M_{prey}). In our analysis, body mass ratio ranges from prey that are 10^4 times bigger than their predators (e.g. insects feeding on trees) to predators that are 10^8 times bigger than their prey (e.g. whales feeding on krill). This range is likely to include most of known predator-prey interactions (Kooijman, 2010). For prey carrying capacity, $1/\omega$ can be understood as a number of different trophic species eaten by the same predator species in a food web (chapter 5). In our analysis, $1/\omega$ ranges from 0 to 10. This range includes almost all values observed in model-based food webs that are consistent with empirical data (e.g. Williams & Martinez, 2000). The sensitivity of our results to parameter ranges is discussed at the end of the section.

Two-dimensional bifurcation diagrams in the plane $(1/\omega, \log_{10}(M_{pred}/M_{prey}))$ were obtained using the Matlab continuations toolboxes Matcont and CL_Matcont (Dhooge *et al.*, 2006). Codimension-one (here curves) and codimension-two (here points) bifurcations were numerically computed using continuation methods (Kuznetsov, 2004). Homoclinic bifurcation curves were estimated by dichotomy for numerous parameter values. Figure 3.3 presents the bifurcation diagrams obtained for both functional responses.

When Holling's disc equation is used (figure 3.3a), more than 99.999 % of the explored param-

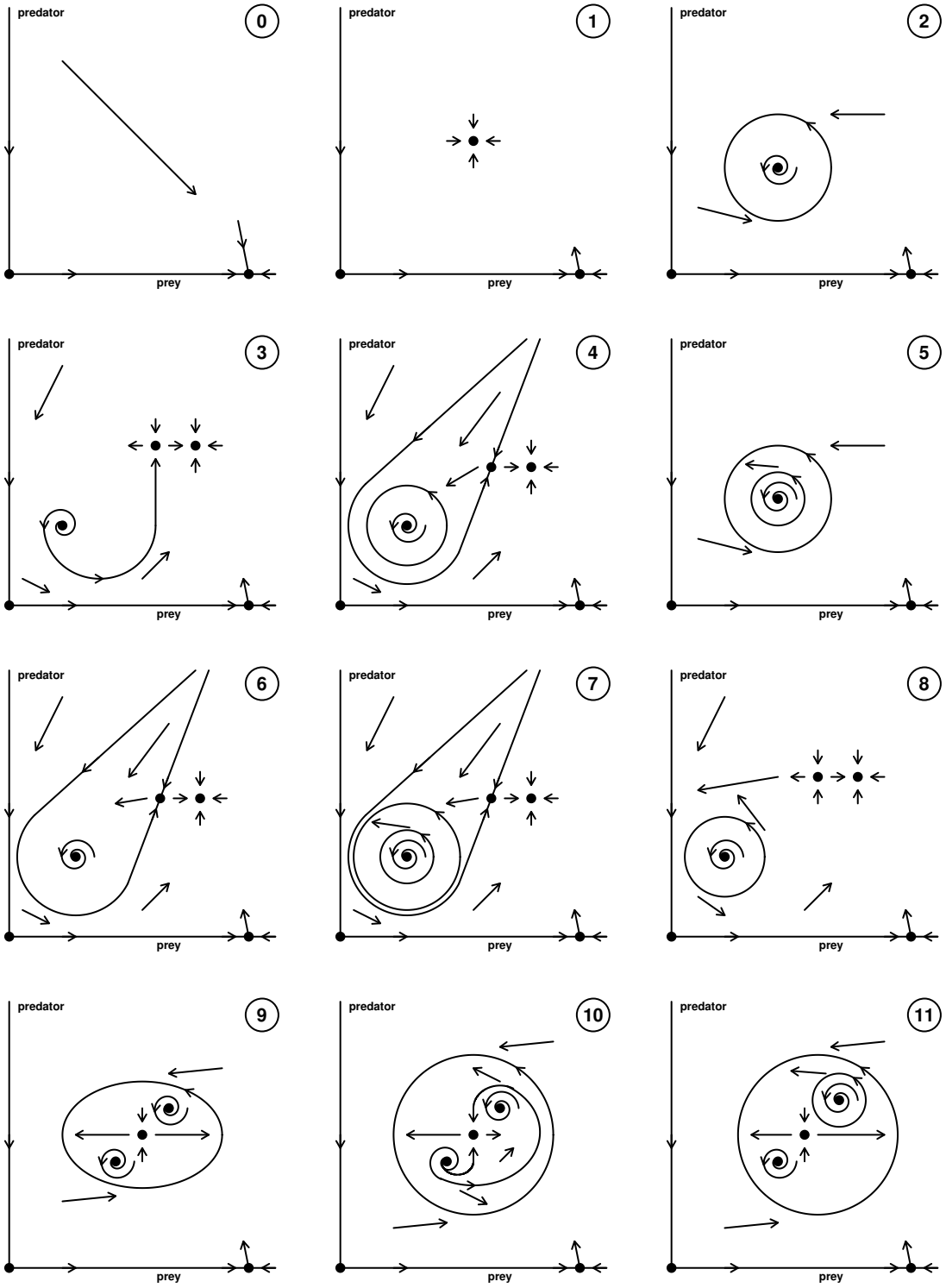

Figure 3.2. Qualitative generic phase portraits of the predator-prey model. Transitions between the different situations corresponds to bifurcations drawn in figure 3.3.

eter space area generate phase portraits #1, #2 or #3. These portraits correspond respectively to a stable equilibrium, an unstable focus with a stable limit cycle and three equilibria (one unstable node or focus, a saddle, one stable node or focus). The area with three equilibria is delimited by the two branches of a saddle-node bifurcation (red curve). Transition between phase portraits #1 and #2 occurs through a Hopf bifurcation, which is either supercritical (dark blue curve) or subcritical (light blue curve). These two branches meet at a Bautin point on this curve. A limit point of cycles bifurcation curve (green curve) starts from this point and stays mostly close to the subcritical Hopf branch. When moving from phase portrait #1 to #2 through this branch and the limit point of cycles, the system exhibits phase portrait #5 in a tiny strip of the parameter space (stable focus and limit cycle separated by an unstable limit cycle). The two branches of the saddle-node bifurcation curves meet at a Cusp bifurcation point. The subcritical branch of the Hopf bifurcation curves meets the bottom-branch of the saddle-node curve at a Bogdanov-Takens point. Close to these points, there are three positive equilibria surrounded by a stable limit cycle (phase portraits #9 to #11). From phase portrait #2 to #3, the limit cycle is destroyed through a homoclinic bifurcation (dashed black curve), which may be a homoclinic to saddle-node bifurcation in most of the bifurcation diagram (see Appendix, section 3.8 for a more detailled technical discussion).

If Ivlev's functional response is used (figure 3.3b), the Bogdanov-Takens point is now located on the top-branch of the saddle-node bifurcation. The homoclinic curve starting from this point is close to the bottom branch of the saddle-node curve in most of the bifurcation diagram (Appendix, section 3.8). Starting from the Bogdanov-Takens point, the Hopf bifurcation is supercritical. In comparison with Holling's disc equation, the Hopf bifurcation curve wraps, which strongly decreases the part of the parameter space where a stable limit cycle exists. This curve becomes a subcritical Hopf bifurcation after the Bautin point. A limit point of cycles curve starts from this Bautin point. As a consequence, various dynamics arise with Ivlev's functional response (see figure 3.3b, bottom zoom). For example, in phase portrait #7 (figure 3.2) the system has three different attractors: a stable focus, a stable limit cycle and a stable node. Their respective attraction basins are delimited by an unstable limit cycle and a saddle. Phase portraits #7 and #8 are not observed with Holling's disc equation in this study or in the bifurcation diagram presented by Kuznetsov (2004). More complex dynamics than phase portraits #1 to #3 occur for roughly $\log_{10}(M_{pred}/M_{prey}) \in [-0.5, 0.5]$ and $1/\omega > 5$ with Ivlev's functional response. This range of body mass ratios corresponds to prey and predator species with similar body mass and metabolic rates, as we assume allometric scaling relationships. This range widens as prey carrying capacity increases.

In terms of structural sensitivity, there are two main differences between the bifurcation di-

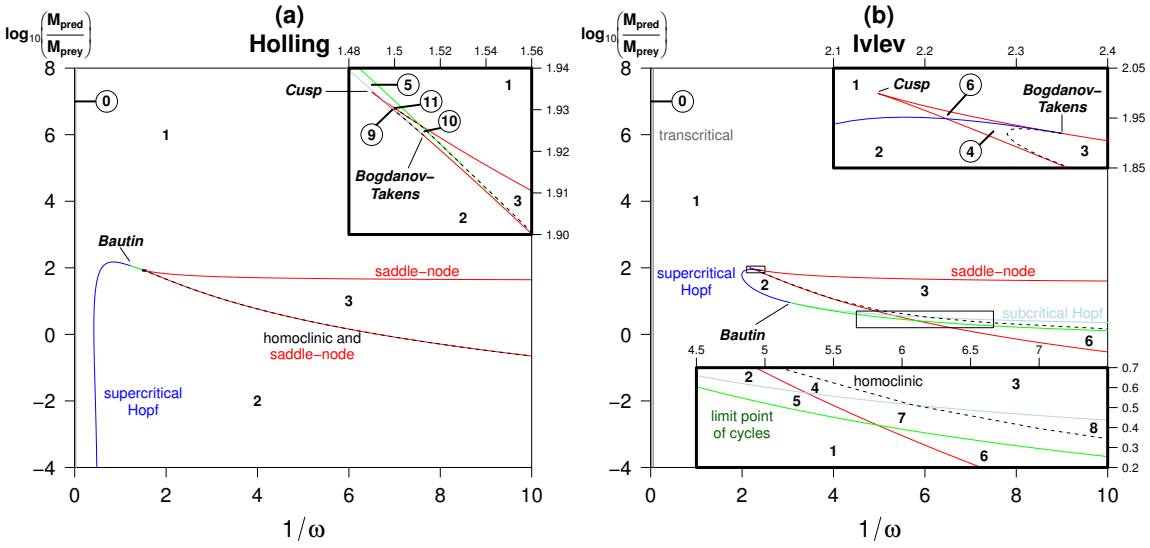

Figure 3.3. Two-dimensional bifurcation diagram of the specific predator-prey model using the functional response proposed by: (a) Holling or (b) Ivlev. Bifurcation diagrams depend on $1/\omega$ (which is proportional to the prey carrying capacity) and the species body mass ratio M_{pred}/M_{prey}. In each diagram, codimension-one bifurcation curves delimit areas of qualitatively different phase portraits. The number in each area indicates the corresponding phase portrait in figure 3.2. The different types of codimension-one bifurcation curves are indicated in different colors. Codimension-two bifurcation points are written in italic.

agrams obtained for Holling's and Ivlev's functional response. The following results are only quantitatively modified by changes in the size of the parameter space investigated (table 3.2). First, there are multiple attractors in 0.1 % to 14.3 % of the bifurcation diagram with Ivlev's functional response (see Appendix, section 3.9 for technical details). This proportion increases if higher $1/\omega$ values (i.e. richer environment) are considered. Second, there is a stable limit cycle (phase portrait #2) with Holling's disc equation and a stable equilibrium (phase portrait #1) with Ivlev's functional response in 26.0 % to 49.4 % of the parameter space explored. This proportion decreases if higher $1/\omega$ values are considered. The opposite situation between functional responses occurs only in a neglectible proportion of the parameter space (near the Cusp and Bogdanov-Takens points). The order of magnitude of these two main results remains similar if any other parameter value is changed by ±20 % (see table 3.3). Depending on the parameter, quantitative changes in our results can be of different amount. However, this impact of each parameter will not be discussed here as the analysis presented in table 3.3 is exploratory.

Table 3.2. Impact of the size of the parameter space explored on results of the bifurcation analysis. These results are the fractions of the parameter space where: (i) there is a stable limit cycle with Holling's disc equation and a stable equilibrium with Ivlev's functional response, (ii) there are multiple attractors with Ivlev's functional response. Constant parameter values are those from table 3.1. We test 9 combinations obtained with 3 ranges of $1/\omega$ values ($[0, 5]$, $[0, 10]$ and $[0, 20]$) and 3 ranges of $\log_{10}(M_{pred}/M_{prey})$ values ($[-2, 4]$, $[-4, 8]$ and $[-8, 16]$). First column shows results obtained with ranges used in figure 3.3. Second column shows the range of results obtained for the 9 parameter subspaces tested. Last two columns are coefficients of the linear regression between results and the range of both parameters. NS means non-significant (p-value $\gg 0.05$). Coefficients for $1/\omega$ are significant (p-value < 0.05).

	reference value	obtained range	sensitivity to explored parameter values $1/\omega$	$\log_{10}(M_{pred}/M_{prey})$
limit cycle vs. equilibrium	0.359	$[0.260, 0.494]$	-0.0084	NS
multiple attractors	0.019	$[0.001, 0.143]$	0.0055	-0.0024 (p-value = 0.07)

Table 3.3. Impact of other parameter values on results of the bifurcation analysis. These results are relative changes from reference values in table 3.2 in the fractions of the parameter space ($1/\omega \in [0, 10], \log_{10}(M_{pred}/M_{prey}) \in [-4, 8]$) where: (i) there is a stable limit cycle with Holling's disc equation and a stable equilibrium with Ivlev's functional response, (ii) there are multiple attractors with Ivlev's functional response. Constant parameter values are those from table 3.1, except for one parameter value that is increased/decreased by 20 %. If this parameter is one of Holling's disc equation (a^H or h^H), both parameters for Ivlev's functional response (a^I and h^I) are re-estimated. For each parameter change, results sensitivity to the size of the parameter space is of similar magnitude as in table 3.2.

		limit cycle vs. equilibrium		multiple attractors	
biological meaning	parameter	-20 %	$+20$ %	-20 %	$+20$ %
mortality rate	α	-0.7 %	-0.3 %	$+50.3$ %	$+45.9$ %
per-capita competition rate	β	-5.4 %	-4.0 %	$+0.5$ %	$+49.9$ %
attack rate	a^H	-5.3 %	-2.7 %	$+52.0$ %	-18.9 %
handling time	h^H	-1.0 %	0 %	$+37.4$ %	-46.3 %
assimilation efficiency	λ	$+3.5$ %	-4.9 %	-77.3 %	$+107.4$ %
resource biomass	B_{res}	0 %	0 %	$+0.1$ %	$+0.1$ %

3.4 Generalized predator-prey model: beyond a specific formulation

In the previous section, we have studied the effect of functional response formulation change on a predator-prey model. Now we use the generalized modelling approach (Gross & Feudel, 2006) to provide another way to interpret the stability of positive equilibria independently of a specific functional response formulation. This helps to understand differences between bifurcation diagrams obtained from different formulations. Model (3.3) also exhibits limit cycles. Like for equilibria, their stability can be studied through generalized modelling. However, the amount of technical work required (even for a predator-prey model without predator competition, Kuehn & Gross, 2011) is beyond the scope of this paper.

We first consider the differential system (3.3) without specifying the functional response and the parameter values. We only claim that the functional response fulfills properties (3.2). So we consider in fact a family of models. Generalized modelling supposes that some models in this family have positive equilibria. The stability of a positive equilibrium is then studied using the Jacobian matrix:

$$\boldsymbol{F_B}(\boldsymbol{B^*}) = \begin{pmatrix} \lambda\overline{q}^{\phi} - B^*_{pred}\dfrac{M_{pred}^{-0.25}}{M_{prey}^{-0.25}}\overline{G}^{\phi\prime}(B^*_{prey}) - \left(\alpha + 2\omega\beta B^*_{prey}\right) & -\overline{G}^{\phi *} \\ \lambda B^*_{pred}\dfrac{M_{pred}^{-0.25}}{M_{prey}^{-0.25}}\overline{G}^{\phi\prime}(B^*_{prey}) & \left(\lambda\overline{G}^{\phi *} - (\alpha + 2\beta B^*_{pred})\right)\dfrac{M_{pred}^{-0.25}}{M_{prey}^{-0.25}} \end{pmatrix}$$

evaluated at a positive equilibrium $\boldsymbol{B^*} = \left(B^*_{prey}, B^*_{pred}\right)^T$, with $\overline{G}^{\phi *} := \overline{G}^{\phi}(B^*_{prey})$. The matrix is expressed using generalized parameters that describe the system close to this equilibrium (table 3.4):

$$\boldsymbol{F_B}(\boldsymbol{B^*}) = \begin{pmatrix} \tau_{prey}(1 - (1-\delta_{prey})\mu_{prey} - \delta_{prey}\gamma_{pred}) & -\tau_{prey}\nu_{prey,pred}\delta_{prey} \\ \tau_{pred}\nu_{pred,prey}\gamma_{pred} & \tau_{pred}(1-\mu_{pred}) \end{pmatrix}.$$

Details on the derivation procedure to define generalized parameters are presented in Gross & Feudel (2006) and Yeakel *et al.* (2011). Equilibrium stability is studied as a function of the generalized parameter values without specific assumptions on the functions and original parameter (such as a^{ϕ} or h^{ϕ}) values behind them.

To study equilbrium stability, let us recall the following statements (that hold under nondegeneracy conditions) from bifurcation theory (see for example Guckenheimer & Holmes, 1983, Perko,

Table 3.4. Formulation and ecological meaning of the generalized parameters used to build the generalized predator-prey model. The scale parameters describe the time scale of species dynamics (for τ_i) and the relative contribution of the different processes to this dynamics. Elasticities measure the non-linearity of processes.

generalized parameter formulation	ecological meaning
scale parameters	
$\tau_{prey} = \lambda\overline{q}^{\phi} = \overline{G}^{\phi*}\frac{B^*_{pred}}{B^*_{prey}}\frac{M^{-0.25}_{pred}}{M^{-0.25}_{prey}} + \left(\alpha + \omega\beta B^*_{prey}\right)$	time scales of species dynamics
$\tau_{pred} = \lambda\overline{G}^{\phi*}\frac{M^{-0.25}_{pred}}{M^{-0.25}_{prey}} = \left(\alpha + \beta B^*_{pred}\right)\frac{M^{-0.25}_{pred}}{M^{-0.25}_{prey}}$	
$\delta_{prey} = \frac{1}{\tau_{prey}}\overline{G}^{\phi*}\frac{B^*_{pred}}{B^*_{prey}}\frac{M^{-0.25}_{pred}}{M^{-0.25}_{prey}}$	fraction of prey losses due to predation
$1-\delta_{prey} = \frac{1}{\tau_{prey}}\left(\alpha + \omega\beta B^*_{prey}\right)$	fraction of prey losses due to intrinsic dynamics
$\nu_{prey,pred} = B^*_{prey}/B^*_{pred}$	biomass ratios between species
$\nu_{pred,prey} = B^*_{pred}/B^*_{prey}$	
elasticities (also called exponent parameters)	
$\mu_{prey} = 1 + \frac{\omega\beta B^*_{prey}}{\alpha + \omega\beta B^*_{prey}} \in [1,2]$	non-linearity of species intrinsic mortality
$\mu_{pred} = 1 + \frac{\beta B^*_{pred}}{\alpha + \beta B^*_{pred}} \in [1,2]$	
$\gamma_{pred} = g^{\phi\prime}(1) \in [0,1]$ with $b_{prey} = \frac{B_{prey}}{B^*_{prey}}$ and $g^{\phi}(b_{prey}) := \frac{\overline{G}^{\phi}(b_{prey}B^*_{prey})}{\overline{G}^{\phi}(B^*_{prey})}$	slope of predator normalized functional response

1996, Kuznetsov, 2004). A saddle-node bifurcation occurs when there is a real zero eigenvalue. A common way to track this bifurcation is to solve $\Psi_{SN} = 0$, with

$$\Psi_{SN} := \det(J) = \tau_{prey}\tau_{pred}\left[(1-\mu_{pred})(1-(1-\delta_{prey})\mu_{prey}) + \mu_{pred}\delta_{prey}\gamma_{pred}\right] \tag{3.5}$$

vanishing only when at least one eigenvalue is equal to zero. A Hopf bifurcation occurs when there is a pair of (conjugate) pure imaginary eigenvalues. A common way to track this bifurcation in planar systems is to solve $\Psi_H = 0$ with

$$\Psi_H := \mathrm{Tr}(J) = \tau_{prey}\left[1-(1-\delta_{prey})\mu_{prey} - \delta_{prey}\gamma_{pred} + \frac{\tau_{pred}}{\tau_{prey}}(1-\mu_{pred})\right]. \tag{3.6}$$

Note that Ψ_H vanishes at a Hopf bifurcation, but as well as if there are two real eigenvalues of opposite sign and same absolute magnitude. In this case the equilibrium is called a neutral saddle. The two situations can be discriminated by looking at the sign of Ψ_{SN} which is positive at a

Hopf bifurcation and negative at a neutral saddle. The limit case between these two situations corresponds to the intersection between a Hopf and a saddle-node bifurcation. It is a codimension-two Bogdanov-Takens bifurcation where two eigenvalues are equal to zero.

A five-dimensional bifurcation diagram is required to explore the whole parameter space. Figure 3.4 displays three-dimensional diagrams that are sufficient to understand the role of all parameters, except for time scales τ_{prey} and τ_{pred}. The ratio τ_{pred}/τ_{prey} has only a scaling impact proportional to μ_{pred} values on the Hopf bifurcation location, as it can be understood by looking at Ψ_H equation (3.6). An equilibrium is stable when prey losses are dominated by density-dependent mortality (low δ_{prey} and high μ_{prey}) and when prey density is sufficiently low to give a high slope to the predator functional response (high γ_{pred}). For $\mu_{pred} = 1$, an unstable equilibrium is always a node or a focus. As the density-dependence of predator mortality increases (μ_{pred} increases), it can be a saddle for an increasing range of γ_{pred} values. For sufficiently high μ_{pred}, an equilibrium is either a stable node (or focus) or a saddle. These results hold for any positive equilibrium of any predator-prey model of the form (3.3).

Axes in figure 3.4 correspond to generalized parameters describing a positive equilibrium. Numerical values of the generalized parameters can be computed for all positive equilibria in the bifurcation diagrams of figure 3.3. By construction, the stability of these equilibria can be interpreted in terms of generalized parameters by mapping their numerical values in the bifurcation diagram of the generalized model (figure 3.4). So, when there are two or more positive equilibria in a specific model such as system (3.3), each equilibrium has a different generalized parameter set. For example, consider parameter values in figure 3.3 close to a saddle-node bifurcation, and where a node (or focus) and a saddle coexist. If generalized parameter values are computed and mapped in figure 3.4, the node is above the saddle-node bifurcation surface and the saddle is below. If a parameter of model (3.3) is moved towards the bifurcation in figure 3.3, generalized parameter values of both equilibria become closer. These values become equal to the saddle-node bifurcation value in figure 3.4 where equilibria collide and disappear, as the parameter of model (3.3) reaches the saddle-node bifurcation in figure 3.3.

Now, we use generalized parameters to interpret the impact of functional response formulation in figure 3.3. Equilibria are computed on a grid by steps of 0.02 for $\log_{10}(M_{pred}/M_{prey})$ and 0.01 for $1/\omega$. Consider values of these two parameters where there is a stable positive equilibrium (phase portrait 1) with Ivlev's functional response and a stable limit cycle (phase portrait 2) with Holling's disc equation. Generalized parameters are computed for the stable equilibrium with Ivlev's functional response and for the unstable focus surrounded by the limit cycle with Holling's disc equation. On average within the considered area, higher μ_{prey}, μ_{pred} and γ_{pred} ($\approx +0.1$) as well as lower δ_{prey} (≈ -0.2) are obtained with Ivlev's functional response. The direction of these

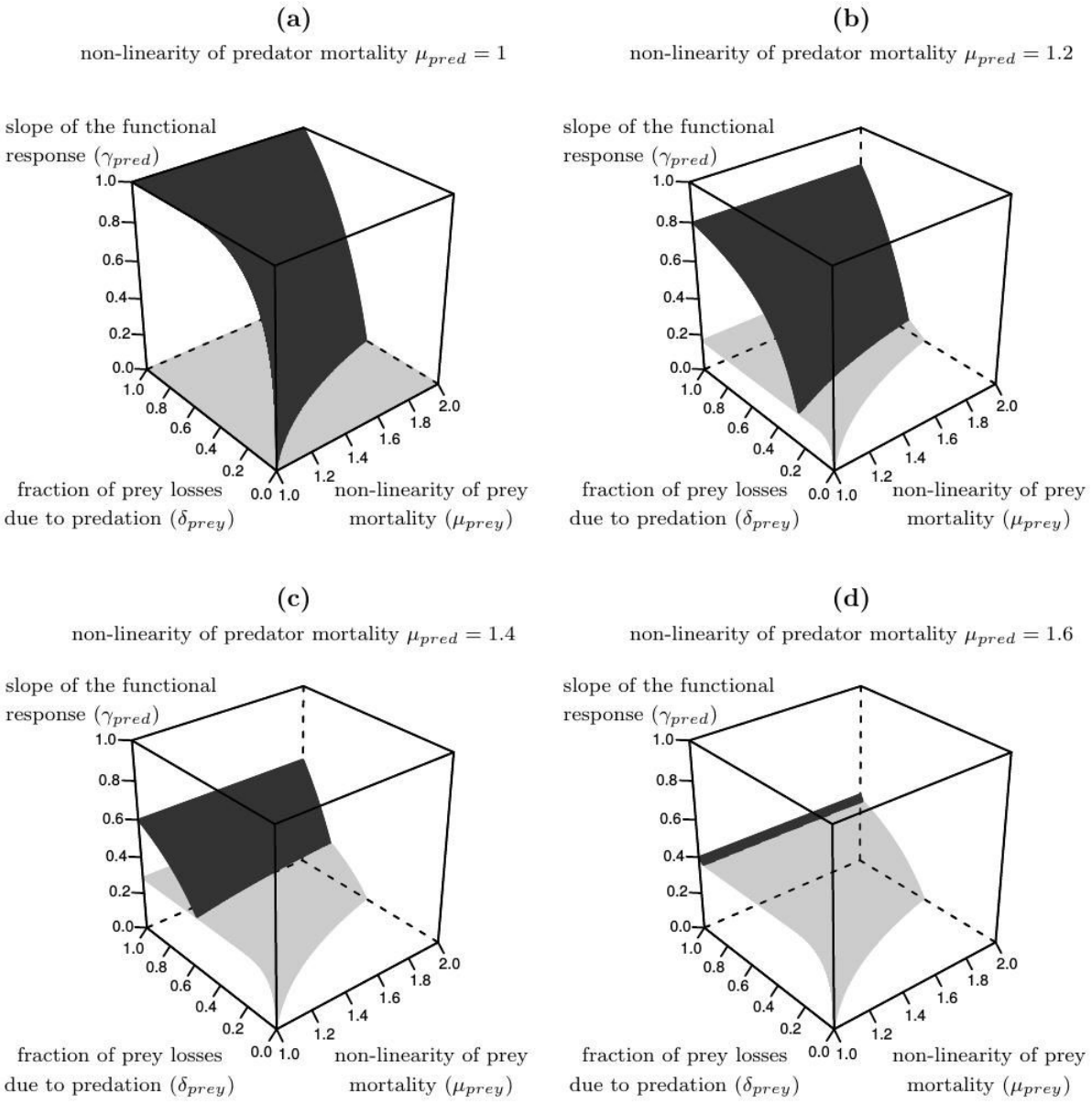

Figure 3.4. Bifurcations of positive equilibria in the generalized predator-prey model. Hopf (dark gray), saddle-node (light gray) and Bogdanov-Takens (surfaces intersection) bifurcations are drawn in the generalized parameters space $(\mu_{prey}, \delta_{prey}, \gamma_{pred})$ for varying μ_{pred} values. The equilibrium is a saddle below the saddle-node surface and a node or a focus above. This node or focus is unstable below the Hopf surface and stable otherwise. Increasing (decreasing) the time scale ratio τ_{pred}/τ_{prey} decreases (increases) the γ_{pred} values where the Hopf bifurcation takes place proportionally to μ_{pred} value. When $\mu_{pred} = 1$ there is another saddle-node bifurcation at $\delta_{prey} = 0$ (not shown for the sake of visibility). It is in fact a transcritical bifurcation (a degenerated case of saddle-node bifurcation) where the positive equilibrium collides with a trivial equilibrium with no predator and disappears.

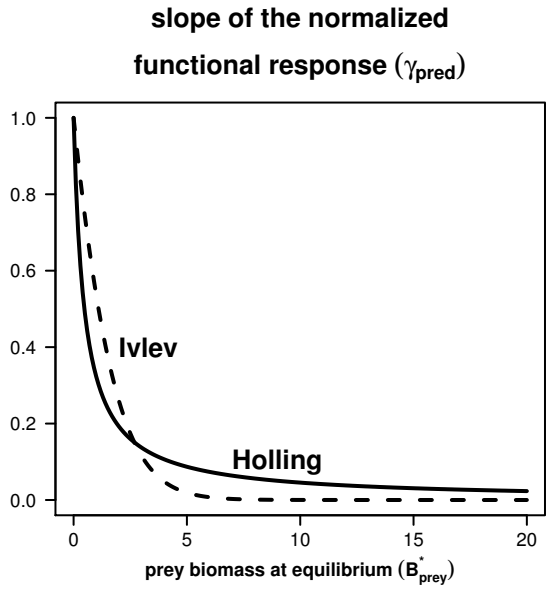

Figure 3.5. Slope of the normalized functional responses (γ_{pred}) used in the model: Holling's disc equation (solid) or Ivlev's functional response (dashed).

changes makes the equilibrium moving from the unstable part of the generalized parameter space (figure 3.4) with Holling's disc equation to the stable part with Ivlev's functional response by crossing the Hopf bifurcation. The increase of μ_{prey} and μ_{pred} can be explained by higher prey and predator biomasses at equilibrium ($\approx +0.1$) with Ivlev's functional response, and thus a higher intra-specific competition. As a consequence, a lower fraction of prey losses are due to predation (lower δ_{prey}). The predator has a stronger response (higher increase of the predation flux) to an increase in prey biomass, as the slope of the functional response near equilibrium is higher with Ivlev's functional response (higher γ_{pred}). Indeed, with this function, the functional response slope is higher within the range of prey biomass at the equilibrium ($B_{prey} \in [0, 2]$, figure 3.5).

3.5 Discussion

3.5.1 Structural sensitivity and model predictions

This chapter shows that the number of attractors (or stable states) is modified if a slight change of functional response formulation occurs. Independently of the functional response formulation, the use of predator quadratic mortality leads to complex system dynamics. Indeed, seven of the twelve generic phase portraits of the predator-prey system display two or three attractors (figure 3.2).

Multiple attractors are found in less than 0.001 % of the parameter space studied with Holling's disc equation and in 1.9 % with Ivlev's functional response (figure 3.3). Fussmann & Blasius (2005) briefly reported a similar situation for Rosenzweig & MacArthur's model. This model has one attractor with Holling's and Ivlev's functional responses, but can have two attractors (an equilibrium and a limit cycle) when the functional response is a hyperbolic tangent function.

Changes in the number of attractors come in addition to changes in attractor type (equilibrium vs. limit cycle). These changes are partly due to differences in local slope of the functional response, as it has been previously reported (Oaten & Murdoch, 1975, Myerscough *et al.*, 1996, Fussmann & Blasius, 2005, Cordoleani *et al.*, 2011, Yeakel *et al.*, 2011, Adamson & Morozov, 2012). We highlighted this effect by studying a generalized predator-prey model. A continuous change in model formulation makes the model exhibits a Hopf bifurcation which destabilizes the equilibrium and gives birth to a stable limit cycle. This bifurcation explains why in 35.9 % of the parameter space explored, the (unique) attractor is a limit cycle with Holling's disc equation and an equilibrium with Ivlev's functional response (figure 3.3).

Both effects of functional response formulation (number and type of attractor(s)) interact to create different system dynamics (figure 3.3). So depending on the formulation, the model can predict very different system responses to disturbances. Disturbances can affect either a parameter or a state variable (Beisner *et al.*, 2003). Figure 3.6 shows an example of model predictions with changing prey carrying capacity due to prey resource(s) and/or habitat alteration. Similarly, figure 3.7 shows another example with changes in prey biomass like a spike of harvesting or introduction of individuals. In both examples, Holling's disc equation predicts a higher system resilience. Indeed, Ivlev's functional response predicts that disturbance puts the system in an alternative stable state. Escaping this alternative state requires a larger modification than going backward (hysteresis phenomena). Such hysteresis phenomena are not predicted by Holling's disc equation because the model has only one attractor with this formulation. In these two examples, state variable and parameter alterations, the system is still deterministic. If a stochastic effect like individual variability was included, a perturbation driving one population close to zero (once or frequently) could lead to species extinction(s).

We studied structural sensitivity by considering two classical type-II functional responses: Holling (1959b, 1965) and Ivlev (1955). A mixed functional response $G^x := xG^H + (1-x)G^I$ can be built to continuously switch between formulations (Cordoleani *et al.*, 2011). Bifurcations that occur during this continuous switch (through the mixing parameter x) explain differences between bifurcation diagrams obtained for different formulations. Nevertheless, the bifurcation analysis of the predator-prey model becomes three-dimensional with respect to parameters (chapter 4), which is beyond the scope of this chapter.

In order to quantify structural sensitivity, Cordoleani *et al.* (2011) compared a distance between model formulations and a distance between model outputs. The strength of this approach is to quantify both quantitative and qualitative changes of the stable state. In the light of our findings, this approach can be extended to quantify different aspects of structural sensitivity, such as changes in the number of stable states and system resilience in situations with hysteresis phenomena (chapter 6).

3.5.2 Combining generalized and specific models

Using a generalized predator-prey model, we found that equilibria in the considered class of model are stabilized by (i) a high slope of the functional response, and (ii) losses mainly driven by density-dependent per-capita intrinsic mortality for both species. In the limit case where predator mortality is linear, these results are consistent with those obtained by Yeakel *et al.* (2011) in a similar model. As stated in the section on generalized modelling, up to two limit cycles can exist in Bazykin's model, which exhibits bifurcations involving periodic orbits (limit point of cycles, homoclinic loops). However, the study of periodic orbits using generalized models is more difficult, even for predator-prey models (Kuehn & Gross, 2011).

We want to highlight the usefulness of studying both a generalized model and specific models belonging to the family represented by the generalized model. The generalized model provides local but generic results on equilibria stability. On the other hand, a specific model provides a specific but global understanding of system dynamics, including periodic orbits and the co-existence of multiple attractors. The generalized model helps to understand the specific model. We used this framework to understand the effects of changing the functional response formulation on equilibria stability. At the opposite, the specific model also helps the interpretation of the generalized model (as also argued by Yeakel *et al.*, 2011). For example, a saddle-node bifurcation in the generalized model is in fact a transcritical bifurcation (a degenerated case of saddle-node bifurcation) where the positive equilibrium disappears (see figure 3.4). Indeed, with the generalized model we suppose that a positive equilibrium exists and thus we cannot focus on its existence conditions. For example, a high slope of the functional response means a higher stability of positive equilibria, but also low prey biomass and potentially predator extinction. This last point cannot be captured by generalized modelling. Positive equilibria with such low prey biomass can exist for some specific models represented by the generalized model. Nevertheless, the distribution of generalized parameter values among all specific models may not be uniform.

From a biological point of view, a specific model allows more insights as processes are explicitly modelled, but a generalized model requires less knowledge of the system to model. Indeed,

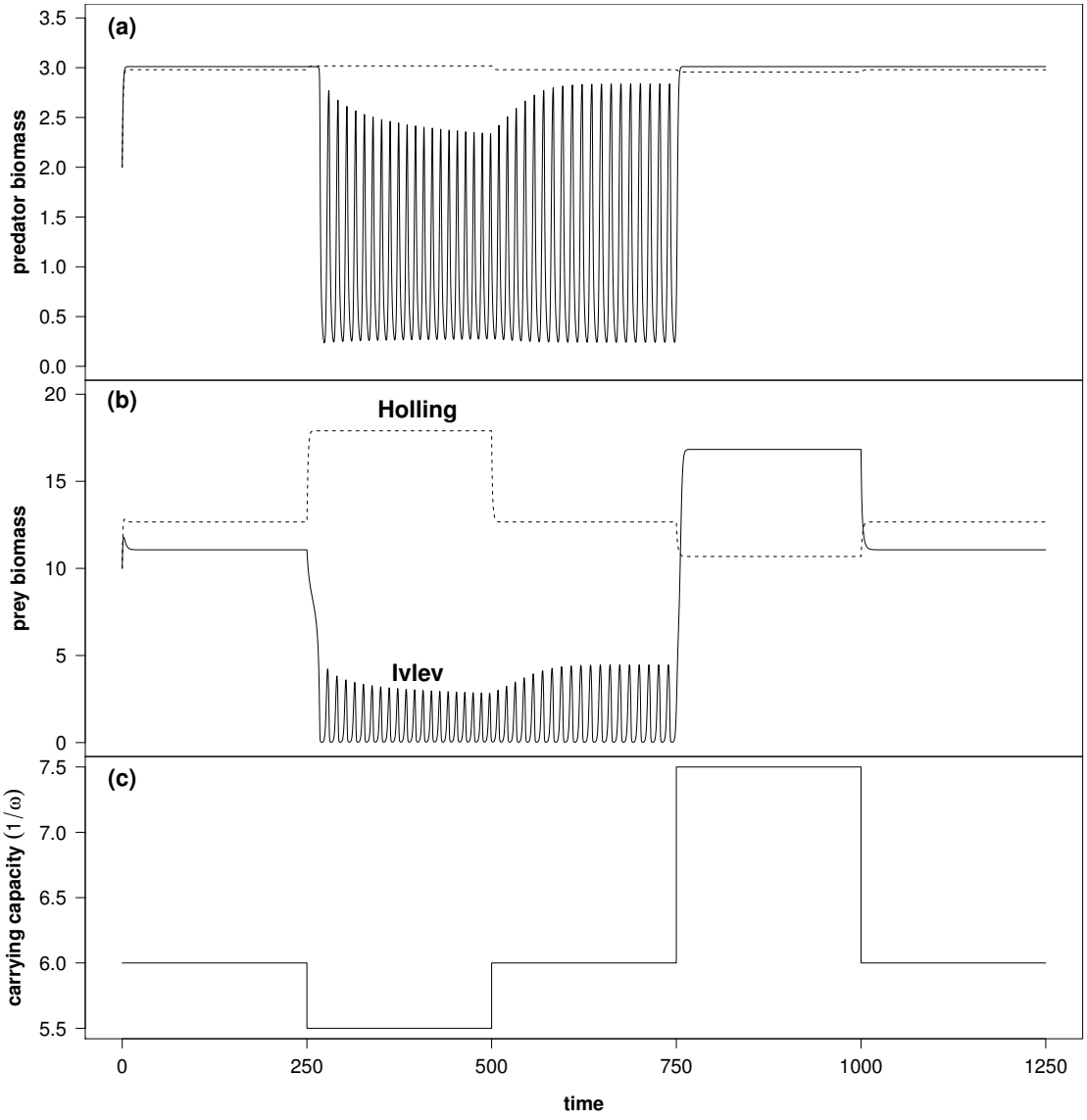

Figure 3.6. Model predictions with disturbances as changes in environmental conditions for both functional responses. Predator (a) and prey (b) dynamics are shown for Holling's disc equation (dashed) and Ivlev's functional response (plain). Prey carrying capacity (c) is modified every 250 time units by changing the environmental parameter $1/\omega$. First, with $1/\omega = 6$, both formulations predict close dynamics. Then $1/\omega$ is decreased by an external disturbance like prey's resource harvesting or habitat loss. Ivlev's functional response predicts that the system reaches an alternative stable state but not Hollingi's disc equation (the change is only quantitative). Now, $1/\omega$ is increased to its original value to end disturbance. While Holling's disc equation predicts a full system recovery, Ivlev's functional response predicts that the system stays trapped in its alternative stable state (hysteresis phenomena). To escape this alternative state, a larger increase of $1/\omega$ is required to destroy this alternative state ($1/\omega$ crosses a bifurcation threshold). Then, after $1/\omega$ is decreased to its original value, Ivlev's functional response predicts that the system goes back to its original state. Parameter value: $\log_{10}(M_{pred}/M_{prey}) = 0.45$. Initial conditions: $B_{prey}(0) = 10$, $B_{pred}(0) = 2$.

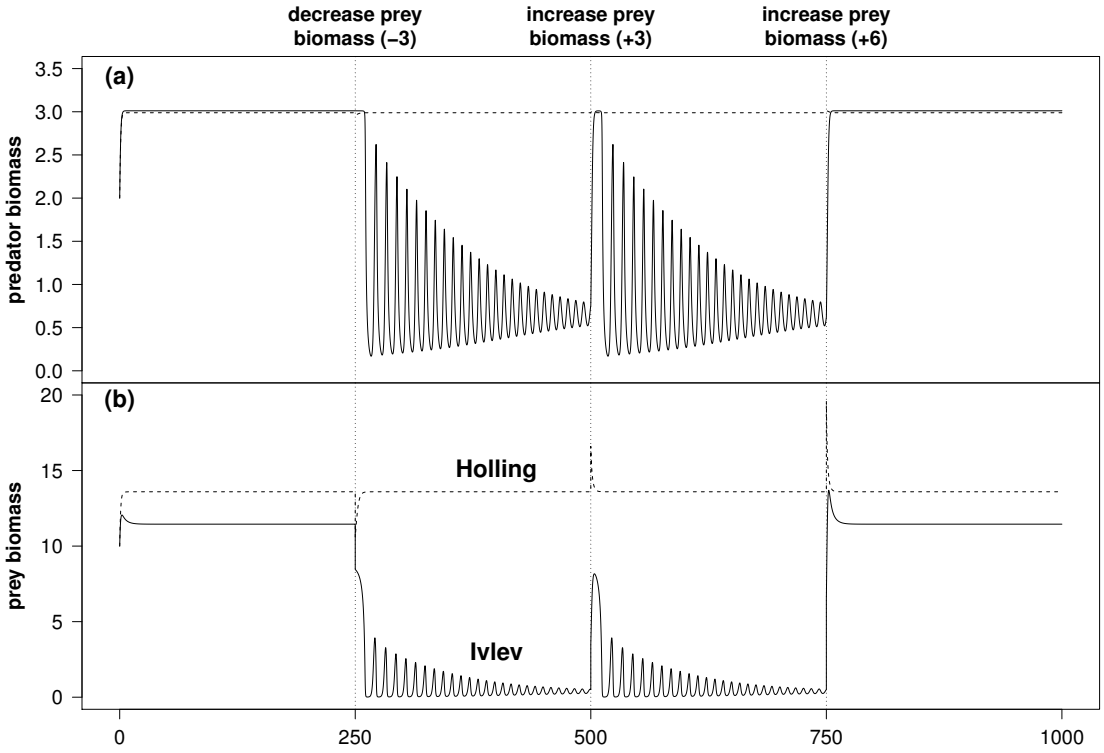

Figure 3.7. Model predictions with disturbances as prey biomass alterations for both functional responses. Predator (a) and prey (b) dynamics are shown for Holling's disc equation (dashed) and Ivlev's functional response (plain). Prey biomass is instantaneously changed every 250 time units. First, both formulations predict close dynamics. Then prey biomass is decreased (-3 biomass units) by an external disturbance like harvesting or a contamination spike. Holling's disc equation predicts (for this alteration and the next ones) that the system goes back to its original state. At the opposite, Ivlev's functional response predicts that the system moves towards an alternative stable state. To escape this alternative state, the increase in prey biomass (e.g. by individuals introduction) has to be larger than the absolute value of the original decrease (hysteresis phenomena). Parameter values: $1/\omega = 6.7$, $\log_{10}(M_{pred}/M_{prey}) = 0.2$. Initial conditions: $B_{prey}(0) = 10$, $B_{pred}(0) = 2$.

generalized modelling describes processes near equilibrium, without specific assumptions on these processes far from this focal equilibrium. In the example of functional response, the generalized model needs only a knowledge of its slope near equilibrium, which can be estimated from empirical data. However, this knowledge allows to predict only system dynamics near equilibrium. Knowing system dynamics far from this equilibrium can be of interest to predict system response to external disturbances (like in figures 3.6-3.7). Such dynamics can be figured out under the assumption that they might be quite simple, for example that there is only one equilibrium. However, more complex dynamics cannot be figured out from the local knowledge of the system near equilibrium. A deeper knowledge of the system is required, like an accurate functional response formulation. In this situation, we leave the generic approach of generalized modelling to study a specific system based on more restrictive assumptions. How far these restrictive assumptions are accurate in the context of the system to model, and how uncertainties in these assumptions influence model predictions, are questions that lead to the study of structural sensitivity.

3.6 Conclusion

We investigated structural sensitivity in a predator-prey model with density-dependent mortality using a bifurcation analysis. The bifurcation diagram, drawn with respect to prey carrying capacity and species body mass ratio, is modified by the choice functional response formulation between close ones in two ways. First, there is a unique stable limit cycle in a smaller part of the parameter space with Ivlev's formulation than with Holling's disc equation. Using generalized modelling, we highlighted the importance of the slope of the functional response in this difference, as it has been previously reported for simpler predator-prey and food chain models. Second, with Ivlev's functional response, dynamics with multiple attractors occur in a significant part of the parameter space where only one attractor exists with Holling's disc equation. With Ivlev's functional response there can be multiple stable states and hysteresis when disturbance appears, whereas there is no such situation with Holling's disc equation.

Because of intrinsic data variability and because model formulation is always a simplified representation of complex biological processes, the choice of the functional response remains uncertain. Here we showed that this uncertainty in the formulation can lead to uncertainties in model predictions through (i) the kind of stable state (equilibrium vs. fluctuations) the system will reach, (ii) the number of alternative stable states, and as a consequence (iii) the system resilience in case of external disturbances. This work rises questions about the choice of functional response formulation in a given situation. For example, how to select a function with enough mechanistic

basis to be more relevant than other ones, while being sufficiently simple and generic? Other questions are: (i) how much complex ecological models can be affected by this sensitivity to model formulation? and (ii) how to deal with these uncertainties in model predictions? This last point can be a challenging way of research for a better assessment of model uncertainties and thus more accurate predictions.

Appendices: Structural sensitivity and resilience in a predator-prey model

3.7 Parameters estimation for Ivlev's functional response

Ivlev's functional response (Ivlev, 1955) was parameterized using the same procedure as in a related study on food web models (chapter 5). Parameter values are set in order to minimize:

$$S\left(a^I, h^I\right) = d^2\left(G^H, G^I\right) = \int_0^{B_{res}} w_{\mathcal{P}}(B_{prey}) \left(G^H(B_{prey}) - G^I(B_{prey})\right)^2 dB_{prey}, \tag{3.7}$$

with a weighting function:

$$w_{\mathcal{P}}(B_{prey}) = \frac{1}{S_{max} B_{res}} \sum_{n=1}^{N} n \text{ with } N = \min\left(\lfloor B_{res}/B_{prey} \rfloor, S_{max}\right). \tag{3.8}$$

This decreasing function gives more weight to low B_{prey} values. Minimizing function (3.7) using $S_{max} = 60$ and $B_{res} = 500$ give the values: $a^I = 3.17$ and $h^I = 0.36$ (simplex method, Nelder & Mead, 1965).

As the functional response is also used to model resource consumption by the prey (q^ϕ), the fit between functional responses is realized over a range of prey biomass $[0, B_{res}] = [0, 500]$. In our study, prey biomass ranges between 0 and $K \approx 62$ (as $1/\omega = 20$ in table 2 of the manuscript). However, our conclusions are not due to an artifact in the fitting range. Indeed, bifurcation diagrams exploring all this range of prey biomass (from 0 to $K \approx 620$ for $1/\omega = 200$) present the same qualitative results in terms of (i) stable equilibrium vs. stable limit cycle, and (ii) presence of multiple attractors (figure 3.8).

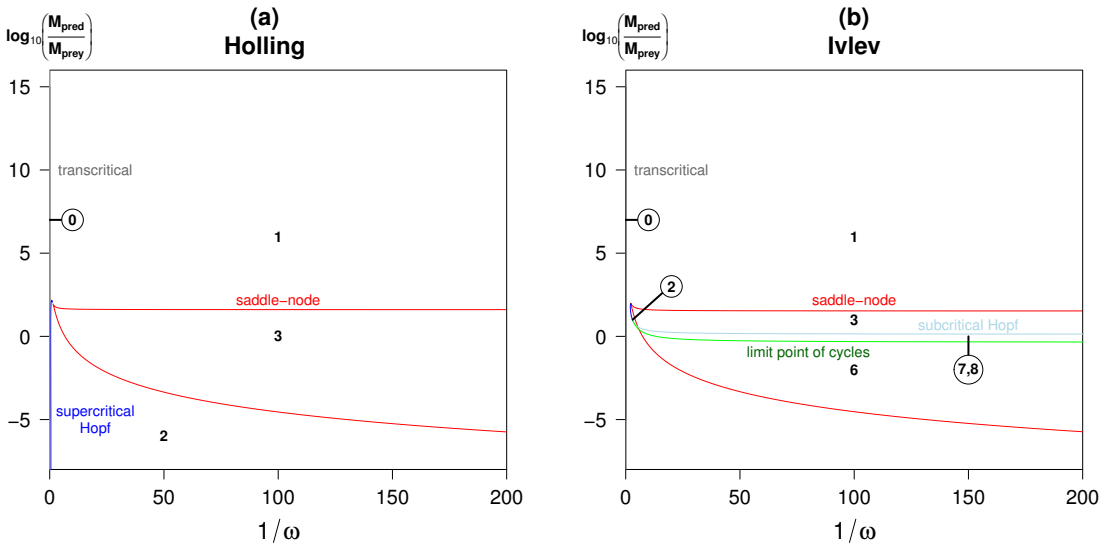

Figure 3.8. Two-dimensional bifurcation diagram (without homoclinic bifurcations) of the specific predator-prey model using the functional response proposed by: (a) Holling or (b) Ivlev. Bifurcation diagrams depend on $1/\omega$ (which is proportional to the prey carrying capacity) and the species body mass ratio M_{pred}/M_{prey}. In each diagram, codimension-one bifurcation curves separate areas of qualitatively different phase portraits. The number in each area indicates the corresponding phase portrait in figure 2 of the manuscript. The different types of codimension-one bifurcation curves are indicated in different colors. Codimension-two bifurcation points are not indicated and are the same as in figure 3 of the manuscript.

3.8 Homoclinic bifurcation curves

The following interpretations are based on a homotopy approach with the bifurcation diagram presented by Kuznetsov (2004), as well as logical requirements for the consistency of transition between phases portraits. We start by discussing the situation with Holling's disc equation. The homoclinic bifurcation curve starting from the Bogdanov-Takens point stays close to the subcritical Hopf curve and then turns clockwise to be close to the top branch of the saddle-node bifurcation curve. Next it turns clockwise again such that it stays close to the limit point of cycles curve. This one ends when the two curves collide. This branch of the homoclinic curve is associated to a "big" homoclinic loop (the limit cycle in phase portrait 10 collides with the saddle). It continues until it reaches the bottom branch of the saddle-node curve and follows it in the rest of the diagram. By homotopy with the bifurcation diagram presented by Kuznetsov (2004), it is likely that branches of the homoclinic curve close to a saddle-node curve are in fact homoclinic-to-saddle-node bifurcations. It implies the existence of three non-central homoclinic-to-saddle-node points in the studied parameter region. Two of these points may be located on the top branch

of the saddle-node curve, delimiting respectively the homoclinic bifurcation, homoclinic-to-saddle-node bifurcation and "big" homoclinic bifurcation. This last one may become a homoclinic-to-saddle-node bifurcation through the third of these points on the bottom branch of the saddle-node bifurcation curve. Tests with Ivlev's functional response do not indicate the presence of such situations. The dashed curve in the right panel of figure 2 is a homoclinic bifurcation curve.

3.9 Area computation in bifurcation analysis

To compute the area of the parameter space corresponding to a given dynamics, we start by defining the boundary hull of this area. It is a closed curve C built from bifurcation curves that delimit the area. The area A is then obtained by integrating counter-clockwise the line integral $A = \oint_C x dy$, where $x := 1/\omega$ and $y := \log_{10}(M_{pred}/M_{prey})$. We compute the area where there is a stable limit cycle (phase portrait #2) with Holling's disc equation and a stable equilibrium (phase portrait #1) with Ivlev's functional response. For multiple attractors with Ivlev's functional response, we compute the area of phase portraits #5 to #8. Area of phase portrait #4 cannot be determined accurately as we have a rough estimate of the homoclinic bifurcation curve. In addition, the area of phase portait 6 near the Cusp and Bogdanov-Takens points cannot be computed as this area is too small regarding to the number of points obtained by continuation to approximate bifurcation curves. However, these two areas are neglectible in comparison to the area of phase portrait 6 for instance.

CHAPTER 4

Structural sensitivity: explaining qualitative changes in bifurcations

"The transition [...] is a bifurcation [...] which could be considered as the ultimate organizing center in (the) model"
SM Baer, BW Kooi, YuA Kuznetsov and HR Thieme,
"Multiparametric bifurcation analysis of a basic two-stage population model" (Baer *et al.*, 2006)

The work presented in this chapter is currently adapted to be submitted for publication as:
Aldebert, C., Kooi, BW., Nerini, D., Gauduchon, M., Poggiale, JC. Three-dimensional bifurcation analysis in a predator-prey model with uncertain formulation. *SIAM Journal on Applied Mathematics*

4.1 Introduction

The previous chapter shows how far the qualitative dynamics of a predator-prey model can be affected by a quantitatively small change in model formulation (structural sentivity). Qualitative changes in model dynamics are due to changes in bifurcations location and type (supercritical vs. subcritical). Bifurcations are organizing centers that explain the qualitative dynamics of the model that occur in different areas of the parameter space. While moving some parameter values, the type of a bifurcation may change at a bifurcation of higher codimension (e.g. a Hopf bifurcation switches from subcritical to supercritical at a Bautin bifurcation). Bifurcations of high codimension can be viewed as "super"-organizing centers as their existence implies the presence of bifurcations of lower codimension (e.g. a codimension-two Bogdanov-Takens bifurcation implies the presence of codimension-one fold, Hopf and homoclinic to saddle bifurcations), and thus explain model qualitative dynamics (Kuznetsov, 2004). Changes in model dynamics that occur between different model formulations can be understood through a bifurcation analysis with respect to an additional parameter that makes a smooth transition between model formulations (Cordoleani *et al.*, 2011).

The question we address in this chapter is: which qualitative changes in bifurcations occur with a small change in model formulation, and what are the organizing centers that explain these changes? As an example of application, we consider the problem of functional response formulation in the same predator-prey model as in chapter 3.

Next section explains how the problem of model formulation can be turned into a parameterization problem. The so-called formulation parameter that controls the choice of model formulation is then considered as a bifurcation parameter. This formulation parameter makes a smooth transition between the two-dimensional bifurcation diagrams of each model formulation (presented in figure 3.3). The resulting three-dimensional bifurcation diagram is presented in section 4.3. This diagram involves a codimension-three bifurcation point. The analysis of this codimension-three bifurcation is completed by the derivation of its critical normal form (section 4.4). Then, the bifurcation diagram of this normal form is built using analytical results as long as it is possible (section 4.5). Dynamics of the normal form are then related to the dynamics of the original system, with a focus on functional response formulation. Finally, we go to a wider discussion about bifurcations that can occur in the model. To complete this qualitative analysis of structural sensitivity, we conclude with some perspectives toward methods that quantify structural sensitivity in a more operational point of view.

4.2 From a problem of model formulation to a problem of model parameterization

We consider the same predator-prey model as in chapter 3, after rescaling:

$$\begin{cases} \dfrac{dB_{prey}}{d\bar{t}} &= \left[\lambda\overline{q}^{\phi} - \alpha - \omega\beta B_{prey}\right] B_{prey} - \overline{G}^{\phi}(B_{prey})B_{pred}(M_{pred}/M_{prey})^{-0.25} \\ \dfrac{dB_{pred}}{d\bar{t}} &= \left[\lambda\overline{G}^{\phi}(B_{prey}) - \alpha - \beta B_{pred}\right] B_{pred}(M_{pred}/M_{prey})^{-0.25}. \end{cases} \tag{4.1}$$

The model and its parameterization are described in section 3.2. The predator functional response $\overline{G}^{\phi}$ (amount of prey eaten per unit of predator and per unit of time) is modelled using either Holling's disc equation (Holling, 1959b, 1965) denoted $\overline{G}^{H}$ (Holling's FR) or Ivlev's functional response (Ivlev, 1955) denoted $\overline{G}^{I}$ (Ivlev's FR):

$$\overline{G}^{H}(B_{prey}) = \frac{a^H B_{prey}}{1 + h^H a^H B_{prey}},\ \overline{G}^{I}(B_{prey}) = \frac{1}{h^I}\left(1 - \exp\left(-h^I a^I B_{prey}\right)\right).$$

To allow a smooth transition from one formulation to the other (figure 4.1), we introduce a new functional response formulation:

$$\overline{G}^{\xi}(B_{prey}) = \xi\overline{G}^{H}(B_{prey}) + (1-\xi)\overline{G}^{I}(B_{prey}),$$

which is a weighted mean of Holling's and Ivlev's FRs. Function $\overline{G}^{\xi}$ corresponds to a linear path in a space of functional responses. Moving the formulation parameter $\xi \in [0,1]$ corresponds to a continuous switch from Ivlev's FR ($\xi = 0$) to Holling's FR ($\xi = 1$). This approach was used by Cordoleani *et al.* (2011) to explore structural sensitivity in a simpler predator-prey model. In model (4.1), primary productivity $\overline{q}^{\phi}$ is modelled using the same function as predation, B_{res} being a constant pool of resource:

$$\overline{q}^{H} = \frac{a^H B_{res}}{1 + h^H a^H B_{res}},\ \overline{q}^{I} = \frac{1}{h^I}\left(1 - \exp\left(-h^I a^I B_{res}\right)\right),\ \overline{q}^{\xi} = \xi\overline{q}^{H} + (1-\xi)\overline{q}^{I}.$$

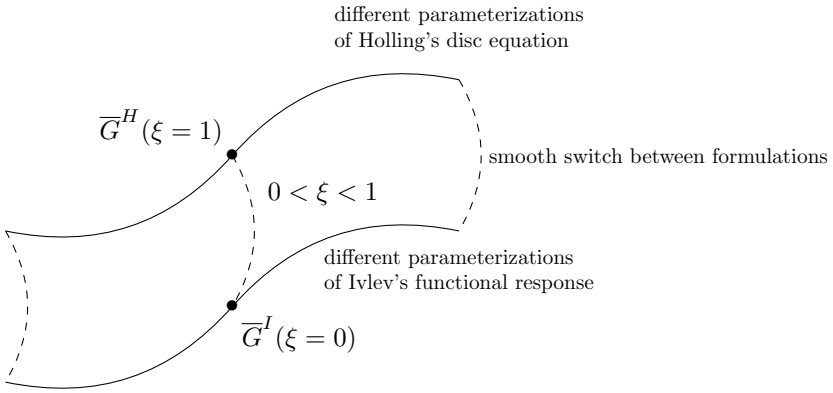

Figure 4.1. Qualitative representation of the functional response in a functional space. When parameter values of Holling's disc equation (resp. Ivlev's functional response) vary, the functional response remains on a particular manifold (here a plain curve) constrains by its mathematical formulation. With any smooth change between mathematical formulations (dashed curve), the functional response explores a wider part of the functional space (here the strip between plain curves). A smooth switch between formulations involves an additional parameter ξ that controls the level of switching. Thus, this approach turns the problem of model formulation into a problem of model parameterization.

4.3 Three-dimensional bifurcation analysis of the predator-prey model

A three-dimensional bifurcation diagram of model (4.1) with respect to $(\xi, 1/\omega, \log_{10}(M_{pred}/M_{prey}))$ is drawn using numerical methods (Matlab toolbox Matcont, Dhooge *et al.*, 2006). Homoclinic bifurcations are estimated by continuing the limit cycle with a fixed, large period close to the global bifurcation (where period tends to infinity). Many mesh points (e.g. 200) are considered for an accurate numerical approximation of the limit cycle.

Due to its complexity, the three-dimensional bifurcation diagram is presented step by step in figures 4.2-4.4 for clarity. Almost all bifurcations are organized around the codimension-three bifurcation point $BT^{=}$ that occurs at $(\xi^{BT^{=}} = 0.801204, 1/\omega^{BT^{=}} = 1.729778, \log_{10}(M_{pred}/M_{prey})^{BT^{=}} = 1.879694)$. A Cusp bifurcation N_e curve passes through $BT^{=}$, allowing the existence of one to three positive equilibria. The triple equilibrium at N_e has a stable (unstable) manifold if $\xi < \xi^{BT^{=}}$ ($\xi > \xi^{BT^{=}}$), the corresponding branch being denoted N_e^s (N_e^u). Starting from N_e, there are two fold bifurcation surfaces T_e. The double equilibrium at T_e has a stable (bifurcation is denoted by T_e^s) or an unstable manifold (bifurcation is denoted by T_e^u), the two cases being delimited by a Bogdanov-Takens bifurcation curve BT on the fold surfaces that passes through $BT^{=}$. The Bogdanov-Takens bifurcation is supercritical BT^{-} (subcritical BT^{+}) if $\xi < \xi^{BT^{=}}$ ($\xi > \xi^{BT^{=}}$) (figure 4.2).

Starting from the supercritical BT^{-} curve (subcritical BT^{+}), a supercritical Hopf bifurcation

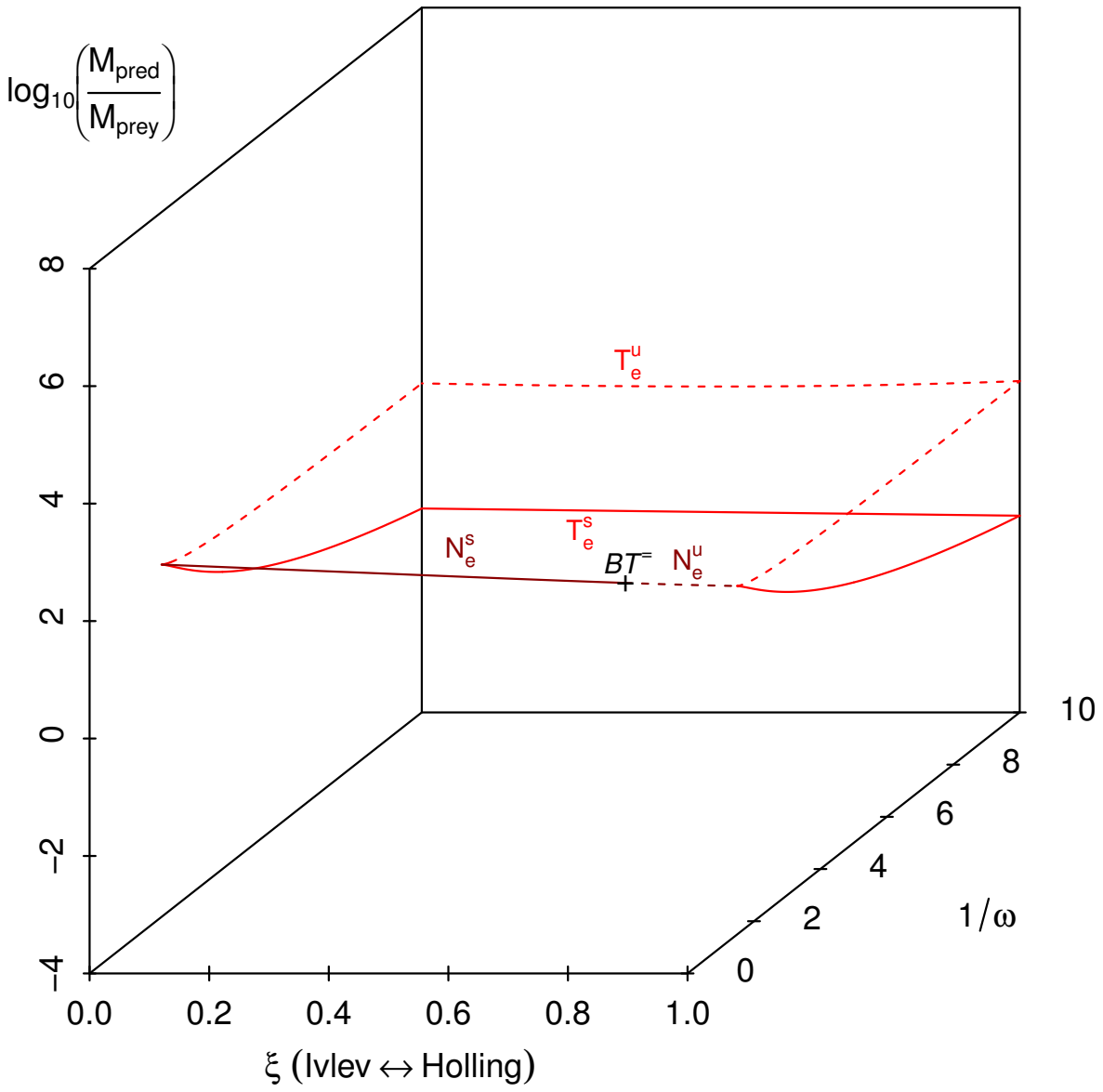

Figure 4.2. Partial three-dimensional bifurcation diagram of the predator-prey model with a continuous switch of functional response formulation from Ivlev's FR ($\xi = 0$) to Holling's FR ($\xi = 1$). Bifurcation diagram also depends on $1/\omega$ (which is proportional to the prey carrying capacity) and the species body mass ratio M_{pred}/M_{prey}. There is one codimension-three bifurcation point, a Bogdanov-Takens bifurcation of triple equilibrium ($BT^{=}$, "+" point). The codimension-two bifurcation curve is a Cusp bifurcation (N_e^u and N_e^s, dark red). The codimension-one bifurcation surface is a tangent bifurcation of equilibria (T_e^+ and T_e^-, red). A superscript "u" (resp. "s") in bifurcation labels indicates that the non-central manifold is unstable (stable) at the bifurcation drawn in dashed (plain) in the figure.

surface H^- (subcritical H^+) gives birth to a stable (unstable) limit cycle (figure 4.3). On the Hopf surface, the transition between the supercritical and the subcritical cases occurs on supercritical two Bautin bifurcation curves B^- (figure 4.4). Note that one of these curves ends at the $BT^=$ point. From each Bautin curve, a surface of tangent bifurcation of cycles T_c^- starts and gives birth to both a stable (outer) and an unstable (inner) limit cycle. Finally, a homoclinic bifurcation surface Hom starts from the BT curve. The types of homoclinic bifurcation that occurs are discussed in section 4.5.6, after the analysis of the normal form of the $BT^=$ bifurcation point.

The slices $\xi = 0$ and $\xi = 1$ in figures 4.2-4.4 are the bifurcation diagrams obtained for Ivlev's FR and Holling's FR respectively (figure 3.3). The main quantitative difference between them is the Hopf bifurcation that wraps in the plane $(1/\omega, \log_{10}(M_{pred}/M_{prey}))$ as ξ decreases ($\xi \in [0.4, 0.6]$ in figure 4.3). Except for the Bautin bifurcation and tangent bifurcation of cycles that occur at low ξ values, all qualitative differences between $\xi = 0$ and $\xi = 1$ are connected to the codimension-three bifurcation point $BT^=$. The codimension-two bifurcation curves associated to this point are shown in figure 4.5. The bifurcations that are connected to the $BT^=$ point indicate that this point is a degenerated Bogdanov-Takens bifurcation of triple point (Kuznetsov, 2004, Baer *et al.*, 2006).

4.4 Reduction to the normal form of the Bogdanov-Takens bifurcation of triple point

To strenghten the previous topological argument, we perform the reduction of the system (4.1) at the point $BT^=$ to its normal form. The work presented in this section has been conducted by Bob Kooi (VU, Amsterdam), who already did a similar study in a model of age-structured population (Baer *et al.*, 2006). Here we summarize the main steps of the procedure.

The parameters are set to their value at the bifurcation $BT^=$. First, the system is scaled to shift the positive equilibrium ($B_{prey}^{BT^=} = 1.495998, B_{pred}^{BT^=} = 2.245037$) to the origin. The obtained system is then projected into its canonical basis, as its Jacobian matrix has an eigenvalue $\lambda_{1,2} = 0$ of multiplicity 2 (Bogdanov-Takens bifurcation). Second, the fourth-order Taylor expansion of the transformed system is performed. This Taylor expansion is rewritten using the fact that the equilibrium is triple (i.e. the Bogdanov-Takens bifurcation is degenerated) and two successive scaling of time and coordinates. The obtained truncated critical normal form is:

$$\begin{cases} \dfrac{dx_1}{dt} &= x_2 \\ \dfrac{dx_2}{dt} &= \beta x_1 x_2 + \epsilon_1 x_1^3 + \epsilon_2 x_1^2 x_2, \end{cases} \tag{4.2}$$

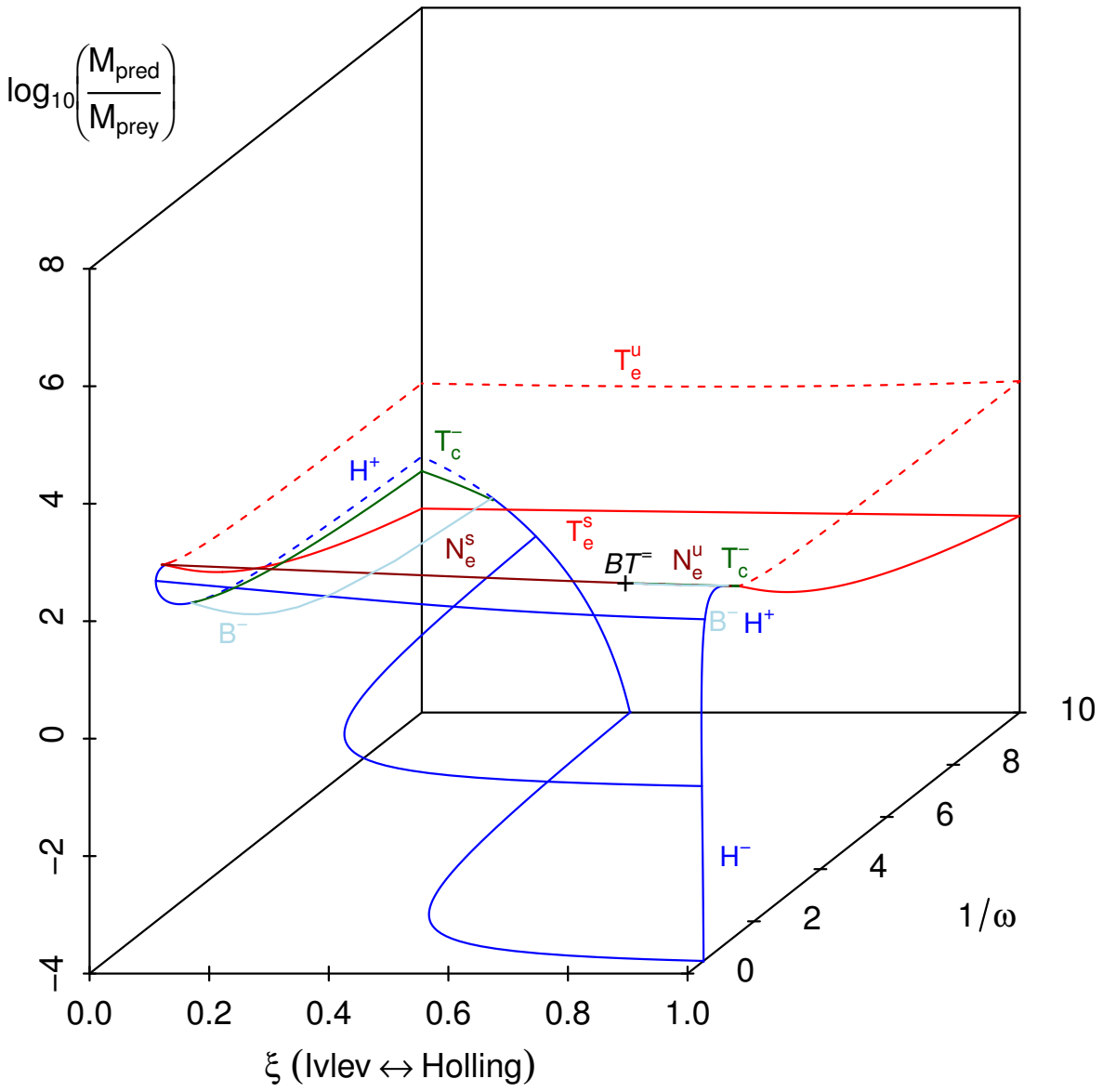

Figure 4.3. Partial three-dimensional bifurcation diagram of the predator-prey model with a continuous switch of functional response formulation from Ivlev's FR ($\xi = 0$) to Holling's FR ($\xi = 1$). Bifurcation diagram also depends on $1/\omega$ (which is proportional to the prey carrying capacity) and the species body mass ratio M_{pred}/M_{prey}. There is one codimension-three bifurcation point, a Bogdanov-Takens bifurcation of triple equilibrium ($BT^{=}$, "+" point). Codimension-two bifurcation curves are a Bautin bifurcation (B^{-}, light blue) and a Cusp bifurcation (N_e^u and N_e^s, dark red). Codimension-one bifurcation surfaces are a tangent bifurcation of equilibria (T_e^+ and T_e^-, red), tangent bifurcations of cycles (T_c^-, green) and a Hopf bifurcation (H^+ and H^-, blue). In bifurcation labels, a superscript "+" (resp. "-") indicates a subcritical (supercritical) bifurcation drawn in dashed (plain) in the figure. For the tangent and Cusp bifurcations of equilibria, a superscript "u" (resp. "s") indicates that the non-central manifold is unstable (stable) at the bifurcation drawn in dashed (plain) in the figure.

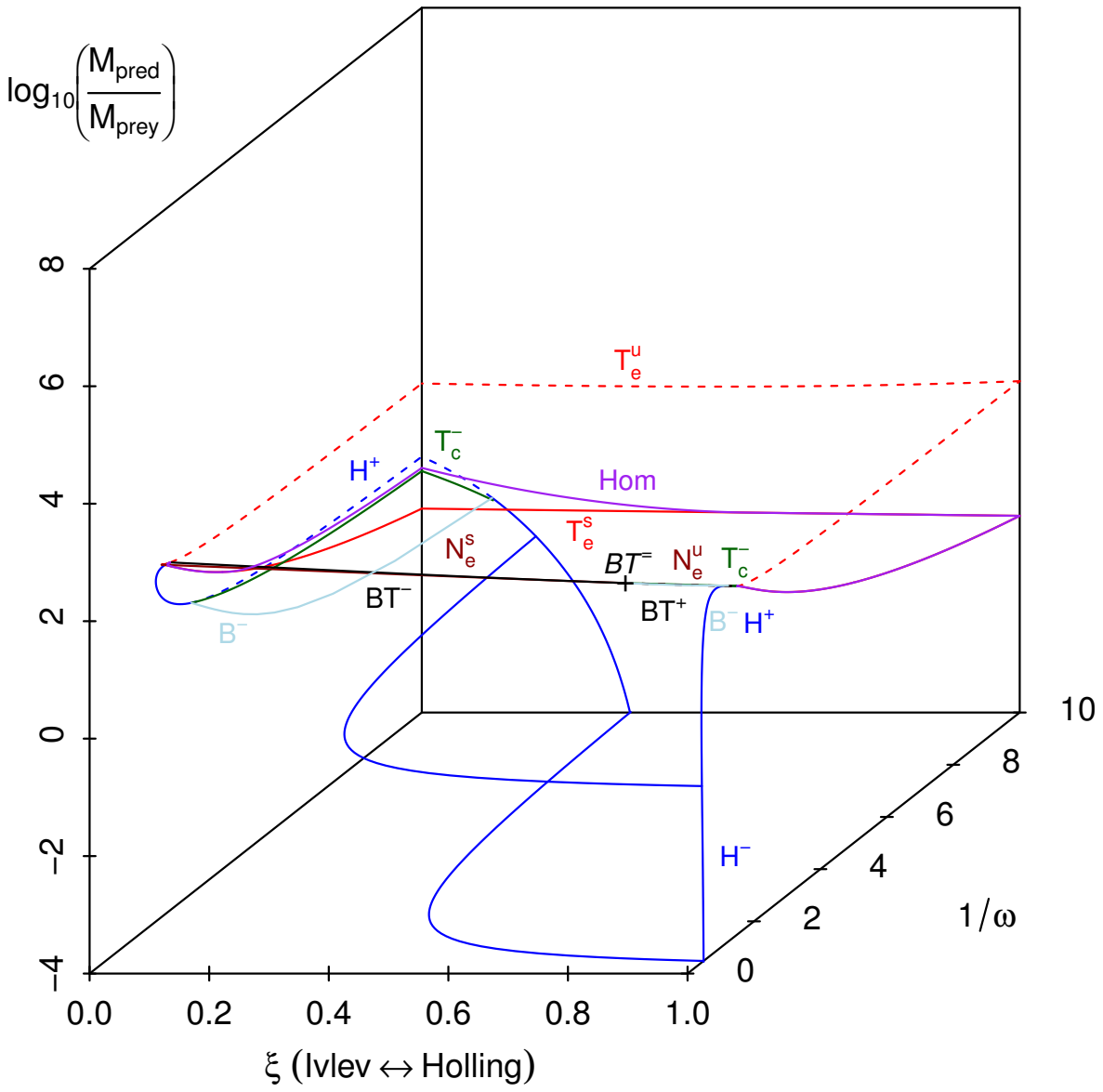

Figure 4.4. Three-dimensional bifurcation diagram of the predator-prey model with a continuous switch of functional response formulation from Ivlev's FR ($\xi = 0$) to Holling's FR ($\xi = 1$). Bifurcation diagram also depends on $1/\omega$ (which is proportional to the prey carrying capacity) and the species body mass ratio M_{pred}/M_{prey}. There is one codimension-three bifurcation point, a Bogdanov-Takens bifurcation of triple equilibrium ($BT^{=}$, "+" point). Codimension-two bifurcation curves are a Bautin bifurcation (B^-, light blue), a Cusp bifurcation (N_e^u and N_e^s, dark red) and a Bogdanov-Takens bifurcation (BT^+ and BT^-, black). Codimension-one bifurcation surfaces are tangent bifurcation of equilibria (T_e^+ and T_e^-, red), tangent bifurcation of cycles (T_c^-, green), Hopf bifurcation (H^+ and H^-, blue) and homoclinic bifurcations (Hom, purple). Homoclinic bifurcation can be of various types (homoclinic to saddle, homoclinic to saddle-node, "big" homoclinic) that are not detailed here. In bifurcation labels, a superscript "+" (resp. "-") indicates a subcritical (supercritical) bifurcation drawn in dashed (plain) in the figure. For the tangent and Cusp bifurcations of equilibria, a superscript "u" (resp. "s") indicates that the non-central manifold is unstable (stable) at the bifurcation drawn in dashed (plain) in the figure.

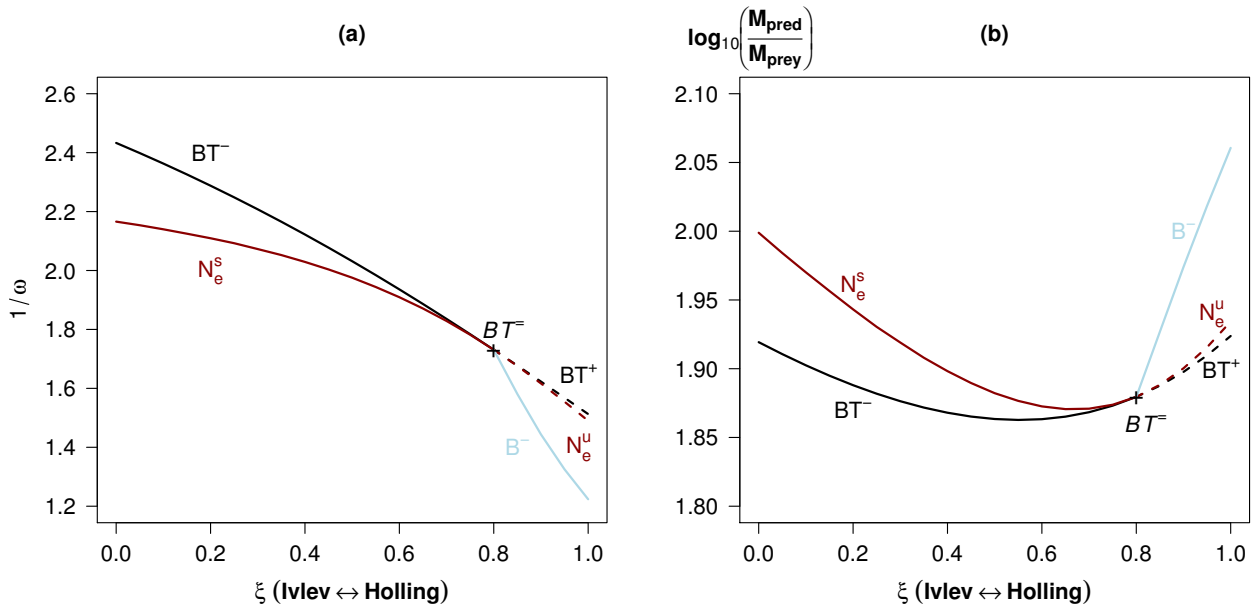

Figure 4.5. Projection of codimension-two bifurcation curves into the planes $(\xi, 1/\omega)$ (a) and $(\xi, \log_{10}(M_{pred}/M_{prey}))$ (b). Labels and colors are the same as in figure 4.4.

where the normal form coefficients $\epsilon_1 = \pm 1$, $\epsilon_2 = \pm 1$ and $\beta \in \mathbb{R}$ depend on coefficients of the Taylor expansion. Note that β does not denote the per-capita density-dependent mortality rate in the remaining of this chapter.

Three topologically different cases have been reported for the Bogdanov-Takens bifurcation of triple equilibrium (Dumortier *et al.*, 1991, p2):

- saddle case with $\epsilon_1 = 1$, any ϵ_2 and β,
- focus case with $\epsilon_1 = -1$ and $0 < \beta < 2\sqrt{2}$, any ϵ_2,
- elliptic case with $\epsilon_1 = -1$ and $2\sqrt{2} < \beta$, any ϵ_2.

Here, we have $\epsilon_1 = \epsilon_2 = -1$ and $\beta = 2.199250 < 2\sqrt{2}$, which corresponds to the focus case.

The truncated critical normal form (4.2) is embedded in the following three-parameter canonical unfolding (Baer *et al.*, 2006):

$$\frac{d\boldsymbol{x}}{dt} = \boldsymbol{f}(\boldsymbol{x}, \boldsymbol{\alpha}) \Leftrightarrow \begin{cases} \dfrac{dx_1}{dt} &= x_2 \\ \dfrac{dx_2}{dt} &= -\alpha_1 - \alpha_2 x_1 + \alpha_3 x_2 + \beta x_1 x_2 - x_1^3 - x_2 x_1^2, \end{cases} \tag{4.3}$$

where $\boldsymbol{x} \in \mathbb{R}^2$ is the vector of state variables and $\boldsymbol{\alpha} \in \mathbb{R}^3$ is the vector of bifurcation parameters. Parameter β remains constant and is assumed to satisfy the focus case conditions. The normal form (4.3) is topologically equivalent to the one presented in Kuznetsov (2004, p386-387).

4.5 Analysis of the canonical unfolding of the Bogdanov-Takens bifurcation of triple point

4.5.1 Equilibria

Differential equations of system (4.3) vanish if:

$$\begin{cases} x_2 = 0 \\ x_1^3 + \alpha_2 x_1 + \alpha_1 = 0. \end{cases} \tag{4.4}$$

At any equilibrium, we have always $x_2^* = 0$, so we focus now on x_1. The second equation of (4.4) has one to three roots. According to Cardano's formula, we have the discriminant:

$$\Delta = -\left(4\alpha_2^3 + 27\alpha_1^2\right).$$

If $\Delta < 0$, there is a unique (real) equilibrium:

$$x_1^{(0)} = \sqrt[3]{\frac{-\alpha_1 + \sqrt{-\Delta/27}}{2}} + \sqrt[3]{\frac{-\alpha_1 - \sqrt{-\Delta/27}}{2}}. \tag{4.5}$$

The superscript in $x_1^{(0)}$ indicates the number of the focus equilibrium (multiple numbers indicate a multiple equilibrium). If $\Delta = 0$ and $\alpha_1 = \alpha_2 = 0$, there is a triple equilibrium $x_1^{(0,1,2)} = 0$. If $\Delta = 0$ with $\alpha_1 \neq 0$ and $\alpha_2 \neq 0$, there are one equilibrium and one double equilibrium:

$$x_1^{(0)} = \frac{3\alpha_1}{\alpha_2},\ x_1^{(1,2)} = \frac{-3\alpha_1}{2\alpha_2}. \tag{4.6}$$

Finally, if $\Delta > 0$, there are three distinct equilibria with $k = 0, 1, 2$:

$$x_1^{(k)} = 2\sqrt{\frac{-\alpha_2}{3}}\cos\left(\frac{1}{3}\arccos\left(\frac{-\alpha_1}{2}\sqrt{\frac{27}{-\alpha_2^3}}\right) + \frac{k2\pi}{3}\right). \tag{4.7}$$

Later, we use $\boldsymbol{x}^*$ when we want to refer to any positive equilibrium of system (4.3).

4.5.2 Fold (tangent) and Cusp bifurcations of equilibria

A fold bifurcation of equilibria T_e is a codimension-one bifurcation that occurs when two equilibria collide and disappear, i.e. when there is a double equilibrium ($\Delta = 0$). Thus, a vector of parameters at a fold bifurcation $\boldsymbol{\alpha}^{T_e}$ has to satisfy:

$$\alpha_1^{T_e} = \pm\frac{2}{3}\alpha_2^{T_e}\sqrt{\frac{-\alpha_2^{T_e}}{3}},\ \forall\alpha_3. \tag{4.8}$$

Another way to find a fold bifurcation of equilibria is by computing the Jacobian matrix of system (4.3):

$$\boldsymbol{f}_{\boldsymbol{x}}(\boldsymbol{x},\boldsymbol{\alpha}) = \begin{pmatrix} 0 & 1 \\ -\alpha_2 + \beta x_2 - 3x_1^2 - 2x_2x_1 & \alpha_3 + \beta x_1 - x_1^2 \end{pmatrix}. \tag{4.9}$$

One can check that $\det(\boldsymbol{f}_{\boldsymbol{x}}(\boldsymbol{x}^{(1,2)},\boldsymbol{\alpha}^{T_e})) = 0$. This implies that the Jacobian matrix:

$$\boldsymbol{f}_{\boldsymbol{x}}(\boldsymbol{x}^{(1,2)},\boldsymbol{\alpha}^{T_e}) = \begin{pmatrix} 0 & 1 \\ 0 & \alpha_3 + \beta x_1^{(1,2)} - x_1^{(1,2)^2} \end{pmatrix}. \tag{4.10}$$

has one real zero eigenvalue, i.e. the first condition for fold-type bifurcation is fulfilled (section 2.3.3).

We now check the genericity conditions of this bifurcation. The real zero eigenvalue of Jacobian matrix (4.10) is associated to the scaled ($\langle \boldsymbol{p},\boldsymbol{q}\rangle = 1$) right and left eigenvectors:

$$\boldsymbol{q} = (1,0)^T, \boldsymbol{p} = \left(1, \frac{-1}{\alpha_3 + \beta x_1^{(1,2)} - x_1^{(1,2)^2}}\right)^T,$$

which satisfy $\boldsymbol{f}_{\boldsymbol{x}}(\boldsymbol{x}^{(1,2)},\boldsymbol{\alpha}^{T_e})\boldsymbol{q} = \boldsymbol{0}$ and $\boldsymbol{p}^T\boldsymbol{f}_{\boldsymbol{x}}(\boldsymbol{x}^{(1,2)},\boldsymbol{\alpha}^{T_e}) = \boldsymbol{0}^T$. To check the transversality condition, we choose α_1 as the bifurcation parameter. As $\boldsymbol{f}_{\alpha_1}(\boldsymbol{x},\boldsymbol{\alpha}) = (0,-1)^T$ and

$$\boldsymbol{p}^T\boldsymbol{f}_{\alpha_1}(\boldsymbol{x}^{(1,2)},\boldsymbol{\alpha}^{T_e}) = 1/(\alpha_3 + \beta x_1^{(1,2)} - x_1^{(1,2)^2}) \neq 0,$$

the transversality condition is fulfilled.

To check the non-degeneracy condition, we need to compute the tensor made of second-order

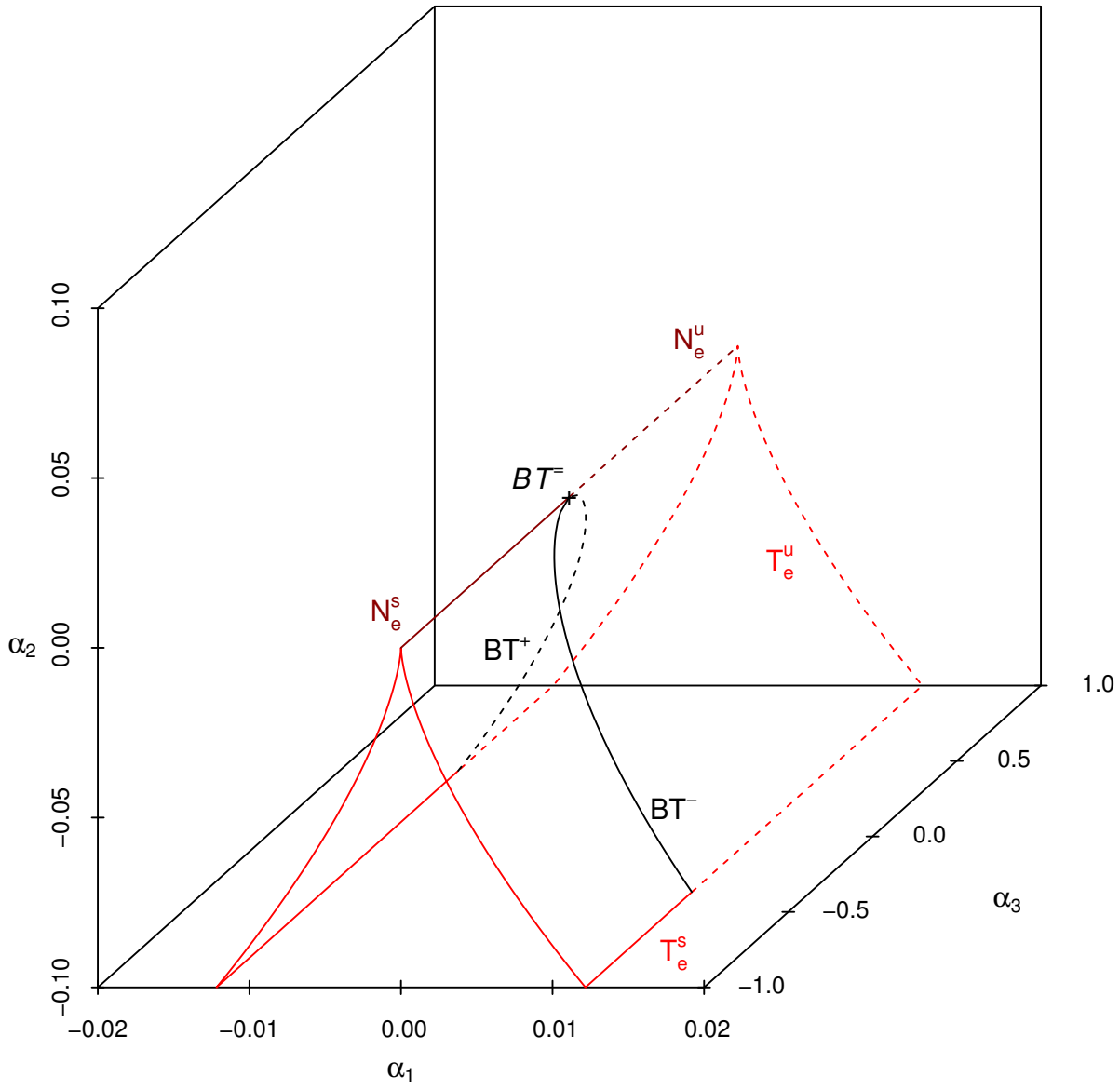

Figure 4.6. Three-dimensional bifurcation diagram (partial) of the normal form of a Bogdanov-Takens bifurcation of triple point ($BT^{=}$) for the focus case. Bifurcation diagram depends on α_1, α_2 and α_3 that serve as unfolding parameters. Codimension-two bifurcation curves are a Cusp bifurcation (N_e^u and N_e^s, dark red) and a Bogdanov-Takens bifurcation (BT^+ and BT^-, black). Codimension-one bifurcation surfaces are tangent bifurcation of equilibria (T_e^+ and T_e^-, red). In bifurcation labels, a superscript "+" (resp. "-") indicates a subcritical (supercritical) bifurcation drawn in dashed (plain) in the figure. For the tangent and Cusp bifurcations of equilibria, a superscript "u" (resp. "s") indicates that the non-central manifold is unstable (stable) at the bifurcation drawn in dashed (plain) in the figure.

partial derivatives of system (4.3) at equilibrium:

$$\boldsymbol{f}_{\boldsymbol{xx}}(\boldsymbol{x}^*, \boldsymbol{\alpha})(\boldsymbol{u}, \boldsymbol{v}) = \begin{pmatrix} 0 \\ -6x_1^* u_1 v_1 + (\beta - 2x_1^*)(u_1 v_2 + u_2 v_1) \end{pmatrix}, \tag{4.11}$$

where $\boldsymbol{u}, \boldsymbol{v} \in \mathbb{R}^2$. Then, the second-order coefficient in the Taylor expansion of the system on the central manifold is:

$$b := \frac{1}{2}\boldsymbol{p}^T \boldsymbol{f}_{\boldsymbol{xx}}(\boldsymbol{x}^{(1,2)}, \boldsymbol{\alpha}^{T_e})(\boldsymbol{q}, \boldsymbol{q}) = \frac{3x_1^{(1,2)}}{\alpha_3 + \beta x_1^{(1,2)} - {x_1^{(1,2)}}^2} = \frac{3x_1^{(1,2)}}{\mathrm{Tr}\left(\boldsymbol{f}_{\boldsymbol{x}}(\boldsymbol{x}^{(1,2)}, \boldsymbol{\alpha}^{T_e})\right)}.$$

This coefficient is defined for $\boldsymbol{\alpha} \in \mathbb{R}^3_*$, $\boldsymbol{\alpha} = \mathbf{0}$ being the degenerated Bogdanov-Takens bifurcation point. The coefficient b can be infinite but does not vanish as long as $x_1^{(1,2)} \neq 0$, which means that the fold bifurcation is generic. The bifurcation becomes non-generic ($b = 0$) only if $\alpha_1 = \alpha_2 = 0$, which means that the equilibrium is triple ($x_1^{(1,2,3)} = 0$), i.e. the system exhibits a Cusp bifurcation.

A Cusp bifurcation of equilibria N_e (codimension two) is a degenerated fold bifurcation that occurs when there is a triple equilibrium, i.e. when $\Delta = 0$ and $\alpha_1 = \alpha_2 = 0, \forall \alpha_3$. One can check that the two saddle-node surfaces meet at the Cusp curve which also fulfills the same transversality condition as the fold bifurcation.

To check the non-degeneracy condition of the Cusp bifurcation, we need to go deeper in the approximation of model dynamics on the central manifold of the fold bifurcation (Kuznetsov, 2004, section 5.4). We first compute the vector of quadratic coefficients in the approximation of model dynamics in the non-central subspace:

$$\boldsymbol{a} := \boldsymbol{f}_{\boldsymbol{xx}}(\boldsymbol{x}^{(1,2)}, \boldsymbol{\alpha}^{T_e})(\boldsymbol{q}, \boldsymbol{q}) - \boldsymbol{p}^T \boldsymbol{f}_{\boldsymbol{xx}}(\boldsymbol{x}^{(1,2)}, \boldsymbol{\alpha}^{T_e})(\boldsymbol{q}, \boldsymbol{q})\boldsymbol{q} = \begin{pmatrix} \dfrac{6x_1^{(1,2)}}{\alpha_3 + \beta x_1^{(1,2)} - {x_1^{(1,2)}}^2} \\ 6x_1^{(1,2)} \end{pmatrix}.$$

The equation:

$$\boldsymbol{f}_{\boldsymbol{x}}(\boldsymbol{x}^{(1,2)}, \boldsymbol{\alpha}^{T_e})\boldsymbol{\omega_2} = -\boldsymbol{a},$$

together with the requirement that $\langle \boldsymbol{p}, \boldsymbol{\omega_2} \rangle = 0$ ($\boldsymbol{\omega_2}$ belongs to the non-central subspace) has a unique solution:

$$\boldsymbol{\omega_2} = \frac{-6x_1^{(1,2)}}{\alpha_3 + \beta x_1^{(1,2)} - {x_1^{(1,2)}}^2} \begin{pmatrix} \dfrac{1}{\alpha_3 + \beta x_1^{(1,2)} - {x_1^{(1,2)}}^2} \\ 1 \end{pmatrix},$$

which is the second-order coefficient of the Taylor approximation of the central manifold. We also need the tensor made of third-order partial derivatives of system (4.3) at equilibrium:

$$\boldsymbol{f}_{\boldsymbol{xxx}}(\boldsymbol{x},\boldsymbol{\alpha})(\boldsymbol{u},\boldsymbol{v},\boldsymbol{w}) = \begin{pmatrix} 0 \\ -2(u_1v_1w_2 + u_1v_2w_1 + u_2v_1w_1) - 6u_1v_1w_1 \end{pmatrix}, \tag{4.12}$$

where $\boldsymbol{u},\boldsymbol{v},\boldsymbol{w} \in \mathbb{R}^2$. The third-order coefficient in the Taylor expansion of the system on the central manifold of the Cusp bifurcation is:

$$c := \frac{1}{6}\boldsymbol{p}^T \boldsymbol{f}_{\boldsymbol{xxx}}(\boldsymbol{x}^{(1,2,3)},\boldsymbol{\alpha}^{N_e})(\boldsymbol{q},\boldsymbol{q},\boldsymbol{q}) + \frac{1}{2}\boldsymbol{p}^T \boldsymbol{f}_{\boldsymbol{xx}}(\boldsymbol{x}^{(1,2)},\boldsymbol{\alpha}^{T_e})(\boldsymbol{q},\boldsymbol{\omega_2}) = \frac{1}{\alpha_3} \neq 0.$$

Thus, the non-degeneracy condition of the Cusp bifurcation is fulfilled. Note that $c \to \pm\infty$ for $\boldsymbol{\alpha} \to \boldsymbol{0}$, i.e. at the degenerated Bogdanov-Takens bifurcation.

For both Cusp and fold bifurcations, the dynamics of the system outside the central manifold is discussed later (see figure 4.6 for an overview of the results). These dynamics can be infered using topological arguments on the link between bifurcations. Thus, we have to wait for the results on other bifurcations that occur in the system.

4.5.3 Bogdanov-Takens bifurcation

A Bogdanov-Takens bifurcation occurs when the Jacobian matrix (4.9) evaluated at the double equilibrium $\boldsymbol{x}^{(1,2)}$ has two real zero eigenvalues. In planar systems, this condition is satisfied when $\mathrm{Tr}(\boldsymbol{f}_{\boldsymbol{x}}(\boldsymbol{x}^{(1,2)},\boldsymbol{\alpha}^{\boldsymbol{BT}})) = 0$ and $\det(\boldsymbol{f}_{\boldsymbol{x}}(\boldsymbol{x}^{(1,2)},\boldsymbol{\alpha}^{\boldsymbol{BT}})) = 0$. Solving $\mathrm{Tr}(\boldsymbol{f}_{\boldsymbol{x}}(\boldsymbol{x}^{(1,2)},\boldsymbol{\alpha}^{\boldsymbol{BT}})) = 0$ leads to:

$$\alpha_3^{BT} = \frac{3\alpha_1^{BT}}{2\alpha_2^{BT}}\left(\beta + \frac{3\alpha_1^{BT}}{2\alpha_2^{BT}}\right).$$

Using the condition for a fold bifurcation (4.8), the previous condition simplifies into:

$$\alpha_3^{BT} = \pm\beta\sqrt{\frac{-\alpha_2^{BT}}{3}} - \frac{\alpha_2^{BT}}{3}.$$

This condition together with (4.8) defines a Bogdanov-Takens bifurcation curve (figure 4.6).

The Jacobian matrix evaluated at the Bogdanov-Takens bifurcation is:

$$\boldsymbol{f}_{\boldsymbol{x}}(\boldsymbol{x}^{(1,2)},\boldsymbol{\alpha}^{BT}) = \begin{pmatrix} 0 & 1 \\ 0 & 0 \end{pmatrix}.$$

Let us define the map:

$$\boldsymbol{F}(\boldsymbol{x},\boldsymbol{\alpha}) = (\boldsymbol{f}(\boldsymbol{x},\boldsymbol{\alpha}), \mathrm{Tr}(\boldsymbol{f}_{\boldsymbol{x}}(\boldsymbol{x},\boldsymbol{\alpha})), \det(\boldsymbol{f}_{\boldsymbol{x}}(\boldsymbol{x},\boldsymbol{\alpha})))^T, \tag{4.13}$$

and consider α_1 and α_2 as bifurcation parameters. One can check that:

$$\det(\boldsymbol{F}_{\boldsymbol{y}}(\boldsymbol{x}^{(1,2)}, \boldsymbol{\alpha}^{BT})) = \beta - 2x_1^{(1,2)}, \tag{4.14}$$

with $\boldsymbol{y} = (x_1, x_2, \alpha_1, \alpha_2)^T$. At the degenerated Bogdanov-Takens point, the determinant (4.14) equals $\beta > 0$. By continuity of equilibrium value, this determinant remains strictly positive at least in a given neighborhood of the degenerated Bogdanov-Takens point. In this neighborhood, the matrix $\boldsymbol{F}_{\boldsymbol{y}}(\boldsymbol{x}^{(1,2)}, \boldsymbol{\alpha}^{BT})$ is invertible and the map (4.13) is regular at the Bogdanov-Takens bifurcation, which is a genericity condition for this bifurcation (Kuznetsov, 2004, p323).

To check the other genericity conditions, we need the generalized eigenvectors:

$$\boldsymbol{q_0} = \boldsymbol{p_0} = (1,0)^T,\ \boldsymbol{q_1} = \boldsymbol{p_1} = (0,1)^T,$$

that are solutions of:

$$\boldsymbol{f}_{\boldsymbol{x}}(\boldsymbol{x}^{(1,2)}, \boldsymbol{\alpha}^{BT})\boldsymbol{q_0} = \boldsymbol{0},\ \boldsymbol{f}_{\boldsymbol{x}}(\boldsymbol{x}^{(1,2)}, \boldsymbol{\alpha}^{BT})\boldsymbol{q_1} = \boldsymbol{q_0},$$

$$\boldsymbol{p_1}^T \boldsymbol{f}_{\boldsymbol{x}}(\boldsymbol{x}^{(1,2)}, \boldsymbol{\alpha}^{BT}) = \boldsymbol{0}^T,\ \boldsymbol{p_0}^T \boldsymbol{f}_{\boldsymbol{x}}(\boldsymbol{x}^{(1,2)}, \boldsymbol{\alpha}^{BT}) = \boldsymbol{p_1}^T,$$

and that satisfy:

$$\langle \boldsymbol{p_0}, \boldsymbol{q_0} \rangle = \langle \boldsymbol{p_1}, \boldsymbol{q_1} \rangle = 1,\ \langle \boldsymbol{p_0}, \boldsymbol{q_1} \rangle = \langle \boldsymbol{p_1}, \boldsymbol{q_0} \rangle = 0.$$

Thus, we can compute the following coefficients (Kuznetsov, 2004, p377):

$$a := \frac{1}{2}\boldsymbol{p_1}^T \boldsymbol{f}_{\boldsymbol{xx}}(\boldsymbol{x}^{(1,2)}, \boldsymbol{\alpha}^{BT})(\boldsymbol{q_0}, \boldsymbol{q_0}) = -3x_1^{(1,2)},$$

$$b := \boldsymbol{p_0}^T \boldsymbol{f}_{\boldsymbol{xx}}(\boldsymbol{x}^{(1,2)}, \boldsymbol{\alpha}^{BT})(\boldsymbol{q_0}, \boldsymbol{q_0}) + \boldsymbol{p_1}^T \boldsymbol{f}_{\boldsymbol{xx}}(\boldsymbol{x}^{(1,2)}, \boldsymbol{\alpha}^{BT})(\boldsymbol{q_0}, \boldsymbol{q_1}) = \beta - 2x_1^{(1,2)}.$$

The coefficient b equals the determinant (4.14). So, it is strictly positive at least in a given neighborhood of the degenerated Bogdanov-Takens point. The coefficient a vanishes only at the degenerated Bogdanov-Takens point, where the genericity condition $a \neq 0$ is violated. In a given neighborhood of this point (because of the other genericity conditions), the Bogdanov-Takens bifurcation is generic. From the equilibrium value (4.6), we know that the Bogdanov-Takens

bifurcation is supercritical ($a < 0$) for $\alpha_1^{BT} > 0$ (and $\alpha_3^{BT} < 0$) and subcritical ($a > 0$) for $\alpha_1^{BT} < 0$ (and $\alpha_3^{BT} > 0$, figure 4.6).

4.5.4 Hopf and Generalized Hopf (Bautin) bifurcations

A Hopf bifurcation is a codimension-one bifurcation that occurs if the Jacobian matrix evaluated at an equilibrium $\boldsymbol{x}^*$ for some parameter values $\boldsymbol{\alpha^H}$ has a pair of conjugated and pure imaginary eigenvalues. This can be detected in planar systems by solving $\mathrm{Tr}(\boldsymbol{f_x}(\boldsymbol{x}^*, \boldsymbol{\alpha^H})) = 0$ with the constraint $\det(\boldsymbol{f_x}(\boldsymbol{x}^*, \boldsymbol{\alpha^H})) > 0$. Solving the trace condition gives:

$$\alpha_3^H = x_1^{*2} - \beta x_1^*. \tag{4.15}$$

The graph of this condition is a surface (figure 4.7), drawn by replacing x_1^* by the different possible equilibrium values (4.5-4.7).

One can check that the Hopf surface passes through the Bogdanov-Takens bifurcation curve. If $\alpha_1 = \alpha_3 = 0$ and $\alpha_2 > 0$, the only equilibrium of system (4.3) is $\boldsymbol{x_1^{(0)}} = \boldsymbol{0}$. This equilibrium satisfies the trace condition (4.15). One can check that the $\det(\boldsymbol{f_x}(\boldsymbol{0}, \boldsymbol{\alpha^H})) = \alpha_2 > 0$. By definition, the determinant of the Jacobian matrix evaluated at equilibrium with parameter values satisfying (4.15) vanishes only at a Bogdanov-Takens bifurcation. Thus, this determinant is positive on the part of the Hopf surface that is above the Bogdanov-Takens curve. Below this curve, the surface satisfying (4.15) indicates a neutral saddle (a saddle where the two real eigenvalues are of same absolute magnitude but of opposite sign).

We now check the genericity conditions for the Hopf bifurcation. Near bifurcation, Jacobian matrix (4.9) has complex eigenvalues λ and $\overline{\lambda}$ with real part $\Re(\lambda) = \Re(\overline{\lambda}) = \mathrm{Tr}(\boldsymbol{f_x}(\boldsymbol{x}^*, \boldsymbol{\alpha}^H))/2$. Taking α_3 as the bifurcation parameter, one can check that the transversality condition is fulfilled:

$$\frac{\partial \mathrm{Tr}(\boldsymbol{f_x}(\boldsymbol{x}^*, \boldsymbol{\alpha}^H))}{\partial \alpha_3} = 1 \neq 0.$$

To check the non-degeneracy condition, we write the Jacobian matrix at the Hopf bifurcation:

$$\boldsymbol{f_x}(\boldsymbol{x}^*, \boldsymbol{\alpha}^H) = \begin{pmatrix} 0 & 1 \\ -\omega^2 & 0 \end{pmatrix},$$

with $\omega^2 = \alpha_2 + 3{x_1^{(0)}}^2$. This matrix has complex eigenvalues $\lambda = \pm i\omega$ with scaled ($\langle \boldsymbol{p}, \boldsymbol{q} \rangle = 1$, with

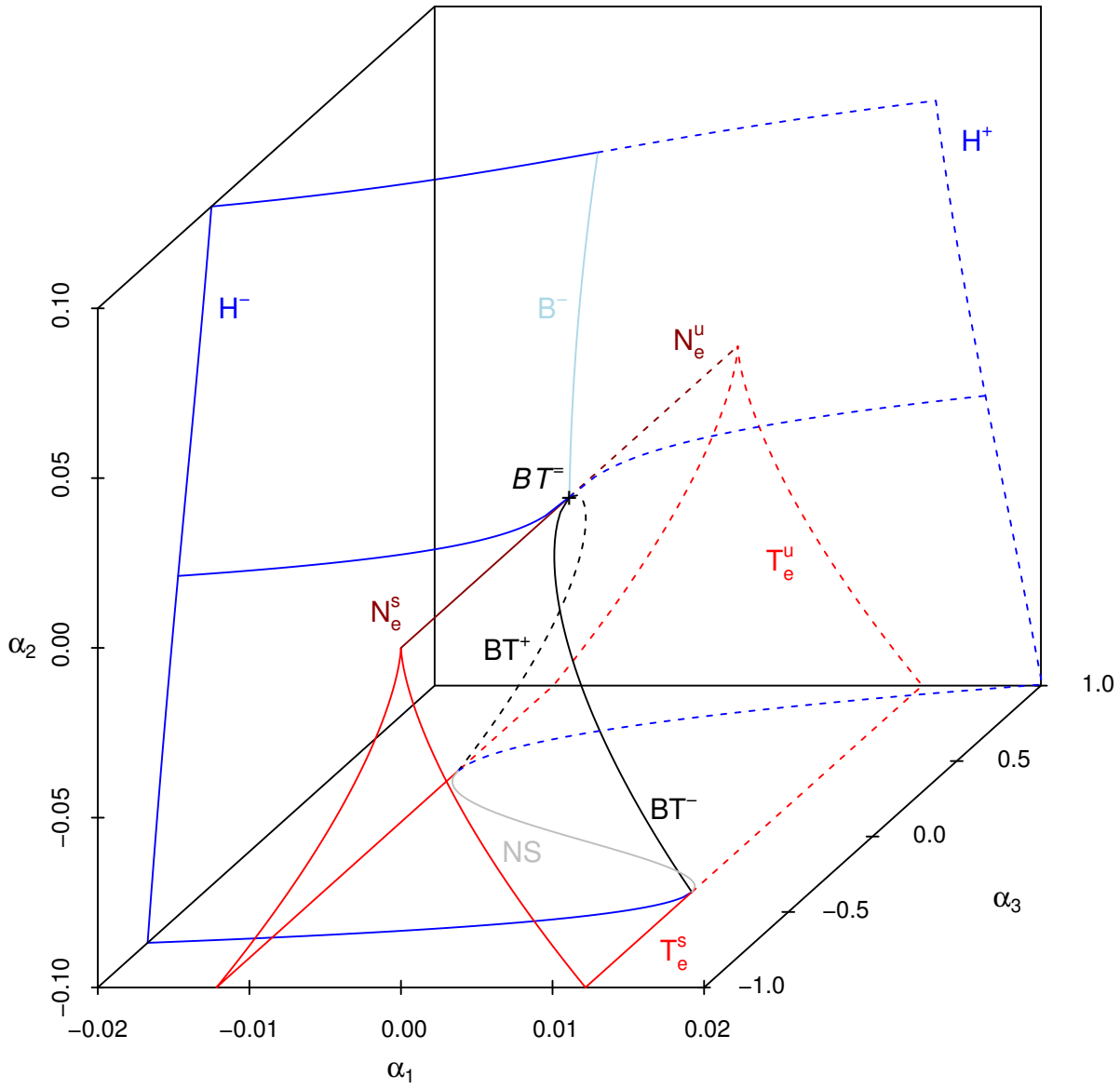

Figure 4.7. Three-dimensional bifurcation diagram (of equilibria) of the normal form of a Bogdanov-Takens bifurcation of triple point ($BT^{=}$) for the focus case. Bifurcation diagram depends on α_1, α_2 and α_3 that serve as unfolding parameters. Codimension-two bifurcation curves are a Bautin bifurcation (B^-, light blue), a Cusp bifurcation (N_e^u and N_e^s, dark red) and a Bogdanov-Takens bifurcation (BT^+ and BT^-, black). Codimension-one bifurcation surfaces are tangent bifurcation of equilibria (T_e^+ and T_e^-, red) and Hopf bifurcation (H^+ and H^-, blue). Homoclinic bifurcation can be of various types (homoclinic to saddle, homoclinic to saddle-node, "big" homoclinic) that are not detailed here. The surface of neutral saddle (NS, gray) is indicated but does not correspond to a bifurcation. In bifurcation labels, a superscript "+" (resp. "-") indicates a subcritical (supercritical) bifurcation drawn in dashed (plain) in the figure. For the tangent and Cusp bifurcations of equilibria, a superscript "u" (resp. "s") indicates that the non-central manifold is unstable (stable) at the bifurcation drawn in dashed (plain) in the figure.

$\langle \cdot, \cdot \rangle$ being the standard Hermitian inner product) proper eigenvectors in the complex space:

$$\boldsymbol{q} = (1, i\omega)^T \,,\ \boldsymbol{p} = (1/2, i/2\omega)^T \,,$$

that satisfies $\boldsymbol{f}_{\boldsymbol{x}}(\boldsymbol{x}^*, \boldsymbol{\alpha}^H)\boldsymbol{q} = i\omega\boldsymbol{q}$ and $\boldsymbol{p}^T\boldsymbol{f}_{\boldsymbol{x}}(\boldsymbol{x}^*, \boldsymbol{\alpha}^H) = -i\omega\boldsymbol{p}^T$ respectively.

Using proper eigenvectors as well as the second- and third-order partial derivatives (4.11,4.12), we compute the following quantities:

$$g_{20} = \langle \boldsymbol{p}, \boldsymbol{f}_{\boldsymbol{xx}}(\boldsymbol{x}^*, \boldsymbol{\alpha}^H)(q, q)\rangle = \frac{3ix_1^*}{\omega} + \beta - 2x_1^*,$$

$$g_{11} = \langle \boldsymbol{p}, \boldsymbol{f}_{\boldsymbol{xx}}(\boldsymbol{x}^*, \boldsymbol{\alpha}^H)(\boldsymbol{q}, \overline{\boldsymbol{q}})\rangle = \frac{3ix_1^*}{\omega},$$

$$g_{21} = \langle \boldsymbol{p}, \boldsymbol{f}_{\boldsymbol{xxx}}(\boldsymbol{x}^*, \boldsymbol{\alpha}^H)(\boldsymbol{q}, \boldsymbol{q}, \overline{\boldsymbol{q}})\rangle = \frac{3i}{\omega} - 1,$$

that give the first Lyapunov coefficient:

$$l_1 := \frac{1}{2\omega^2}\Re\left(ig_{20}g_{11} + \omega g_{21}\right) = \frac{1}{2\omega^2}\left(\frac{-3\beta x_1^{(0)}}{\omega} + \frac{6{x_1^{(0)}}^2}{\omega} - \omega\right).$$

The Hopf bifurcation is supercritical if $l_1 < 0$, i.e. if:

$$\alpha_2^H > 3\alpha_3^H \,, \tag{4.16}$$

or subcritical if the reverse inequality is satisfied. In both cases, the non-degeneracy condition is satisfied as $l_1 \neq 0$, which means that the Hopf bifurcation is generic.

The Hopf bifurcation becomes non-generic when $l_1 = 0$, i.e. when $\alpha_2 = 3\alpha_3$. This corresponds to a Bautin bifurcation (one can check its genericity numerically). As the Bautin bifurcation occurs on a Hopf surface, one has to find α_1^H values that satisfy the Hopf condition (4.15) with $\alpha_2^H = 3\alpha_3^H$ numerically.

To identify the type of Hopf bifurcation, consider a Bautin point where $\alpha_2 = 3\alpha_3$. If α_3 is decreased while α_2 is held constant (α_1 varies to remain on the Hopf surface), the condition for a supercritical Hopf bifurcation (4.16) is fulfilled. One can check that the other branch of the Hopf surface is subcritical. The subcritical (supercritical) branch of the Hopf surface ends at the subcritical (supercritical) branch of the Bogdanov-Takens bifurcation curve (figure 4.7), which is consistent with the knowledge of generic Bogdanov-Takens bifurcation.

Based on the knowledge of generic Bogdanov-Takens bifurcation in the plane, we know that at the branch of the fold surface tangent to the supercritical (subcritical) Hopf bifurcation, the double equilibrium has a stable (unstable) manifold. The double equilibrium has a stable (unstable) manifold on both branches of the fold bifurcation if $\alpha_3 < 0$ ($\alpha_3 > 0$). So, the triple equilibrium at the Cusp bifurcation has a stable manifold if $\alpha_3 < 0$ ($\alpha_3 > 0$, figure 4.7).

4.5.5 Global and cycle bifurcations

The other bifurcations of system (4.3) are computed numerically using the same procedure as for figures 4.2-4.4. A codimension-one surface of tangent bifurcation of cycles emerges tangentially to the subcritical Hopf bifurcation figure 4.8 from the Bautin curve when $\alpha_2 > 0$. When $\alpha_2 < 0$, the tangent bifurcation of cycles emerges from the intersection curve (not shown in figure 4.8) between the neutral saddle surface and the homoclinic bifurcation surface. The homoclinic bifurcation surface connects the two branches of the Bogdanov-Takens bifurcation curve. Homoclinic bifurcation is of various types (homoclinic to saddle, homoclinic to saddle-node, "big" homoclinic) along the surface. These different types of homoclinic bifurcation can be detected using the software Auto HomCont (Doedel *et al.*, 1997). Here, our interpretation of homoclinic bifurcations is based on an homotopy approach with some results presented in Bazykin (1998, section 3.5.2) and Baer *et al.* (2006), as well as logical requirements between the observed phase portraits (e.g. disappearence of a stable vs. unstable limit cycle).

Bifurcations presented in the previous paragraph can be better understood by looking at a cross-section of figure 4.8. The cross-section $\alpha_2 = -0.1$ allows us to discuss the type of homoclinic bifurcations (figure 4.9). Homoclinic bifurcation involves either a stable or an unstable limit cycle (e.g. Hom^- between phase portraits #4 and #3 vs. Hom^+ between phase portraits #11 and #10). In addition, homoclinic bifurcation is either an homoclinic to saddle $Hom^\pm$ (e.g. phase portraits #4 to #3), an homoclinic to saddle-node $HSN^\pm$ (e.g. phase portraits #2 to #3) or a "big" homoclinic bifurcation $Hom^{b\pm}$ (e.g. phase portraits #12 to #10). Transitions between these cases occur at codimension-two bifurcation points. Points D_i are saddle-node homoclinic points where the homoclinic orbit is non-smooth and returns to the saddle-node along a non-central manifold. For the different types of homoclinic bifurcations that we briefly discussed, the interested reader is refered to figures 6.7, 6.8, 6.16, 7.2 and 8.12 in Kuznetsov (2004) for a graphical overview and to Baer *et al.* (2006, p1351) for a more detailed description. The last codimension-two bifurcation point is F, where the "big" homoclinic curve $Hom^{b\pm}$ and the neutral saddle curve cross each other. From this intersection, a tangent bifurcation of limit cycles T_c^- emerges and has an infinite-order tangency with the "big" homoclinic curve (Nozdracheva, 1982 *in* Baer *et al.*, 2006). Between these

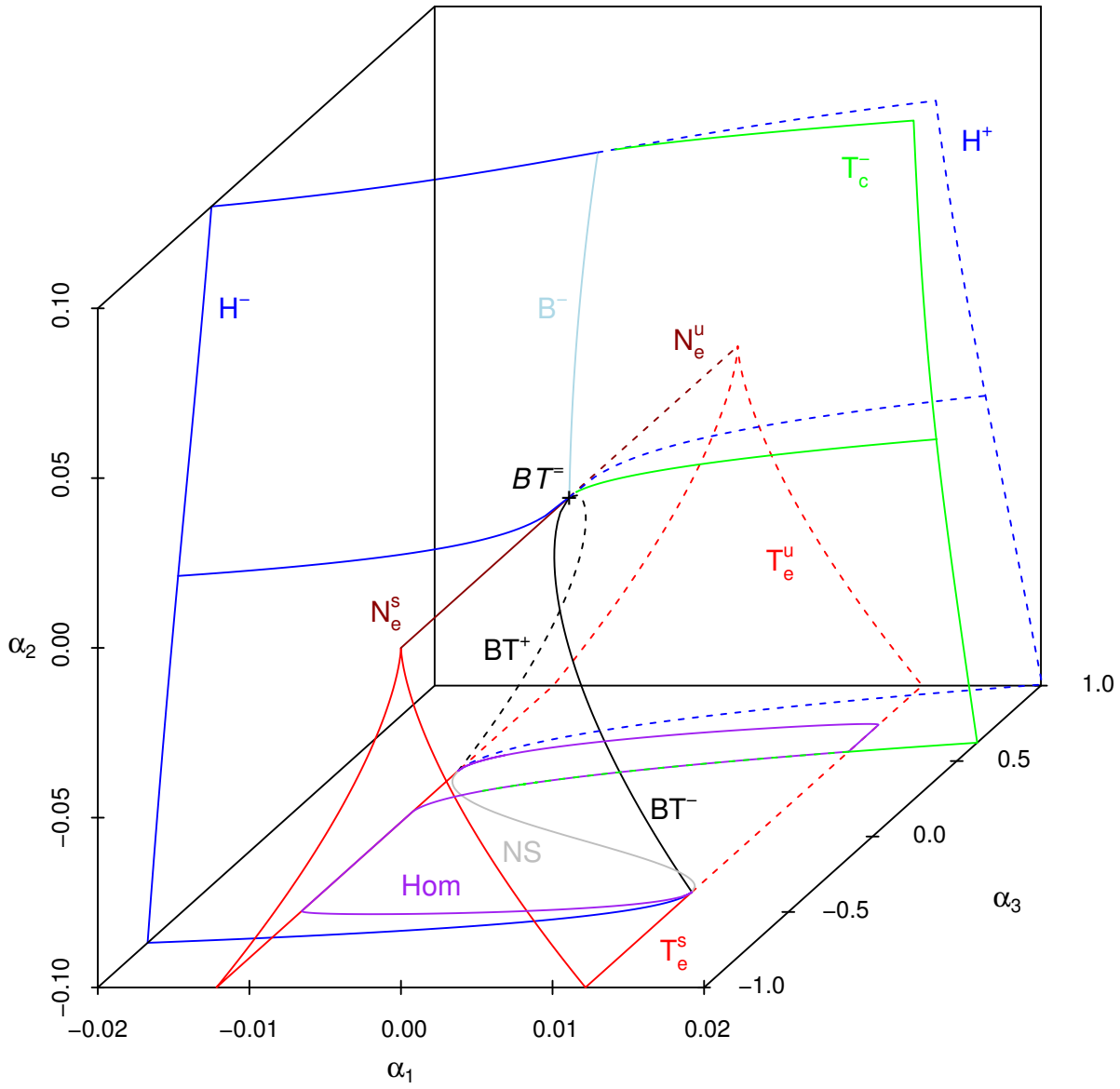

Figure 4.8. Three-dimensional bifurcation diagram of the normal form of a Bogdanov-Takens bifurcation of triple point ($BT^{=}$) for the focus case. Bifurcation diagram depends on α_1, α_2 and α_3 that serve as unfolding parameters. Codimension-two bifurcation curves are a Bautin bifurcation (B^-, light blue), a Cusp bifurcation (N^u_e and N^s_e, dark red) and a Bogdanov-Takens bifurcation (BT^+ and BT^-, black). Codimension-one bifurcation surfaces are tangent bifurcation of equilibria (T^+_e and T^-_e, red), tangent bifurcation of cycles (T^-_c, green, partly dashed for lisibility), Hopf bifurcation (H^+ and H^-, blue) and homoclinic bifurcations (Hom, purple). Homoclinic bifurcation can be of various types (homoclinic to saddle, homoclinic to saddle-node, "big" homoclinic) that are not detailed here. The surface of neutral saddle (NS, gray) is indicated but does not correspond to a bifurcation. In bifurcation labels, a superscript "+" (resp. "-") indicates a subcritical (supercritical) bifurcation drawn in dashed (plain) in the figure. For the tangent and Cusp bifurcations of equilibria, a superscript "u" (resp. "s") indicates that the non-central manifold is unstable (stable) at the bifurcation drawn in dashed (plain) in the figure.

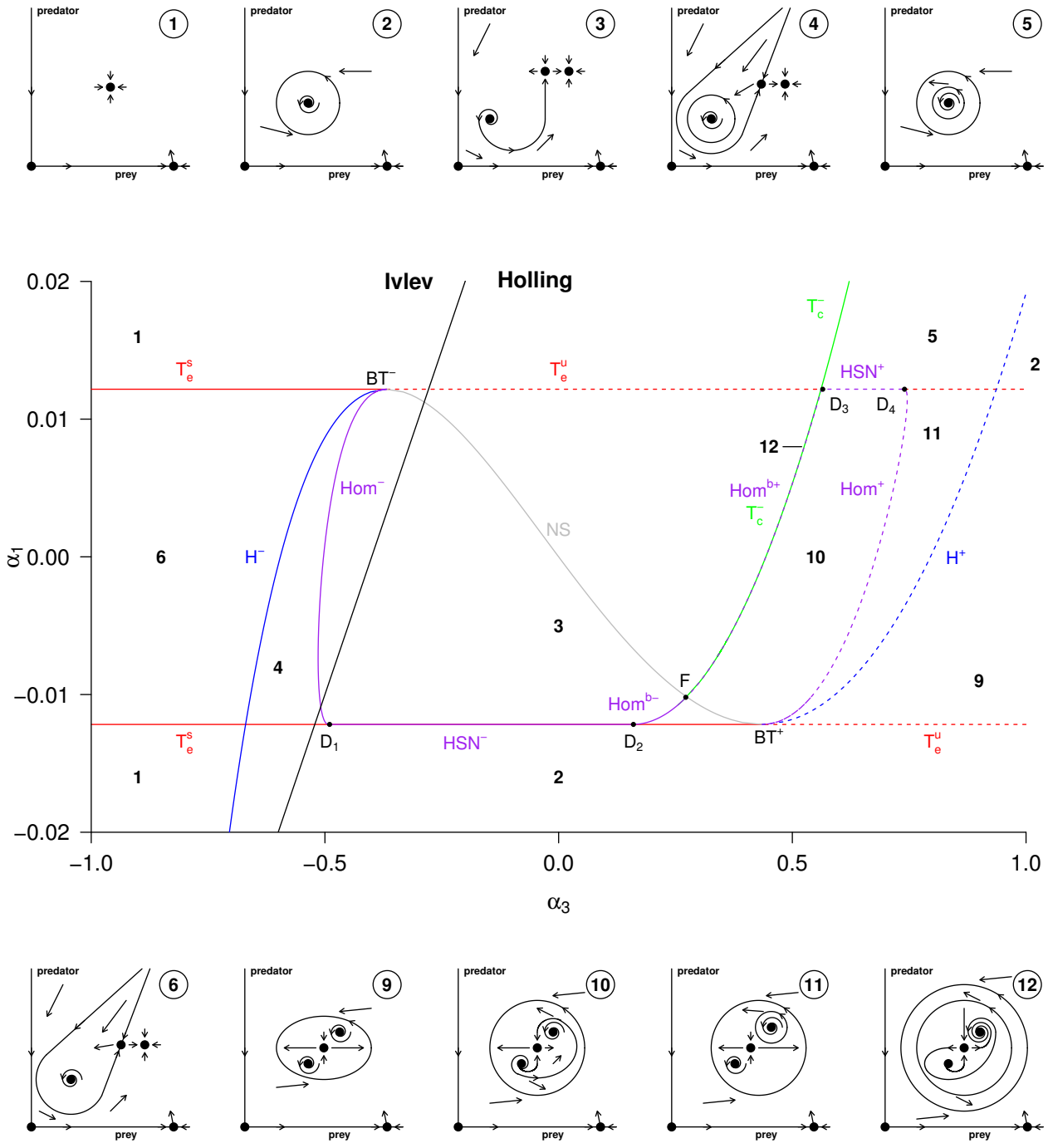

Figure 4.9. Two-dimensional slice of figure 4.8 at $\alpha_2 = -0.1$ with the corresponding phase portraits of the predator-prey model (small panels and numbers). Colors and labels indicate the same bifurcations as in figure 4.8. Homoclinic bifurcation (purple) is either a homoclinic to saddle (Hom^{b+} and Hom^{b-}), a homoclinic to saddle-node (HSN^+ and HSN^-) or a "big" homoclinic bifurcation (Hom^{b+} and Hom^{b-}). Labels indicate that the bifurcation involves a stable limit cycle (superscript "-") or an unstable limit cycle (superscript "+"). Codimension-two bifurcation points F and D_1 to D_4 are described in the main text. The black line qualitatively splits the diagram between dynamics that are observed near the Bogdanov-Takens bifurcation with Ivlev's FR and Holling's FR respectively.

two curves, the predator-prey model exhibits phase portrait #12 in a tiny strip of the parameter space. This strip has to exist for consistency of the bifurcation diagram. In practice, we never observed phase portait #12 here or in the previous chapter.

4.5.6 Interpretation in term of the original predator-prey model

The bifurcation diagram of the normal form of the Bogdanov-Takens bifurcation of triple equilibrium can be interpreted in terms of dynamics in the original predator-prey model (panels in figure 4.9). Indeed, the bifurcation diagram of the normal form can be splitted in two qualitative parts that corresponds to the dynamics of model (4.1) near the Bogdanov-Takens bifurcation predicted either by Holling's FR or Ivlev's FR. With Ivlev's FR, nothing indicates homoclinic bifurcations like HSN^- and D_1 and D_2 in the analysis presented in the previous chapter (figure 3.3b). Despite we do not use a bifurcation continuation method like Auto HomCont (Doedel *et al.*, 1997) for homoclinic bifurcations, consistency between phase portaits implies that the homoclinic bifurcation with Ivlev's FR is of type Hom^-. Conversely, the same reasoning indicates that all the types of homoclinic bifurcation in figure 4.9 occur with Holling's FR. This argument explains the location of the qualitative separation line we proposed in figure 4.9. The most striking result with this separation, is that more complex dynamics occur with Holling's FR than with Ivlev's FR near the Bogdanov-Takens bifurcation. The opposite result is obtained when the whole bifurcation diagram of the predator-prey model is considered, especially if we focus on the size of the parameter space where multiple attractors coexist (chapter 3).

4.6 Discussion and perspectives

We found that a three-dimensional bifurcation diagram of the predator-prey model exhibits a codimension-three Bogdanov-Takens bifurcation of triple equilibrium when one bifurcation parameter (called formulation parameter) corresponds to a smooth switch between two functional response formulations. With Holling's FR, this bifurcation also occurs in a three-dimensional bifurcation diagram with respect to three model parameters (density-dependent mortality of both species, saturation parameter of the functional response, figure 3.5.5 in Bazykin, 1998). Considering another parameter in our analysis would give a codimension-four bifurcation. For example, Baer *et al.* (2006) observed a codimension-four bifurcation from the focus to the elliptic case of the degenerated Bogdanov-Takens bifurcation of triple equilibrium. However, they argued that this bifurcation may not affect the dynamics of the system away from the degenerated Bogdanov-Takens bifurcation. Indeed, the normal form (4.3) has the same bifurcation diagram in the focus

and elliptic cases (our figure 4.7 vs. figure 4.4 in Baer *et al.*, 2006). The difference between the two cases is that in the elliptic case, there is an elliptic sector around the critical equilibrium at the degenerated bifurcation. Baer *et al.* (2006) argued that this difference is of minor interest from an applied point of view. Thus, adding a fourth parameter in the bifurcation analysis may not affect the results obtained with three parameters. In our case, fixed parameter values are estimated from empirical data sets (table 3.1). Uncertainty in the estimation of one parameter can be taken into account by adding this parameter to the bifurcation analysis. However, the above discussion about codimension-four bifurcation suggests that our results might be robust to uncertainty in this parameter value.

The bifurcation analysis in this chapter explains all qualitative differences between the two bifurcation diagrams of Holling's and Ivlev's functional response formulation models, except the Bautin bifurcation that occurs close to Ivlev's FR (low ξ). This codimension-two bifurcation is not connected to the degenerated Bogdanov-Takens bifurcation of triple equilibrium. There is only one generic Bogdanov-Takens bifurcation in the parameter space we investigated. However, Bazykin (1998) found two generic Bogdanov-Takens bifurcations in the two-dimensional bifurcation diagram of the scaled model with respect to other parameters. Thus, a second Bogdanov-Takens bifurcation may exist outside the range of parameters we investigated. We checked that there are no such bifurcation when $1/\omega \to +\infty$. However, if this second bifurcation exists, it can also degenerate into a codimension-three Bogdanov-Takens bifurcation for a given ξ value. This codimension-three bifurcation might give birth to the "unexplained" Bautin curve.

This chapter deals with the qualitative aspect of structural sensitivity, namely qualitative changes in the bifurcations and phase portraits of the system. This qualitative analysis is interesting to understand some changes. However, most of these qualitative changes concern only a small part of the parameter space considered in our example of predator-prey model (see previous chapter). Thus, it would be interesting to also consider the quantitative aspects of structural sensitivity, namely changes in bifurcations and attractors location. In the one-attractor case, Cordoleani *et al.* (2011) proposed to quantify a distance between model predictions that takes into account both a change in attractor location (e.g. equilibrium value) and type (e.g. transition from an equilibrium to a limit cycle through a Hopf bifurcation). As multiple attractors can coexist in the predator-prey model we considered here, chapter 6 presents an extension of this approach to systems with multiple attractors. Indeed, multiple attractors are of particular interest to study the resilience disturbed systems and their coexistence can be highly dependent of model formulation (chapter 3 and this chapter).

CHAPTER 5

Does structural sensitivity alter complexity-stability relationships in food web models?

"Not only do ecological communities harbor a multitude of different species, but even the interaction of just two individuals can be amazingly complex."
JD Yeakel, D Stiefs, M Novak and T Gross,
"Generalized modeling of ecological population dynamics" (Yeakel *et al.*, 2011)

The work presented in this chapter has been published into Aldebert *et al.* (2016a):
Aldebert, C., Nerini, D., Gauduchon, M., Poggiale, JC. 2016. Does structural sensitivity alter complexity-stability relationships? *Ecological Complexity*

5.1 Introduction

Predictions made by mathematical models can be sensitive to model formulation (Fulton *et al.*, 2003b, Fussmann & Blasius, 2005, Anderson *et al.*, 2010, among others). However, this sensitivity has rarely been tested in theoretical and operational ecosystem models (Fulton *et al.*, 2003a, Arhonditsis & Brett, 2004). In ecological models with multiple interacting populations, phenomena observed at the community scale are usually represented by simplifying smaller scale processes. For instance, collective and individual behaviours as well as physiological processes involved in predation are collapsed into one function, the functional response (Jeschke *et al.*, 2002, Gentleman *et al.*, 2003). Numerous mathematical formulations of a given biological phenomenon are relevant in the sense that: (i) their properties and assumptions about underlying processes are consistent with the knowledge of the system to model, (ii) they equivalently fit empirical data (Mullin *et al.*, 1975, Cordoleani *et al.*, 2011). Moreover, some of these functions may have the same mathematical properties (pointwise properties, monotonicity, convexity, ...). However, the choice of a particular function among relevant ones can affect the dynamics predicted by the same model. Differences occur in predicted steady-state values, equilibrium vs. oscillating dynamics and in the system response to external disturbances (chapters 3 and 4). Uncertainty due to this choice of a function is coined as "structural sensitivity" (*sensu* Cordoleani *et al.*, 2011).

Structural sensitivity has been theoretically studied in simple models with a few state variables, mainly predator-prey and food chain models (Myerscough *et al.*, 1996, Gross *et al.*, 2004, Fussmann & Blasius, 2005, Adamson & Morozov, 2012, 2014). The aim of this study is to extend these results to more complex models such as food webs. Previous results on predator-prey models may suggest that food web models are sensitive to the choice of type-II functional response. We propose to compare food web dynamics under changes in both functional response formulation and trophic complexity (number of trophic species and trophic links).

Trophic complexity is known to affect food web dynamics and stability. Complexity-stability relationships have been conceptually studied by MacArthur (1955) and then more formally by May (1972, 1973). May's work has led to a long-standing debate which is still open after decades of field and theoretical researches (May, 1999, McCann, 2000, Loreau, 2010). Food webs exhibit a huge number of different structures. A relevant analysis of their common properties requires to reproduce their diversity. Numerous food webs with empirically consistent structural properties and a desired trophic complexity can be built by simple random models (Williams & Martinez, 2000, Cattin *et al.*, 2004, among others). These models have been used to statistically investigate complexity-stability relationships in food web models based on different ecological phenomena (Williams & Martinez,

2004, Brose *et al.*, 2006, Uchida & Drossel, 2007, Williams, 2008, Kartascheff *et al.*, 2009, 2010, Stouffer & Bascompte, 2010, 2011, Heckmann *et al.*, 2012, Plitzko *et al.*, 2012).

The questions we address in this chapter are: (i) are dynamics predicted by a food web model more impacted by structural sensitivity or by trophic complexity? (ii) Does structural sensitivity alter complexity-stability relationships?

Next section presents the studied food web model. This model is an extension of the predator-prey model studied in chapters 3 and 4. Structural sensitivity in the food web model is compared to the impact of trophic complexity in subsection 5.3.1. Observed results are then explained from the knowledge of predator-prey models (subsection 5.3.2) and their robustness to changes in the method used to fit functional responses is tested (subsection 5.3.3). Then, the relative importance of trophic complexity, functional response formulation and parameter values is estimated (subsection 5.3.4). Next, robustness to changes in model assumptions is assessed, and complexity-stability relationships are compared to empirical findings (subsection 5.3.5). Chapter ends with a more general discussion about structural sensitivity and modelling of biological systems (subsection 5.3.6).

5.2 Models

5.2.1 Food web structure

Food webs are composed by S species (*sensu* trophic species) and one resource. Species are linked by L trophic interactions, so that food web connectance is $C = L/S^2$ (directed connectance, Martinez, 1991). The niche model (Williams & Martinez, 2000) is used to randomly build numerous food webs with the desired number of species and connectance. The niche model generates quickly numerous food webs with patterns that are consistent with empirical data (Williams & Martinez, 2000, Cattin *et al.*, 2004, Allesina *et al.*, 2008). It is based on the principle of ecological niche (Hutchinson, 1957). A species i is characterized by a niche value n_i uniformly drawn in the interval $[0, 1]$, the niche axis.

The niche model is described in Appendix (section 5.5). Food webs are made of distinct species, that are either a primary producer or a predator. Attribution of trophic links allows for cannibalism and trophic loops. We added a rejection step after food webs construction to avoid unrealistic patterns. We only studied food webs with a realized connectance that deviated at most by 0.01 of the expected one, that are connected (no disconnected parts), and in which all predators feed (as a prey or through a food chain) upon at least one primary producer.

5.2.2 Food web dynamics

Food web dynamics is modeled using a dynamical system of S differential equations. It is a bio-energetic model extended for a multi-species system (Yodzis & Innes, 1992, Plitzko *et al.*, 2012, among others). This deterministic model is continuous in time with unstructured populations. Each species i is described by its biomass B_i, with dynamics given by the ordinary differential equation:

$$\frac{dB_i}{dt} = \lambda q_i^{\phi} B_i + \lambda \sum_{j \in R_i} G_{i,j}^{\phi} B_i - \sum_{j \in C_i} G_{j,i}^{\phi} B_j - \alpha_i B_i - \beta_i B_i^2 \quad i = 1, ..., S. \tag{5.1}$$

Right terms of model (5.1) handle respectively a gain in biomass by primary production, sum of gains by predation, sum of losses by predation, linear mortality and respiration, density-dependent mortality (intra-specific competition, diseases). Species i possesses a set of prey (predator) species denoted as R_i (C_i). By definition, primary producers have $R_i = \varnothing$ and top-predators have $C_i = \varnothing$. The parameter λ is the assimilation efficiency. For the sake of simplicity, λ is assumed to be the same for all species. Parameter α_i is the linear mortality rate and parameter β_i is the per-capita intra-specific competition rate of species i. The letter ϕ indicates the specific formulation used for the Holling-type II functional response $G_{i,j}^{\phi}$. For simplicity, all species are assumed to have the same formulation. This one is either Holling's disc equation (1959b, 1965) denoted as $G_{i,j}^{H}$ or Ivlev's functional response (1955) denoted as $G_{i,j}^{I}$ (later called Holling's FR and Ivlev's FR):

$$G_{i,j}^{H} = \frac{a_i^H f_{i,j} B_j}{1 + h_i^H a_i^H T_i}, \; G_{i,j}^{I} = \frac{1}{h_i^I} \left(1 - \exp\left(-h_i^I a_i^I T_i\right)\right) \frac{f_{i,j} B_j}{T_i} \text{ with } T_i = \sum_{j \in R_i} f_{i,j} B_j.$$

Both functional responses are extended for a predator with multiple prey species by assuming that it does not switch between preys (Gentleman *et al.*, 2003). For Holling's FR, parameters a_i^H and h_i^H are respectively the attack rate and the handling time of the predator. For Ivlev's FR, parameter $1/h_i^I$ is the maximal digestion rate and $a_i^I h_i^I$ is the satiation coefficient of the predator. The total amount of prey available for species i is the weighted sum of its prey species biomass T_i. The weighting parameter $f_{i,j}$ is constant and it can be considered as the foraging effort or the feeding preference of predator i for its prey species j (obviously, $f_{i,j} = 0$ and $G_{i,j}^{\phi} = 0$ if $j \notin R_i$). This means that the total functional response of a predator $G_i^{\phi,tot}(T_i) = \sum_{j \in R_i} G_{i,j}^{\phi}$ is a function of T_i (figure 5.1) and that $G_{i,j}^{\phi} = G_i^{\phi,tot} f_{i,j} B_j / T_i$. Both functional responses also fulfills properties:

$$G_i^{\phi,tot} \in \mathcal{C}^2, \; G_i^{\phi,tot}(0) = 0, \; G_i^{\phi,tot}(T_i) \geq 0, \; G_i^{\phi,tot\,\prime}(T_i) > 0, \; G_i^{\phi,tot\,\prime\prime}(T_i) < 0, \; \lim_{T_i \to +\infty} G_i^{\phi,tot}(T_i) < +\infty,$$

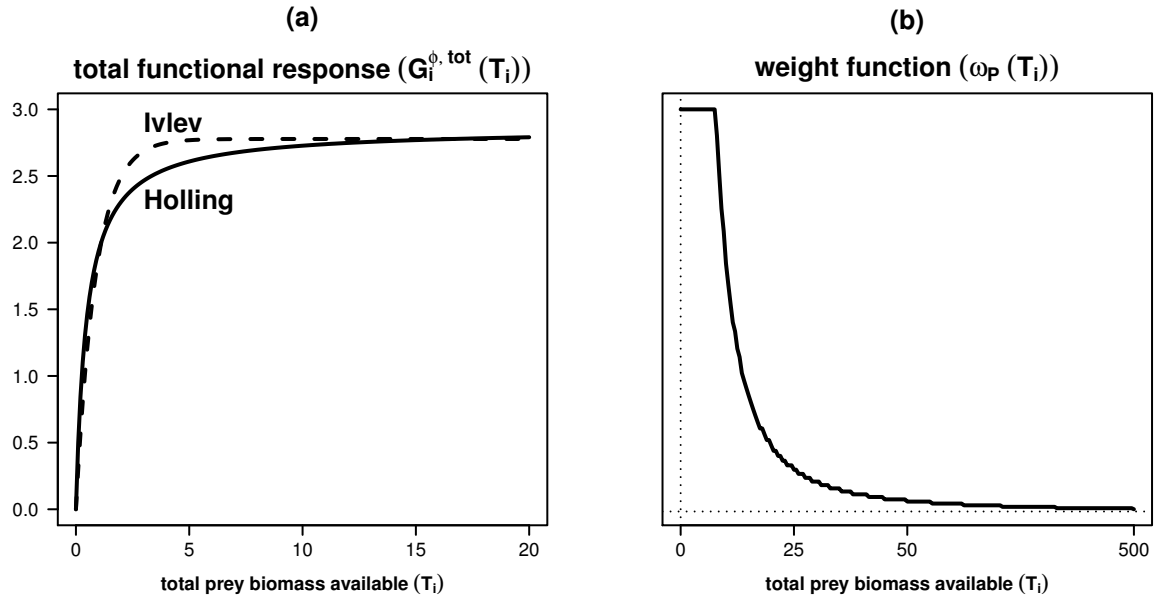

Figure 5.1. Functional responses used in the model. a: total functional response of species i (total amount of preys eaten by predator and by time unit) calculated as a function of its total prey biomass available, using Holling's disc equation (solid) or Ivlev's functional response (dashed). The latter is parameterized in order to minimize the weighted Euclidean distance between the two formulations. For the sake of visibility, only a part of the fitting range is shown. b: weighting function used to calculate the distance between formulations. See section 5.2.2 for formulations and section 5.2.3 for parameterization.

with $\mathcal{C}^2$ being the class of twice continuously differentiable functions. Other properties means that $G^{\phi,tot}$ is null in absence of prey, increases with prey biomass, is concave and saturates at high prey biomass.

Functional response's parameters have the same mathematical meaning in both formulations:

$$G_i^{\phi,tot\,\prime}(0) = a_i^{\phi},\ \lim_{T_i \to +\infty} G_i^{\phi,tot}(T_i) = \frac{1}{h_i^{\phi}}.$$

Thus, a_{pred}^{ϕ} gives the slope of the functional response at the origin, and $1/h_{pred}^{\phi}$ gives the asymptotic value of the functional response when it saturates at high prey biomass.

The term of primary productivity q_i^{ϕ} has the same equation as the functional response $G_{i,j}^{\phi}$ with a constant pool of resources B_{res}:

$$q_i^H = \begin{cases} \dfrac{a_i^H B_{res}}{1 + h_i^H a_i^H B_{res}} & \text{if } i \in P_I \\ 0 & \text{otherwise} \end{cases},\ q_i^I = \begin{cases} \dfrac{1}{h_i^I}\left(1 - \exp\left(-h_i^I a_i^I B_{res}\right)\right) & \text{if } i \in P_I \\ 0 & \text{otherwise.} \end{cases}$$

This term vanishes for predators, with P_I being the set of primary producers. Setting a constant pool of resource implies two assumptions. First, the time scale of the resource dynamics is such that it is always at quasi-equilibrium in comparison to the time scale of population dynamics. Second, the equilibrium value is independent of the food web dynamics, it only depends on the environment, which is supposed to be constant.

Let $M_i = 10^{xn_i}$ be the body mass of species i, with a scale parameter x. We assume that some parameter values scale allometrically across species (Brown *et al.*, 2004):

$$a_i^\phi = a^\phi M_i^{-1/4},\ h_i^\phi = h^\phi M_i^{1/4},\ \alpha_i = \alpha M_i^{-1/4},\ \beta_i = \beta M_i^{-1/4}.$$

As species abundance is quantified in terms of biomass, the scaling exponent $-1/4$ corresponds to an increase of individual metabolic rate with body mass power $3/4$, divided by individual body mass. The $3/4$ exponent is controversial. Empirical data and theoretical studies indicate values between $2/3$ and 1 (Kooijman, 2010). Nevertheless, the exact value of this exponent has a limited impact on species extinctions in similar food web models (Kartascheff *et al.*, 2010).

Note that if two species have the same trophic interactions and parameter values, model (5.1) is sensitive to the aggregation of these identical species as no direct inter-specific competition is considered. It has no impact on our numerical results as identical (or infinitely close) species are infinitely rare in food webs built by the niche model. This problem in model consistency can be solved by considering an inter-specific competition term, with a competition strength that decreases with a measure of distance between species.

5.2.3 Parameterization and numerical study

Parameter values are displayed in table 5.1. The range of trophic complexity (20 to 60 species, connectance of 0.10 to 0.30) is set to include values used in previous studies (Gross *et al.*, 2009, Kartascheff *et al.*, 2009, 2010, Plitzko *et al.*, 2012, among others) for comparison. The number of simulations is limited by assuming that a species i has the same feeding preference $f_{i,j} = 1/|R_i|$ for all its prey species $j \in R_i$ (with $|R_i|$ being the number of prey species of species i). This choice implies that T_i is the average biomass of prey species $\sum_{j \in R_i} B_j / |R_i|$ (weak generalist model, *sensu* Williams, 2008).

Parameters in Ivlev's FR are chosen to minimize the weighted Euclidean distance between both functional responses:

$$S_{A,\omega}\left(a^I, h^I\right) = d^2_{A,\omega}\left(G_i^{H,tot}, G_i^{I,tot}\right) = \int_A \omega(T_i)\left(G_i^{H,tot}(T_i) - G_i^{I,tot}(T_i)\right)^2 dT_i, \tag{5.2}$$

Table 5.1. Parameter values used in the food web model. Parameter values from Heckmann *et al.* (2012) were estimated from empirical data sets (up to > 700 organisms from unicellular eukaryotes to plants and mammals, which span 20 orders of magnitude in body mass, Brown *et al.*, 2004, Brose *et al.*, 2006) using allometric scaling or set to values similar to other studies for comparison (like Kartascheff *et al.*, 2009, 2010).

biological meaning	parameter	value	source	unit
mortality rate	α	0.3	(Heckmann *et al.*, 2012)	time^{-1}
per-capita competition rate	β	0.5	(Heckmann *et al.*, 2012)	$\text{biomass}^{-1}\text{time}^{-1}$
assimilation efficiency	λ	0.65	(Heckmann *et al.*, 2012)	-
resource biomass	B_{res}	500	(Heckmann *et al.*, 2012)	biomass
magnitude of body mass range	x	8	(Plitzko *et al.*, 2012)	-
Holling's disc equation:				
attack rate	a^H	6	(Heckmann *et al.*, 2012)	$\text{biomass}^{-1}\text{time}^{-1}$
handling time	h^H	0.35	(Heckmann *et al.*, 2012)	time
Ivlev's functional response:				
maximal consumption rate	$1/h^I$	1/0.36	see text	time^{-1}
satiation coefficient	$a^I h^I$	3.17×0.36	see text	biomass^{-1}

with a weighting function $\omega(T_i)$ on a fitting range A of T_i values. Total prey biomass ranges from 0 to constant resource biomass for primary producers, so we set $A = [0, B_{res}]$. For a fixed amount of total prey biomass $\sum_{j \in R_i} B_j$, the resulting T_i depends on $|R_i|$. To balance this effect *a priori*, the distance is weighted by (figure 5.1):

$$\omega_{\mathcal{P}}(T_i) = \frac{1}{S_{max} T_{max}} \sum_{n=1}^{N} n \text{ with } N = \min\left(\lfloor T_{max}/T_i \rfloor, S_{max}\right) \text{ and } T_{max} = \max(A), \tag{5.3}$$

which is the frequency distribution of T_i values for $\sum_{j \in R_i} B_j \in A$ and for a predator's number of prey species which ranges between one and $S_{max} = 60$. Minimizing the cost function $S_{[0,B_{res}],\omega_{\mathcal{P}}}$ using the simplex method by Nelder & Mead (1965) give values $a^I = 3.17$ and $h^I = 0.36$. The sensitivity of our results to choices in A and $\omega(T_i)$ is discussed in section 5.3.3.

The algorithm presented in Appendix (section 5.6), with a discussion about its limits) is used to automatically determine the kind of asymptotic dynamics reached by a food web. The proposed algorithm classifies asymptotic dynamics in three types: dynamics in which at least one species goes extinct, equilibrium in which all species coexist, fluctuating dynamics (e.g. limit cycle, torus, strange attractor) in which all species coexist. The proportion of food webs in which all species coexist (at equilibrium or with fluctuating dynamics) is a measure of food web persistence. The proportion of persistent food webs (i.e. food webs in which all species coexist) which exhibit a fluctuating dynamics is a measure of food web variability. Food webs construction and simulation were achieved by C++ programs using GNU Scientific Library for C/C++ (Galassi *et al.*, 2013).

Post-simulation analysis and figures were performed using R language (R Core Team, 2013).

5.3 Results and Discussion

5.3.1 Structural sensitivity vs. trophic complexity

Both functional responses predict similar patterns of food web persistence as a function of trophic complexity (figure 5.2a,c). Within this range, Ivlev's FR predicts less extinctions than Holling's FR does (from −11 % to +1 % food webs with at least one species extinction). With both functional responses, the proportion of non-persistent food webs increases with trophic complexity. This increase is higher with the number of species (×1.4 with Holling's FR and ×1.5 with Ivlev's FR) than with connectance (×1.2 and ×1.3). Functional responses are parameterized to predict quantitatively close predation fluxes, which explains their similar predictions of food web persistence.

Conversely, food web variability is mainly driven by functional response formulation within the tested range of trophic complexity (figure 5.2b,d). Ivlev's FR predicts 2.3 times more equilibrium dynamics (from 98 % to 99 % of persistent food webs reach an equilibrium) than Holling's FR does (from 25 % to 80 %). The proportion of equilibrium dynamics increases more with connectance (on average ×3.2 with Holling's FR and +1 % with Ivlev's FR) than with the number of species (×1.1 with Holling's FR, no trend with Ivlev's FR). Even if the effect of trophic complexity can change with other measures of food web persistence and variability, the latter is still higher with Ivlev's FR (Appendix, section 5.9).

5.3.2 Understanding structural sensitivity in food webs

Model (5.1) applied to a one-predator/one-prey system owns an equibrium which is stable with Ivlev's FR and unstable with Holling's FR in 26 % to 49 % of the parameter space explored in chapter 3. With Holling's FR, dynamics converge on a stable limit cycle. Equilibrium stability is different because the slope of Holling's FR at equilibrium is lower. The slope of the functional response at equilibrium in food webs can be described by its elasticity:

$$\gamma_i := g_i^{\phi\prime}(1) \in [0,1] \text{ with } t_i := \frac{T_i}{T_i^*} \text{ and } g_i^{\phi}(t_i) := \frac{G_i^{\phi,tot}(t_i T_i^*)}{G_i^{\phi,tot}(T_i^*)},$$

where the normalized functional response equals 1 at equilibrium ($g_i^{\phi}(1) = 1$). A high elasticity γ_i stabilizes equilibria in predator-prey (Yeakel *et al.*, 2011, section 3.4 of this thesis) and food web models (Appendix, section 5.10).

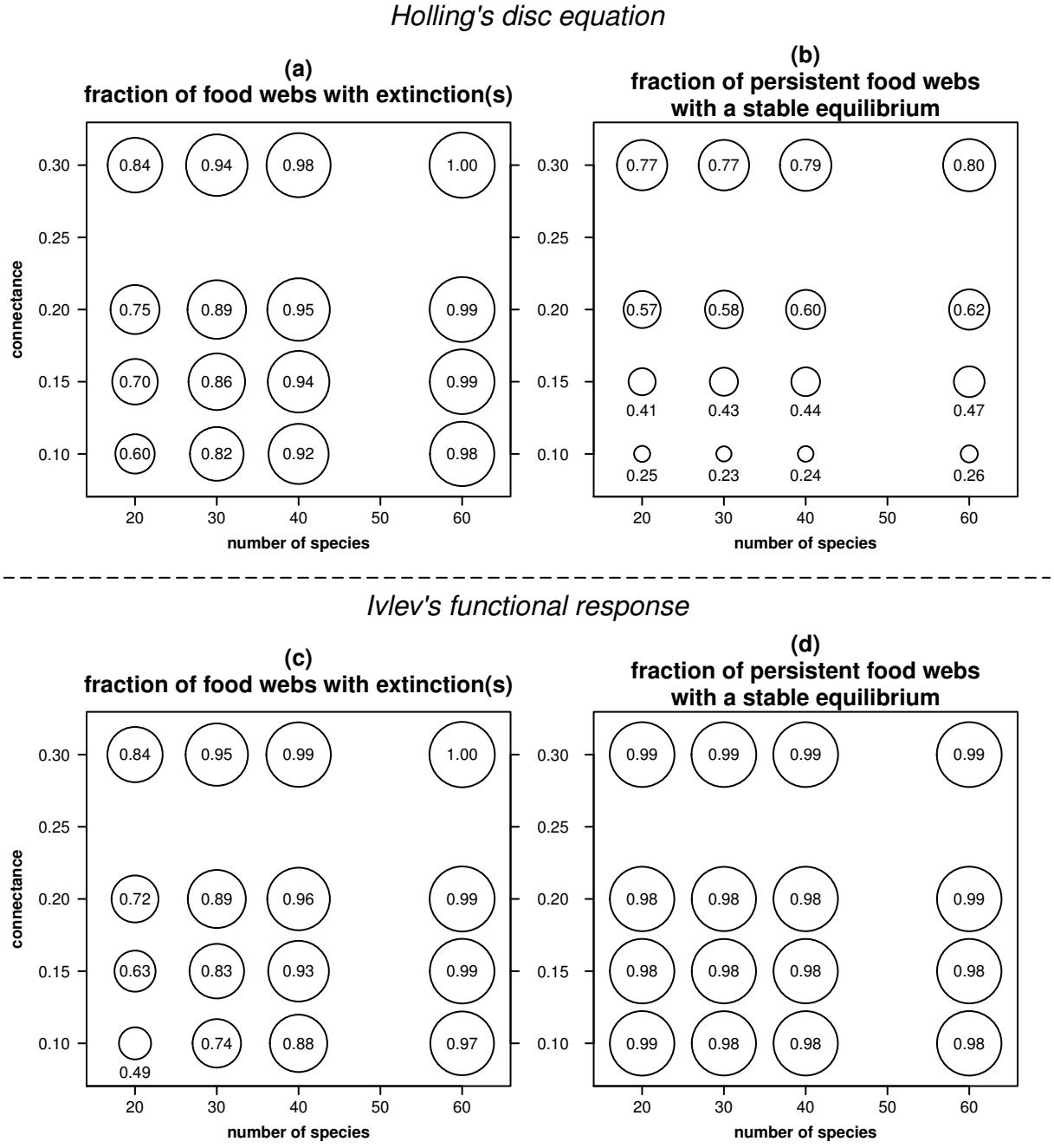

Figure 5.2. Food web dynamics as a function of trophic complexity predicted by Holling's (a, b) and Ivlev's functional responses (c, d). a, c: proportion of food webs with at least one species extinction. b, d: proportion of persistent food webs with a stable positive equilibrium. The number of food webs studied for each pair of parameters is enough to obtain 10 000 food webs with a stable positive equilibrium.

The elasticity depends on prey biomass at equilibrium, which has a similar distribution between functional responses (figure 5.3). However, Ivlev's FR has a higher elasticity than Holling's FR for low prey biomass values (figure 5.4b). As a consequence, the realized γ_i distribution in food web simulations is 1.6 times higher with Ivlev's FR ($\bar{\gamma} = 0.60$) than with Holling's FR ($\bar{\gamma} = 0.37$, figure 5.4a). With the latter, one can expect that stable equilibria are closer to a bifurcation threshold (with respect to γ_i). Thus, more food webs are likely to be on the unstable side of this bifurcation with Holling's FR. This can explain why this function leads more frequently to fluctuating dynamics. This reasoning extends the previous mechanism found in predator-prey models (Fussmann & Blasius, 2005) to the scale of complex food webs.

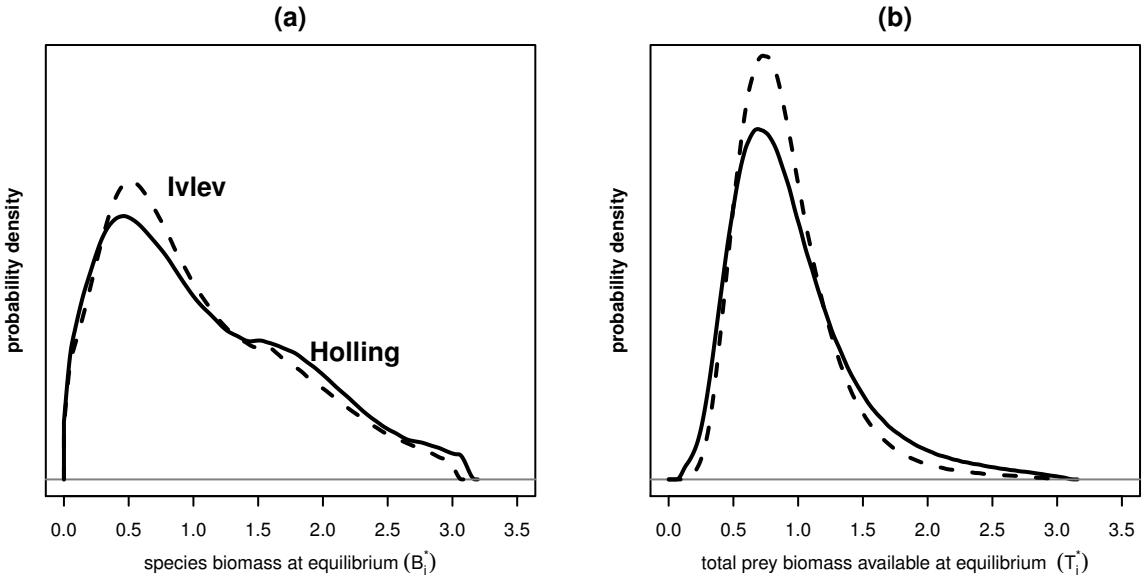

Figure 5.3. Estimated densities of species biomass (a) and total prey biomass available for predator species (b) in food webs reaching a positive equilibrium with Holling's (plain) or Ivlev's (dashed) functional response. Computed from 160 000 food webs of varying complexity (4 levels of connectance and 4 numbers of species, 10 000 food webs by pair of values). Density estimates are realized using non-parametric kernel methods (Simonoff, 1996).

5.3.3 Structural sensitivity and the method used to fit the functional responses

As the slope of the functional response drives food web variability, one can think about different ways to parameterize Ivlev's FR. The relevance of these different approaches from a biological point of view is discussed in section 5.3.6. Here, we focus on robustness to changes in parameter values estimated for Ivlev's FR. Different parameter sets are estimated by minimizing the

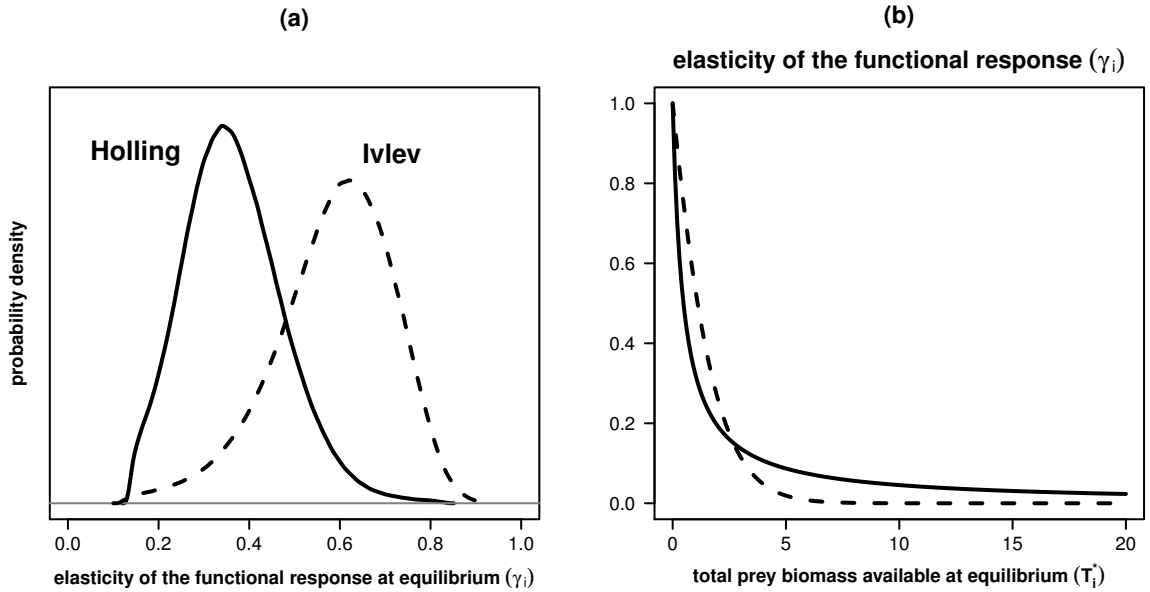

Figure 5.4. Elasticity of the functional response: estimated density in food webs reaching a positive equilibrium (a) and as a function of total prey biomass available (b) with Holling's (plain) or Ivlev's (dashed) functional response. Computed for predator species from 160 000 food webs of varying complexity (4 levels of connectance and 4 numbers of species, 10 000 food webs by pair of values). Density estimates are realized using non-parametric kernel methods (Simonoff, 1996).

weighted distance (5.2): (i) over different ranges of T_i values, and (ii) using either the weighting function $\omega_{\mathcal{P}}$ (5.3) (figure 5.1) or a uniform weighting function $\omega_{\mathcal{U}}(T_i)$. One last parameter set is estimated using the empirical distribution of total prey biomass observed in persistent food webs at equilibrium with Holling's FR (figure 5.3b).

Parameter sets that give a better fit to Holling's FR at low prey biomass (closer a^ϕ value) predict a closer value of food web variability between functional responses (table 5.2 and figure 5.5). However, they also predict more distant primary productivity ($\approx 1/h^\phi$ value) and predicted value of food web persistence. Furthermore, equilibrium dynamics are still more frequent with Ivlev's FR within the tested range of trophic complexity (Appendix, section 5.7). The parameter set that leads to the closer food web variability ($\omega_{\mathcal{P}}$ within $[0, 3.5]$) does not lead to the best fit of functional responses within the range of prey biomass observed (column $S_{\omega_{\mathcal{U}},[0,3.5]}$ in table 5.2), as it is optimized for even smaller biomass values. In other words, this parameter set optimizes only the slope at the origin (a^ϕ), as we know that the functional response slope drives food web variability. Only one parameter set is usually considered in previous studies on structural sensitivity in predator-prey models (Myerscough *et al.*, 1996, Fussmann & Blasius, 2005, Cordoleani *et al.*, 2011, chapter 3). We checked here with different parameter sets that functional response formulation influences food web variability, even if this influence is lower with some fitting methods.

Table 5.2. Impact of the method used to fit the functional responses. The columns indicate respectively: the weighting function used, the range of T_i values within which the weighted distance between functions is minimized, the pair of parameters values obtained (a^ϕ and h^ϕ) for Ivlev's functional response, the corresponding distance (computed with the same weighting function for comparison) between functions at low ($[0, 3.5]$) and high ($[3.5, 500]$) total prey biomass available, the predicted dynamics (proportion of food webs with extinction(s), proportion of persistent food webs reaching an equilibrium) in 30-species food webs with a connectance of 0.15. The number of food webs studied for each pair of parameters is enough to obtain 1 000 food webs with a stable positive equilibrium. The bold line corresponds to the parameters values used in the rest of the study. In addition, one parameter set for Ivlev's functional response has been estimated using the empirical distribution of T_i observed in persistent food webs at equilibrium with Holling's disc equation (figure 5.3b). Dynamics predicted by Holling's disc equation are indicated for comparison.

weighting function	$T_i \in A$	a^ϕ	h^ϕ	$S_{\omega_\mathcal{U},[0,3.5]}$	$S_{\omega_\mathcal{U},[3.5,500]}$	extinction(s)	equilibrium
$\omega_\mathcal{U}$	$[0, 500]$	2.70	0.35	0.049	< 0.001	0.79	1.00
	$[0, 20]$	3.12	0.37	0.026	0.021	0.83	0.99
	$[0, 15]$	3.22	0.37	0.025	0.021	0.84	0.98
	$[0, 10]$	3.39	0.38	0.017	0.046	0.85	0.96
	$[0, 3.5]$	4.03	0.41	0.004	0.165	0.89	0.89
$\omega_\mathcal{P}$	$\mathbf{[0, 500]}$	**3.17**	**0.36**	**0.036**	**0.005**	**0.83**	**0.98**
	$[0, 20]$	4.67	0.41	0.007	0.165	0.91	0.72
	$[0, 15]$	4.82	0.42	0.007	0.215	0.92	0.68
	$[0, 10]$	4.98	0.43	0.010	0.269	0.92	0.60
	$[0, 3.5]$	5.31	0.45	0.023	0.387	0.93	0.51
T_i distribution from fig. 5.3b		4.50	0.44	0.015	0.327	0.91	0.80
Holling's disc equation		6	0.35			0.86	0.43

5.3.4 Structural sensitivity vs. parameter sensitivity

Even with the simplifying assumption that parameter values scale allometrically, a full parameter sensitivity analysis requires a high computational effort. Indeed, to be reasonably exhaustive it is necessary to study thousands of food webs with different numbers of species and connectance levels for each parameter set. However, we investigate the robustness of our results to the functional response parameter values. We vary the parameter values used for Holling's FR (a^H and h^H) within a range $[-20\,\%, +20\,\%]$ (discretized by steps of 10 %) and re-estimate the parameters for Ivlev's FR by fitting the two functions. The relative variation considered is comparable to uncertainties in parameter estimation from empirical data (Cordoleani *et al.*, 2011). Food webs with the same numbers of species and connectance levels as in figure 5.2 are studied for each parameter set and each functional response, for a total amount of $\approx 6.10^7$ food webs studied.

Within the tested range of trophic complexity, food web persistence is strongly correlated (0.76) to the number of species, whereas food web variability is strongly correlated (0.82) to functional response formulation (table 5.3). Both persistence and variability are also correlated (0.37 and 0.36) to connectance. In comparison, food web dynamics are weakly correlated to parameter

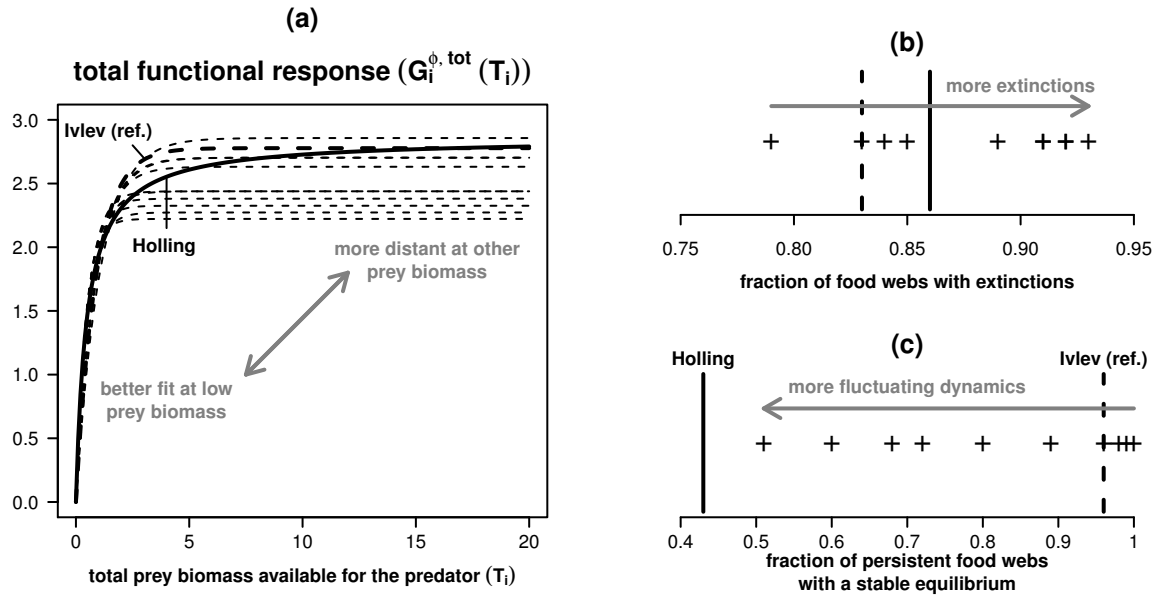

Figure 5.5. Impact of the method used to fit the functional responses. a: Holling's disc equation (plain), Ivlev's functional response with the parameter set used in the study (bold dashed) and with parameter sets obtained with different fitting methods (thin dashed, see table 5.2). b and c: food web dynamics (30 species, connectance of 0.15) predicted for these parameter sets. Gray labels and arrows summarize the main trend of results: a better fit at low prey biomass (a) leads to a closer predicted food web variability (c), but also to more distant functions at other prey biomass values (a) and more distant predicted food web persistence (b).

values. A change in parameter values has a weaker impact on model dynamics than a change in model formulation, even if both changes correspond to a quantitatively similar variation measured between the functional responses (Wood & Thomas, 1999, Cordoleani *et al.*, 2011, Adamson & Morozov, 2012, 2014). Indeed, for a quantitatively similar variation, a change of formulation may affect the function shape and lead to a higher change in functional response slope near equilibrium, i.e. in equilibrium stability.

5.3.5 Model assumptions, complexity-stability relationships and biological systems

Different combinations of model assumptions are made by recent studies on food webs, often for simplifying reasons (Brose *et al.*, 2006, Williams, 2008, Gross *et al.*, 2009, Kartascheff *et al.*, 2010, Stouffer & Bascompte, 2010, 2011, Heckmann *et al.*, 2012, Plitzko *et al.*, 2012). The impact of these assumptions is detailled in Appendix (section 5.8) of SOM and summarized in table 5.4. In all cases, equilibrium dynamics are more frequent with Ivlev's FR than with Holling's FR. In addition, both functional responses show the same qualitative effect of each assumption.

Table 5.3. Correlations between food web dynamics, trophic complexity, the functional response used and its parameterization. We simulated food webs of varying complexity (4 numbers of species times 4 connectance levels) with different functional response formulation (Holling's or Ivlev's FRs) and parameterization (5 values of a^ϕ times 5 values of h^ϕ), leading to $n = 800$ combinations. For each one, food web dynamics is summarized by the proportion of food webs with extinction(s) and the proportion of persistent food webs reaching a stable equilibrium. A positive correlation with the functional response corresponds to an increase with Ivlev's FR. NS means that the corresponding p-value is higher than 0.01 (Student's test on the regression coefficient). For each combination, the number of food webs studied is enough to obtain 1 000 food webs with a stable positive equilibrium. The total number of food webs simulated is $\approx 6.10^7$.

	number of species	connectance	a^ϕ	h^ϕ	functional response
extinction(s)	**0.76**	0.37	0.12	0.07	-0.17
equilibrium	NS	0.36	-0.22	0.07	**0.82**

Table 5.4. Model assumptions and complexity-stability relationships. Three changes in model assumptions are tested: studying food webs with a fixed number of five primary producer species (PP), setting the body mass of primary producers to 1 and deleting cannibalistic links. For each changes, results (proportion of food webs with extinction(s) and proportion of persistent food webs that reach an equilibrium) are summarized for Holling's and Ivlev's functional responses. Trophic complexity (number of species S and connectance C) is varied within the same range as in figure 5.2. The obtained range of results and the mean impact of trophic complexity are shown. The "-" indicates that the impact of the number of species is not discussed because the number of persistent food webs studied has been decreased for computational reasons.

		extinction(s)			equilibrium		
assumption	functional response	range	S	C	range	S	C
number of PP	Holling	$[0.48, 1.00]$	$\times 1.6$	$\times 0.8$	$[0.15, 0.78]$	-	$\times 4.3$
	Ivlev	$[0.47, 1.00]$	$\times 1.7$	$\times 0.9$	$[0.92, 0.99]$	-	$\times 1.03$
body mass of PP	Holling	$[0.48, 0.99]$	$\times 1.6$	$\times 1.2$	$[0.38, 0.86]$	$\times 1.02$	$\times 2.2$
	Ivlev	$[0.43, 1.00]$	$\times 1.7$	$\times 1.3$	1.00	$=$	$=$
body mass of PP	Holling	$[0.60, 1.00]$	$\times 1.4$	$\times 1.2$	$[0.35, 0.81]$	$\times 1.05$	$\times 2.2$
+ no cannibalism	Ivlev	$[0.51, 1.00]$	$\times 1.5$	$\times 1.3$	1.00	$=$	$=$

These changes in model assumptions show that food web persistence decreases with connectance due to a decrease of the proportion of primary producer species in food webs made by the niche model (Appendix, figure 5.7). However, persistence is increased by the connectance *per se*, i.e. the number of pathways where energy can flow. Furthermore, connectance increases the occurrence of equilibrium dynamics and improves species survival by keeping their dynamics far from the extinction threshold. More equilibrium dynamics occur at high connectance because it increases the number of weak trophic links. Weak links stabilize equilibria by dampening predator-prey oscillations (McCann *et al.*, 1998).

The impact of the number of species on system dynamics can be related to general questions on the effect of biodiversity on ecosystem functioning (May, 1999, McCann, 2000). Jiang & Pu (2009) have made a meta-analysis of empirical studies on the effect of biodiversity. Both observational and experimental studies on multi-trophic communities indicate that the temporal variability of state variables (biomasses, processes, etc.) decreases at the population level (15 studies), and even more at the community level (25 studies). These trends are predicted by the model, which predicts more equilibrium dynamics (figure 5.2 and table 5.4) and a lower temporal variability of population biomass (Appendix, section 5.9) in larger persistent food webs. In addition, larger food webs have a lower variability of their predicted total biomass (data not shown). Note that in the model we used, there is no feedback of population dynamics on the trophic structure, which is set *a priori*. Thus, the link between diversity and ecosystem persistence can be better explored using evolutionary models that build persistent networks of interaction based on population dynamics (Drossel *et al.*, 2001, Loeuille & Loreau, 2005, Rossberg *et al.*, 2006).

5.3.6 Structural sensitivity and modelling biological systems

We have shown that quantitatively close mathematical functions can lead to qualitatively different food web dynamics. However, the amount of differences in dynamics depends on the way the functions were parameterized. In general, parameterization is realized by either fitting the functions to data on the process itself (Fussmann *et al.*, 2000, Anderson *et al.*, 2010, Cordoleani *et al.*, 2011, Poggiale *et al.*, 2010), or fitting the full model predictions (other parameters can be optimized at the same time) to data on the temporal evolution of the system (Canale *et al.*, 1973, Kooi & Kooijman, 1994b).

Here, we used the first method in different ways. The most classical ones, namely a fit with a uniform weight over the range of biomass observed or a fit using the empirical biomass distribution, lead to significant differences in model dynamics between functional responses. These differences become lower only if the fit is done so that functions are close in term of property that drives

model dynamics (here the functional response slope at the origin). So, model dynamics have to be known *a priori* to be able to use this approach, which is in fact more similar to the second method of fit.

The second method focuses on the dynamics predicted by the model. Different functions can be parameterized in order to predict close dynamics. However, these dynamics are specific to the set of environmental conditions (i.e. other parameter values) used. If these conditions are changed (e.g. resource availability, mortality due to external factors), the different functions are likely to predict different dynamics as they are outside the range of optimization. The underlying idea is similar to the method of generalized modelling (Gross & Feudel, 2006) and the approach proposed by Adamson & Morozov (2012). These approaches do not specify model formulation and describe only the local properties of the model (like the slope of a function) near an equilibrium. So, results on equilibrium stability are independent of a specific formulation. However, these approaches provide no information on the system dynamics far from this equilibrium, like the existence of alternative stable states. In conclusion, if different functions are parameterized to predict similar dynamics in a given situation, this is likely to work only in the vicinity of this given situation (e.g. a given equilibrium). Choosing to do so or to use the first method depends on the purpose of the study.

Stable equilibria and limit cycles can coexist in the food web model applied to a predator-prey system, due to density-dependent mortality (chapters 3 and 4). Density-dependent mortality allows the coexistence of different asymptotic states that depend on functional response formulation. As a consequence, functional response formulation drives model predictions in situations where external disturbances and recovery policies are applied (resilience, hysteresis phenomena). Such situations have not been investigated in food webs in this study, as we did one dynamical simulation per food web. Multiple simulations with different initial conditions are required for each food web to try to detect different asymptotic dynamics. Indeed, the existence of such dynamics cannot be fully determined using bifurcation analysis in systems with tens of state variables like food webs. However, quantifying uncertainties in food web model predictions in situations with external disturbances would be an important step toward more accurate model predictions.

5.4 Conclusion

We investigated the sensitivity of a food web model to the choice of functional response formulation (Holling's or Ivlev's FRs). We found a little effect of functional response formulation on food web persistence, whereas food web variability is significantly lower with Ivlev's functional response.

Functional response slope at equilibrium explains this lower variability. In addition, food web variability is more driven by functional response formulation than by its parameter values and the tested range of trophic complexity (number of species, connectance). However, complexity-stability relationships are not qualitatively affected by functional response formulation. These conclusions are robust both to different combinations of model assumptions (cannibalism, primary production) and to different fitting methods to parameterize functional responses.

Because of intrinsic data variability and because model formulation is always a simplified representation of complex biological processes, the choice of functional response may remain uncertain for many species. The results demonstrate that this uncertainty in the formulation of a food web model can lead to uncertainties in the type of asymptotic dynamics it predicts. In addition, uncertainties in predicted system resilience in case of external disturbances are known to arise in some predator-prey models, and so are likely to occur in food web models. The quantification of these potential uncertainties in food web resilience may be a challenging way of research toward more accurate model predictions.

Appendices: Does structural sensitivity alter complexity-stability relationships in food web models?

5.5 Niche model, primary producers and cannibal species

Food webs are composed by S species (*sensu* trophic species) and one resource. Species are linked by L trophic interactions, so that food web connectance is $C = L/S^2$ (directed connectance, as defined by Martinez, 1991). In order to statistically investigate the effect of trophic complexity, we need to produce millions of different food webs. We use the niche model (Williams & Martinez, 2000) to randomly build food webs with the desired number of species and an *a priori* fixed connectance. This stochastic model generates quickly numerous food webs with patterns that are roughly empirically consistent (Williams & Martinez, 2000, Cattin *et al.*, 2004, Allesina *et al.*, 2008). It is based on the principle of ecological niche (Hutchinson, 1957). A species i is characterized by a niche value n_i, that indicate its position on the segment $[0, 1]$, the niche axis (figure 5.6). Each species is also characterized by a continuous feeding range, a sub-interval of this axis. Species i feeds on all species whose niche value belongs to this range. It is defined by its center c_i and its relative width r_i. So this feeding range is $[c_i \pm n_i r_i/2]$. The niche value n_i is uniformly drawn in the interval $[0, 1]$. The relative width of the feeding range r_i is drawn from a beta distribution $\mathcal{B}\left(1, \frac{1}{2C} - 1\right)$, where C is the desired food web connectance. If C is high (low), the expected width of the feeding range is also high (low), and thus the expected number of prey species is high (low) too. The center of the feeding range c_i is uniformly drawn in the interval $[n_i r_i/2, \min(n_i, 1 - n_i r_i/2)]$ so that the feeding range is always a sub-interval of $[0, 1]$ (Williams & Martinez, 2004). Species whose feeding range does not contain any other species niche value do

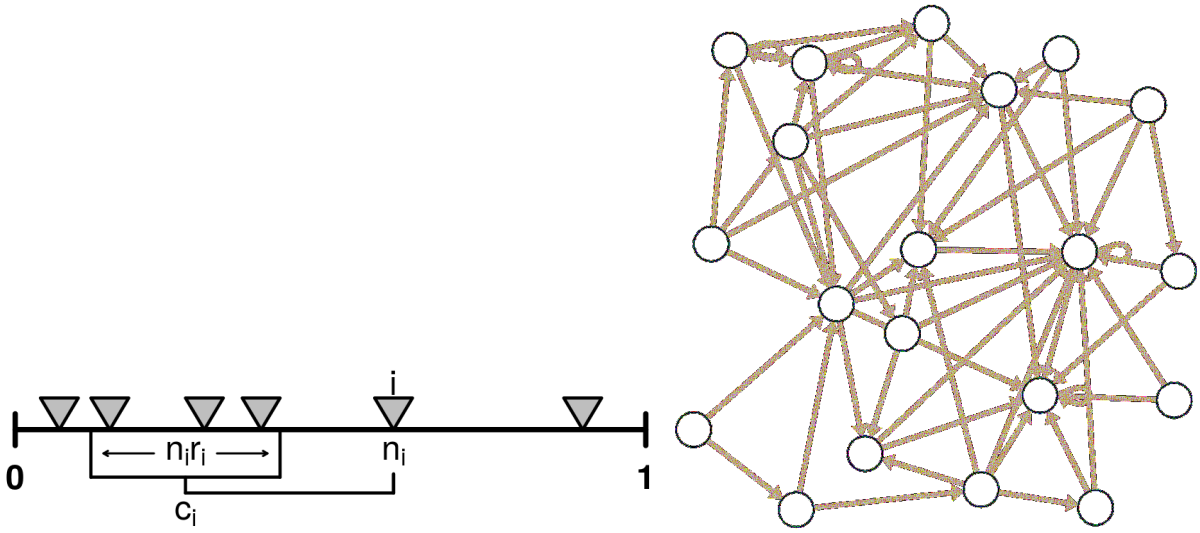

Figure 5.6. Scheme of the principle of the niche model (left, redrawn from Williams & Martinez, 2000, 2004) and an example of a 20 species food web generated by this model (right). This model is used to build all food webs studied in the remaining of the paper. The left scheme represents a food web with $S = 6$ species. The set of all possible ecological niches is summarized by the segment $[0, 1]$. The ecological niche of each species i is summarized by a niche value $n_i \in [0, 1]$. Each species feeds on a continuous range of prey species defined by its center c_i and its relative width r_i. Species which do not have any prey species in their feeding range are defined as primary producers. See section 5.5 for details on how the parameters values are randomly drawn.

not feed on any prey species and define primary producers. Other species are called predators. Species whose niche value does not belong to any other species feeding range define top predators. Construction of the feeding range intervals allows the possibility that the feeding range of a species contains its own niche value, so that it becomes its own prey (this is cannibalism). A predator may even feed on prey of higher niche value than itself, what may generate trophic loops in resulting food webs. In order to have at least one primary producer in the food web, the species with the lowest n_i has always $r_i = 0$.

The construction method in the niche model is such that the average connectance among numerous generated food webs is equal to the desired *a priori* connectance (through the second parameter of the beta distribution). Nevertheless, due to the variability of random draws, all food webs do not have exactly this desired connectance. Beside that, some generated food webs present unrealistic patterns. So we added a rejection step after food webs construction. We only studied food webs with a connectance that deviated at most by 0.01 of the desired one, that are connected (no disconnected parts), and in which all predators feed (as a prey or through a food chain) upon at least one primary producer. The average number of primary producers and the average proportion of cannibal species in food webs generated by the niche model are shown in

figure 5.7.

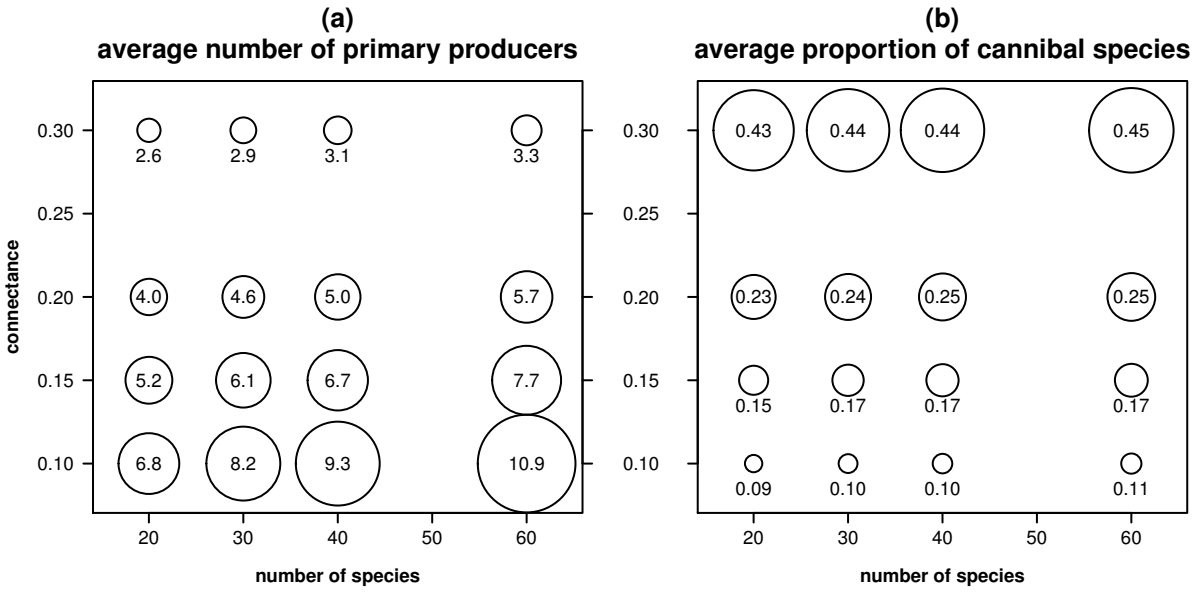

Figure 5.7. Average number of primary producers and proportion of cannibal species in the food webs studied. These numbers vary with trophic complexity (number of species and connectance). Estimations are realized on 10 000 food webs generated using the niche model proposed by Williams & Martinez (2000, 2004) for each trophic complexity.

5.6 Algorithm to classify asymptotic dynamics

In order to characterize the asymptotic dynamics of the numerous food webs studied, we built the following automatized classification algorithm. The algorithm starts by a time T_{ini} of initial simulation in order to limit transient effects due to the arbitrary initial condition. After that, the asymptotic dynamics is considered as associated to extinction(s) if at least one species has a biomass that becomes lower than an arbitrary extinction threshold B_{min}. Else, if the system converges to a point in the phase space (criterion $\sum_{i \in S} |dB_i/B_i dt| < \varepsilon_{cv}$) where all eigenvalues of the jacobian matrix have negative real parts, the asymptotic dynamics is a positive equilibrium. As long as no criterion is reached, the simulation continues. The whole simulation is divided in subparts of length T_{sub}. After each subpart, jacobian's eigenvalues at the temporal average of the dynamic during the current subpart are computed. If all eigenvalues have a negative real part the simulation continues, and finally an equilibrium is reached in all our simulations ending before T_{max} (see below). If at least one eigenvalue has a positive real part and if fluctuations do not change significantly between subparts of the simulation ($\sum_{i \in S} |\bar{B_i}^m - \bar{B_i}^{m-1}| < \varepsilon_{mean}$, with $\bar{B_i}^m$ being

the average of $B_i(t)$ for $t \in [T_{ini}, T_{ini} + mT_{sub}]$), the asymptotic dynamics will be considered as a fluctuating dynamic without any extinction. This is done because the multiple estimations of the jacobian matrix indicate that the flow is divergent at the average of the fluctuating dynamics. This means that the presence of a stable equilibrium around this average is very unlikely. Sometimes, reaching one of the criteria needs a long time of simulation. So we fixed a maximal time of simulation T_{max}. If the algorithm fails to classify a food web dynamics in one of the three classes before the simulation end, the dynamics is consider as unknown.

The algorithm used to solve ODEs is a Runge-Kutta-Fehlberg-4,5 numerical scheme, with absolute and relative error tolerances set to 10^{-6}. Preliminary tests showed that the choice of a specific numerical scheme among those tested does not affect the results. Tests were also done to choose the values of absolute and relative error tolerance. The parameter values used for our algorithm were tuned after preliminary tests to improve the algorithm efficiency. We set $T_{ini} = 500$, $T_{sub} = 5\ 000$, $T_{max} = 50T_{sub} + T_{ini}$, $B_{min} = 10^{-6}$, $\varepsilon_{cv} = 10^{-6}$ and $\varepsilon_{mean} = 0.01$. Results are the same if a lower B_{min} value is used to define extinctions. All simulations start with the arbitrary initial condition $B_i(0) = 1\ \forall i$. We used only one initial condition. Tests with 10 random initial conditions on 20-species food webs (connectance equals to 0.15) indicate that a small fraction of these food webs ($< 1\,\%$) can reach significantly different asymptotic dynamics depending on the initial condition. For computational reasons, we choose to use only one initial condition per food web.

The algorithm failed to classify food web dynamics before reaching T_{max} in 0.2 % of the food webs with Holling's FR and 2 % with Ivlev's FR. However, a study of the calculus made by the algorithm along the simulation allows to determine which asymptotic dynamics the system is likely to reach is the simulation continues. The proportion of these food webs which will likely reach a positive equilibrium is close to the proportion observed in food webs for which the algorithm determines the dynamics before T_{max} is reached. For example, among the 2 % of unknown dynamics with Ivlev, 98.5 % are likely to reach a positive equilibrium ($\varepsilon_{cv} < \sum_{i \in S} |dB_i/B_i dt| < 10^{-5}$) on average within the tested range of trophic complexity. This proportion is roughly equal to that observed in food webs for which dynamics have been determined (figure 5.2). So using a greater T_{max} will not significantly affect our results.

For some food webs which dynamics seems to converge on a positive equilibrium, the point reached is unstable. We found for some of these food webs that in fact the dynamics converges on a limit cycle which size is such that the algorithm considers it as an equilibrium. This happens when the food web is closed to a Hopf bifurcation (i.e. a pair of complex conjugated eigenvalues have small positive real parts). For some other food webs, we supposed that the dynamics fluctuates around one (or more) saddle(s) connected by an homoclinic or an heteroclinic loop (one eigenvalue

is real and slightly positive), but stays bounded in a set of the phase space which size is again such that the algorithm considers it as an equilibrium. This phenomenon is negligible with Holling's FR, with less than 10 cases observed among the hundreds thousands positive equilibria studied. With Ivlev's FR, it concerns up to 4.5 % of the food webs with a positive equilibrium. This proportion decreases with trophic complexity, mainly with connectance. When functional response fit at low prey densities is improved (section 5.3.3), it concerns up to 30 % of the food webs with a positive equilibrium. We consider these food webs as food webs which reach a positive equilibrium, because the ecological meaning of such small fluctuating dynamics is the same as an equilibrium. Considering these food webs as food webs with fluctuating dynamics, or neglecting them, do not affect our qualitative results and conclusions.

5.7 Different parameter sets for Ivlev's functional response

Table 5.2 in the article presents the dynamics of 30 species food webs (with a connectance of 0.15) predicted by different parameter sets for Ivlev's FR. These parameter sets come from different ways to fit the functional responses. To test the robustness of our main conclusions to the method of fit, some of these parameter sets are used to predict complexity-stability relationships with Ivlev's FR. We used the parameter sets obtained with a fitting range $T_i \in [0, 3.5]$ with both weight functions (uniform $\omega_{\mathcal{U}}$ and $\omega_{\mathcal{P}}$ presented in figure 5.1b), as well as the parameter set obtained using the empirical distribution of total prey biomass available predicted by Holling's FR (figure 5.3b).

The three parameter sets predict the same qualitative complexity-stability relationships as the ones presented in figure 5.2 (figures 5.8-5.10). The two parameter sets obtained with the more classical methods (see discussion in section 5.3.6) predict a higher frequency of equilibrium dynamics than Holling's FR ($\times$2.1 for the uniform weight function, figure 5.8, and $\times$1.9 for the empirical distribution, figure 5.10). A higher frequency of equilibrium dynamics is also predicted by the parameter set derived using $\omega_{\mathcal{P}}$ over $T_i \in [0, 3.5]$, despite the difference is quantitatively lower ($\times$1.2, figure 5.9).

5.8 Changes in model assumptions

We tested the influence of three assumptions on food web dynamics: fixing the number of primary producer species in food webs, deleting cannibalistic links, setting the body mass of primary producers equals to 1. Some of these assumptions are made in some previous studies about complexity-stability relationships in food webs, but the same combination is not always use. So

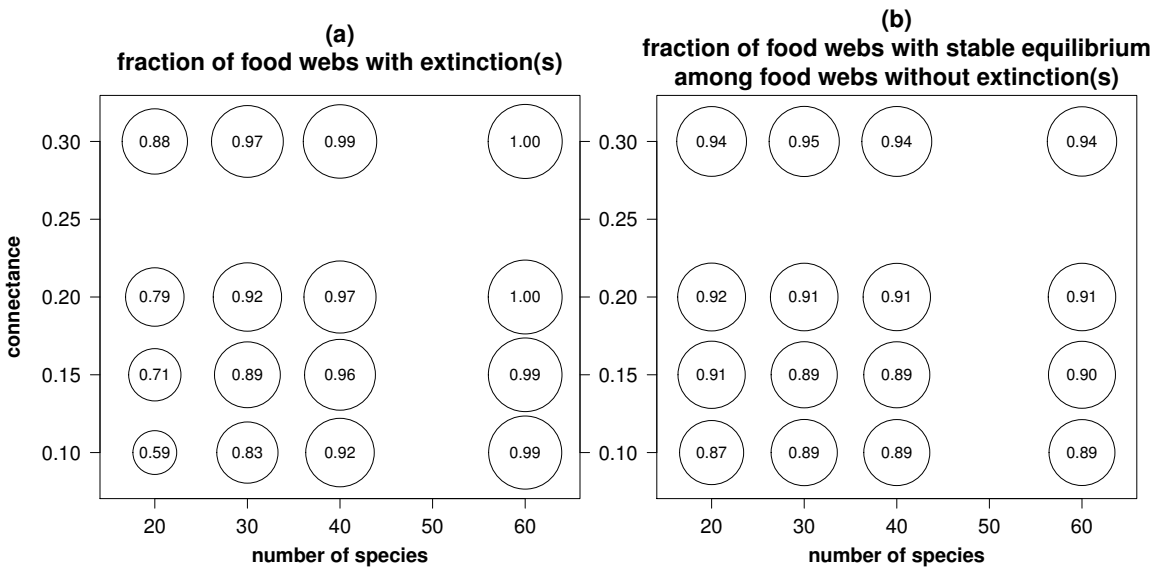

Figure 5.8. Food web dynamics as a function of trophic complexity predicted by Ivlev's functional response, fitted using a uniform weight function over $T_i \in [0, 3.5]$. a: fraction of food webs with at least one species extinction. b: fraction of persistent food webs with a stable positive equilibrium. The number of food webs studied for each pair of parameters is enough to obtain 1 000 food webs with a stable positive equilibrium.

we tested their influence in order to get the widest picture as possible. These results are used in section 5.3.5 in the article to explain the complexity-stability relationships predicted by the model. Here, we present the dynamics obtained within the tested range of trophic complexity for different combinations of assumptions, as well as a short description of their trends.

When food webs with a fixed number of five primary producer species are considered (figure 5.11), Ivlev's FR predicts on average less extinctions than Holling's FR (from −10 % to +3 %). Their frequency increases with the number of species (on average ×1.6 with Holling's FR and ×1.7 with Ivlev' FR) and decreases with connectance (×0.8 and ×0.9). On average, there are 2.6 times more equilibrium dynamics with Ivlev's FR (from 92 % to 99 %) than with Holling's FR (from 15 % to 78 %). The frequency of equilibrium dynamics increases with connectance (×4.3 with Holling's FR and +3 % with Ivlev's FR). We do not discuss any effect of the number of species as the number of food webs studied is lower for food webs with 40 and 60 species.

When body mass is set to 1 for primary producers (figures 5.12a,b and 5.13a,b), Ivlev's FR predicts on average less extinctions than Holling's FR (from −5 % to +2 %). Their frequency increases more with the number of species (×1.6 with Holling's FR and ×1.7 with Ivlev's FR) than with connectance (×1.2 with Holling's FR and ×1.3 with Ivlev's FR). Within the tested range of trophic complexity, the proportion of persistent food webs reaching an equilibrium is

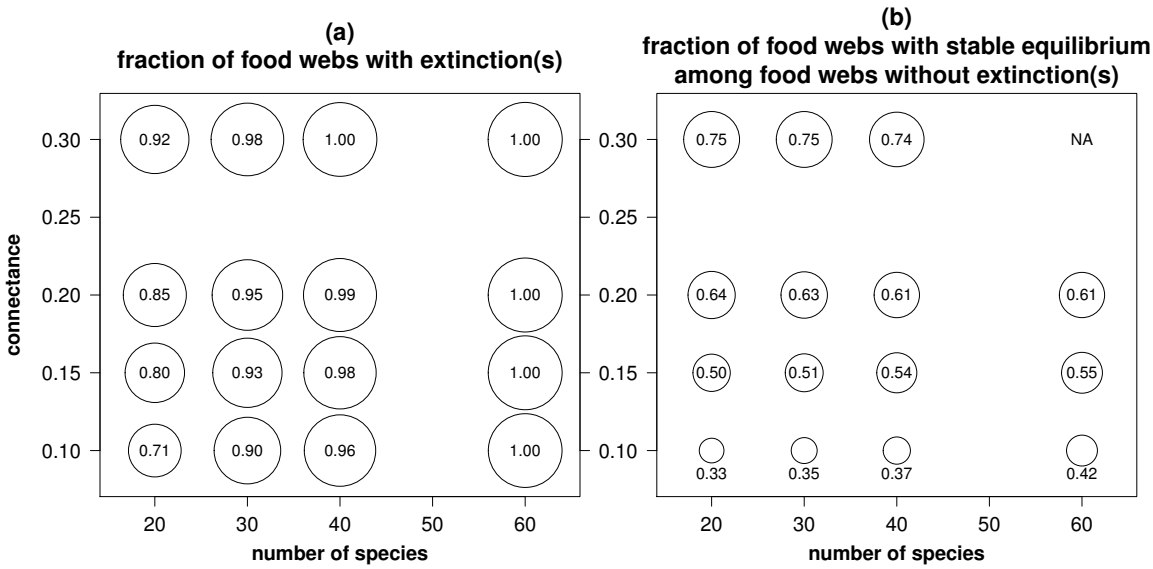

Figure 5.9. Food web dynamics as a function of trophic complexity predicted by Ivlev's functional response, fitted using the weight function $\omega_{\mathcal{P}}$ over $T_i \in [0, 3.5]$. a: fraction of food webs with at least one species extinction. b: fraction of persistent food webs with a stable positive equilibrium. NA means that the precise data has not been acquired for computational reasons (fraction of food webs with extinction(s) close to 1). The number of food webs studied for each pair of parameters is enough to obtain 1 000 food webs with a stable positive equilibrium.

always 100 % with Ivlev's FR and ranges from 38 % to 86 % with Holling's FR. With the latter, this proportion increases with connectance (×2.2) and does not show a clear trend with the number of species (from −3 % to +4 % depending on connectance).

When cannibalistic link are deleted and body mass is set to 1 for primary producers (figures 5.12c,d and 5.13c,d), Ivlev's FR predicts less extinction(s) than Holling's FR (from −9 % to no difference). Their frequency increases more with the number of species (×1.4 with Holling's FR and ×1.5 with Ivlev's FR) than with connectance (×1.2 and ×1.3). Within the tested range of trophic complexity, the proportion of persistent food webs reaching an equilibrium is always 100 % with Ivlev's FR and ranges from 35 % to 81 % with Holling's FR. With the latter, this proportion increases more with connectance (×2.2) than with the number of species (from −2 % to +7 % depending on connectance).

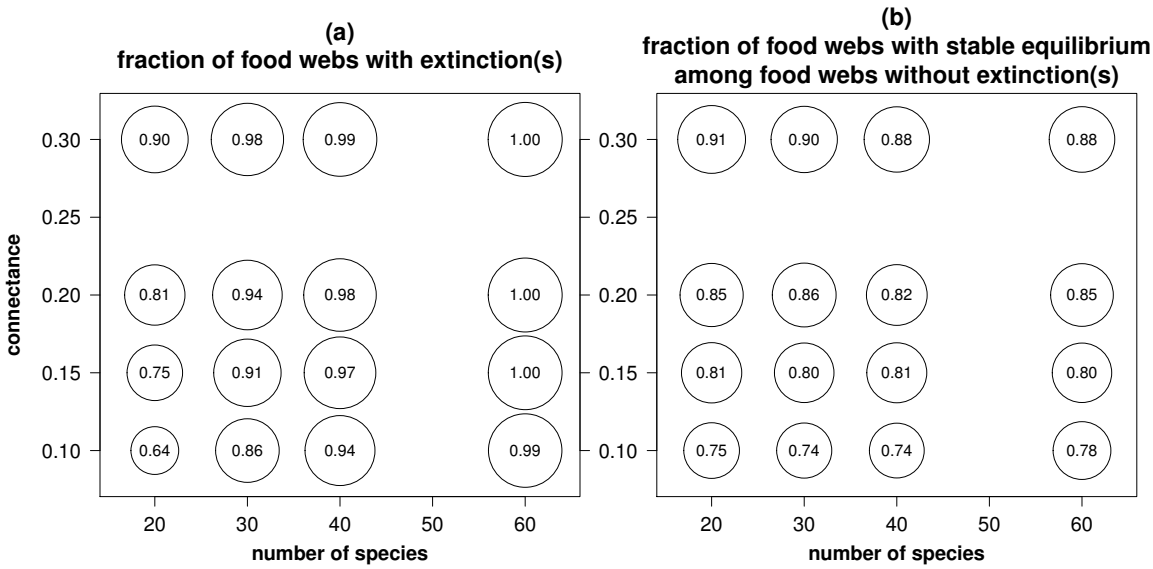

Figure 5.10. Food web dynamics as a function of trophic complexity predicted by Ivlev's functional response, fitted using the empirical distribution of prey biomass observed with Holling's disc equation (figure 3b in the article). a: fraction of food webs with at least one species extinction. b: fraction of persistent food webs with a stable positive equilibrium. The number of food webs studied for each pair of parameters is enough to obtain 1 000 food webs with a stable positive equilibrium.

5.9 Different metrics to quantify food web persistence and variability

We tested different metrics to quantify food web persistence and variability. Their estimation is based on the analysis of species biomass after a simulation of 100 000 time steps. Mean and variation coefficient were computed for each species over the last 10 000 time steps of the simulation.

Relationships between these metrics and those used in the article are presented in figures 5.14 and 5.15 for Holling's FR and Ivlev's FR respectively. Both functional responses again predict similar food web persistence if it is quantified using the average proportion of extincted species in networks (mean species biomass below 10^{-6}, panel a in both figures). Using this metrics, food web persistence also decreases more with the number of species than with connectance. Food web variability is again significantly lower with Ivlev's FR (non-overlapping ranges of values between formulations) when different metrics are used. Metrics based on the variation coefficient predict different complexity-stability relationships between formulations (panels c and d). However, we will not discuss relationships obtained with Ivlev's FR as the estimated values are close to 0 and within a small range of variations. Opposite complexity-stability relationships are also obtained if

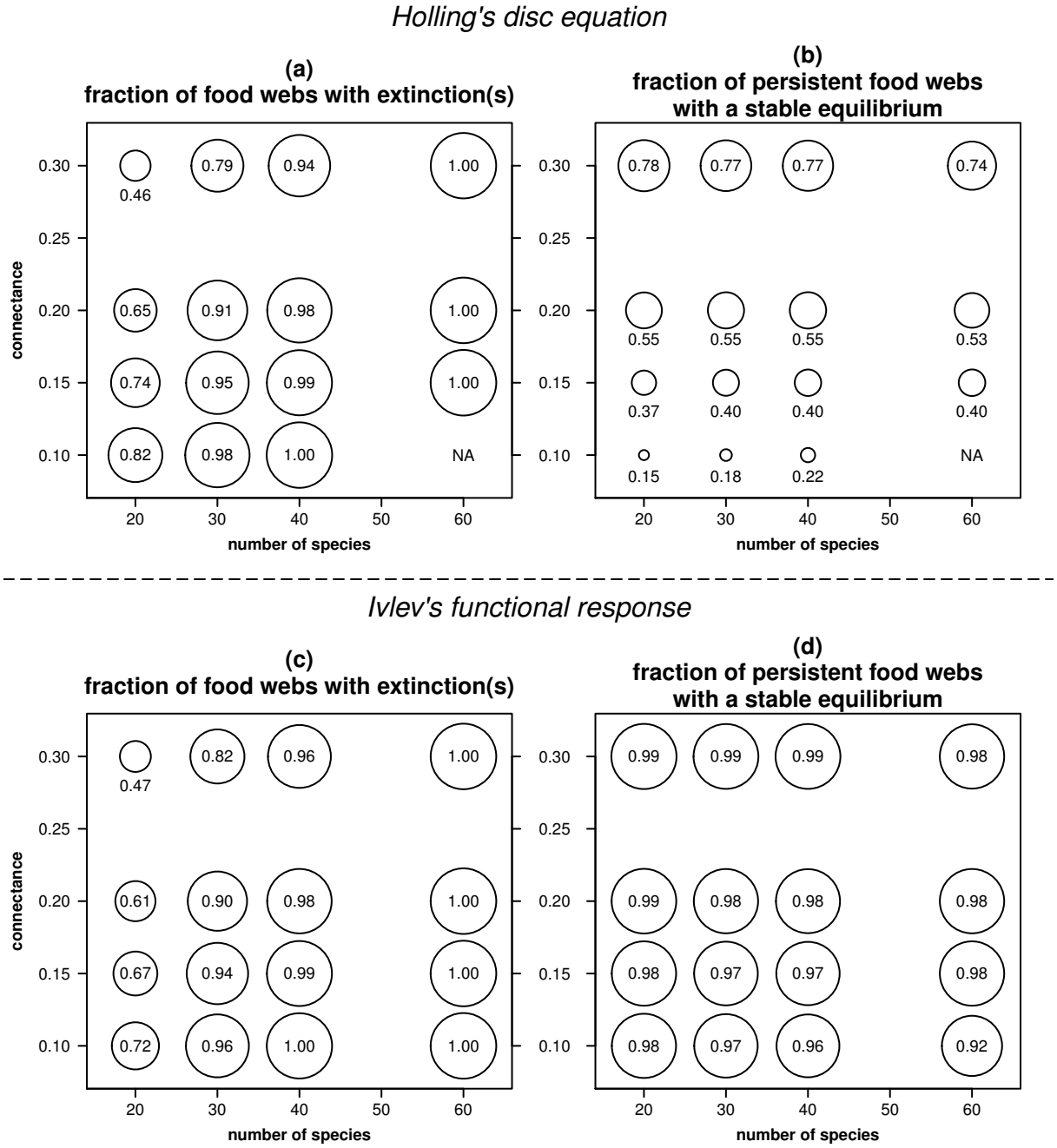

Figure 5.11. Food web dynamics as a function of trophic complexity predicted by Holling's (a, b) and Ivlev's functional responses (c, d) for food webs with a fixed number of five primary producer species. a, c: fraction of food webs with at least one species extinction. b, d: fraction of persistent food webs with a stable positive equilibrium. NA means that the precise data has not been acquired for computational reasons (fraction of food webs with extinction(s) close to 1). The number of food webs studied for each pair of parameters is enough to obtain N food webs with a stable positive equilibrium. For computational reasons, the value of N depends on the number of species (S), $N = 100$ if $S = 60$, $N = 1\,000$ if $S = 40$ and $N = 10\,000$ otherwise.

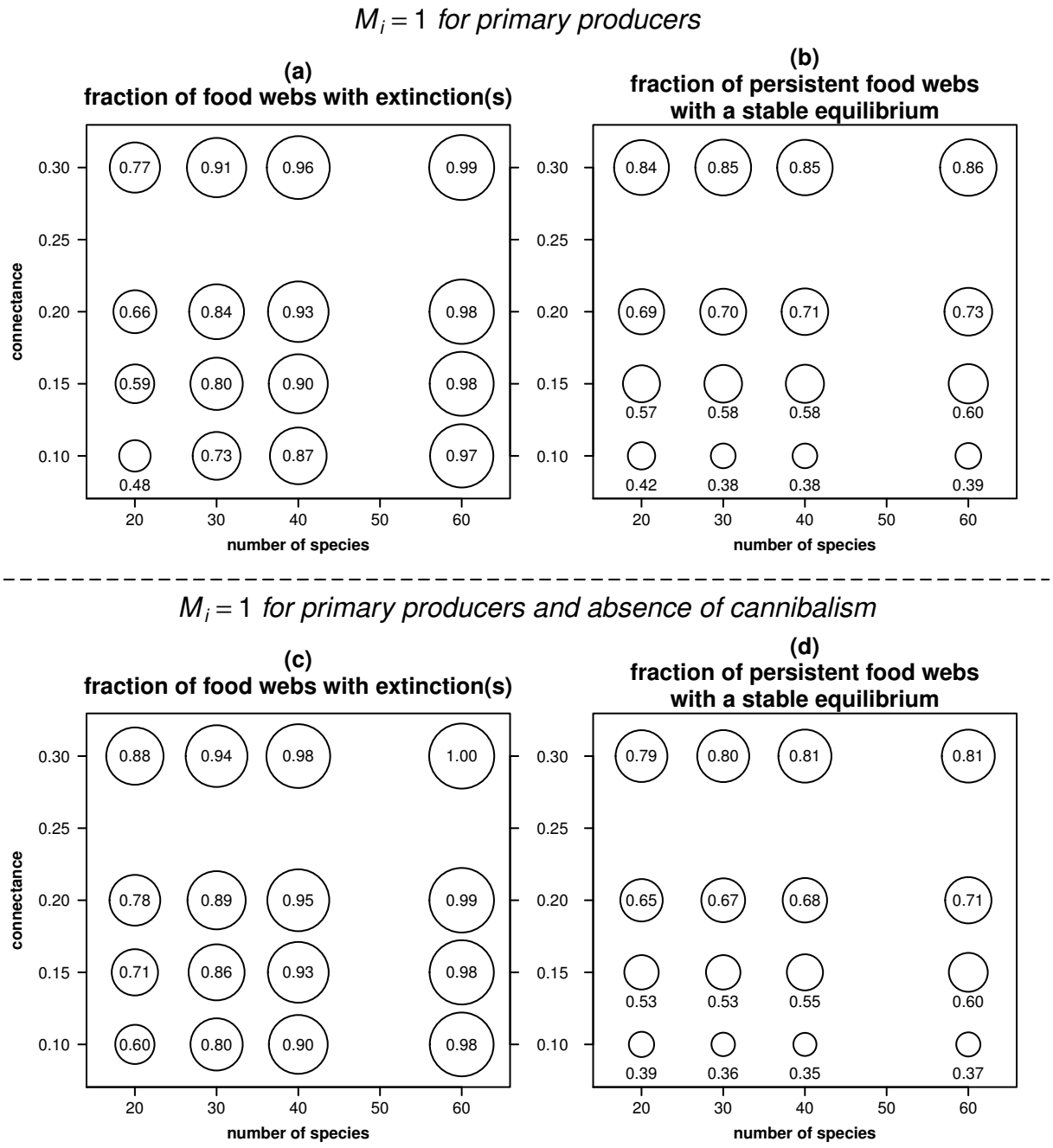

Figure 5.12. Food web dynamics as a function of trophic complexity predicted by Holling's disc equation, if the body mass M_i of all primary producer species is set to 1, for food webs in which cannibalistic links are kept (a, b) or removed (c, d). a, c: fraction of food webs with at least one species extinction. b, d: fraction of persistent food webs with a stable positive equilibrium. The number of food webs studied for each pair of parameters is enough to obtain 10 000 food webs with a stable positive equilibrium.

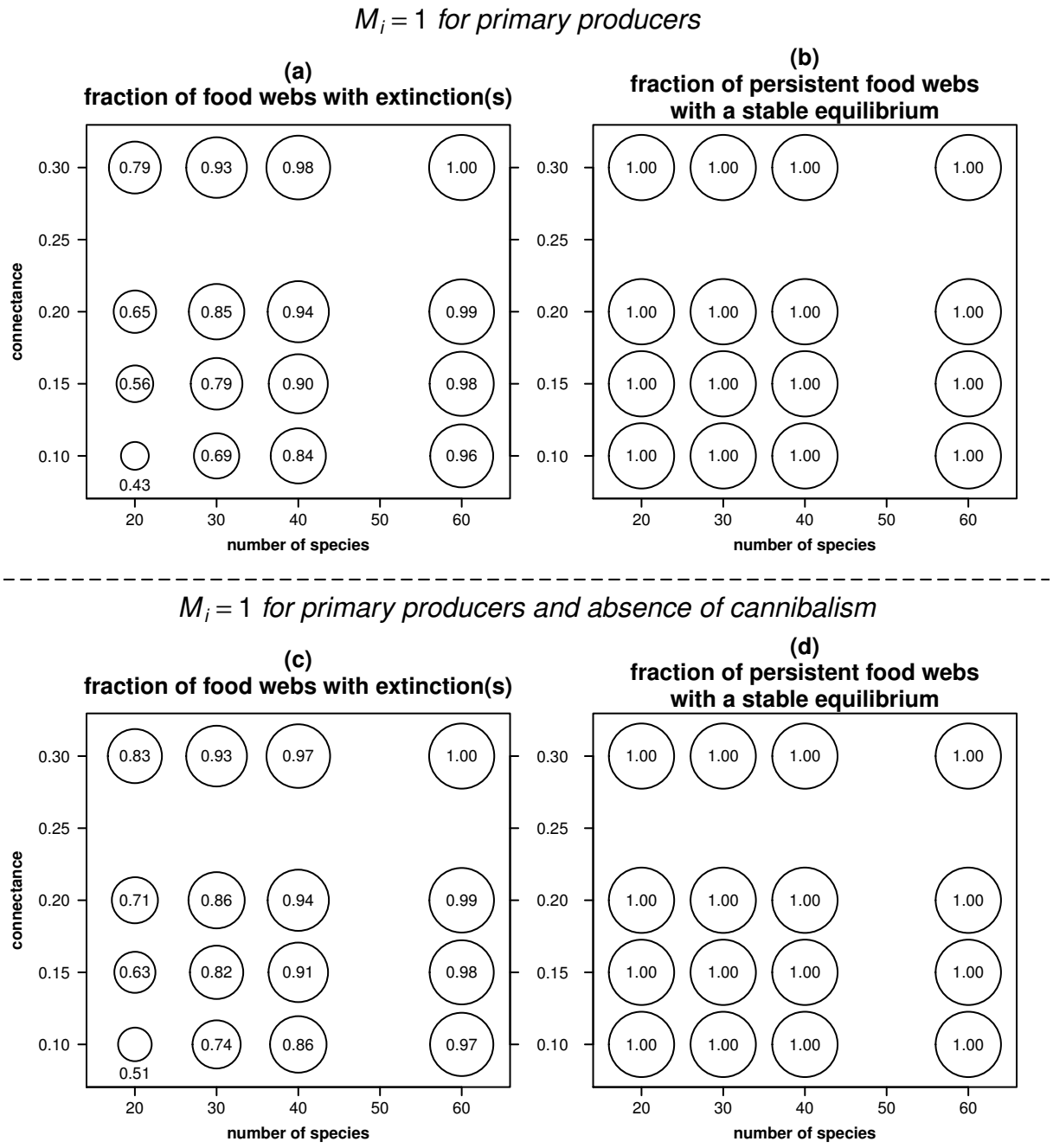

Figure 5.13. Food web dynamics as a function of trophic complexity predicted by Ivlev's functional response, if the body mass M_i of all primary producer species is set to 1, for food webs in which cannibalistic links are kept (a, b) or removed (c, d). a, c: fraction of food webs with at least one species extinction. b, d: fraction of persistent food webs with a stable positive equilibrium. The number of food webs studied for each pair of parameters is enough to obtain 10 000 food webs with a stable positive equilibrium.

we focus on the fraction of food webs with fluctuating dynamics, whatever the number of species extinctions that occured (panel b). However, the predicted food web variability is still lower with Ivlev's FR. Furthermore, considering food webs with extinctions, as for all these metrics, introduces a bias as the number of species and connectance are changed during simulation.

5.10 Identification of stabilizing factors through Generalized Modelling

We want to identify the stabilizing factors in the food web model for any type-II functional response and use them to explain our results from dynamical simulations. Here, we start by explaining how we derived the generalized model use to identify these factors expressed in terms of generalized parameters. Then we summarize the key results about the role of generalized parameters in equilibria stability. Finally, these generalized parameters are calculated in food webs at equilibrium in our dynamical simulations to explain why more equilibrium dynamics are predicted by Ivlev's FR.

To build the generalized model, we first consider the differential system made of S equations corresponding to S species (see section 5.2.2 for details):

$$\frac{dB_i}{dt} = \lambda q_i^{\phi} B_i + \lambda \sum_{j \in R_i} G_{i,j}^{\phi} B_i - \sum_{j \in C_i} G_{j,i}^{\phi} B_j - \alpha_i B_i - \beta_i B_i^2 \equiv F_i^{\phi}(\boldsymbol{B}), \quad i = 1, ..., S$$

with $\boldsymbol{B} = (..., B_i, ...)^T$, without specifying the functional response $G_{i,j}^{\phi}$ and the parameter values. We only claim that the functional response assumes no prey switching with constant fractional foraging effort, fulfills properties):

$$G_i^{\phi,tot} \in \mathcal{C}^2,\ G_i^{\phi,tot}(0) = 0,\ G_i^{\phi,tot} \geq 0,\ G_i^{\phi,tot\,\prime}(T_i) > 0,\ G_i^{\phi,tot\,\prime\prime}(T_i) < 0,\ \lim_{T_i \to +\infty} G_i^{\phi,tot}(T_i) < +\infty.$$

So we consider in fact a family of models. Generalized modelling supposes that some models in this family have positive equilibria. The qualitative stability of a positive equilibrium is then studied using the Jacobian matrix:

$$\frac{\partial F_i^{\phi}(\boldsymbol{B^*})}{dB_i} = \lambda \left[q_i^{\phi} + G_i^{\phi,tot*} + B_i^* \left. \frac{\partial G_i^{\phi,tot}}{\partial B_i} \right|_{\mathbf{B}^*} \right] - G_{i,i}^{\phi *} - \sum_{k \in C_i} B_k^* \left. \frac{\partial G_{k,i}^{\phi}}{\partial B_i} \right|_{\mathbf{B}^*} - \alpha_i - 2\beta_i B_i^*, \quad i = 1, ..., S,$$

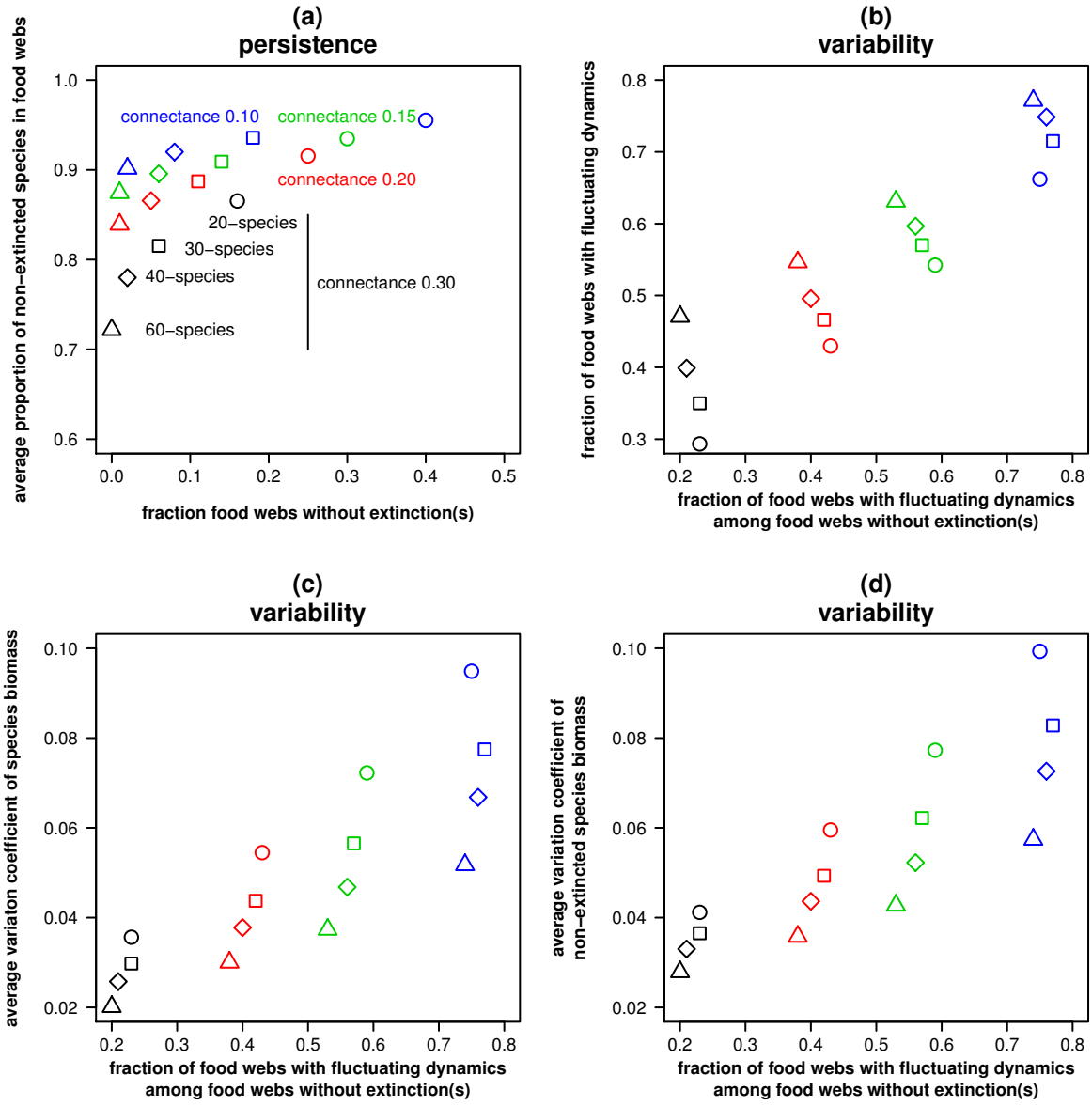

Figure 5.14. Relationships between different measures of the persistence (a) and the variability (b-d) of the food webs modeled using Holling's disc equation. The x-axis corresponds to the measure used in our study whereas the y-axis corresponds to another one. Each point indicates the values obtained for 10 000 food webs with the same number of species and connectance. Sixteen pairs of values are studied: four number of species (20: circle, 30: square, 40: diamond, 60: triangle) times four connectance levels (0.10: blue, 0.15: green, 0.20: red, 0.30: black). Simulations of 100 000 time units were performed to estimate the measures which are not used in the remaining of our study. The average and the standard deviation of species biomass were calculated across the 10 000 last time units. Extincted species are those with an average biomass below 10^{-6}.

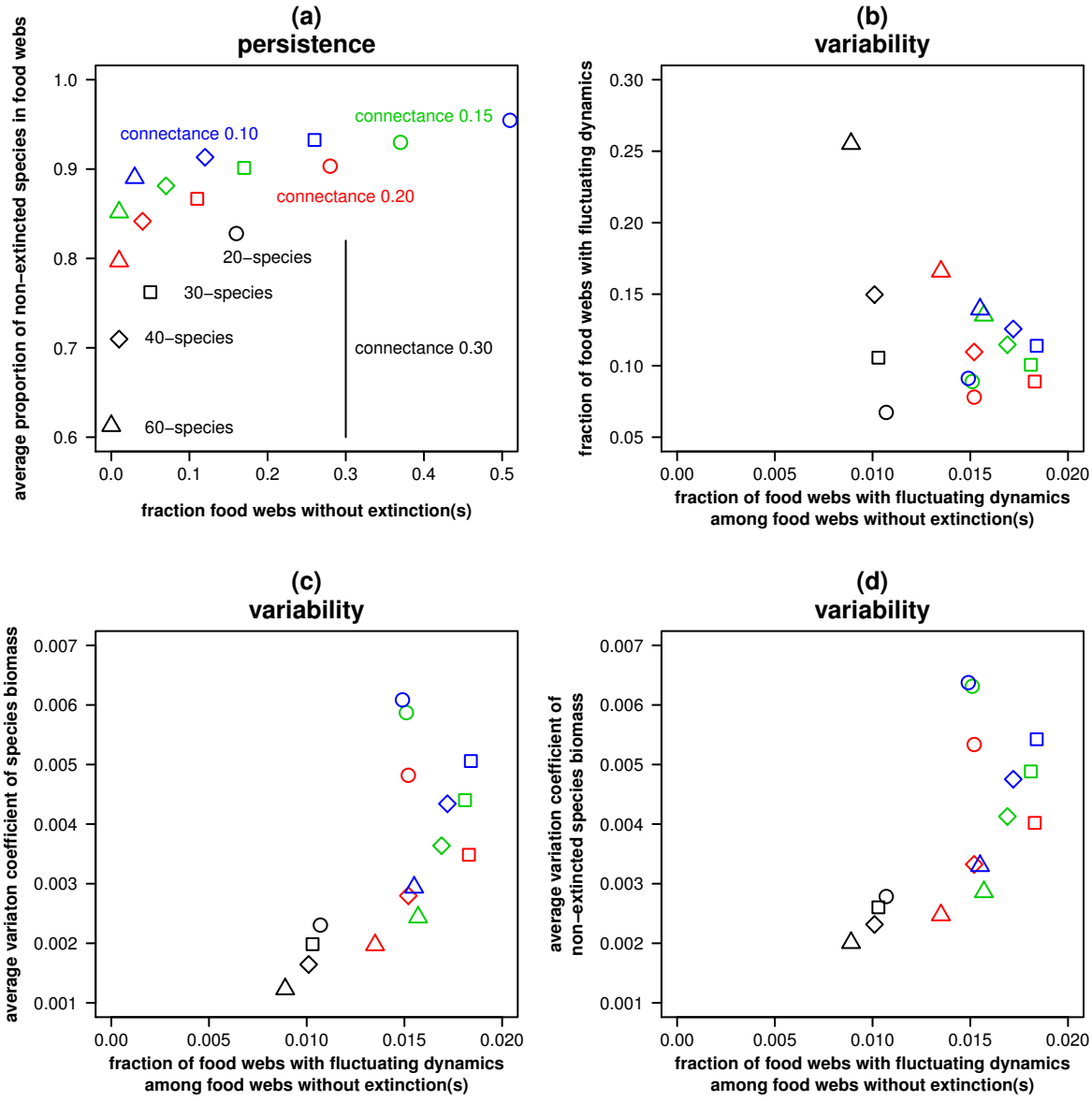

Figure 5.15. Relationships between different measures of the persistence (a) and the variability (b-d) of the food webs modeled using Ivlev's functional response. The x-axis corresponds to the measure used in our study whereas the y-axis corresponds to another one. Each point indicates the values obtained for 10 000 food webs with the same number of species and connectance. Sixteen pairs of values are studied: four number of species (20: circle, 30: square, 40: diamond, 60: triangle) times four connectance levels (0.10: blue, 0.15: green, 0.20: red, 0.30: black). Simulations of 100 000 time units were performed to estimate the measures which are not used in the remaining of our study. The average and the standard deviation of species biomass were calculated across the 10 000 last time units. Extincted species are those with an average biomass below 10^{-6}.

$$\frac{\partial F_i^{\phi}(\boldsymbol{B^*})}{dB_j} = \lambda B_i^* \left.\frac{\partial G_i^{\phi,tot}}{\partial B_j}\right|_{\mathbf{B}^*} - G_{j,i}^{\phi *} + \sum_{k\in C_i} \left.\frac{\partial G_{k,i}^{\phi}}{\partial B_j}\right|_{\mathbf{B}^*}, \quad i,j = 1,...,S,\ j \neq i,$$

evaluated at a positive equilibrium $\mathbf{B}^* = (..., B_i^*, ...)$. Then we re-write this matrix using generalized parameters that describe the system close to this equilibrium (table 5.5):

$$\begin{cases} \dfrac{\partial F_i^{\phi}(\boldsymbol{B^*})}{dB_i} &= \tau_i \left[1 - (1-\delta_i)\mu_i - \delta_i \left(\rho_{i,i}(1-\lambda\gamma_i) + \sum\limits_{k\in C_i} \rho_{k,i}[(\gamma_k - 1)\chi_{k,i} + 1]\right)\right], \\ \dfrac{\partial F_i^{\phi}(\boldsymbol{B^*})}{dB_j} &= \tau_i \nu_{i,j} \left[\theta_i \gamma_i \chi_{i,j} - \delta_i \left(\rho_{j,i} + \sum\limits_{k\in C_i} \rho_{k,i}(\gamma_k - 1)\chi_{k,j}\right)\right], \quad i,j = 1,...S,\ i \neq j. \end{cases} \tag{5.4}$$

Details on the derivation procedure to define generalized parameters are presented in Gross & Feudel (2006) and Yeakel *et al.* (2011). Then, equilibrium stability is studied as a function of the generalized parameter values without specific assumptions on the functions and original parameter (such as a^{ϕ} or h^{ϕ}) values behind them.

This generalized model is an extension of a model proposed by Plitzko *et al.* (2012). First, we correct a mistake in Plitzko *et al.* (2012)'s calculus by adding the parameter $\nu_{i,j}$ (a biomass ratio) to non-diagonal terms. We checked that this mistake does not affect results presented by Plitzko *et al.* (2012) under the assumptions they made for their numerical study. Second, we also complete the diagonal terms to take cannibalism into account. Finally, we provide a generalized parameter formulation independent of a specific functional response.

For food webs made with S species, there are $5S(S+1)/2$ degrees of freedom in the parameter set of the generalized model (5.4) if no special assumption is made. It is not possible to realize a bifurcation analysis like for a predator-prey model (section 3.4). Furthermore, results depend on the trophic complexity and food web structure. So, numerous food webs have to be studied to obtain statistical results. To avoid unreasonable computing costs, we need to make some assumptions to decrease the number of degrees of freedom and study only some parameters of interest. As in all this study, we first assume that a species is either a primary producer ($\theta_i = 0$) or a predator ($\theta_i = 1$), the selection being done during food web construction by the niche model (see section 2.1 in the article for details). Since Gross *et al.* (2009) reported that the time scale τ_i does not significantly affect equilibria stability, it is arbitrarily set to 1 for all species. Then, as the mean biomass ratio is $\bar{\nu} = 1$ by definition, we assume $\nu_{i,j} = 1\ \forall i,j$. It implies that $B_i^* = B_j^*\ \forall i,j$ and so that $\chi_{i,j} = 1/|R_i|$ if $j \in R_i$ (0 otherwise). Note that $1/|R_i|$ is also by definition the mean fraction of total prey biomass represented by each prey of species i. Similarly, $1/|C_i|$ is by definition the mean fraction of total predative losses represented by each predator of species i. We assume $\rho_{j,i} = 1/|C_i|$ if $j \in C_i$ (0 otherwise). Values of other parameters are assumed to be constant across a food

Table 5.5. Formulation and ecological meaning of the generalized parameters used to build the generalized model. Generalized parameters are used in the generalized model to describe the local dynamics of the system close to an equilibrium. Their value are independent of the specific formulation of the functional response because they only describe a local dynamics. So the stability of an equilibrium depends only of their value at these equilibrium. The scale parameters describe the time scale of species dynamics (for τ_i) and the relative contribution of the different processes to this dynamics. Elasticities (called exponent parameters by some authors) measure the non-linearity of processes.

generalized parameter formulation	**ecological meaning**
scale parameters	
$\tau_i = \lambda\left(q_i^\phi + G_i^{\phi,tot*}\right)$ $= \sum_{j\in C_i} G_{j,i}^{\phi*}\frac{B_j^*}{B_i^*} + (\alpha+\beta B_i^*)\, M_i^{-0.25}$	time scale of species i's dynamics
$\theta_i = \frac{1}{\tau_i^\phi}\lambda G_i^{\phi,tot*}$	fraction of gains of species i obtained by predation
$1-\theta_i = \frac{1}{\tau_i^\phi}\lambda q_i^\phi$	fraction of gains of species i obtained by primary production
$\delta_i = \frac{1}{\tau_i^\phi}\sum_{j\in C_i} G_{j,i}^{\phi*}\frac{B_j^*}{B_i^*}$	fraction of losses of species i due to predation
$1-\delta_i = \frac{1}{\tau_i^\phi}(\alpha+\beta B_i^*)\, M_i^{-0.25}$	fraction of losses of species i due to intrinsic dynamics
$\chi_{i,j} = \begin{cases} \frac{B_j^*}{T_i^*} & \text{if } j\in R_i \\ 0 & \text{otherwise} \end{cases}$	fraction of gains by predation of species i from species j
$\rho_{i,j} = \begin{cases} \frac{1}{\tau_i^\phi \delta_i^\phi} G_{j,i}^{\phi*}\frac{B_j^*}{B_i^*} & \text{if } i\in R_j \\ 0 & \text{otherwise} \end{cases}$	fraction of losses by predation of species i due to species j
$\nu_{i,j} = B_i^*/B_j^*$	biomass ratio between species i and j
elasticities (also called exponent parameters)	
$\mu_i = 1 + \frac{\beta B_i^*}{\alpha+\beta B_i^*} \in [1,2]$	non-linearity of intrinsic mortality for species i
$\gamma_i = g_i^{\phi\prime}(1) \in [0,1]$ with $t_i = \frac{T_i}{T_i^*}$ and $g_i^\phi(t_i) := \frac{G_i^{\phi,tot}(t_i T_i^*)}{G_i^{\phi,tot}(T_i^*)}$	slope of the normalized functional response of species i

web. Numerical simulations were realized with $\mu_i = \mu \in \{4/3, 3/2, 5/3\}$, $\delta_i = \delta \in \{1/3, 1/2, 2/3\}$ if species i has predators and $\delta_i = 0$ if species i is a top-predator, $\gamma_i = \gamma \in [0,1]$ (discretized by step of 0.01) and $\lambda \in \{0, 1/4, 1/2, 3/4, 1\}$. We studied food webs of varying number of species $S \in \{20, 30, 40, 60\}$ and connectance $C \in \{0.10, 0.15, 0.20, 0.30\}$ as in the rest of this study.

According to the jacobian matrix of the generalized model (5.4), the proportion of food webs with a stable positive equilibrium is higher if density-dependent mortality is high (high value of μ) and/or if there is a small fraction of losses due to predation (low value of δ, figure 5.16). This corresponds to a high value of $(1-\delta)\mu$, which plays a negative role in the diagonal elements of the

jacobian matrix. Negative terms in diagonal elements of the jacobian matrix are known to increase local stability of equilibria in some food web models (Takeuchi, 1996). If $(1-\delta)\mu$ is high, more food webs have a stable equilibrium for intermediate values of γ, whatever the trophic complexity. Otherwise, the proportion of all the food webs with a stable equilibrium increases on average with γ values.

For each set of generalized parameter valued, we use a statistical linear model to quantify the effect of the number of species and connectance on the proportion of food webs with a stable positive equilibrium (arrows in figure 5.16). For low values of γ (high prey biomass), there is a positive complexity-stability relationship. It is mainly due to connectance, which affect more the fraction of food webs with a stable equilibrium than the number of species. For intermediate values of γ, the fraction of food webs with a stable equilibrium is increased by connectance and decreased by the number of species. For high values of γ (low prey biomass), there is a negative complexity-stability relationship, with a similar impact of the number of species and connectance. The assimilation efficiency λ slightly affects the quantitative results, but not the qualitative trends (figures 5.17 and 5.18). The highest proportions of food webs with a stable equilibrium are obtained in the limit case of $\lambda = 0$, and the lowest in the opposite limit case $\lambda = 1$. On average, deleting cannibalistic links decreases the proportion of food webs with a stable equilibrium but do not affect the qualitative results on complexity-stability relationships (figure 5.19). Considering only food webs with a fixed number of primary producers has only a little quantitative impact on the results (figures 5.20 and 5.21) as the positive equilibrium is assumed to exist.

To summarize, the stabilizing factors of positive equilibria found in a predator-prey model (section 3.4 and by Yeakel *et al.*, 2011) are also observed at the food web scale. Nevertheless they are less straightforward, because of the interplay with trophic complexity. For example, highest stability is found for a high or intermediate slope of the functional response γ, depending on other parameter values and trophic complexity.

We calculated generalized parameters for food webs at positive equilibrium simulated in figure 5.2. Generalized parameters can be viewed as indicators of the food web functioning close to this equilibrium. Because the statistical distributions of species biomass at equilibrium are similar between functional responses (figure 5.22a), similar distributions for the parameters (such as δ_i) and for the non-linearity of species mortality μ_i are also observed (figure 5.22c,d). At the opposite, different distributions are observed for the normalized slope of the functional response γ_i (figure 5.22b). The average value obtained with Ivlev's FR ($\bar{\gamma} = 0.60$) is 1.6 times higher than the average obtained with Holling's functional response ($\bar{\gamma} = 0.37$).

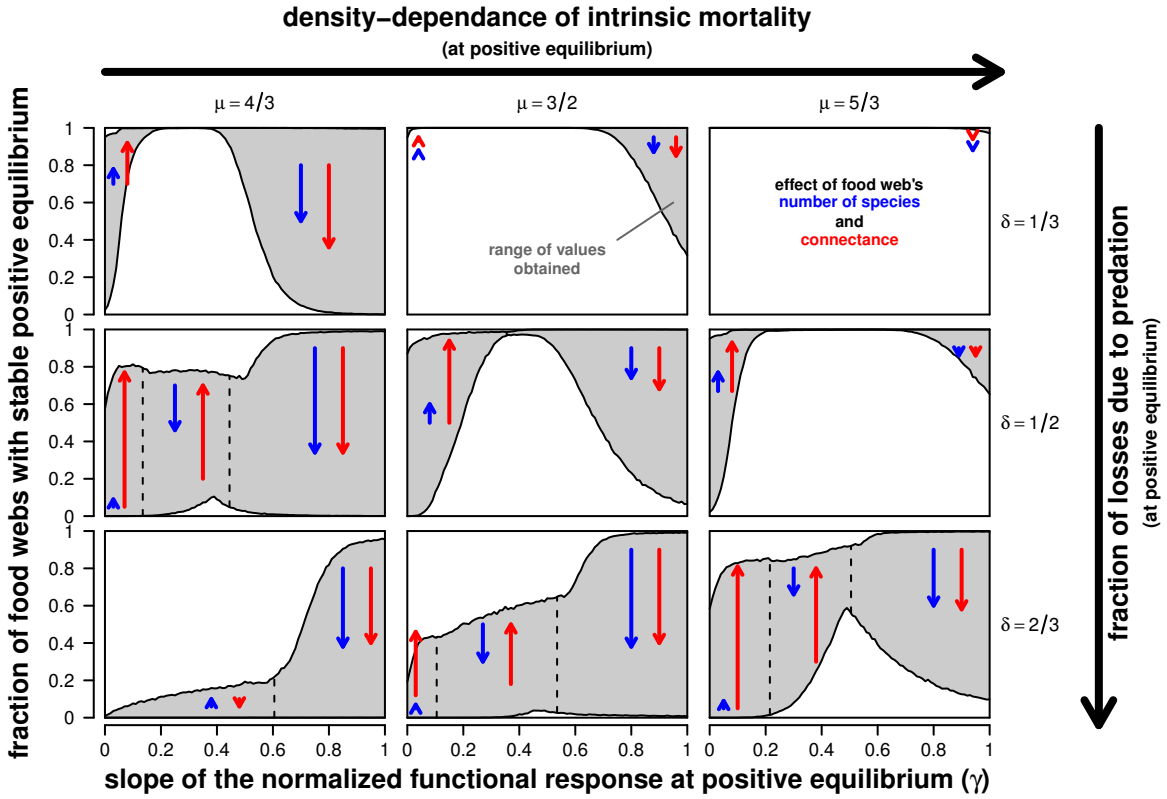

Figure 5.16. Fraction of food webs with a stable positive equilibrium for the generalized model, as a function of generalized parameters values and trophic complexity (number of species and connectance). Food web topology is generated using niche model (Williams & Martinez, 2000, 2004). For each set of parameters, 10000 food webs are studied. Assimilation efficiency λ is set to 0.75 (the value has a little impact on the results).

Results are presented for 9 pairs of density-dependence of mortality (μ, varying across columns) and fraction of losses due to predation (δ, varying across rows). In each panel, the fraction of food webs with a stable positive equilibrium is presented as a function of the slope of the normalized functional response (γ, discretized by step of 0.01). Results were estimated for 16 pairs of connectance ($C \in \{0.10, 0.15, 0.20, 0.30\}$) and number of species ($S \in \{20, 30, 40, 60\}$). The grey area on each graph indicates the range of values obtained. For each value of γ, a linear model $y = z_1 + z_2 S + z_3 C + \varepsilon$ (with y the fraction of stable food webs, $z = {}^t(z_1, z_2, z_3) \in \mathbb{R}^3$ the vector of parameters and ε the error of prediction) is used to estimate the respective effect of the number of species and connectance on the proportion of food webs with a stable positive equilibrium. Changes in the sign of z_2 and/or z_3 occur at values of γ corresponding to vertical dashed lines. Blue and red arrows represent respectively the average z_1 and z_2 between two vertical dashed lines. The length of the arrow's tail is equal to the average value of its associated parameter (normalized value of the parameter readable on the left axis with a ± 0.01 precision).

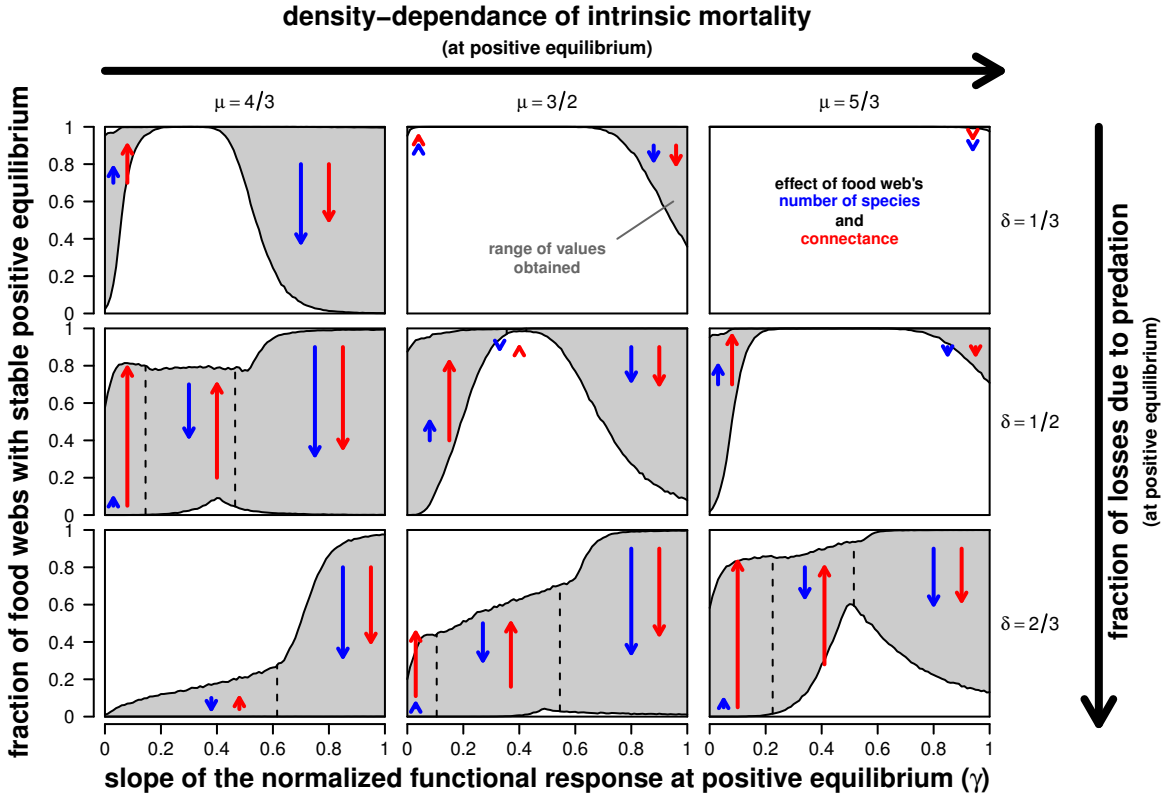

Figure 5.17. Fraction of food webs with a stable positive equilibrium for the generalized model, as a function of generalized parameters values and trophic complexity (number of species and connectance) when assimilation efficiency λ is set to 0. Food web topology is generated using niche model (Williams & Martinez, 2000, 2004). For each set of parameters, 10000 food webs are studied.
Results are presented for 9 pairs of density-dependence of mortality (μ, varying across columns) and fraction of losses due to predation (δ, varying across rows). In each panel, the fraction of food webs with a stable positive equilibrium is presented as a function of the slope of the normalized functional response (γ, discretized by step of 0.01). Results were estimated for 16 pairs of connectance ($C \in \{0.10, 0.15, 0.20, 0.30\}$) and number of species ($S \in \{20, 30, 40, 60\}$). The grey area on each graph indicates the range of values obtained. For each value of γ, a linear model $y = z_1 + z_2 S + z_3 C + \varepsilon$ (with y the fraction of stable food webs, $z = {}^t(z_1, z_2, z_3) \in \mathbb{R}^3$ the vector of parameters and ε the error of prediction) is used to estimate the respective effect of the number of species and connectance on the proportion of food webs with a stable positive equilibrium. Changes in the sign of z_2 and/or z_3 occur at values of γ corresponding to vertical dashed lines. Blue and red arrows represent respectively the average z_1 and z_2 between two vertical dashed lines. The length of the arrow's tail is equal to the average value of its associated parameter (normalized value of the parameter readable on the left axis with a ± 0.01 precision).

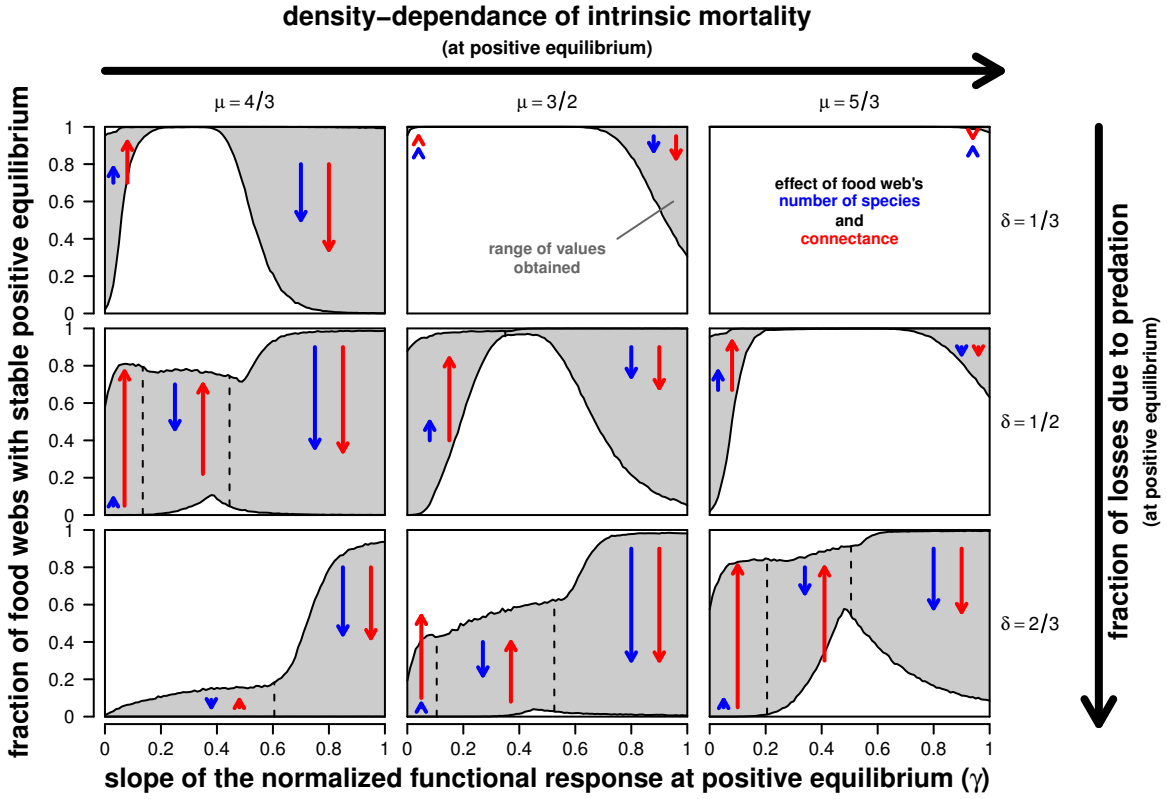

Figure 5.18. Fraction of food webs with a stable positive equilibrium for the generalized model, as a function of generalized parameters values and trophic complexity (number of species and connectance) when assimilation efficiency λ is set to 1. Food web topology is generated using niche model (Williams & Martinez, 2000, 2004). For each set of parameters, 10000 food webs are studied.
Results are presented for 9 pairs of density-dependence of mortality (μ, varying across columns) and fraction of losses due to predation (δ, varying across rows). In each panel, the fraction of food webs with a stable positive equilibrium is presented as a function of the slope of the normalized functional response (γ, discretized by step of 0.01). Results were estimated for 16 pairs of connectance ($C \in \{0.10, 0.15, 0.20, 0.30\}$) and number of species ($S \in \{20, 30, 40, 60\}$). The grey area on each graph indicates the range of values obtained. For each value of γ, a linear model $y = z_1 + z_2 S + z_3 C + \varepsilon$ (with y the fraction of stable food webs, $z = {}^t(z_1, z_2, z_3) \in \mathbb{R}^3$ the vector of parameters and ε the error of prediction) is used to estimate the respective effect of the number of species and connectance on the proportion of food webs with a stable positive equilibrium. Changes in the sign of z_2 and/or z_3 occur at values of γ corresponding to vertical dashed lines. Blue and red arrows represent respectively the average z_1 and z_2 between two vertical dashed lines. The length of the arrow's tail is equal to the average value of its associated parameter (normalized value of the parameter readable on the left axis with a ± 0.01 precision).

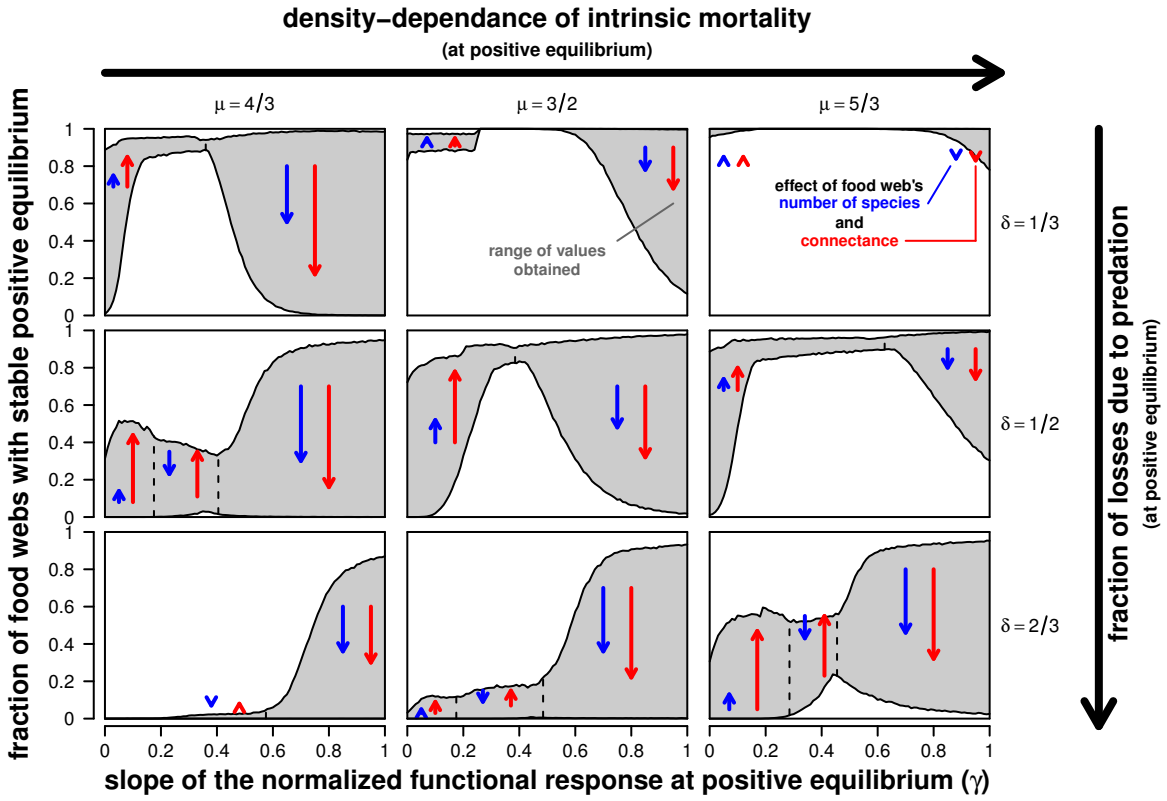

Figure 5.19. Fraction of food webs with a stable positive equilibrium for the generalized model, as a function of generalized parameters values and trophic complexity (number of species and connectance) in absence of cannibalism. Food web topology is generated using niche model (Williams & Martinez, 2000, 2004). For each set of parameters, 10000 food webs in which cannibalistic links have been removed are studied. Results are presented for 9 pairs of density-dependence of mortality (μ, varying across columns) and fraction of losses due to predation (δ, varying across rows). In each panel, the fraction of food webs with a stable positive equilibrium is presented as a function of the slope of the normalized functional response (γ, discretized by step of 0.01). Results were estimated for 16 pairs of connectance ($C \in \{0.10, 0.15, 0.20, 0.30\}$) and number of species ($S \in \{20, 30, 40, 60\}$). The grey area on each graph indicates the range of values obtained. For each value of γ, a linear model $y = z_1 + z_2 S + z_3 C + \varepsilon$ (with y the fraction of stable food webs, $z = {}^t(z_1, z_2, z_3) \in \mathbb{R}^3$ the vector of parameters and ε the error of prediction) is used to estimate the respective effect of the number of species and connectance on the proportion of food webs with a stable positive equilibrium. Changes in the sign of z_2 and/or z_3 occur at values of γ corresponding to vertical dashed lines. Blue and red arrows represent respectively the average z_1 and z_2 between two vertical dashed lines. The length of the arrow's tail is equal to the average value of its associated parameter (normalized value of the parameter readable on the left axis with a ± 0.01 precision).

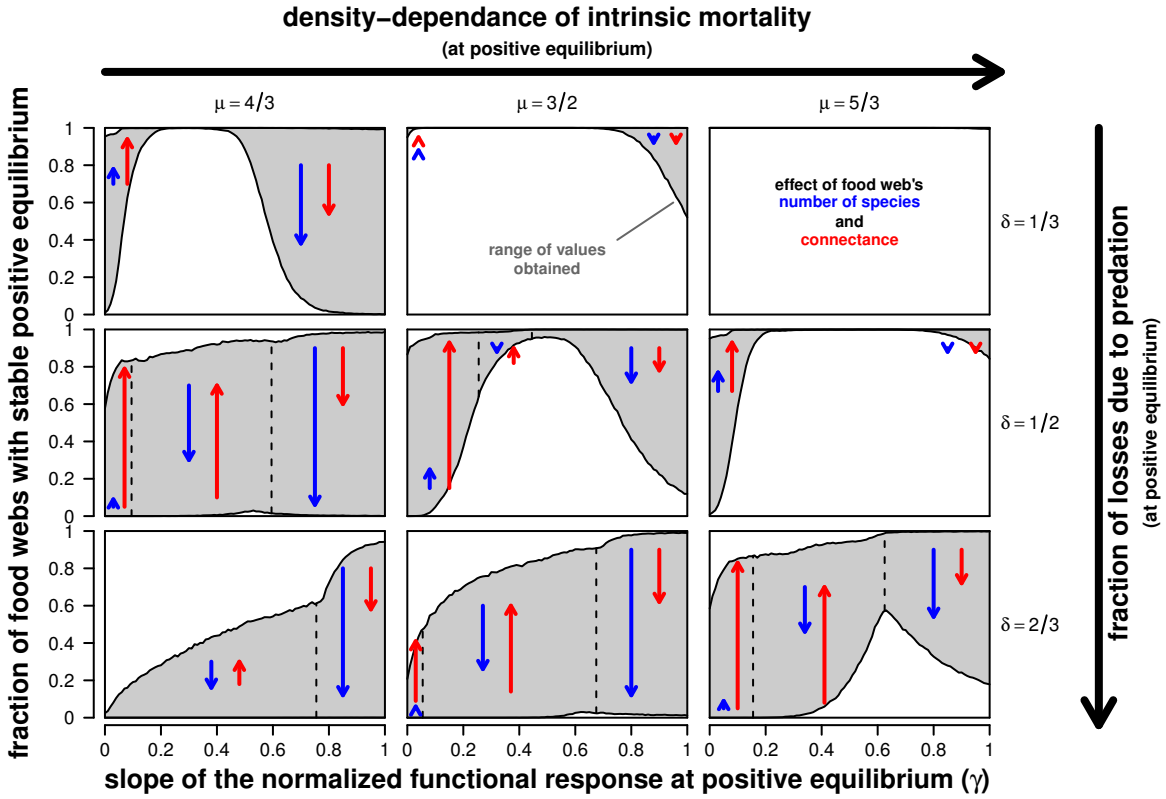

Figure 5.20. Fraction of food webs with a stable positive equilibrium for the generalized model, as a function of generalized parameters values and trophic complexity (number of species and connectance) for food webs with a fixed number of primary producer species. Food web topology is generated using niche model (Williams & Martinez, 2000, 2004). For each set of parameters, 10000 food webs with five primary producers are studied. Assimilation efficiency λ is set to 0.75 (the value has a little impact on the results).
Results are presented for 9 pairs of density-dependence of mortality (μ, varying across columns) and fraction of losses due to predation (δ, varying across rows). In each panel, the fraction of food webs with a stable positive equilibrium is presented as a function of the slope of the normalized functional response (γ, discretized by step of 0.01). Results were estimated for 16 pairs of connectance ($C \in \{0.10, 0.15, 0.20, 0.30\}$) and number of species ($S \in \{20, 30, 40, 60\}$). The grey area on each graph indicates the range of values obtained. For each value of γ, a linear model $y = z_1 + z_2 S + z_3 C + \varepsilon$ (with y the fraction of stable food webs, $z = {}^t(z_1, z_2, z_3) \in \mathbb{R}^3$ the vector of parameters and ε the error of prediction) is used to estimate the respective effect of the number of species and connectance on the proportion of food webs with a stable positive equilibrium. Changes in the sign of z_2 and/or z_3 occur at values of γ corresponding to vertical dashed lines. Blue and red arrows represent respectively the average z_1 and z_2 between two vertical dashed lines. The length of the arrow's tail is equal to the average value of its associated parameter (normalized value of the parameter readable on the left axis with a ± 0.01 precision).

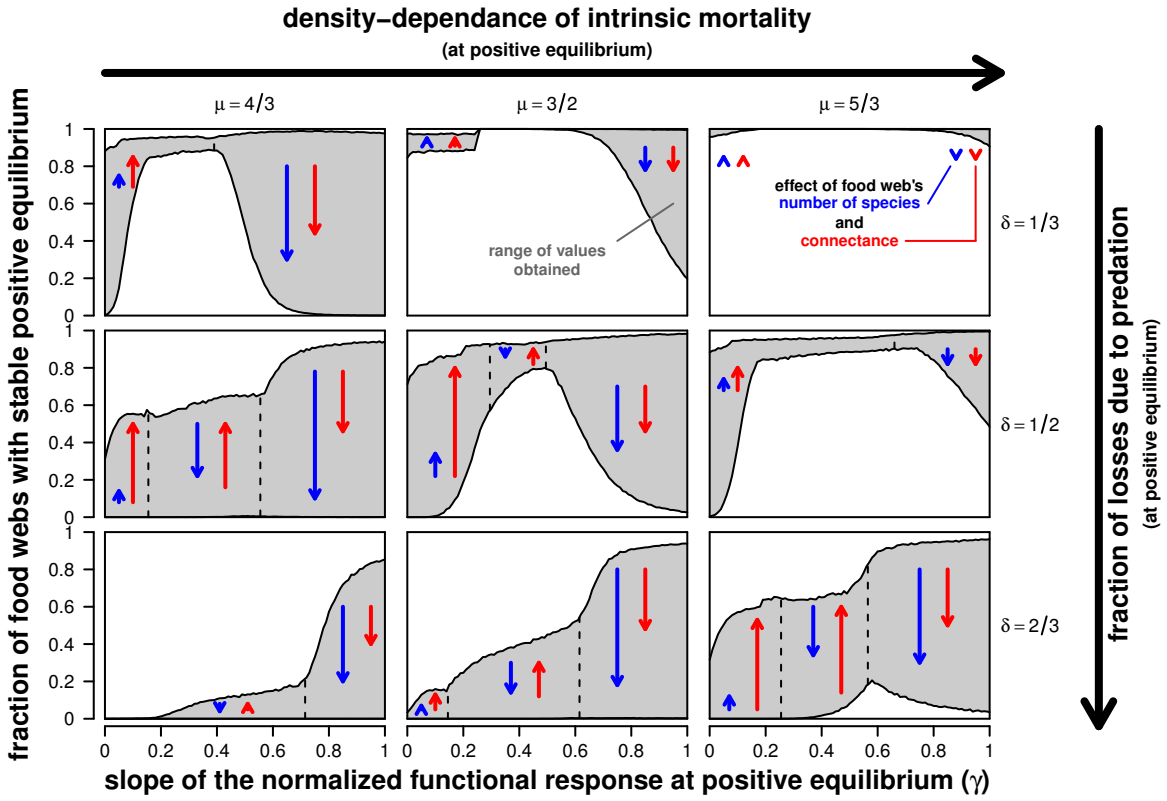

Figure 5.21. Fraction of food webs with a stable positive equilibrium for the generalized model, as a function of generalized parameters values and trophic complexity (number of species and connectance) for food webs with a fixed number of primary producer species and in absence of cannibalism. Food web topology is generated using niche model (Williams & Martinez, 2000, 2004). For each set of parameters, 10000 food webs with five primary producers and in which cannibalistic links have been removed are studied.

Results are presented for 9 pairs of density-dependence of mortality (μ, varying across columns) and fraction of losses due to predation (δ, varying across rows). In each panel, the fraction of food webs with a stable positive equilibrium is presented as a function of the slope of the normalized functional response (γ, discretized by step of 0.01). Results were estimated for 16 pairs of connectance ($C \in \{0.10, 0.15, 0.20, 0.30\}$) and number of species ($S \in \{20, 30, 40, 60\}$). The grey area on each graph indicates the range of values obtained. For each value of γ, a linear model $y = z_1 + z_2 S + z_3 C + \varepsilon$ (with y the fraction of stable food webs, $z = {}^t(z_1, z_2, z_3) \in \mathbb{R}^3$ the vector of parameters and ε the error of prediction) is used to estimate the respective effect of the number of species and connectance on the proportion of food webs with a stable positive equilibrium. Changes in the sign of z_2 and/or z_3 occur at values of γ corresponding to vertical dashed lines. Blue and red arrows represent respectively the average z_1 and z_2 between two vertical dashed lines. The length of the arrow's tail is equal to the average value of its associated parameter (normalized value of the parameter readable on the left axis with a ± 0.01 precision).

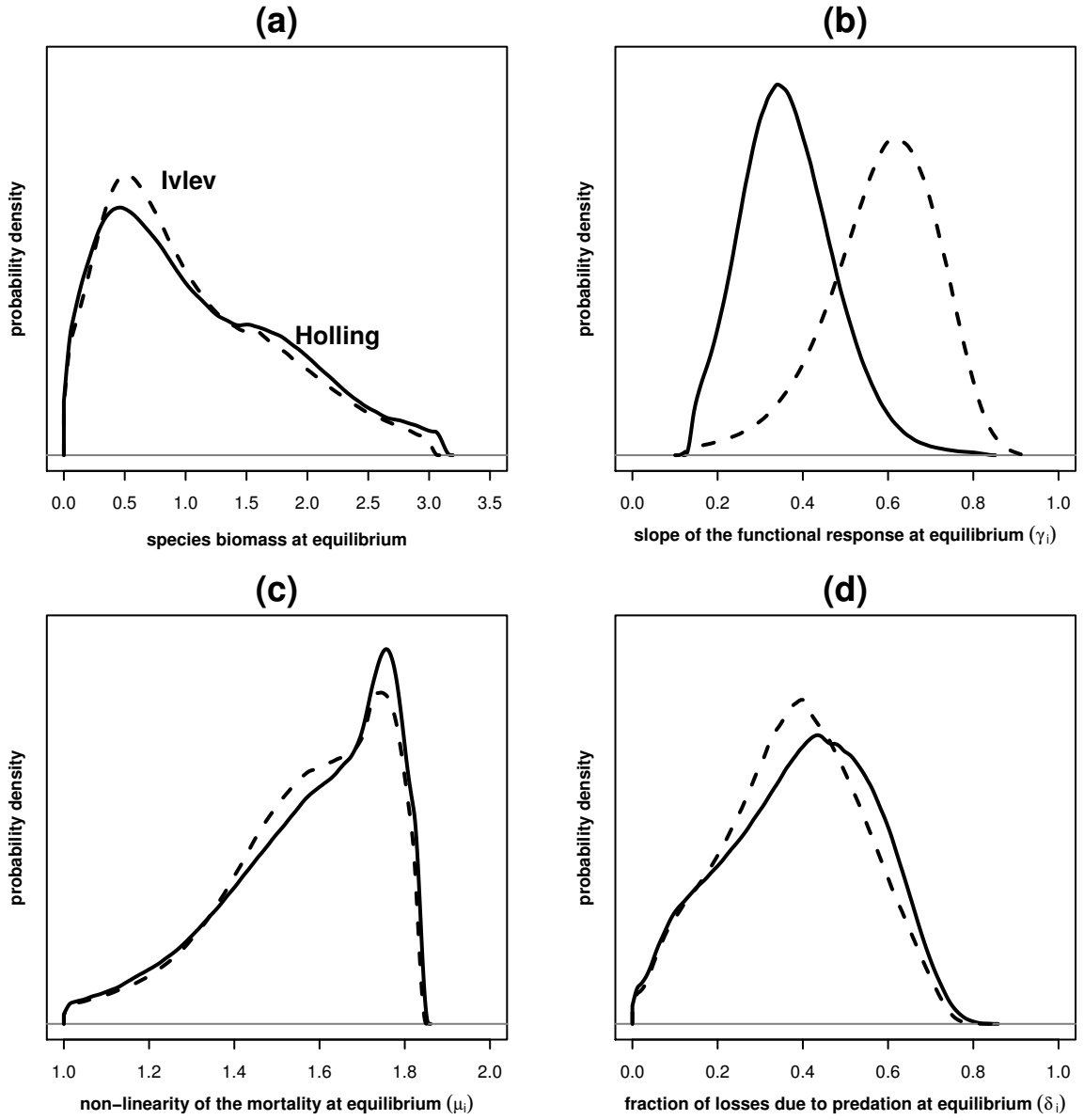

Figure 5.22. Estimated probability densities of the species biomass and 3 generalized parameters for food webs which reach a positive equilibrium at the end of the dynamical simulations for Holling's disc equation (plain) and Ivlev's functional response (dashed). Generalized parameters are here used as indicators to describe system dynamics close to equilibrium. Results are obtained from 160 000 food webs with 16 pairs of number of species and connectance values (10 000 food webs by pair of values). The null values (γ_i for primary producers and δ_i for top-predators) are not taken into account. Density estimates are realized using non-parametric kernel methods (Simonoff, 1996) with the same weight for all simulated food webs.

Part III

How to deal with structural sensitivity?

CHAPTER 6

Toward a quantification of structural sensitivity in models with multiple stable states

""To measure is to know."
"If you cannot measure it, you can not improve it."
Lord Kelvin

The work presented in this chapter corresponds to ongoing research involving **Aldebert, C.**, D. Nerini, M. Gauduchon and JC. Poggiale.

6.1 Introduction

The previous part of this thesis showed that structural sensitivity affects the predicted dynamics of models with up to tens of state variables. Even in a two-dimensional predator-prey model, functional response formulation deeply affects the predicted number and type of stable states, as well as system resilience (chapter 3). System resilience has not been investigated in our structural sensitivity analysis at the scale of complex food webs (chapter 5). Indeed, these systems are too large to allow a bifurcation analysis like the one realized on the predator-prey model (chapters 3 and 4). In addition, a simulation-based analysis of numerous food webs would be both computationally prohibitive and non-exhaustive. However, a non-exhaustive and exploratory analysis can still provide an overview of system dynamics. Changes in system dynamics occur with changes in parameter values and/or model formulation. These changes in model dynamics might be quantified to estimate model sensitivity. Different ways to do that are explored in this chapter which is a preliminary study.

Cordoleani *et al.* (2011) proposed a method that quantifies two aspects of structural sensitivity, namely changes in the type of stable state (bifurcation) and in its location in phase space. This method allows a formal definition of structural sensitivity, and also to compare the respective impact of a change in formulation and a change in parameter values. However, this method is suited for models with one stable state and does not provide any quantitative measure of differences between the dynamics of model with multiple stable states. Different dynamics are mostly the results of qualitative changes in the phase portrait of the system through bifurcations. These bifurcations are highlighted by computing a distance between asymptotic dynamics.

The questions we address in this chapter are: (i) how can we quantify structural sensitivity in models predicting multiple stable states? And (ii) how to compare the respective model sensitivity to its formulation and its parameter values in such models?

To better understand which quantitative changes will be observed at a given bifurcation, any quantification method should be first tested on a small model with a known bifurcation diagram. After that, unknown bifurcation diagrams of more complex systems could be guessed on the basis of the quantification analysis. Next section introduces the quantitative definition of structural sensitivity proposed by Cordoleani *et al.* (2011). Then, section 6.3 recalls briefly the predator-prey model (already studied in chapters 3 and 4) that we use as an example to apply our methods. Different metrics to quantify differences between asymptotic dynamics of models with multiple stable states are proposed and tested in section 6.4. Section 6.5 proposes and tests a method to compare the respective sensitivity of a model to a change in its formulation and a change in

a parameter value. Finally, chapter ends with a discussion of our preliminary results, and some perspectives for future developments.

6.2 Method proposed by Cordoleani et al. (2011)

We call a model M a differential system with a given mathematical formulation and parameter values. Thus, two models are said to be different if their formulation and/or their parameter values are different. Consider any differential system of the form:

$$\frac{d\boldsymbol{x}}{dt} = \boldsymbol{f}(\boldsymbol{x}), \tag{6.1}$$

with $\boldsymbol{x} \in \mathbb{R}^n$ the vector of state variables and $\boldsymbol{f}(\boldsymbol{x}) : \mathbb{R}^n \to \mathbb{R}^n$ a vector function. We denote $\Lambda \subset \mathbb{R}^n$ the bounded set where $\boldsymbol{x}$ remains during the study (e.g. $\Lambda =]0, K]$ for the logistic growth model in section 2.2.2, with K being the carrying capacity). We denote $\boldsymbol{f}^M(\boldsymbol{x})$ the vector function associated to a given model M. The method proposed by Cordoleani *et al.* (2011) is based on a distance between models (i.e. the vector field they define) and a distance between asymptotic dynamics of the models (i.e. attractors of the flow defined by the vector field).

First, we use the p-distance in a functional space to define a distance between the formulation and parameterization of two models M and M' (with weights γ_i):

$$d^p_{model}(M, M') = \sum_{i=1}^{n} \gamma_i \left(\int_\Lambda \left| \boldsymbol{f}_i^M(\boldsymbol{x}) - \boldsymbol{f}_i^{M'}(\boldsymbol{x}) \right|^p d\boldsymbol{x} \right)^{1/p}. \tag{6.2}$$

Estimating the previous distance may require a high computational effort in large systems, because functions are integrated over $\Lambda \subset \mathbb{R}^n$. As a shortcut, if the model changes (formulation and parameter values) considered affect only a function defined on subset of Λ, the distance can be computed over this subset. For example, if only a function $g(x) : \mathbb{R}^+ \to \mathbb{R}^+$ (e.g. a functional response) is modified, one can consider the distance:

$$d^p_{model}(M, M') = \left(\int_\Lambda \left| g^M(x) - g^{M'}(x) \right|^p dx \right)^{1/p}. \tag{6.3}$$

with $\Lambda \subset \mathbb{R}^+$, even if the model is defined over a subset of $\mathbb{R}^n$. Indeed, the purpose of this distance is to compare the relative impact of different model changes according to a reference model. So, the absolute distance has a minor importance.

Second, the distance between asymptotic dynamics uses the fact that ω-limit sets are by defini-

tion compact sets. For a given model M, we denote $\omega^M(\boldsymbol{x})$ the ω-limit set reached by the system from a given initial condition $\boldsymbol{x}$:

$$\omega^M(\boldsymbol{x}) = \bigcap_{T>0} \overline{\bigcup_{t>T} \phi_t^M(\boldsymbol{x})}, \tag{6.4}$$

with $\phi_t^M(\boldsymbol{x})$ the flow defined by model M. A given ω-limit set written ω_i^M has an attraction basin $B_i \subset \Lambda$ defined as the set of initial conditions that reach ω_i^M:

$$B_i = \left\{ \boldsymbol{x} \in \Lambda | \omega^M(\boldsymbol{x}) = \omega_i^M \right\}. \tag{6.5}$$

The set of all distinct ω-limit sets in Λ is denoted:

$$\Omega^M = \bigcup_{i \in I} \omega_i^M,$$

with I the sequence of labels of those sets and $|\Omega^M|$ is their number (we assume that this number is finite for simplicity). Consider the simple case where both M and M' have only one ω-limit set in Λ:

$$|\Omega^M| = |\Omega^{M'}| = 1,\ \omega^M := \Omega^M = \omega_1^M,\ \omega^{M'} := \Omega^{M'} = \omega_1^{M'} \tag{6.6}$$

The distance between model asymptotic dynamics is defined as the Hausdorff distance between ω^M and $\omega^{M'}$. This is possible because an ω-limit set is compact. We first need the p-distance between two points $\boldsymbol{x}, \boldsymbol{y} \in \mathbb{R}^n$:

$$d^p(\boldsymbol{x}, \boldsymbol{y}) = \left(\sum_{i=1}^{n} (x_i - y_i)^p \right)^{1/p}, \tag{6.7}$$

and then a distance between a point $\boldsymbol{x} \in \mathbb{R}^n$ and a compact set $A \subset \mathbb{R}^n$:

$$d_s^p(\boldsymbol{x}, A) = \min_{\boldsymbol{y} \in A} \left(d^p(\boldsymbol{x}, \boldsymbol{y}) \right), \tag{6.8}$$

to finally define the Hausdorff distance between two compact sets $A, B \subset \mathbb{R}^n$:

$$d_H^p(A, B) = \max \left(\max_{\boldsymbol{x} \in B} \left(d_s^p(\boldsymbol{x}, A) \right), \max_{\boldsymbol{x} \in A} \left(d_s^p(\boldsymbol{x}, B) \right) \right). \tag{6.9}$$

If A and B are the ω-limit sets of two models, this distance takes into account both quantitative (e.g. equilibrium value) and qualitative differences (e.g. an equilibrium vs. a limit cycle) between model asymptotic dynamics.

Cordoleani *et al.* (2011) proposed the following definition of structural sensitivity. A model M is ρ-structurally σ-sensitive if there exists a model M' such that $d^p_{model}(M, M') < \rho$ and at least one of the following conditions is fulfilled:

(i) model M' is not structurally stable,

(ii) there is an initial condition $\boldsymbol{x_0} \in \Lambda$ such that for all $\boldsymbol{x}$ satisfying $\omega^M(\boldsymbol{x}) = \omega^M(\boldsymbol{x_0})$, then $d^p_H(\omega^M(\boldsymbol{x}), \omega^{M'}(\boldsymbol{x})) > \sigma$.

The last condition means that a close model predict sufficiently different dynamics, even if the difference is only quantitative. This definition is also appropriate for multiple ω-limit sets. If at least one ω-limit set fulfills condition (ii) ("there is an initial condition"), then the model is ρ-structurally σ-sensitive. This approach does not take into account the respective importance (size of the attraction basin) of each ω-limit set. In addition, each ω-limit set is considered individually and no distance between all asymptotic dynamics is provided. Different distances between asymptotic dynamics of models with multiple stable states are proposed in the remaining of this chapter.

6.3 Example of application: Bazykin's predator-prey model

We consider the same predator-prey model as in chapters 3 and 4, after rescaling:

$$\begin{cases} \dfrac{dB_{prey}}{d\bar{t}} &= \left[\lambda \overline{q}^{\xi} - \alpha - \omega\beta B_{prey}\right] B_{prey} - \overline{G}^{\xi}(B_{prey}) B_{pred} (M_{pred}/M_{prey})^{-0.25} \\ \dfrac{dB_{pred}}{d\bar{t}} &= \left[\lambda \overline{G}^{\xi}(B_{prey}) - \alpha - \beta B_{pred}\right] B_{pred} (M_{pred}/M_{prey})^{-0.25}. \end{cases} \tag{6.10}$$

The model and its parameterization are described in sections 3.2 and 4.2. The predator functional response $\overline{G}^{\xi}$ (amount of prey eaten per unit of predator and per unit of time):

$$\overline{G}^{H}(B_{prey}) = \frac{a^H B_{prey}}{1 + h^H a^H B_{prey}}, \; \overline{G}^{I}(B_{prey}) = \frac{1}{h^I}\left(1 - \exp\left(-h^I a^I B_{prey}\right)\right),$$

$$\overline{G}^{\xi}(B_{prey}) = \xi \overline{G}^{H}(B_{prey}) + (1 - \xi)\overline{G}^{I}(B_{prey}), \tag{6.11}$$

is a weighted mean of Holling's disc equation (Holling, 1959b, 1965) denotes $\overline{G}^{H}$ (Holling's FR) and Ivlev's functional response (Ivlev, 1955) denotes $\overline{G}^{I}$ (Ivlev's FR). Moving parameter $\xi \in [0, 1]$ corresponds to a smooth transition from Ivlev's FR ($\xi = 0$) to Holling's FR ($\xi = 1$). This approach

was used by Cordoleani *et al.* (2011) and in chapter 4 to turn the problem of model formulation into a problem of model parameterization. In model (6.10), primary productivity $\overline{q}^{\xi}$ is modelled using the same function as predation, B_{res} being a constant pool of resource:

$$\overline{q}^{H} = \frac{a^{H} B_{res}}{1 + h^{H} a^{H} B_{res}},\ \overline{q}^{I} = \frac{1}{h^{I}} \left(1 - \exp\left(-h^{I} a^{I} B_{res}\right)\right),\ \overline{q}^{\xi} = \xi \overline{q}^{H} + (1 - \xi)\overline{q}^{I}. \tag{6.12}$$

Model 6.10 exhibits all possible codimension-two bifurcations in planar systems. As a result of these bifurcations, the model have up to three positive equilibria and two limit cycles. For our preliminary tests in this chapter, we focus on one of the most interesting part of the parameter space of this model. We set $1/\omega = 6$ (scaling coefficient of prey carrying capacity) and study the range of species body mass ratio $\log_{10}(M_{pred}/M_{prey}) \in [0.2, 0.7]$. The reader is refered to figures 3.2 and 3.3 for a graphical illustration of the corresponding dynamics. First consider that we use Ivlev's FR ($\xi = 0$). Starting from the lowest body mass ratio, the system has only one stable positive equilibrium (phase portrait 1 in figure 3.2) associated to low population biomasses. As the ratio increases, the system crosses a fold bifurcation of equilibria and has two stable equilibria and a saddle between them (phase portrait 6). For higher ratios, the system undergoes a fold bifurcation of cycles and has three attractors: the stable equilibrium with low biomasses is surrounded by two limit cycles, the outer one being stable and the inner one being unstable (phase portrait 7). Then, the unstable limit cycle disappears through a subcritical Hopf bifurcation that makes the low-biomasses equilibrium becoming unstable (phase portait 4). Finally, if the ratio is increased again, the stable limit cycle disappears through a homoclinic to saddle bifurcation and the system has only one stable equilibrium associated to high population biomass and two unstable equilibria (phase portrait 3). Second, consider now that we use Holling's FR. For $\log_{10}(M_{pred}/M_{prey}) \in [0.2, 0.7]$, the system has always three positive equilibria. Only the one with high population biomasses is stable (phase portrait 3). The smooth transition between the dynamics predicted Ivlev's and Holling's FRs is depicted in figure 4.4.

6.4 Different metrics between multiple attractors

In this section, we present different metrics to extend the distance (6.9) to quantify differences between several attractors. Each proposed metric is applied to model (6.10) with Ivlev's FR and the above-mentioned parameter values to test how the metric behaves in the different situations. For all numerical tests, we defined $\Lambda = B_{prey}, B_{pred} \in \mathbb{R}^2_+ | B_{prey} \in]0, K],\ B_{pred} \in]0, 4]$ (the carrying capacity K is given in equation 3.4). The Euclidean distance ($p = 2$) between points is used to

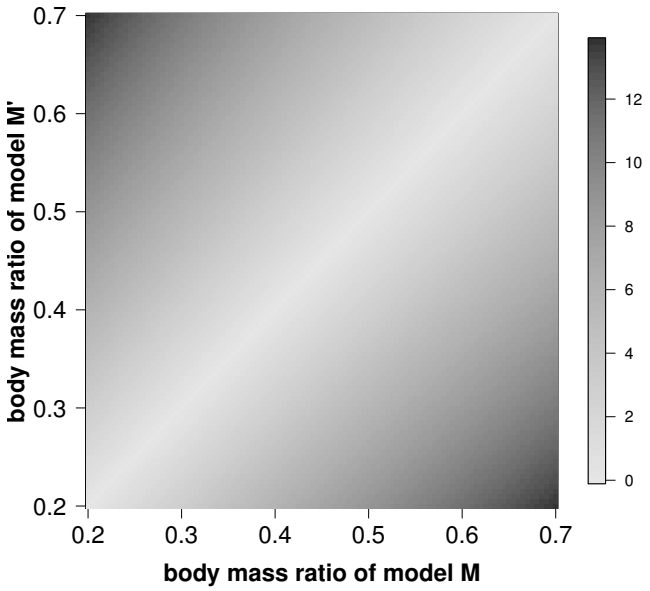

Figure 6.1. Distance between the formulation and parameterization of two models M and M' as a function of their respective species body mass ratios. The distance d^2_{model} is computed using equation (6.2), the integral being approximated using a zero-degree approximation with steps of 0.01 for each dimension.

derive all the more complex distances. For our tests, we consider 101 models with evenly distributed $\log_{10}(M_{pred}/M_{prey}) \in [0.2, 0.7]$ values. The distance (6.2) between all these models is presented in figure 6.1. The distance between models increases smoothly with the distance between body mass ratios when we compare models with more distant parameter values.

6.4.1 Average distance among initial conditions

The average distance between model dynamics is the weighted mean distance between the ω-limit sets of models M and M' for all initial conditions in Λ:

$$d^p_{mean}(M, M') = \int_\Lambda g(\boldsymbol{x}) d^p_H(\omega^M(\boldsymbol{x}), \omega^{M'}(\boldsymbol{x})) d\boldsymbol{x}. \tag{6.13}$$

The weight function $g(\boldsymbol{x}) : \mathbb{R}^n \to \mathbb{R}^+$ satisfies $\int_\Lambda g(\boldsymbol{x}) d\boldsymbol{x} = 1$. This distance quantifies changes in ω-limit sets (size and location) weighted by changes in their attraction basins (size and location). Attraction basins can be sharply affected by some bifurcations (like fold bifurcations of equilibria or cycles) which would result in a sharp change in distance (6.13).

Distance (6.13) quantifies the average difference in the futur predicted by models. It follows

the mathematical definition of a distance. From a practical point of view, this distance can be approximated by considering a finite sample of initial conditions $\lambda \subset \Lambda$. Sampling a high number of initial conditions to be exhaustive (at least 10^n) is the main limit of this distance, for computational reasons. However, the computational cost can be significantely decreased by stopping numerical integration when the system is sufficiently close (using equations 6.7-6.8) to a known ω-limit set that will be reached if the simulation goes on.

Numerical tests are realized with 10 000 initial conditions, located on a regular grid of uniform samples of 100 values for each state variable. This grid is used to compute a zero-degree approximation of the integral in (6.13). The average distance (figure 6.2) increases with model distance (figure 6.1) and shows three thresholds corresponding to bifurcations. The first threshold (low body mass ratio) is sharp as the fold bifurcation of equilibria creates a new attractor with an important attraction basin (it is the bigger of the two basins). The second threshold is less sharp, even if the fold bifurcation of cycles also creates a new attractor. Indeed, the high-biomass stable equilibrium and its attraction basin are not affected by this bifurcation. The next bifurcation (subcritical Hopf) does not lead to a visible change in the average distance. Indeed, this distance is weighted by the size of the attraction basin, and the basin of the stable equilibrium becomes neglectible before the bifurcation that makes it unstable. The last bifurcation (homoclinic to saddle) leads to sharp changes in the average distance as the stable limit cycle disappear and there is only one attractor remaining (the high-biomass equilibrium). Comparing the one attractor situations with a low-biomass and a high-biomass stable equilibrium gives the higher average distance. In this case, the distance reflects the difference in numerical equilibrium locations. Intermediate situations with more than one attractor have at least one attractor with low or high population biomasses. Thus, these asymptotic dynamics are less distant to the one-attractor cases. Between the sharp transitions related to bifurcations, there are smooth changes in the average distance due to smooth quantitative changes in attractor location and attraction basins with species body mass ratio.

6.4.2 Metrics between the closest attractors

The idea of the following metrics is that the distance between a given ω-limit set of one model with all ω-limit sets of the other model is the smallest Hausdorff distance between the set of the first model and all of the second model. The procedure is repeated for all ω-limit sets of the first model. The weigthed sum (with weights α_i^M) or the maximum of these distances is taken. The same is done using either M or M' as a "first model" and the distance between asymptotic dynamics is

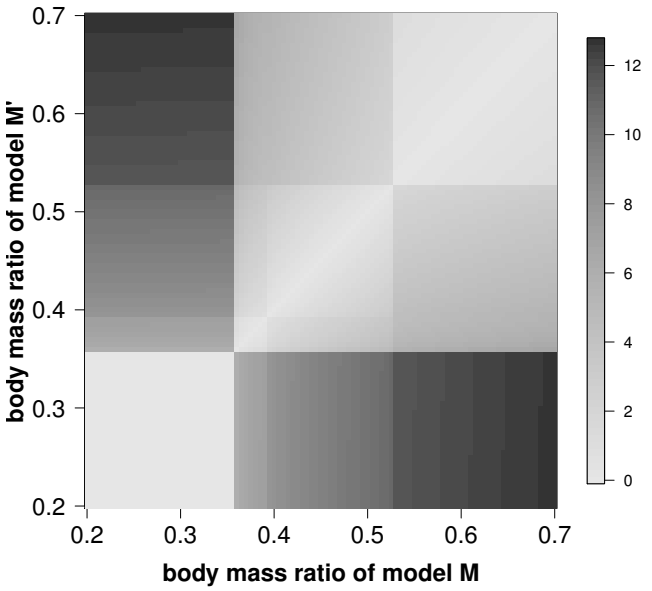

Figure 6.2. Average distance d^2_{mean} between asymptotic dynamics of two models M and M' as a function of their respective species body mass ratios.

the maximum value obtained, which guarantees symmetry:

$$d^p_{close,sum}(M, M') = \max\left(\sum_{i\in I} \alpha_i^M \min_{j\in I'}(d^p_H(\omega_i^M, \omega_j^{M'})), \sum_{i\in I'} \alpha_i^{M'} \min_{j\in I}(d^p_H(\omega_j^M, \omega_i^{M'}))\right), \tag{6.14}$$

$$d^p_{close,max}(M, M') = \max\left(\max_{i\in I}\left(\min_{j\in I'}(d^p_H(\omega_i^M, \omega_j^{M'}))\right), \max_{i\in I'}\left(\min_{j\in I}(d^p_H(\omega_j^M, \omega_i^{M'}))\right)\right). \tag{6.15}$$

These two metrics quantify differences in the number of ω-limit sets and their respective size/location.

As it can be expected, the maximum distance (6.15) hides the information about the distance between other pairs of ω-limit sets (figure 6.3a). For example, the distance is high between the situation with the low-biomass (high-biomass) stable equilibrium and any situation with multiple attractors as one of them is associated to high (low) biomasses in our example. The practical interest of the maximum distance is to highlight the most distant asymptotic dynamics that can be observed between the models.

The sum distance (6.14) with the same weight for all attractor ($\alpha_i^M = 1\ \forall i \in I$) shows clearly all the bifurcations that occur (figure 6.3b). Indeed, each attractor is taken into account and its apparition or disparition will result in a sharp change in distance, even if the change is smooth if we consider the attraction basin (like for the subcritical Hopf bifurcation in the previous subsection).

Thus, the distance is high between models with three attractors ω-limit sets and those with one stable equilibrium, especially if this equilibrium is associated to high biomasses (two attractors correspond to low biomasses in the three-attractors case). The practical interest of the sum distance is to highlight changes in the complexity of the phase portrait (number of attractors).

Using the sum distance (6.14) as a mean ($\alpha_i^M = 1/|\Omega^M|$) or weighted mean ($\alpha_i^M$ is an estimation the relative size of the attraction basin) distance give similar results despite bifurcations appear less clearly with the weighted mean. Indeed, the weighted mean provides the same informations as the average distance (6.13). The mean distance gives kind of mixed results between the sum and the weighted mean. Its main drawback is the lack of theoretical support for the use of a mean instead of a weighted mean. It is neither an "average distance"-like distance (it is insensitive to changes of the attraction basins size) or a distance which quantifies the phase portrait complexity (the addition of a new ω-limit set does not necessarily lead to a sharp increase in the distance due to averaging effect).

6.4.3 Transition between models

To define the next metrics, we first have to define what we call a transition between models. We consider a system first describes by model M and then by model M' after an instantaneous disturbance. We suppose that the system has initially reached an ω-limit set ω_i^M of model M. Then we estimate the probability $p_{ij}^{M,M'}$ that trajectories starting from any initial condition $\boldsymbol{x} \in \omega_i^M$ reach each ω-limit set $\omega_j^{M'}$ of model M':

$$p_{ij}^{M,M'} = \int_{\omega_i^M} \delta\left(\omega_j^{M'}, \omega^{M'}(\boldsymbol{x})\right) g_{\omega_i^M}(\boldsymbol{x}) d\boldsymbol{x} \text{ with } \delta(A,B) = \begin{cases} 1 & \text{if } d_H^p(A,B) = 0, \\ 0 & \text{otherwise.} \end{cases} \tag{6.16}$$

The weight function $g_A(\boldsymbol{x}) : \mathbb{R}^n \to \mathbb{R}^+$ satisfies $\int_A g_A(\boldsymbol{x}) d\boldsymbol{x} = 1$ with $g_A(\boldsymbol{x}) > 0$ if $\boldsymbol{x} \in A$ and $g_A(\boldsymbol{x}) = 0$ otherwise, for any set $A \subset \mathbb{R}^n$. This weight function can be uniform or be the probability density of a system trajectory on the ω-limit set. Using the discrete points returned by an adaptive step-size solver for ODEs (as done actually for preliminary tests) is not the best method because the time between two points only depends on trajectory stiffness.

We denote $P^{M,M'}$ the matrix made of elements $p_{ij}^{M,M'}$. We also define the matrix $\Pi^{M,M'} = P^{M,M'} P^{M',M}$. It corresponds to transitions between ω-limit sets of a system following model M through a switch to model M' and a switch back to model M. Transfert probabilities $\pi_{ij}^{M,M'}$ are valid under the assumption that time scales allow the system to reach one of its ω-limit set before switching the model. Matrix $P^{M,M'}$ and $\Pi^{M,M'}$ both correspond to Markovian processes.

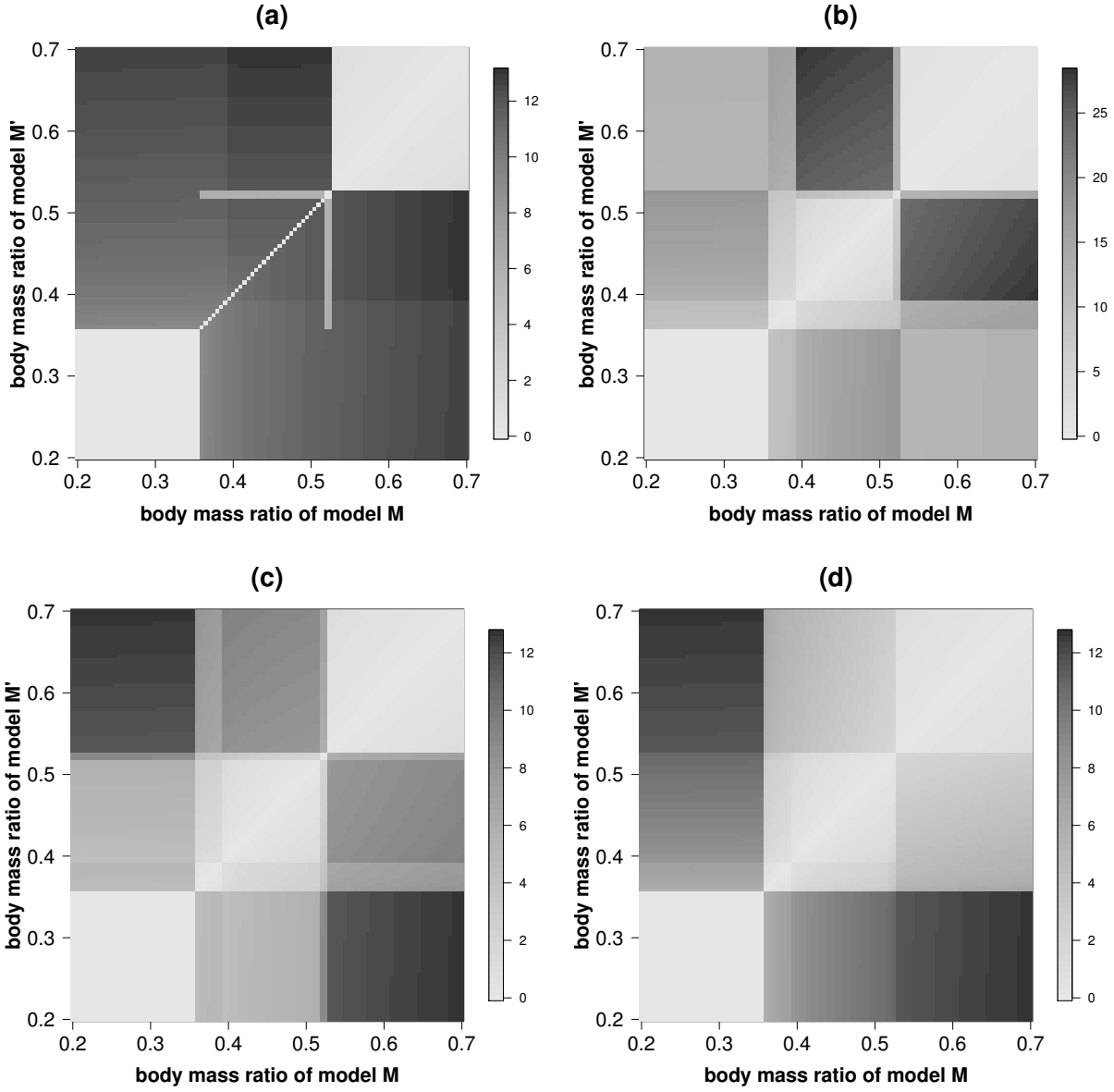

Figure 6.3. Distances between closest attractors of two models M and M' as a function of their respective species body mass ratios: maximum distance $d^2_{close,max}$ (a), sum of distances $d^2_{close,sum}$ with $\alpha_i^M = 1$ (b), mean of distances $d^2_{close,sum}$ with $\alpha_i^M = 1/|\Omega^M|$ (c) and mean of distances weighted by the size of the attraction basins $d^2_{close,sum}$ with α_i^M an estimation od the relative size of the attraction basin (d).

6.4.4 Metrics of attractor switching

This method consider that the distance between two models dynamics is the sum of the Hausdorff distance between all pairs of ω-limit sets weighted by the probability transition between the two sets (6.16). Since this probability transition depends on if we switch from model M to M' or the reverse, we first define the following directed metric (which is not a distance) with weights α_i^M:

$$d^p_{d-switch}(M, M') = \sum_{i \in I} \sum_{j \in I'} \alpha_i^M p_{ij}^{M,M'} d^p_H(\omega_i^M, \omega_j^{M'}). \tag{6.17}$$

The same can be done by taking either M or M' as the "original model". The distance between the models dynamics is then the maximum value obtained, which guarantees symmetry:

$$d^p_{switch}(M, M') = \max\left(d^p_{d-switch}(M, M'), d^p_{d-switch}(M', M)\right). \tag{6.18}$$

These metrics are expected to stay low if the new attractor reached is qualitatively the same as in the original model, but with some quantitative differences. Conversely, they are expected to be larger if the new attractor is qualitatively different to the one in the original model.

The main results highlighted by these metrics are similar to the ones given by the metrics based on closest attractors (section 6.4.2). Bifurcation thresholds are more visible using a sum metric or distance ($\alpha_i^M = 1 \ \forall i \in I$, figure 6.4a,b). This metric/distance is higher when the original model has three attractors and the new model has one stable equilibrium, especially if it is associated to high biomasses. Conversely, the mean ($\alpha_i^M = 1/|\Omega^M|$) and weighted mean ($\alpha_i^M$ is an estimation the relative size of the attraction basin) distances and metrics are high between models with a low-biomasses and a high-biomasses equilibrium as unique attractor (figure 6.4c-f). Indeed, changes due to multiple attractors are less visible due to the averaging effect between attractors. Again, the mean distance is less interesting than the two others. Furthermore, despite the directed metric (6.17) can be of interest for some practical applications (e.g. to study a sudden and directed change of environmental conditions), the distance (6.18) is of lower interest as it gives the same results as the metrics based on closest attractors (section 6.4.2) at a higher computational cost.

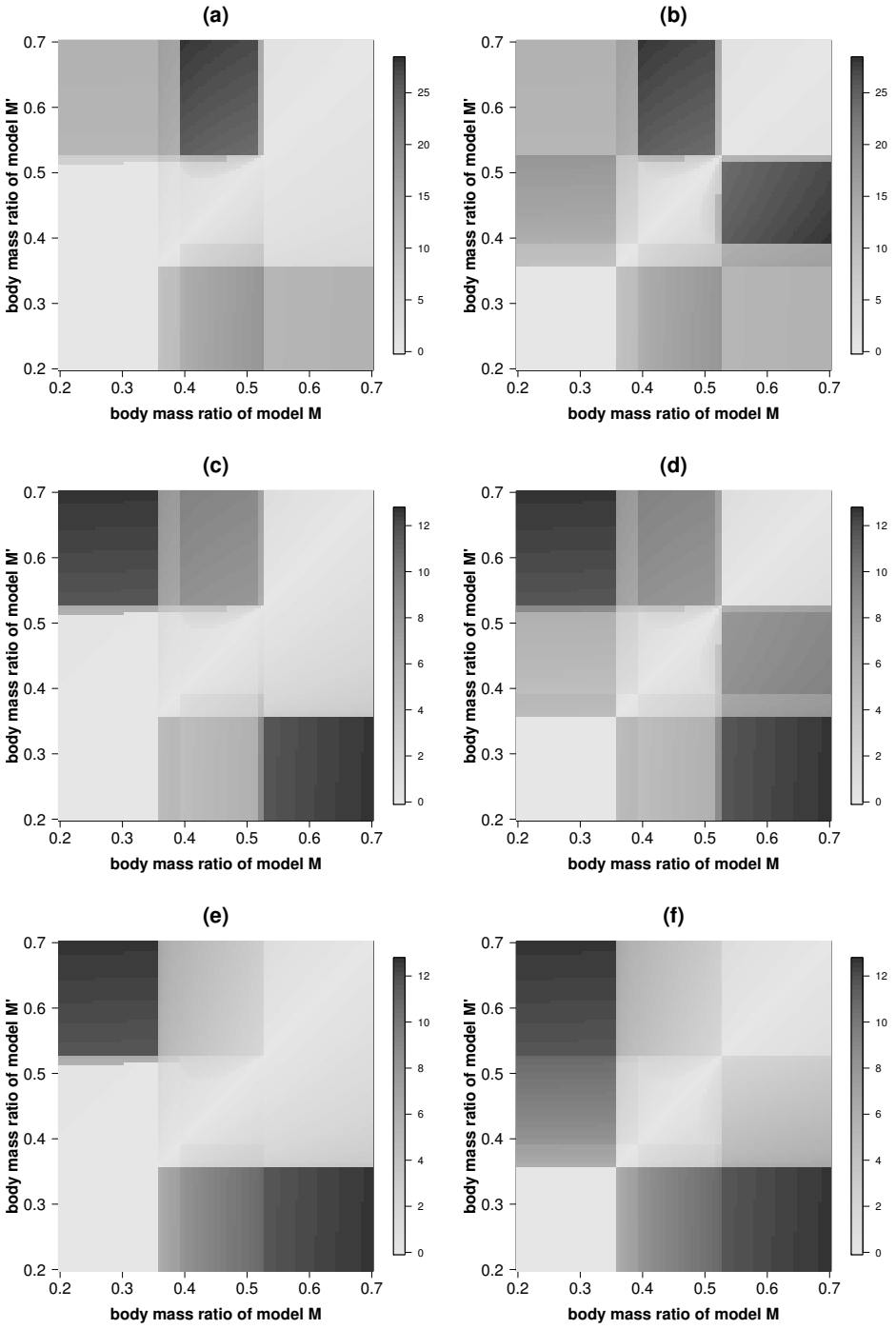

Figure 6.4. Metrics based on the distances between attractors before and after a switch from model M to model M'. Directed metrics (a,c,e) and distances (b,d,f) are based on the sum of distances (a,b), mean of distances (c,d) and mean of distances weighted by the size of the attraction basins (e,f).

6.4.5 Metrics of potential for hysteresis

With the same idea as in previous subsection, the following metrics and distances can be defined when we consider a switch back to the original model:

$$d^p_{d-hyst}(M, M') = \sum_{i\in I}\sum_{j\in I} b_i \pi_{ij}^{M,M'} d^p_H(\omega_i^M, \omega_j^M), \tag{6.19}$$

$$d^p_{hyst}(M, M') = \max\left(d^p_{d-hyst}(M, M'), d^p_{d-hyst}(M', M)\right). \tag{6.20}$$

The distance is zero if the system goes back to its original state after reverse perturbation, whereas it is positive if it stays on another attractor, i.e. in case of hysteresis phenomenon.

These metrics with the same types of weights as in section 6.4.4 are always zero if the original model has only one attractor, as it is impossible to have hysteresis phenomena (figure 6.5). The hysteresis distance makes bifurcations more visible if it is used as a sum ($\alpha_i^M = 1\ \forall i \in I$). Maximum values are obtained when the original model has three attractors and the switch is through a model with only one stable equilibrium. If this equilibrium is the one with high biomasses, the sum distance is maximal (two original attractors have low biomasses). Conversely, the weighted distance is maximal if the equilibrium is the one with low biomasses (the high biomasses equilibrium that disappears during model transitions has a large attraction basin).

6.5 Parameter sensitivity vs. formulation sensitivity

In the previous section, the obtained results allow a comparison between different parameter changes, like "are model outputs more sensitive to an increase or a decrease of 0.2 of the body mass ratio?". Such comparisons are possible because we can quantify a parameter change: the value is increased or decreased of a certain amount. To compare a parameter and a formulation changes, we will now use the distance between models (6.2). So, the kind of questions we try to answer is: "are model outputs more sensitive to a change in formulation or to a parameter change of the same amount (*sensu* distance between models) ?".

Consider a model M with a given formulation and parameterization. Suppose that we want to compare the impact of one change in model formulation quantified through a switching parameter ξ with the impact of one parameter value. As the change in formulation is bounded ($\xi \in [0, 1]$), we denote M^{fmax} the model with the maximum change in model formulation and the same parameter values. The distance $d^p_{model}(M, M^{fmax})$ gives the maximum model change to investigate. For a discrete value $d_{sample} \in [0, d^p_{model}(M, M^{fmax})]$ of distance between model, the corresponding

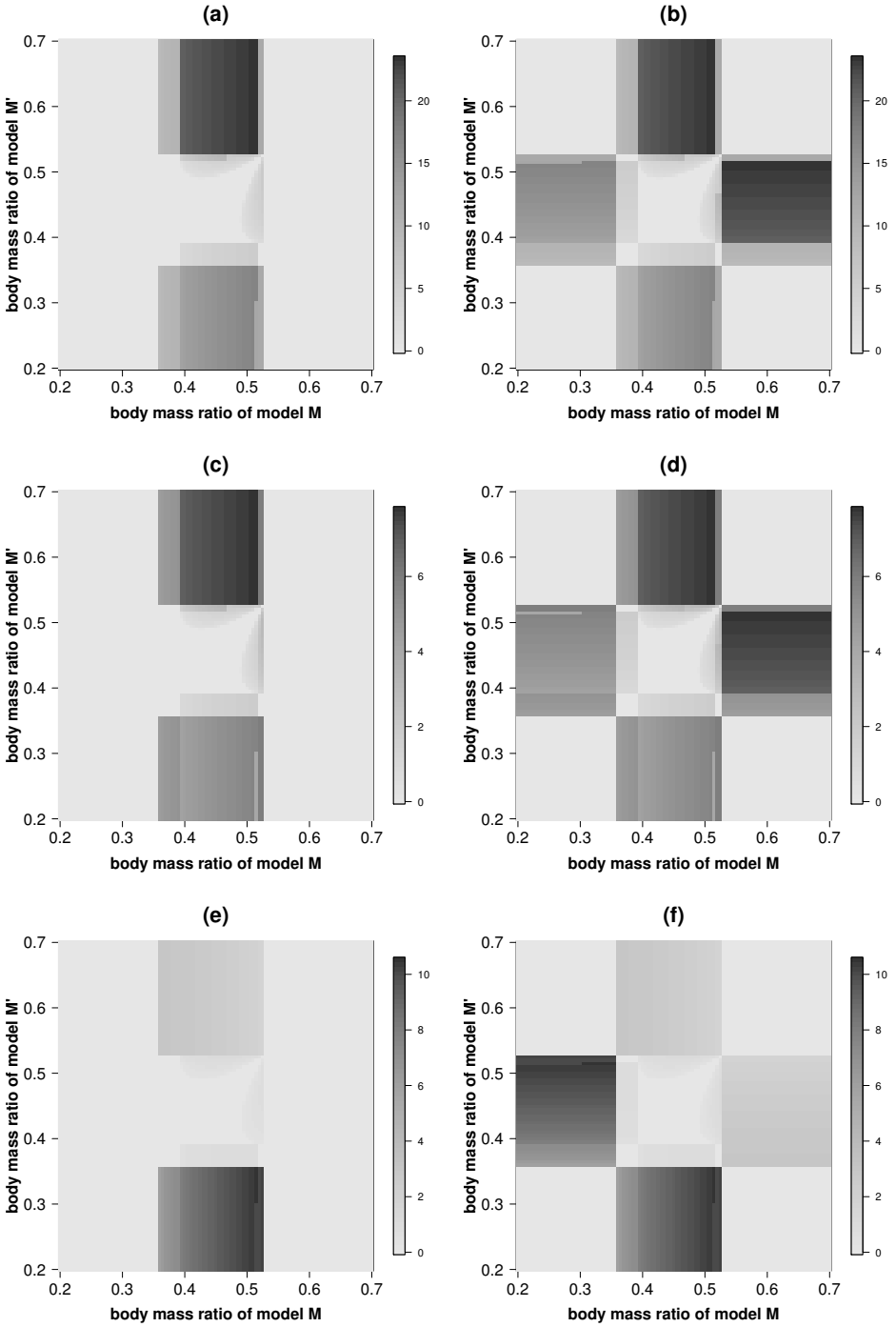

Figure 6.5. Metrics to detect hysteresis phenomena, based on the distances between attractors before and after a switch from model M to model M' and then back to model M. Directed metrics (a,c,e) and distances (b,d,f) are based on the sum of distances (a,b), mean of distances (c,d) and mean of distances weighted by the size of the attraction basins (e,f).

amount of formulation change (through ξ) is numerically estimated and defines a new model M^f. The same is done for an increase (M^{p+}) and a decrease (M^{p-}) of the parameter value with the reference model formulation. Thus, the three models M^f, M^{p+} and M^{p-} are located at the same distance d_{sample} of the reference model M. Their respective distance to the reference model in term of asymptotic dynamics can be compared. To compare model sensitivity to the change in model formulation and to changes in parameter, we propose the following index:

$$I_{p+}(M, d_{sample}) = 2\left(\frac{d^p_{\cdot}(M, M^f)}{d^p_{\cdot}(M, M^f) + d^p_{\cdot}(M, M^{p+})} - 0.5\right) \in [-1, 1], \tag{6.21}$$

$$I_{p-}(M, d_{sample}) = 2\left(\frac{d^p_{\cdot}(M, M^f)}{d^p_{\cdot}(M, M^f) + d^p_{\cdot}(M, M^{p-})} - 0.5\right) \in [-1, 1], \tag{6.22}$$

with $d^p_{\cdot}(\cdot, \cdot)$ being any distance or metric discussed in section 6.4. The index is set to zero if $d^p_{\cdot}(M, M^f) = d^p_{\cdot}(M, M^{p+}) = 0$ ($d^p_{\cdot}(M, M^f) = d^p_{\cdot}(M, M^{p-}) = 0$). This index is bounded between -1 and 1. It is positive if a higher change in model dynamics is obtained with the formulation change, and negative otherwise. Doing this for different values $d_{sample} \in [0, d^p_{model}(M, M^{fmax})]$ gives an estimate of how much changes in the model result in a change in model dynamics.

Figure 6.6 provides some examples of application to Bazykin's model (6.10) using the average distance (6.13). With this distance, model sensitiviy depends on the reference parameter value. Depending on this value, the model is either more sensitive to species body mass ratio or to functional response formulation. For both changes, sudden changes in distance between dynamics and in the index value occur at bifurcation thresholds. For example, figure 6.6a shows that a bifurcation is crossed for a small change in functional response formulation, whereas it happens only for a higher change in parameter values, and only if it is an increase of the body mass ratio. As a consequence, the reference model is more sensitive to functional response formulation (figure 6.6b). Conversely, figure 6.6e shows that a bifurcation is only crossed for a decrease in body mass ratio, resulting in a higher sensitivity of the model to this parameter value (figure 6.6f).

In figure 6.6, only the sensitivity of one reference model with one parameter value is investigated. Exploring this sensitivity for a range of reference parameter values adds another dimension to the study. A way to summarize the results of each reference value is to use quantiles of the structural sensitivity index ($I_{p+}(M, d_{sample})$ or $I_{p-}(M, d_{sample})$) curve in figure 6.6. Two examples using either the average distance (6.13) and the sum of distances between closest attractors (6.14) ($\alpha_i^M = 1$) are provided in figures 6.7 and 6.8. Both distance indicates that the model is more sensitive to the functional response formulation. However, the model is more sensitive to a decrease in body

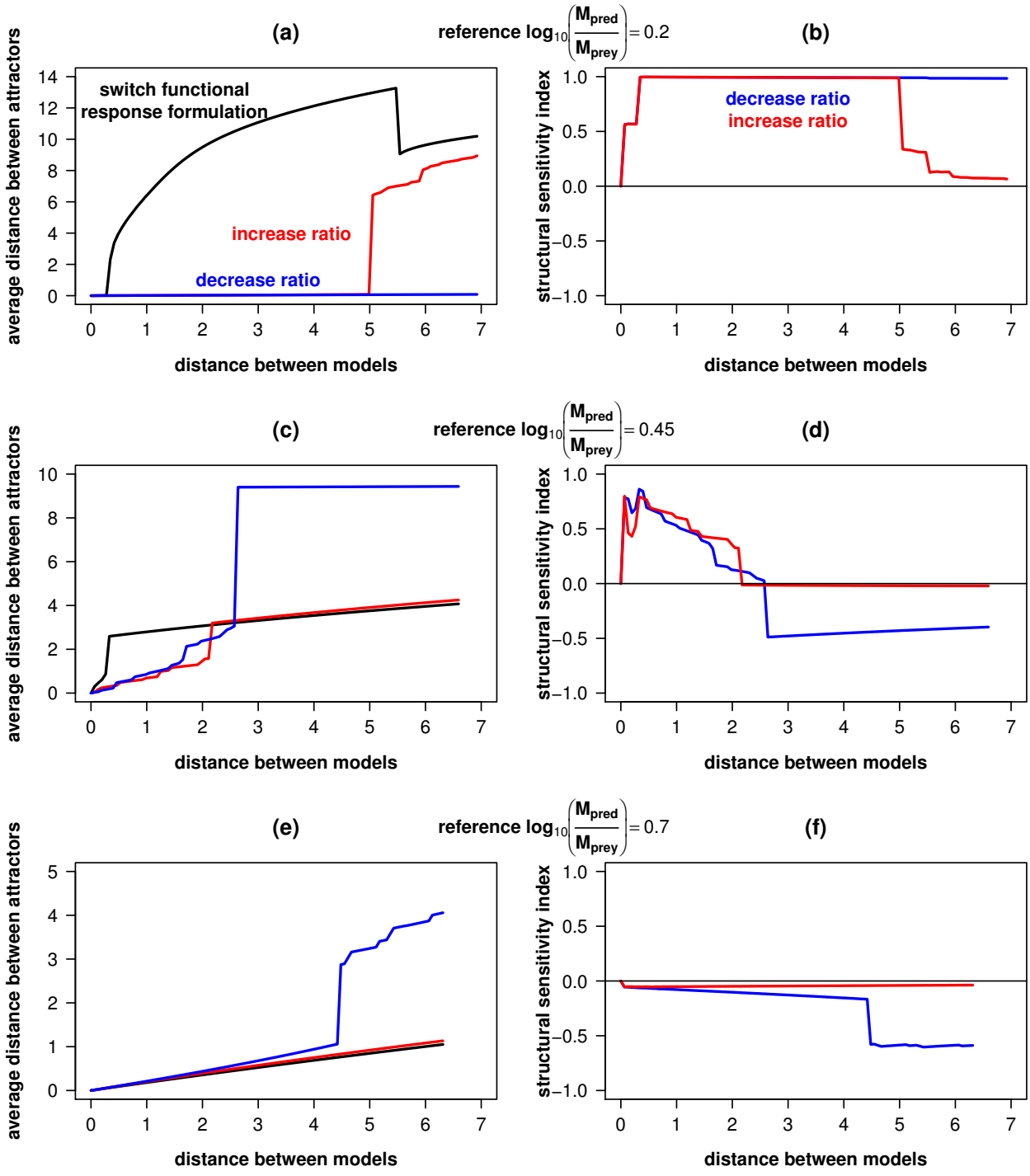

Figure 6.6. Average distance between model asymptotic dynamics as a function of distance between models (a,c,e) for a change in functional response formulation (black) or species body mass ratio (red, blue), and the resulting index of structural sensitivity (b,d,f). The reference model M uses Ivlev's functional response with $1/\omega = 6$ and three different species body mass ratio (panels line). Depending on the reference body mass ratio, the reference model is more sensitive to functional response formulation (positive index) or body mass ratio value (negative index). For each curve, 101 evenly distributed d_{sample} values are taken for the distance between models. For each model, 100 initial conditions are used to estimate model dynamics.

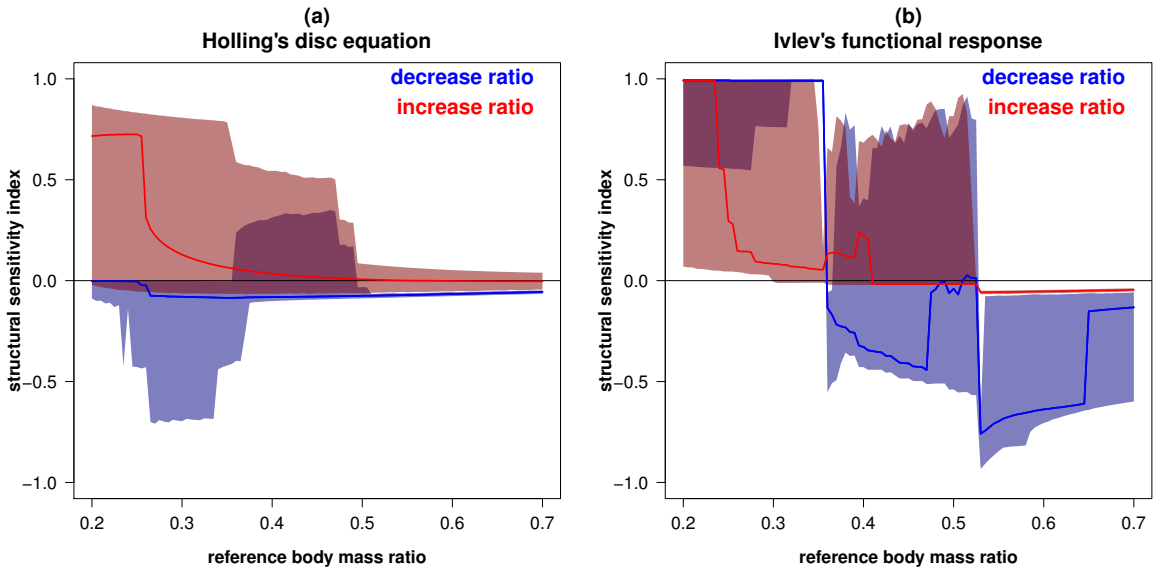

Figure 6.7. Index of structural sensitivity using the average distance between asymptotic dynamics using either Holling's disc equation (a) or Ivlev's functional response (b) as a reference model. For each reference body mass ratio, the index is computed for an increase (red) or a decrease (blue) of species body mass ratio. The obtained curve $I_{p\pm}(M, d_{sample})$ is summarized in the figure by its median (curve) and its $[2.5\ \%, 97.5\ \%]$ inter-quantiles range (shaded area).

mass ratio for the lowest tested values of body mass ratio with Holling's FR and the higher values with Ivlev's FR. In these situations, the decrease in body mass ratio makes the system crosses bifurcation(s) whereas a change of functional response formulation only results in quantitative changes in equilibrium value.

6.6 Discussion and perspectives

Among the five proposed distances that make a direct comparison between models asymptotic dynamics, two of them are of particular interest and provide a complementary information. Bifurcations location and differences in the complexity of the phase portrait of the system are spotted by the sum of distances between closest attractors (6.14) (with $\alpha_i^M = 1$). Conversely, the average distance (6.13) highlights changes in the average dynamics predicted by the system among a set of initial conditions. Initial conditions allow to take into account the size of the attraction basin of each attractor, which hides some bifurcations that are of little quantitative importance for predicted dynamics. Quantitative changes in predicted dynamics like changes in equilibrium value are also visible with both distances. Directed metrics based on model transitions (6.17,6.19) allow to quantify the potential for attractor switching and hysteresis phenomena. These events can be

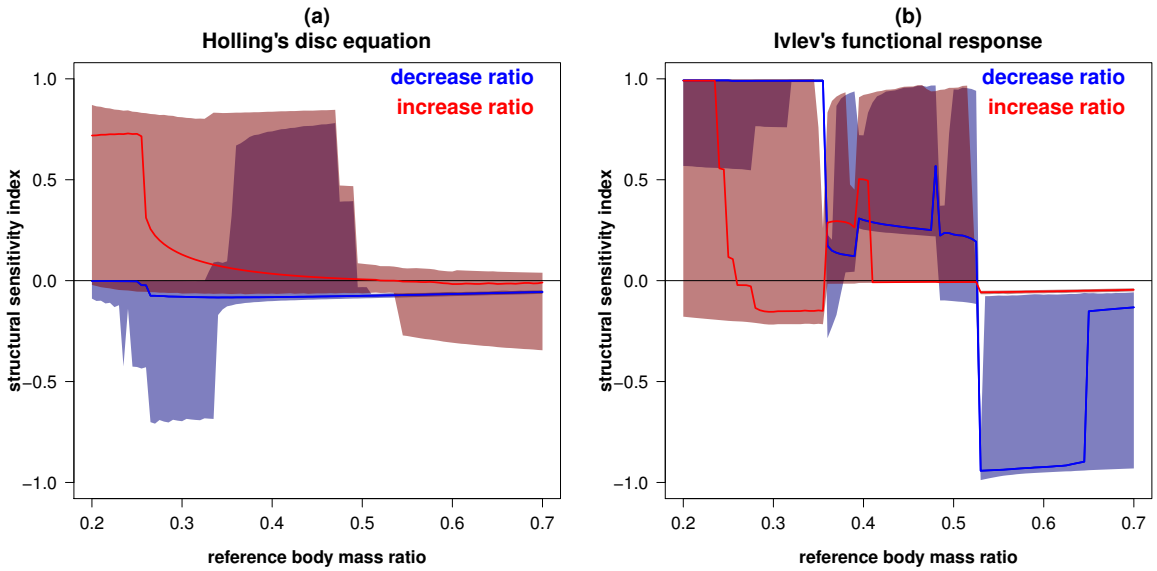

Figure 6.8. Index of structural sensitivity using the sum of distances between closest attractors using either Holling's disc equation (a) or Ivlev's functional response (b) as a reference model. For each reference body mass ratio, the index is computed for an increase (red) or a decrease (blue) of species body mass ratio. The obtained curve $I_{p\pm}(M, d_{sample})$ is summarized in the figure by its median (curve) and its $[2.5\ \%, 97.5\ \%]$ inter-quantiles range (shaded area).

studied using different distances. The sum of distances among attractors reflects changes in the phase portrait complexity, whereas the mean weigthed by the relative size of each attraction basin highlights differences in the average predicted dynamics.

All these distances can be used to define structural sensitivity in a slightly different way than originally proposed by Cordoleani *et al.* (2011). This new definition might be: a model M is said to be ρ-structurally σ-sensitive if there exists a model M' such that $d^p_{model}(M, M') < \rho$ and $d^p_{\cdot}(M, M') > \sigma$, where $d^p_{\cdot}$ can be any distance between model dynamics (like the ones in section 6.4). Depending on the distance used, a different aspect of stuctural sensitivity is highlighted. Note that with this definition, a model might not be structurally sensitive if a bifurcation that occurs between M and M' does not lead to a significant change in the distance used (e.g. subcritical Hopf bifurcation with the average distance). This possibility is consistent with the notion of "sensitivity", i.e. a quantitative response to a given amount of change. The proposed definition can be used by considering any possible change in the model such that $d^p_{model}(M, M') < \rho$, or by considering a directional change like changing a given function formulation.

Previous distances can also be used to compare the impact of different model changes, based on the procedure proposed in section 6.5. Even if the implementation of this procedure can be improved (numerical approximations, sampling of initial conditions on attractors), it allows to

compare the respective effect of one parameter value and one model formulation on model dynamics (figures 6.6-6.8). Multiple changes in model formulation and parameter values can be compared at the same time with this approach. The main issue is how to summarize the results. This is a recurrent problem in global sensitivity analysis where information is aggregated statistically (ten Broeke *et al.*, 2016). Conversely to classical sensitivity analysis which are not designed to detect bifurcations, our proposed approach gives a good estimate of bifurcations location.

Adamson & Morozov (2012, 2014) proposed to study structural sensitivity by considering the vicinity of a reference model (defined using the distance between model formulation and parameterization) in the function space. The infinite-dimensional function space is projected into a finite-dimensional space that is enough to know model dynamics. For example, the stability of the coexistence equilibrium of a predator-prey model is a function of equilibrium value and functional response derivative at this equilibrium. One can notice that the spirit of this approach is similar to the method of generalized modelling (Gross & Feudel, 2006) that we already used in chapters 3 and 5. This idea might be extended to the analysis of dynamics with multiple attractors. Attractors can be detected and distances to the reference model can be quantified for a finite sample of functions within its neighborood. Projecting this neighborhood into a finite-dimensional space that is enough to summarize multiple attractor dynamics would be the main issue. Indeed, extending the method of generalized modelling to the analysis of periodic orbits in planar systems requires the use of Floquet's theory and Fourier analysis (Kuehn & Gross, 2011).

Applying the proposed distances and procedure to larger systems will be limited by numerical issues like the sampling of initial conditions to detect all attractors. The convergence of our method to estimate a quantitative measure of structural sensitivity needs to be known to allow a rigorous interpretation of any results. Performing such analysis on a simple model will be the next step of this work. This method might show limits of application in large systems, like any other method. However, it is an intermediate approach that bridges bifurcation analysis and numerical simulations. It may help to have a better mathematical understanding of model dynamics, as well as their sensitivity to model formulation and parameterization in large systems.

CHAPTER 7

Structural sensitivity in predator-prey models based on Dynamic Energy Budget theory: importance of metabolism

"Life started as an individual in evolutionary history [...]
and individuals are the units of selection and
the survival machines of life"
SALM Kooijman,
"Dynamic Energy Budget for metabolic organisation" (Kooijman, 2010)

The work presented in this chapter is currently adapted to be submitted for publication as: **Aldebert, C.**, Kooi, BW., Nerini, D., Gauduchon, M., Poggiale, JC. Metabolism and predation: what may drive the dynamics of a predator-prey system? *The American Naturalist*

7.1 Dynamic Energy Budget theory

7.1.1 General introduction and motivation

Dynamic Energy Budget theory, or DEB theory, has been developped by SALM Kooijman and many collaborators since 1977 (Kooijman, 2010, 2015, Jusup *et al.*, in press). This reductionist theory aims to represent all living organims within a single coherent framework that focuses on individuals. Individual is a level of organization that allows for relatively easy (in comparison to ecosystems) mass and energy budgets. Energy budget is the core of DEB theory as it follows conservation law and because all organisms require energy. Energy allocation within organisms is represented by a generic scheme in DEB theory (standard DEB model, figure 7.1). This scheme is common to most known organisms, due to evolution. Thus, organisms can be classified according to their metabolic properties as defined within the DEB scheme. The main scheme of energy allocation may be refined by adding and/or simplifying processes depending on the organism and the scope of the study. Thus, the study of an organism does not lead to a single DEB model, but to a variety of models including more or less details on energy allocation, organism's chemical composition, its life history, aging process, etc. All these models are consistently related to each others as they are all derived from the same coherent theory. A coherent upscaling from individual to population dynamics can also be performed. The strength of DEB theory is to propose a coherent biological framework that can be adapted to a given situation using testable assumptions.

Assumptions that specify the standard DEB model are listed in table 7.1 to give a brief overview of the general concepts of DEB theory. DEB theory is a unifying theory in biology and thus is more than a set of mathematical models. To underline this idea, the mathematical formulation of the standard DEB model is not provided here and we focus on concepts. DEB theory has many advantages, but it also has some drawbacks from a practical point of view. A major problem is that all the twelve parameters of the standard DEB model cannot be quantified directly from data (like the fraction of energy allocation to soma κ). Their quantification requires to estimate functions of these parameters (like respiration). This intermediate step and the number of parameters rise technical issues for parameter estimation. For instance, some parameter values may be less constrained by data than others and remain uncertain. However, the problem of the number of parameters can be partly tackle by the use of more or less complex DEB models depending on data availability (Lika *et al.*, 2011a,b). Another drawback of DEB theory concerns its spread among the scientific community, as it is based on different disciplines from microbiology to animal ecology through chemistry and mathematics. For the sake of synthesis, DEB theory uses its own vocabulary and mathematical notations (in Kooijman, 2010, p469-477 summarize these notations

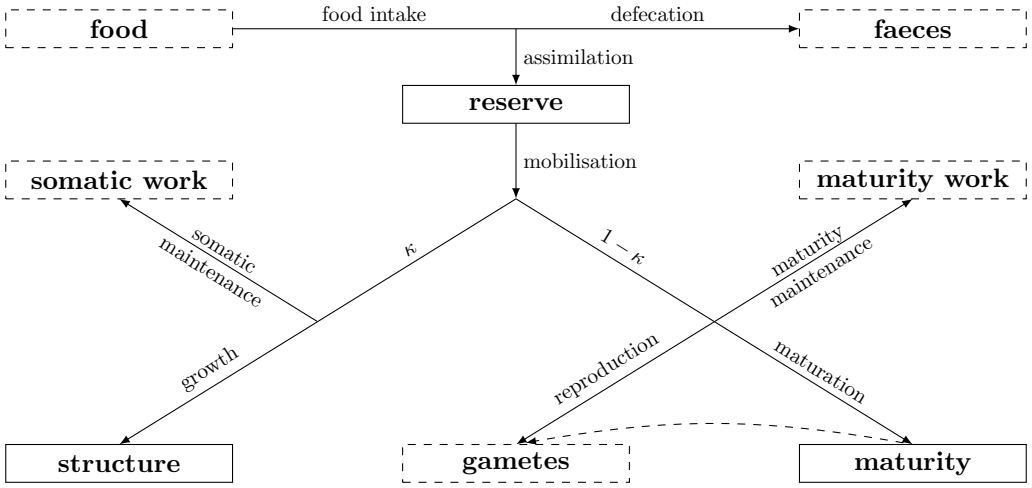

Figure 7.1. Scheme of the standard DEB model. Adapted from figure 2.1 in Kooijman (2010). Plain boxes denote the three state variables that describe an individual, dashed boxes indicate sources and sinks. A fixed fraction of food intake is egested and the rest (assimilation efficiency) is assimilated into reserve. A fixed fraction κ of mobilised reserve is allocated to somatic maintenance plus growth (the κ-rule). The dashed arrow represents the allocation switch between maturation and reproduction that occurs at puberty.

and symbols). For example, the dot in $\dot{x}$ does not mean the time derivative of x, but that the quantity x is a rate expressed per unit of time. Despite it may cause some difficulty to people discovering DEB theory, these unusual notations keep the number of symbols acceptable and allow a quick understanding of dimensions when reading an equation.

Two main aspects of DEB theory are of particular interest in the scope of this thesis. First, previous chapters emphasize that qualitative and quantitative uncertainties in model predictions can arise from small changes in model formulation. Within the infinite number of model formulations that can be built, the framework provided by DEB theory is useful to derive mechanistic models that remain coherent from a biological point of view. Second, in most population models like those considered in previous chapters, population growth rate is assumed to be proportional to its instantaneous feeding rate, i.e. the functional response. As functional response formulation affects model dynamics, one may ask if this sensitivity can be dampened by including more physiological details that act as a buffer between between feeding and population growth. Three of these buffers are (i) the reserve compartment between feeding and individual growth, (ii) maintenance costs that has to be paid to maintain organism integrity, and (iii) the difference between individual growth in various life stages due to ontogenic development and reproduction. These three buffers can be included or not in a model based on DEB theory.

The question we adress in this chapter is: how far changes in the formulation of feeding and the level of details in the metabolism representation can affect a predator-prey model? We consider

Table 7.1. Assumptions that define the standard DEB model. Adapted from table 2.4 in Kooijman (2010). Assumptions that start with an asterisk are not directly required to understand the DEB models for unicellular organisms used latter in this chapter. However, these assumptions are relevant to understand how these models are derived from the standard DEB model and how they fit within the DEB theory framework.

1. The amounts of reserve, structure and maturity are the state variables of the individual; reserve and structure have a constant chemical composition (strong homeostasis) and maturity represents information (about ontogenic development of the individual). Reserve is a mixture of compounds (from ribosomal RNA to lipids) waiting for being used.
2. * Substrate (food) uptake is initiated (birth) and allocation to maturity is redirected to reproduction (puberty) if maturity reaches certain threshold values.
3. Food is converted into reserve and reserve is mobilised at a rate that depends on the state variables only to fuel all other metabolic processes.
4. * The embryonic stage has initially a negligibly small amount of structure and maturity (but a substantial amount of reserve). The reserve density (amount of reserve per unit of structure) at birth equals that of the mother at egg formation (maternal effect). Foetuses develop in the same way as embryos in eggs, but at a rate unrestricted by its reserve availability as it lives on its mother's reserves.
5. The feeding rate is proportional to the surface area of the individual and the food handling time is independent of food density.
6. The reserve density (amount of reserve per unit of structure) at constant food density does not depend on the amount of structure (weak homeostasis).
7. Somatic maintenance is proportional to structural volume, but some components (osmosis in aquatic organisms, heating in endotherms) are proportional to structural surface area.
8. * Maturity maintenance is proportional to the level of maturity.
9. * A fixed fraction of mobilised reserves is allocated to somatic maintenance plus growth, the rest to maturity maintenance plus maturation or reproduction (the κ-rule).
10. * The individual does not change in shape during growth (isomorphism). This assumption applies to the standard DEB model only.

four predator-prey models in chemostat used by Kooi & Kooijman (1994b) to model unicellular organisms. Unicellular organisms can be easily modelled at the population scale in DEB theory, as population growth rate is equal to individual growth rate (next subsection). Thus, the buffers between feeding and population growth are the reserve and the maintenance. Models with (section 7.2) and without (section 7.3) reserve, and with or without maintenance are considered, leading to four models derived from DEB theory. These models include the well-known Droop (1973, 1983), Marr-Pirt (Marr *et al.*, 1963, Pirt, 1965) and Monod (1942, *in* Kooijman 2010) models. Each model was parameterized by Kooi & Kooijman (1994b) to fit data on the transient dynamics of a chemostat experiment on *Dictyostelium discoideum* (Myxamoeba) feeding on *Escherischia coli* (Dent *et al.*, 1976). This trophic interaction is modelled using different type-II functional responses (Holling, 1965) for each model. For each model and functional response, a bifurcation analysis is conducted with respect to environmental parameters (throughput rate of the chemostat and resource concentration in the feed).

7.1.2 DEB theory and unicellular organisms

DEB theory includes some useful assumptions to simplify the standard DEB model (figure 7.1 and table 7.1) for unicellular organisms. Unicellular organisms that divide into two daughter cells have a volume that ranges from a factor one to two. Due to this relatively small range, their volume-to-surface area relationship can be approximated by a linear relationship, i.e. their volume is proportional to their surface area (V1-morph organisms, Kooijman, 2010, section 4.2.2). Furthermore, there is no flux allocated to reproduction as organisms divide. Division is the only threshold in the life history of the organism[1], so there is no need to evaluate maturity explicitely if we assume that it is proportional to growth. In addition, maturity and somatic maintenance costs can be combined as they are both proportional to volume (due to the V1-morph assumption). This combined maintenance cost allows to delete maturity dynamics by setting $\kappa = 1$ (even if it is not true, it avoids the use of new notations without loss of generality).

According to previous simplifications of the standard DEB model, a dividing unicellular organism of species i can be modelled by the following structure (expressed as a volume V_i) and reserve (expressed as energy E_i) dynamics:

$$\frac{dV_i}{dt} = \frac{\dot{k}_E^i E_i - \dot{k}_M^i g_i [E_m^i] V_i}{E_i + g_i [E_m^i] V_i} V_i, \tag{7.1}$$

[1] In DEB theory, unicellular organisms with asexual reproduction are treated as juveniles as they feed and do not reproduce (Kooijman, 2010, section 1.1.4). Division occurs when the individual reaches the maturity threshold corresponding to puberty.

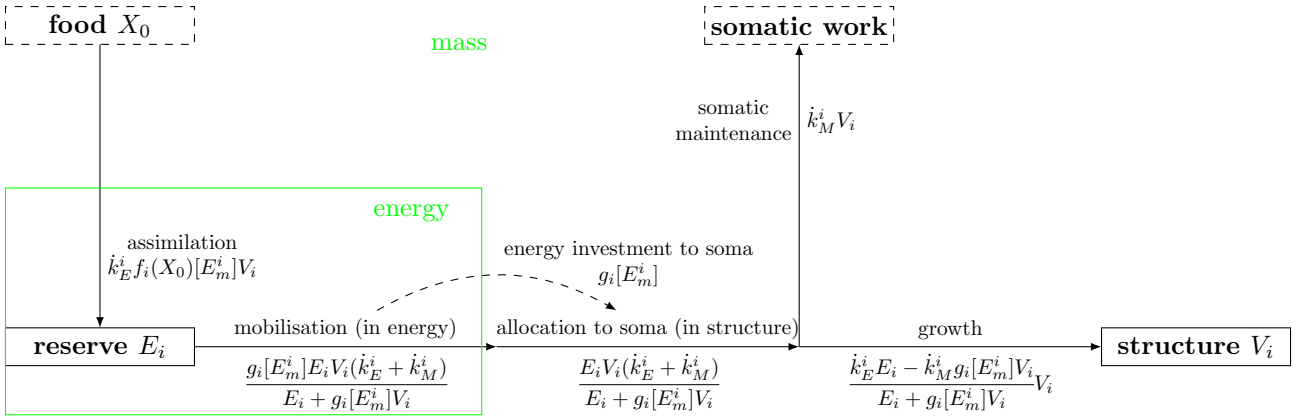

Figure 7.2. Scheme of the DEB model for a dividing unicellular organism. An unstructured population of such organisms can be represented by the same model (Kooi & Kooijman, 1994a). Fluxes are expressed as total amounts and come from equations (7.1-7.2). Plain boxes denote the two state variables that describe the population as a super-individual, dashed boxes indicate sources and sinks. Stocks and fluxes are expressed in a mass framework, except those within the green box that are expressed in an energy framework. Thus, the dashed arrow represents the conversion of the mobilised energy flux into an amount of structure.

$$\frac{dE_i}{dt} = \left(\dot{k}_E^i f_i(X_0) - \frac{E_i g_i(\dot{k}_E^i + \dot{k}_M^i)}{E_i + g_i[E_m^i]V_i}\right)[E_m^i]V_i \text{ where } f_i(X_0) = \frac{X_0}{X_0 + K_i}, \tag{7.2}$$

which are summarized in figure 7.2. This model assumes that there is no additional somatic maintenance due to processes at the cell surface, like osmosis regulation. The first term in equation (7.2) is the assimilation flux (feeding minus excretion), where $\dot{k}_E^i$ is the specific energy conductance (expressed per unit of time) and $[E_m^i]$ is the maximum value of reserve density $[E_i] = E_i/V_i$, which is the amount of reserve per unit of structure (brackets indicate that quantities are expressed per unit of volume). The scaled functional response $f_i(X_0)$ is taken as a Holling's type II functional response (as usually done in DEB theory). Its half saturation coefficient K_i has the same dimension as the food X_0, which can be either a constant or a variable.

The second term in equation (7.2) is the flux of mobilised reserve (see Kooijman, 2010, section 2.4 for details on its derivation), where $\dot{k}_M^i$ is the somatic maintenance rate coefficient (expressed per unit of time) and g_i is the investment ratio into growth and somatic maintenance, a dimensionless parameter that quantifies the cost of building structure relatively to $[E_m^i]$. Thus, the energy investment required for a unit of structure is $g_i[E_m^i]$ and the flux allocated to soma (growth plus somatic maintenance) expressed in amount of structure is:

$$\frac{E_iV_i(\dot{k}_E^i + \dot{k}_M^i)}{E_i + g_i[E_m^i]V_i}.$$

This flux is splitted into a somatic maintenance flux $\dot{k}_M^i V_i$ that is dissipated and an increase of structure (growth rate) given by the right-hand side of equation (7.1). Equations (7.1-7.2) can be conveniently re-written:

$$\frac{dV_i}{dt} = \frac{\dot{k}_E^i e_i - \dot{k}_M^i g_i}{e_i + g_i} V_i, \tag{7.3}$$

$$\frac{de_i}{dt} = \dot{k}_E^i \left(f_i(X_0) - e_i\right) \text{ where } f_i(X_0) = \frac{X_0}{X_0 + K_i}, \tag{7.4}$$

using the rescaling $e_i = E_i/([E_m^i]V_i)$, where $e_i \in [0,1]$ is the scaled reserve density. The scaled reserve density can be understood as the physiological state of the organism (well-fed vs. depleted).

Model (7.3-7.4) remains appropriate if $\kappa_i < 1$, as there is no explicit flux allocated to reproduction and explicit maturity is not required. Maturation may be implicitely taken into account by an increase of g_i value (as $g_i \propto 1/\kappa_i$, Kooijman, 2010, p48), i.e. a higher mobilisation flux of energy is needed to obtain the same allocation flux to somatic maintenance plus growth. A higher somatic maintenance rate $\dot{k}_M^i$ may implicitely take into account the cost of maturity maintenance. Maturation by unicellular organisms ($\kappa_i < 1$) means that cells make a significant investment in cell differentiation relatively to cell growth, "a point still open to debate" according to Kooijman (2010, p123).

Moving now from the individual to the population scale, we denote $n_i(t, e_i, V_i)$ the number of individual at time t which have a scaled reserve density e_i and a volume V_i. The total volume of the population is:

$$V_i^{tot}(t) = \int_{V_i} \int_{e_i} n_i(t, e_i, V_i) V_i de_i dV_i,$$

with a temporal dynamics given by:

$$\frac{dV_i^{tot}}{dt} = \int_{V_i} \int_{e_i} n_i(t, e_i, V_i) \frac{dV_i}{dt} de_i dV_i.$$

If we assume that the functional response f_i is a function of time (through food abundance), the scaled reserve density of each individual converges exponentially toward the same trajectory. So e_i can be viewed as the scaled reserve density of a randomly chosen individual (Kooi & Kooijman, 1994a). Using boundary conditions imposed by cell division, Kooi & Kooijman (1994a) showed that the growth rate of the unstructured population is the same as the individual growth rate:

$$\frac{dV_i^{tot}}{dt} = \frac{\dot{k}_E^i e_i - \dot{k}_M^i g_i}{e_i + g_i} V_i^{tot}.$$

This equation can be rescaled using $X_i = V_i^{tot}/V_{cult}$ to express structure as a concentration within a batch or a chemostat with volume V_{cult}:

$$\frac{dX_i}{dt} = \frac{\dot{k}_E^i e_i - \dot{k}_M^i g_i}{e_i + g_i} X_i,$$

where the dynamics of reserve density is given by (7.4).

7.2 Predator-prey models with reserve

7.2.1 Original model by Kooi & Kooijman (1994b)

Using DEB theory and empirical data by Dent *et al.* (1976), Kooi & Kooijman (1994b) proposed the following model to describe a predator-prey system in chemostat:

$$\frac{d\boldsymbol{x}}{dt} = \boldsymbol{F}(\boldsymbol{x}) \Leftrightarrow \left\{ \begin{array}{rcl} \dfrac{de_1}{dt} & = & \dot{k}_E^1 \left(f_1(X_0) - e_1\right) \\ \dfrac{de_2}{dt} & = & \dot{k}_E^2 \left(f_2(X_1) - e_2\right) \\ \dfrac{dX_0}{dt} & = & \dot{h}(X_r - X_0) - f_1(X_0) j_{XAm}^1 X_1 \\ \dfrac{dX_1}{dt} & = & \left(\dfrac{\dot{k}_E^1 e_1 - \dot{k}_M^1 g_1}{e_1 + g_1} - \dot{h}\right) X_1 - f_2(X_1) j_{XAm}^2 X_2 \\ \dfrac{dX_2}{dt} & = & \left(\dfrac{\dot{k}_E^2 e_2 - \dot{k}_M^2 g_2}{e_2 + g_2} - \dot{h}\right) X_2, \end{array} \right. \tag{7.5}$$

where $\boldsymbol{x} = (e_1, e_2, X_0, X_1, X_2)^T$. The prey (*Escherichia coli*, with structure X_1 and scaled reserve density e_1) feeds on an inorganic resource (glucose, with concentration X_0) and is eaten by a predator (*Dictyostelium discoideum*, with structure X_2 and scaled reserve density e_2). Biological parameters are listed in table 7.2 and they are all assumed to be strictly positive except if it is stated otherwise. Two environmental parameters describe the chemostat, its throughput rate $\dot{h}$ (in h^{-1}) and the resource concentration in the feed X_r (in mg cm^{-3}). Reserve dynamics and growth rates of both prey and predator come from equations (7.3-7.4). This model assumes that the predator consumes only prey's structure. Adding reserve digestion does not improve the fit between empirical data and the model (Kooijman, 2010, p357). In this model (and in DEB theory in general), the scaled functional response f_i is taken as a normalized Holling's disc equation

(Holling, 1959b) with half-saturation constant K_i:

$$f_1(X_0) = \frac{X_0}{X_0 + K_1} \text{ and } f_2(X_1) = \frac{X_1}{X_1 + K_2}. \tag{7.6}$$

To obtain generic results, we consider in the following that the scaled functional response is any function that fulfills properties:

$$f_i : \mathbb{R}^+ \to [0,1],\ f_i(0) = 0,\ f_i'(X_{i-1}) > 0,\ \lim_{X_{i-1}\to+\infty} f_i(X_{i-1}) = 1,\ i = 1,2.$$

These properties imply that f_i is a type-II or a type-III functional response (Holling, 1965).

7.2.2 Overview of the study

In the remaining of the study, prey functional response f_1 is taken as Holling's disc equation (7.6). This assumption is supported by two arguments. First, assumptions beyond Holling's disc equation (which is equivalent to Michaëlis-Menten's uptake function) are consistent with the feeding behaviour of a micro-organism feeding on an inorganic substrate. Second, preliminary tests with the same functional responses as for the predator indicated that changing prey functional response among type-II functional responses has only a neglectible impact on model dynamics, regarding to its sensitivity to predator functional response.

For predator functional response, the choice of a formulation is less straightforward than for the prey. Indeed, its feeding behaviour might be more complex than the uptake of an inorganic substrate. Three scaled functional responses are considered for the predator:

$$f_2^H(X_1) = \frac{X_1}{X_1 + K_2^H},\ f_2^I(X_1) = 1 - \exp(-X_1/K_2^I),\ f_2^t(X_1) = \tanh(X_1/K_2^t). \tag{7.7}$$

Holling's disc equation f_2^H (Holling, 1959b) has a strong theoretical support based on handling time. Ivlev's functional response f_2^I (Ivlev, 1955) also has a theoretical background, based on satiation. There is no theoretical support for the hyperbolic tangent function f_2^t but it is sometimes used in population dynamics (Jassby & Platt, 1976, Fussmann & Blasius, 2005, Cordoleani *et al.*, 2011). In a given situation, even if one functional response is relevant from a theoretical point of view, it is still an approximation of the observed trophic interaction. This interaction might be quantitatively closer to other functional response formulations. Our purpose here is not to debate whether we should use a mechanistic or an empirical formulation when the latter has a better fit to data. Our aim is to quantify the impact of this choice on dynamics predicted by the model, in order to assess

Table 7.2. State variables and biological parameters used in the study. Parameters values are given for the four models studied. DEB and Droop models correspond to model (7.5) with or without maintenance costs. Marr-Pirt and Monod models correspond to model (7.12) with or without maintenance costs. Parameter values come from Kooi & Kooijman (1994b) and were obtained using experimental data by Dent *et al.* (1976), with a throughput rate $\dot{h} = 0.064$ h^{-1} and a glucose concentration in the feed $X_r = 1$ mg cm^{-3}.

variable	range	unit	meaning
e_1	$[0,1]$	-	scaled reserve density of the prey
e_2	$[0,1]$	-	scaled reserve density of the predator
X_0	$\mathbb{R}^+$	mg cm^{-3}	resource concentration
X_1	$\mathbb{R}^+$	mm^3 cm^{-3}	structure concentration of the prey
X_2	$\mathbb{R}^+$	mm^3 cm^{-3}	structure concentration of the predator

parameter	DEB	Droop	Marr-Pirt	Monod	unit	meaning
K_1	4.10^{-4}	4.10^{-4}	$6.1.10^{-4}$	0.001	mg cm^{-3}	half-saturation coefficient of the prey
K_2	0.18	0.23	0.23	0.34	mm^3 cm^{-3}	half-saturation coefficient of the predator
j^1_{XAm}	0.65	0.95	0.91	0.72	mg mm^{-3} h^{-1}	maximum ingestion rate of the prey
j^2_{XAm}	0.26	0.27	0.55	0.49	h^{-1}	maximum ingestion rate of the predator
g_1	0.86	0.92	-	-	-	energy investment ratio of the prey
g_2	4.43	1.72	-	-	-	energy investment ratio of the predator
$\dot{k}^1_E$	0.67	0.45	-	-	h^{-1}	specific energy conductance of the prey
$\dot{k}^2_E$	2.05	0.69	-	-	h^{-1}	specific energy conductance of the predator
μ_1	-	-	0.54	0.43	h^{-1}	maximum growth rate of the prey
μ_2	-	-	0.49	0.33	h^{-1}	maximum growth rate of the predator
$\dot{k}^1_M$	0.008	0	0.008	0	h^{-1}	somatic maintenance rate coef. of the prey
$\dot{k}^2_M$	0.16	0	0.16	0	h^{-1}	somatic maintenance rate coef. of the predator

the relevance of this debate on model construction in bio-ecological modelling.

To parameterize the different functional responses (7.7), we consider the total functional responses $j^{2,\phi}_{Xam} f^{\phi}_2(X_1)$, where $\phi \in \{H, I, t\}$ indicates the formulation used. Parameter values for Holling's disc equation are already known (Kooi & Kooijman, 1994b, and table 7.2). For the two other functional responses, parameter values are estimated in order to minimize their Euclidean distance with Holling's disc equation:

$$d^2_{H,\phi}(j^{2,\phi}_{XAm}, K^{\phi}_2) = \int_A \left(j^{2,H}_{XAm} f^H_2(X_1) - j^{2,\phi}_{XAm} f^{\phi}_2(X_1) \right)^2 dX_1 \tag{7.8}$$

with $A = [0, 10]$ using the simplex method by Nelder & Mead (1965). The range A over which minimization is carried out captures most of the functional response shape, from the absence of prey to the saturating part of the functional response. In addition, we already showed that changes in this range do not affect the qualitative conclusions about structural sensitivity in a food web model (chapter 5).

To assess the effect of functional response formulation, a bifurcation analysis is performed for each formulation. Bifurcation diagrams are drawn with respect to the two environmental parameters: the throughput rate of the chemostat $\dot{h}$ and the resource concentration in the feed X_r. First, some analytical results are derived for any functional response formulations f_1 and f_2. Then, above-mentioned examples of functional response formulations (7.6, 7.7) are considered for a numerical analysis using the Matlab continuation toolbox Matcont (Dhooge *et al.*, 2006). This numerical analysis completes our analytical results for bifurcations involving limit cycle(s) (i.e. oscillating dynamics).

This work is achieved for nested models with more or less physiological details. Three simpler models than model (7.5) are also considered. These three models are specific cases of model (7.5), which is called "original DEB model" in the following. Its analytical study is presented in the next subsection, followed by a numerical analysis with and without explicit somatic maintenance ($\dot{k}^i_M = 0$, Droop model). The next section derives a simpler model without explicit reserve dynamics (Marr-Pirt model). This model is also studied analytically and numerically, both with and without explicit somatic maintenance ($\dot{k}^i_M = 0$, Monod model).

For each of the four models, biological parameters were estimated[2] by Kooi & Kooijman (1994b, see table 7.3) and are used to obtain the parameter values (table 7.3) of the different predator

[2]If the same parameter values are used, conversion efficiencies are greater than 1 in the Marr-Pirt and Monod models. This unrealistic pattern does not occur if parameter values are estimated for each case. Furthermore, the biological relevance of this study remains consistent between models if the parameterization gives the best fit to empirical data by Dent *et al.* (1976) for each model.

Table 7.3. Predator functional response: parameter values for each formulation and model. Ivlev's functional response and the hyperbolic tangent are parameterized in order to mimize their Euclidean distance with Holling's disc equation.

model	parameter	Holling	Ivlev	Hyperbolic tangent
original DEB	$\dot{j}_{XAm}^{2,\phi}$	0.26	0.249	0.248
	K_2^ϕ	0.18	0.336	0.444
Droop	$\dot{j}_{XAm}^{2,\phi}$	0.27	0.257	0.255
	K_2^ϕ	0.23	0.416	0.551
Marr-Pirt	$\dot{j}_{XAm}^{2,\phi}$	0.55	0.523	0.521
	K_2^ϕ	0.23	0.416	0.550
Monod	$\dot{j}_{XAm}^{2,\phi}$	0.49	0.459	0.456
	K_2^ϕ	0.34	0.578	0.767

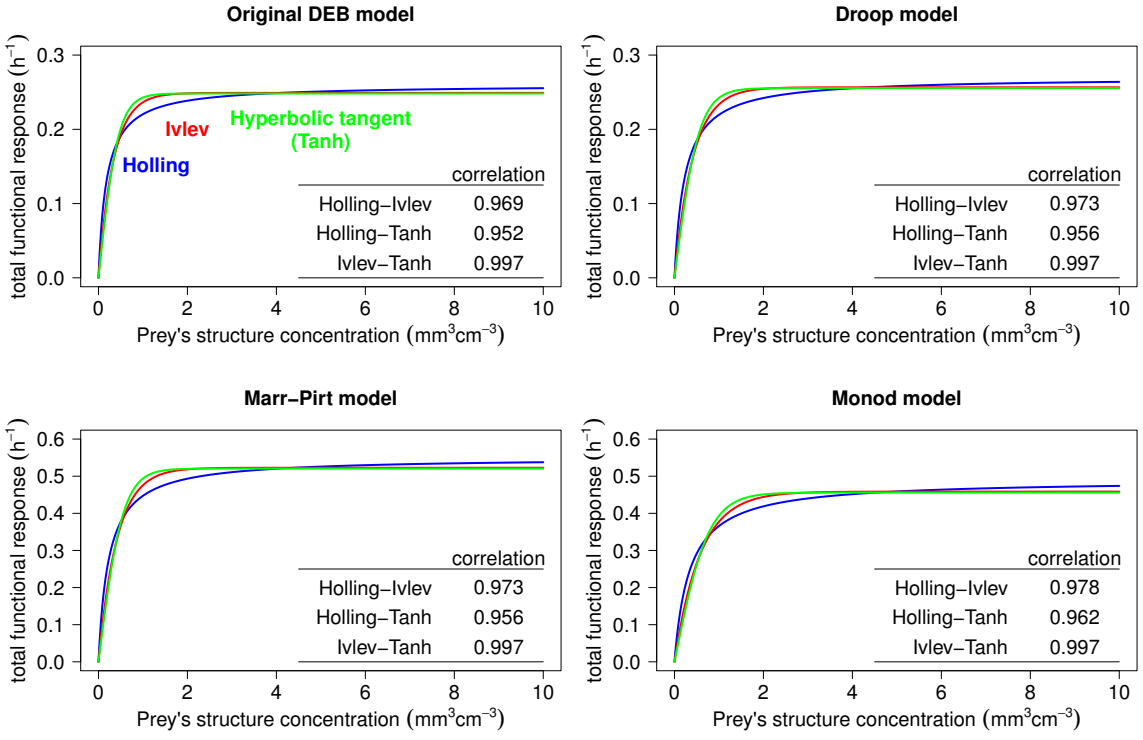

Figure 7.3. Three predator functional responses for each model and correlation between them. Ivlev's functional response and the hyperbolic tangent are parameterized in order to mimize their Euclidean distance with Holling's disc equation (see table 7.3).

functional responses drawn in figure 7.3. Functions (7.7) are such that for each model, Ivlev's functional response and the hyperbolic tangent are closer to each other than to Holling's disc equation (higher correlation coefficient). More precisely, Holling's disc equation is slightly closer to Ivlev's functional response than to the hyperbolic tangent. Note that differences between functional responses mostly occur for intermediate prey concentration in the range $[0.5, 3]$ $\mathrm{mm^3 cm^{-3}}$. In addition, there is a scaling of a factor ≈ 2 between functional responses of models with and without reserve, so that these models fit empirical data.

7.2.3 Some generic results on equilibria and their bifurcations

Model (7.5) has up to three equilibria. For each one, the right hand side of equations (7.5) vanishes. Function $F_5(\boldsymbol{x})$ vanishes if $X_2 = 0$ or if $e_2 = e_2^{(2)} := g_2(\dot{h} + \dot{k}_M^2)/(\dot{k}_E^2 - \dot{h})$. First, consider the case where $X_2 = 0$. Function $F_4(\boldsymbol{x})$ vanishes if $X_1 = 0$ or if $e_1 = e_1^{(1)} := g_1(\dot{h} + \dot{k}_M^1)/(\dot{k}_E^1 - \dot{h})$. There is a unique equilibrium without prey and predator:

$$\boldsymbol{x^{(0)}} = (f_1(X_r), 0, X_r, 0, 0)^T,$$

which exists for all parameter values. At $\boldsymbol{x^{(0)}}$, the resource concentration equals that of the feed X_r. Note that even if the prey has a positive scaled reserve density ($e_1^{(0)} = f_1(X_r) > 0$) at this equilibrium, there is no prey reserve as prey is absent ($E_i^{(0)} \propto X_i^{(0)} = 0$).

Second, consider the case where $X_2 = 0$ and $e_1 = e_1^{(1)}$ from $F_4(\boldsymbol{x}) = F_5(\boldsymbol{x}) = 0$. Function $F_1(\boldsymbol{x})$ vanishes if $X_0 = X_0^{(1)} := f_1^{-1}(e_1^{(1)})$ (where $u^{-1} \circ u = \mathrm{id}$ for any function u). There is a unique $X_0^{(1)}$, as f_1 is a strictly increasing function. Thus, there is a unique equilibrium with prey and without predator:

$$\boldsymbol{x^{(1)}} = \left(e_1^{(1)} := g_1 \frac{\dot{h} + \dot{k}_M^1}{\dot{k}_E^1 - \dot{h}}, f_2(X_1^{(1)}), X_0^{(1)} := f_1^{-1}(e_1^{(1)}), X_1^{(1)} := \frac{\dot{h}(X_r - X_0^{(1)})}{j_{XAm}^1 e_1^{(1)}}, 0 \right)^T,$$

which exists if the conditions:

$$\dot{h} \leq \dot{k}_E^1,\ \dot{h} \leq \frac{\dot{k}_E^1 - \dot{k}_M^1 g_1}{g_1 + 1},\ \dot{h} \leq \dot{h}^{(0,1)} := \frac{\dot{k}_E^1 f_1(X_r) - \dot{k}_M^1 g_1}{f_1(X_r) + g_1}$$

are satisfied. The first two conditions are always satisfied if $\dot{h} \leq \dot{h}^{(0,1)}$, which is both a necessary and sufficient condition for equilibrium existence. This condition means that prey growth rate is higher than the throughput rate of the chemostat if prey is rare (i.e. resource concentration equals that

of the feed), and thus the prey can invade the system. If $\dot{h} = \dot{h}^{(0,1)}$, there is a double equilibrium $\boldsymbol{x^{(0,1)}} := \boldsymbol{x^{(0)}} = \boldsymbol{x^{(1)}}$. As for equilibrium $\boldsymbol{x^{(0)}}$, the predator has a positive scaled reserve density but there is no predator reserve and structure. An increase of resource concentration in the feed X_r increases the concentration of prey at equilibrium. However, it does not affect its scaled reserve density (i.e. its physiological state) and the resource concentration in the chemostat. They both depend on the throughput rate of the chemostat and prey parameters.

Finally, consider the case where $e_2 = e_2^{(2)}$ from $F_5(\boldsymbol{x}) = 0$. Function $F_2(\boldsymbol{x})$ vanishes if $X_1 = X_1^{(2)} := f_2^{-1}(e_2^{(2)})$, $X_1^{(2)}$ being unique as f_2 is a strictly increasing function. Function $F_3(\boldsymbol{x})$ vanishes if:

$$G(X_0) := X_r - X_0 - \frac{f_1(X_0) j^1_{XAm} X_1^{(2)}}{\dot{h}} = 0. \tag{7.9}$$

Function $G(X_0)$ has the following properties:

$$G'(X_0) = -1 - \frac{j^1_{XAm} X_1^{(2)}}{\dot{h}} f_1'(X_0) < 0,\ G(0) = X_r > 0,\ \lim_{X_0 \to +\infty} G(X_0) = -\infty, \tag{7.10}$$

from properties of f_1. As a consequence, equation $G(X_0) = 0$ has one root $X_0^{(2)}$ and there is a unique equilibrium with prey-predator coexistence:

$$\boldsymbol{x^{(2)}} = \left(e_1^{(2)} := f_1(X_0^{(2)}), e_2^{(2)} := g_2 \frac{\dot{h} + \dot{k}_M^2}{\dot{k}_E^2 - \dot{h}}, X_0^{(2)}, X_1^{(2)} := f_2^{-1}(e_2^{(2)}), \right.$$
$$\left. X_2^{(2)} := \left[\frac{\dot{k}_E^1 e_1^{(2)} - \dot{k}_M^1 g_1}{e_1^{(2)} + g_1} - \dot{h} \right] \frac{X_1^{(2)}}{j^2_{XAm} e_2^{(2)}} \right)^T,$$

which exists if the conditions:

$$\dot{h} \leq \dot{k}_E^2,\ \dot{h} \leq \dot{h}^{(1,2)} := \min \left(\frac{\dot{k}_E^1 e_1^{(2)} - \dot{k}_M^1 g_1}{e_1^{(2)} + g_1}, \frac{\dot{k}_E^2 - \dot{k}_M^2 g_2}{g_2 + 1} \right)$$

are satisfied. The first condition is always satisfied if $\dot{h} \leq \dot{h}^{(1,2)}$, which is both a necessary and sufficient condition for equilibrium existence. This condition means that (i) prey growth rate at equilibrium is higher than the throughput rate of the chemostat $\dot{h}$ and thus it can support losses through predation, (ii) predator growth rate is higher than $\dot{h}$ if prey concentration is high enough (i.e. $e_2 = f_2(X_1) \to 1$), thus there is an intermediate prey concentration $X_1^{(2)}$ such that predator growth rate equals $\dot{h}$. If $\dot{h} = \dot{h}^{(1,2)}$, there is a double equilibrium $\boldsymbol{x^{(1,2)}} := \boldsymbol{x^{(1)}} = \boldsymbol{x^{(2)}}$. Note that $\dot{h}^{(1,2)}$ depends on $\dot{h}$ through $e_1^{(2)}$. An increase of resource concentration in the feed

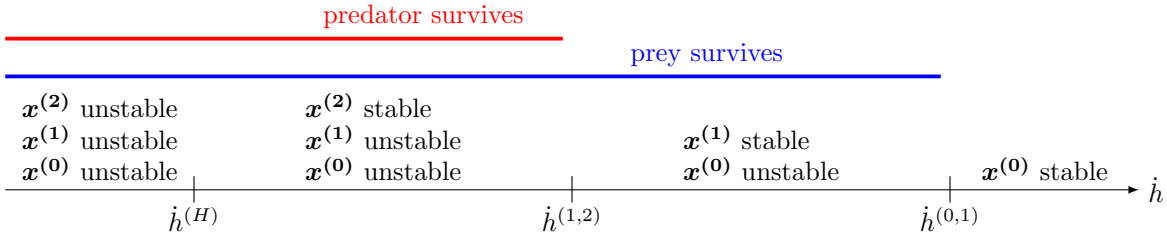

Figure 7.4. Stability and bifurcations of equilibria in the original DEB model as a function of the throughput rate of the chemostat $\dot{h}$. Equilibrium stability is indicated if it exists. All bifurcations do not always occur depending on other parameter values. For fixed other parameter values, the existence of a given bifurcation implies the existence of those that occur at higher $\dot{h}$ values. Note that bifurcation thresholds $\dot{h}^{(H)}$ and $\dot{h}^{(1,2)}$ depends on $\dot{h}$ and thus can be crossed multiple times. Numerical analysis indicates no other bifurcations of equilibria, despite we do not prove it analytically.

X_r does not increase the concentration of prey at equilibrium, which depends on the throughput rate of the chemostat and predator parameters. However, it increases both resource and predator concentrations. Indeed, if $\dot{k}_E^i > \dot{k}_M^i$ (a logical requirement satisfied by the parameter values in table 7.2), then the growth rate of a population (7.3) is an increasing function of scaled reserve density. In addition, $X_0^{(2)} < X_r$ due to equation (7.9) and f_1 is a strictly increasing function, which means that $\dot{h}^{(1,2)} < \dot{h}^{(0,1)}$. This inequality implies that there is no predator-prey coexistence if the prey cannot survive without predator.

The stability of these equilibria and their bifurcations are summarized in figure 7.4 (see section 7.6 in Appendix for details). The trivial equilibrium is stable if $\dot{h} > \dot{h^{(0,1)}}$, i.e. if the $\boldsymbol{x^{(1)}}$ does not exist and thus the prey cannot invade. The prey (resp. the predator) can invade if $\dot{h} < \dot{h^{(0,1)}}$ (resp. $\dot{h} < \dot{h^{(1,2)}}$). This threshold corresponds to a transcritical bifurcation where equilibria $\boldsymbol{x^{(0)}}$ and $\boldsymbol{x^{(1)}}$ (resp. $\boldsymbol{x^{(1)}}$ and $\boldsymbol{x^{(2)}}$) collide and exchange their stability when equilibrium $\boldsymbol{x^{(1)}}$ (resp. $\boldsymbol{x^{(2)}}$) starts to exist. The stability of the coexistence equilibrium $\boldsymbol{x^{(2)}}$ changes when it crosses an Hopf bifurcation at $\dot{h} = \dot{h}^{(H)}$, where $\dot{h}^{(H)}$ is a function of $\dot{h}$. At this bifurcation, a limit cycle appears. Its stability depends on the first Lyapunov coefficient evaluated at the Hopf bifurcation that has to be computed numerically for a given functional response formulation and parameter values. When the first Lyapunov coefficient is negative (positive), there is a stable (unstable) limit cycle when the equilibrium is unstable (stable). In our numerical analysis, the original DEB model and Droop model do not exhibit other bifurcations of equilibria, despite we do not prove it analytically. All the analytical results on the original DEB model presented in this subsection also hold for the Droop model. For this model, the only difference is that both somatic maintenance coefficients $\dot{k}_M^1$ and $\dot{k}_M^2$ are equal to zero (see table 7.2).

7.2.4 Numerical analysis of the original DEB model with different predator functional responses

For the three different predator functional responses, bifurcations between the asymptotic dynamics of model (7.5) (figure 7.5) are qualitatively similar (figure 7.6), despite some quantitative differences that we discuss later. Species survival requires that the throughput rate of the chemostat $\dot{h}$ is high enough to provide resource supply, but not too large as it acts as a linear loss term. In addition, the resource concentration in the feed X_r needs to be sufficient to cover maintenance costs and losses by dilution. For a fixed $\dot{h}$ (resp. X_r), environment enrichment by increasing X_r (resp. decreasing or increasing $\dot{h}$) allows the classical succession of species, with first possibility of invasion by the prey ($\dot{h} < \dot{h}^{(0,1)}$) and then by the predator ($\dot{h} < \dot{h}^{(1,2)} < \dot{h}^{(0,1)}$). For higher enrichment levels, the coexistence equilibrium becomes unstable due to a Hopf bifurcation ($\dot{h} = \dot{h}^{(H)}$) and species coexist on a stable limit cycle. This enrichment paradox (Rosenzweig, 1971) is less straightforward than in the classical Rosenzweig & MacArthur's predator-prey model (1963). In the latter, enrichment destabilizes the coexistence equilibrium through a supercritical Hopf bifurcation which gives birth to a stable limit cycle. Here, enrichment makes an unstable limit cycle collides with the coexistence equilibrium that becomes unstable at a subcritical Hopf bifurcation. The stable limit cycle is not involved in this bifurcation. It comes from a limit point of cycles bifurcation that occurs for a lower enrichment level, where both the stable and unstable limit cycles collide and (dis)appear. The two cycles coexist between the bifurcation of cycles and the Hopf bifurcation, where model (7.5) has two stable states that can be reached depending on initial conditions, the coexistence equilibrium and the stable limit cycle (figure 7.5, panel 4). Such dynamics were unexpected for this type of models, based on previous studies (Kooi & Kooijman, 1994a).

The proportion of the bifurcation diagram that lead to different dynamics between functional responses is quantified. Each area is computed as in chapter 3, using a curve integral over its boundary. To compute proportions, we focus our study on the parameter space where the prey can survive (i.e. equilibrium $\boldsymbol{x^{(1)}}$ exists) for X_r lower than an arbitrary value X_r^{thres}:

$$\Gamma = \left[0, \dot{h}^{(0,1)}\right] \times \left[f_1^{-1}\left(g_1 \frac{\dot{k}_M^1 + \dot{h}^{(0,1)}}{\dot{k}_E^1 - \dot{h}^{(0,1)}}\right), X_r^{thres}\right].$$

This domain is independant on the choice of predator functional response, and thus is common to the three bifurcation diagrams.

Most differences between bifurcation diagrams occur for $X_r < 5$ (figure 7.6). Thus, an increase of X_r^{thres} value decreases the proportions of different dynamics (table 7.4). By decreasing

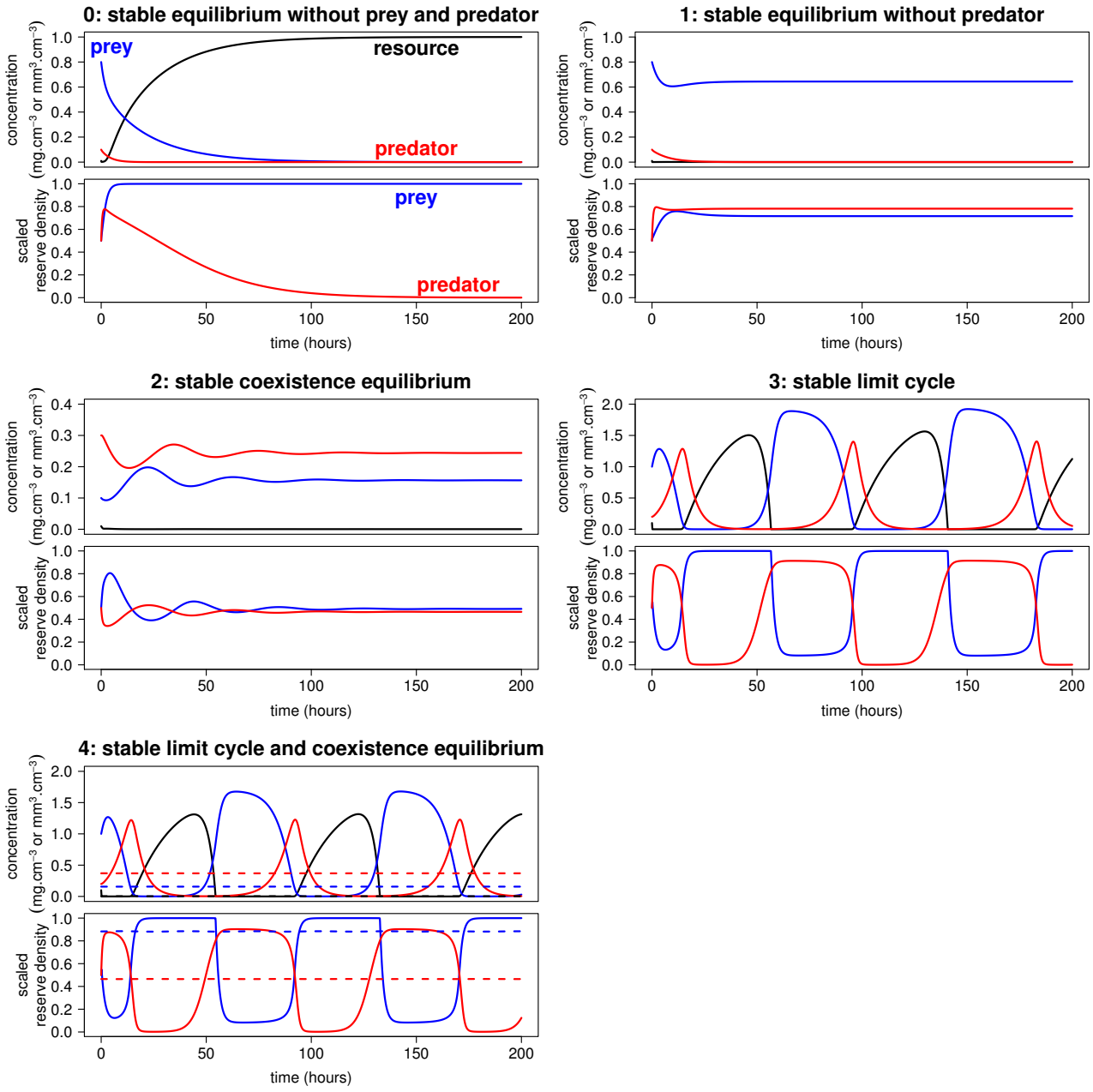

Figure 7.5. Simulations of the original DEB model showing all the qualitative dynamics found in this study. Different asymptotic dynamics with Holling's disc equation are obtained by changing environmental conditions: the throughput rate of the chemostat $\dot{h}$ and the resource concentration in the feed X_r. For panels 0 to 2: $X_r = 1$ and $\dot{h} = \{0.4, 0.3, 0.05\}$ respectively. For panels 3 and 4: $\dot{h} = 0.05$ and $X_r = \{1.8, 2\}$ respectively. In panel 4, plain and dashed curves correspond to different initial conditions to show the two alternative asymptotic dynamics.

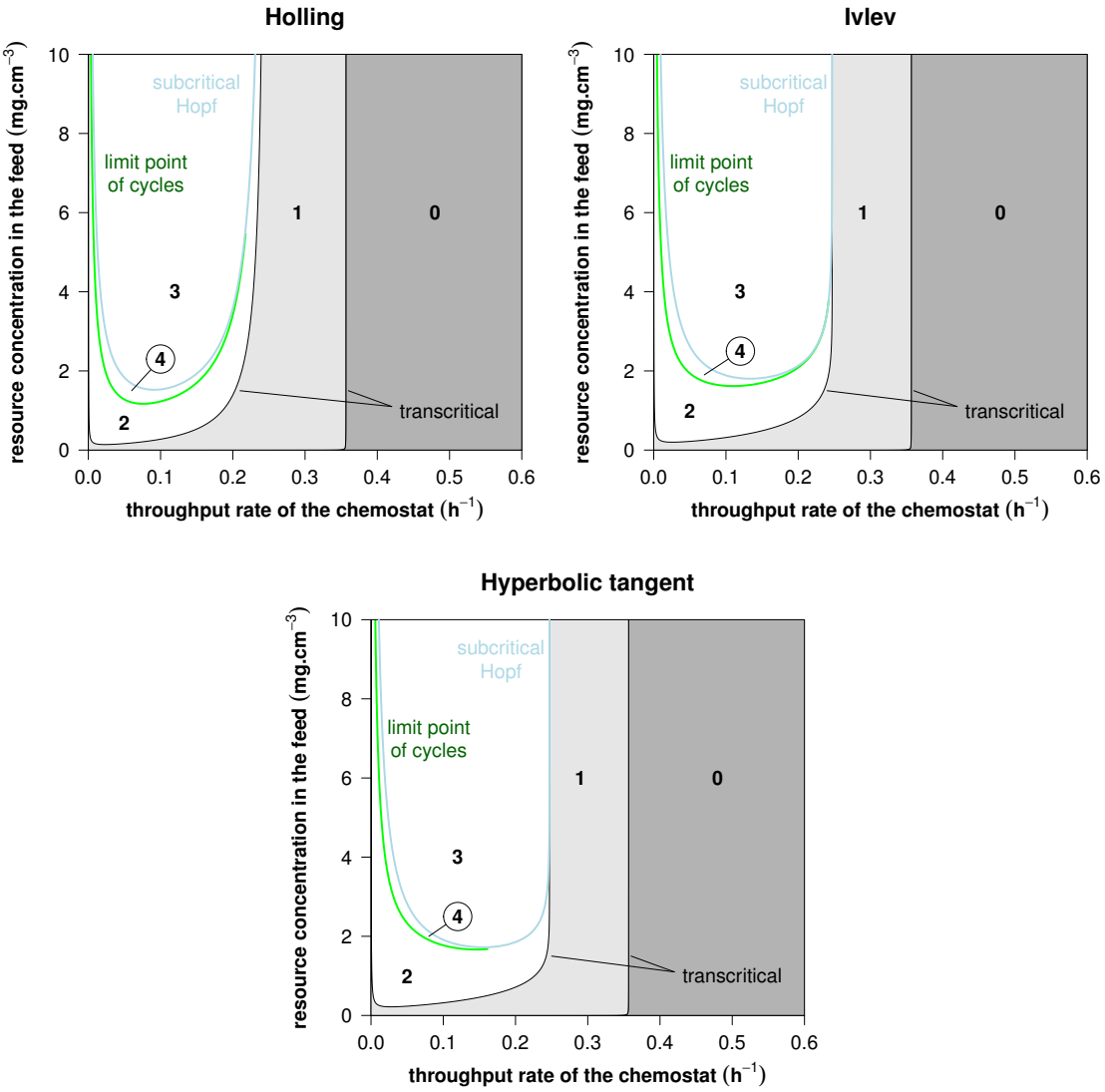

Figure 7.6. Bifurcation diagrams of the original DEB model with respect to environmental parameters, using different predator functional responses. The number in each region of the parameter space means that system dynamics is qualitatively equivalent to the corresponding panel in figure 7.5. In region 0, only the trivial equilibrium ($\boldsymbol{x^{(0)}}$) without prey and predator exists and is stable. It becomes unstable at the transcritical bifurcation between regions 0 and 1 ($\dot{h} = \dot{h}^{(0,1)}$), where the prey can invade at a stable prey-resource equilibrium ($\boldsymbol{x^{(1)}}$). This equilibrium becomes unstable at the transcritical bifurcation between regions 1 and 2 ($\dot{h} = \dot{h}^{(1,2)}$), where the predator can invade at a stable coexistence equilibrium ($\boldsymbol{x^{(2)}}$). This equilibrium becomes unstable at the subcritical Hopf bifurcation between regions 2 and 3 ($\dot{h} = \dot{h}^{(H)}$). In region 3, long-term coexistence occurs on a stable limit cycle. This stable limit cycle expands from the limit point of cycles bifurcation, where it appears with a saddle limit cycle which disappears at the subcritical Hopf bifurcation. This unstable limit cycle exists only in region 4, where there are a stable coexistence equilibrium and a stable limit cycle (asymptotic dynamics depends on initial condition). Note that all bifurcation curves might be very close, but they do not intersect with each others.

Table 7.4. Proportion of qualitatively different dynamics between functional responses in the original DEB model. The reference area corresponds to the parameter space where the prey can survive for resource concentration in the feed lower than an arbitrary value X_r^{thres}. For each pair of functional responses, the following proportions are indicated for different X_r^{thres} values: different predator survival (existence of $\boldsymbol{x^{(2)}}$), predator survives and there is an only stable state with predator-prey fluctuations (stability of $\boldsymbol{x^{(2)}}$ when it exists), existence of multiple stable states (stability of $\boldsymbol{x^{(2)}}$ when it exists and existence of a stable limit cycle). This classification is made to ease comparisons between models. Note that the first proportion does not overlap with the two others. Conversely, the latter two can overlap with each other.

functional responses	X_r^{thres}	predator survival	only oscillations	multi-stability
Holling - Ivlev	5	0.060	0.094	0.085
	10	0.045	0.071	0.051
	20	0.030	0.047	0.030
Holling - Tanh	5	0.069	0.109	0.070
	10	0.050	0.081	0.050
	20	0.032	0.053	0.031
Ivlev - Tanh	5	0.008	0.027	0.026
	10	0.004	0.016	0.018
	20	0.002	0.009	0.012

order, most frequent differences concern the stability of the coexistence equilibrium (from 0.9 % to 10.9 %), the existence of multiple stable states (from 1.1 % to 8.5 %, which partly overlap with the stability of the coexistence equilibrium), and finally the existence of a coexistence equilibrium (i.e. predator survival, from 0.2 % to 6.9 %). For all differences in qualitative dynamics, the closest bifurcation diagrams are those obtained with the hyperbolic tangent and Ivlev's functional response. Ivlev's functional response gives a bifurcation diagram slightly closer to that of Holling's disc equation than the hyperbolic tangent does. This sorting of pairs of bifurcation diagrams is consistent with the closeness between functional responses (measured by correlation coefficient, figure 7.3).

As changing the functional response formulation affects model (7.5) qualitative dynamics (figure 7.6), this model is structurally sensitive (figure 7.6). However, evaluating the importance of this sensitivity from the previous analysis remains a subjective issue. Indeed, no quantitative measure of structural sensitivity (like the one proposed by Cordoleani *et al.*, 2011, or in chapter 6 of this thesis) is used, and our quantification of proportions of qualitatively different dynamics depends on the parameter space consider. Nevertheless, structural sensitivity of model (7.5) to the predator functional response can be considered as low. This statement is supported by two arguments. First, the qualitative shape of the bifurcation diagram is not affected by the functional response formulation (figure 7.6). For each formulation, model (7.5) exhibits the same qualitative dynamics and bifurcations. Bifurcations occur roughly at the same parameter values, despite some differ-

ences. The second argument is that these differences are quantitatively lower than those observed for example in the predator-prey model studied in chapter 3. In this model, different dynamics are predicted by two functional responses in almost half of the parameter space. Furthermore, exploring a larger parameter space in that model still leads to different dynamics, whereas most differences remain in bounded part of the parameter space with model (7.5) (figure 7.6). Using the original DEB model (7.5) as a reference, we now evaluate structural sensitivity in models with less details on species metabolism.

7.2.5 No somatic maintenance: the Droop model

Droop model is a special case of the original DEB model (7.5), where somatic maintenance of organisms is not explicitely taken into account, i.e. $\dot{k}_M^i = 0$. However, some effects of somatic maintenance are indirectly taken into account by other parameter values, which are re-estimated in order to fit empirical data (tables 7.2-7.3).

Similar bifurcation diagrams are obtained for the three different functional responses (figure 7.7), as for the original DEB model. The main difference with the original DEB model is that there is no possibility for multiple stable states (only dynamics 0 to 3 in figure 7.5 are observed). One stable state (equilibrium or limit cycle) occurs for all tested parameter values, because there is no bifurcation of limit cycles and the Hopf bifurcation is supercritical. This supercritical Hopf bifurcation destabilizes the coexistence equilibrium and gives birth to a stable limit cycle as environment is enriched. This enrichment paradox occurs in a different way than in the original DEB model (it occurs like in the classical model by Rosenzweig & MacArthur, 1963), whereas we have the same succession of species. However, the succession of species occurs for increasing X_r or decreasing $\dot{h}$ value. Indeed, $\dot{h}$ value does not need to be high enough to provide a sufficient amount of resource to overcome maintenance costs. As there are no maintenance costs, bifurcations occur at different parameter values than in the original DEB model. A synthetic comparison between models will be provided after the analysis of the four models.

In Droop model, most differences between bifurcation diagrams occur for $X_r < 5$ (figure 7.7). Thus, an increase of X_r^{thres} value decreases the proportions of different dynamics (table 7.5). Differences concern more the stability of the coexistence equilibrium (from 1.4 % to 11.5 %) than its existence (i.e. predator survival, from 0.1 % to 3.5 %). The sorting of closest pairs of bifurcation diagrams is the same as for the original DEB model. Based upon the same arguments as for the original DEB model, the structural sensitivity to the predator functional response is low in Droop model.

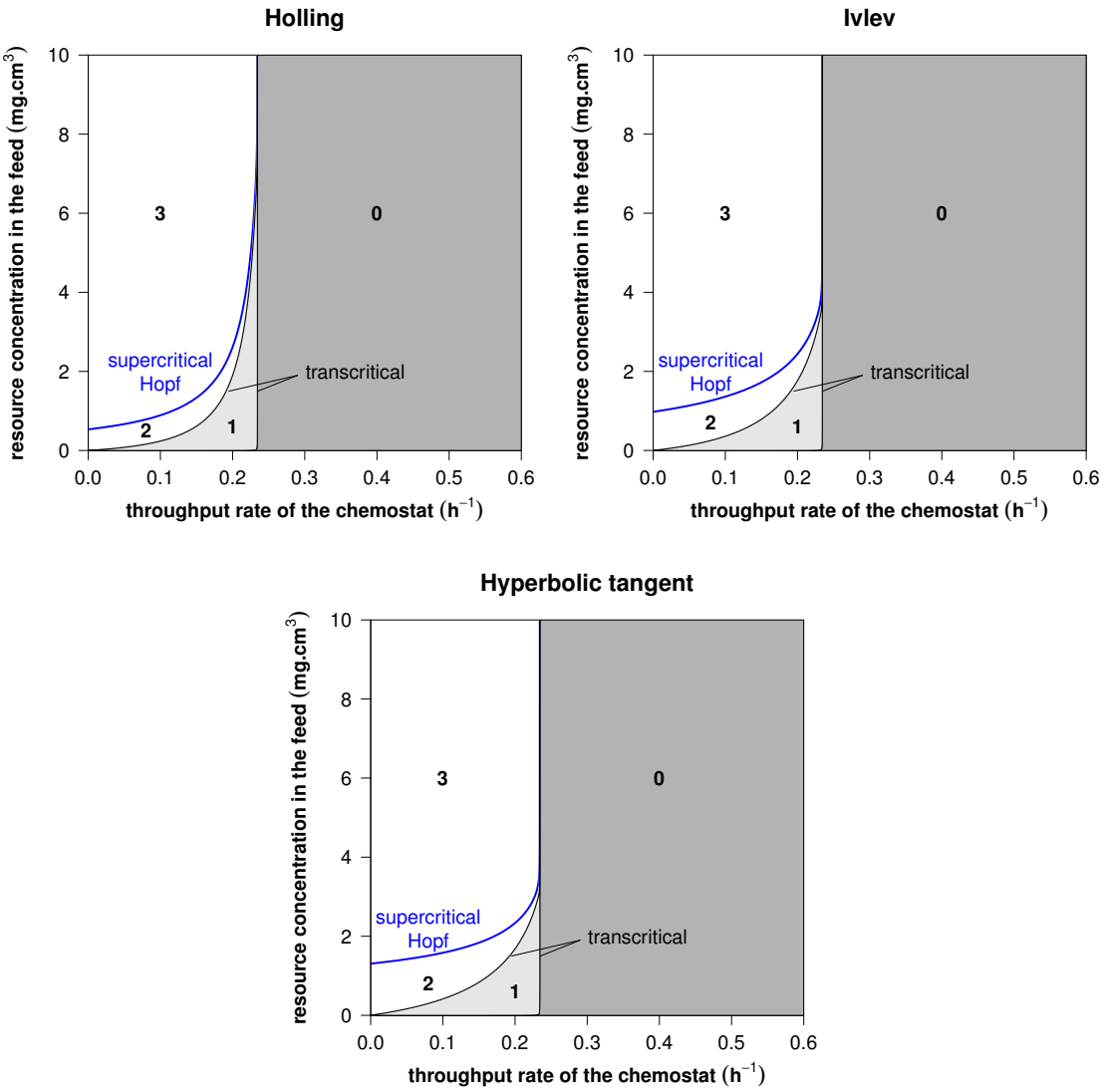

Figure 7.7. Bifurcation diagrams of the Droop model with respect to environmental parameters, using different predator functional responses. The number in each region of the parameter space means that system dynamics is qualitatively equivalent to the corresponding panel in figure 7.5. In region 0, only the trivial equilibrium ($\boldsymbol{x^{(0)}}$) without prey and predator exists and is stable. It becomes unstable at the transcritical bifurcation between regions 0 and 1 ($\dot{h} = \dot{h}^{(0,1)}$), where the prey can invade at a stable prey-resource equilibrium ($\boldsymbol{x^{(1)}}$). This equilibrium becomes unstable at the transcritical bifurcation between regions 1 and 2 ($\dot{h} = \dot{h}^{(1,2)}$), where the predator can invade at a stable coexistence equilibrium ($\boldsymbol{x^{(2)}}$). This equilibrium becomes unstable at the supercritical Hopf bifurcation between regions 2 and 3 ($\dot{h} = \dot{h}^{(H)}$). In region 3, long-term coexistence occurs on a stable limit cycle. Note that all bifurcation curves might be very close, but they do not intersect with each others.

Table 7.5. Proportion of qualitatively different dynamics between functional responses in the Droop model. The reference area corresponds to the parameter space where the prey can survive for resource concentration in the feed lower than an arbitrary value X_r^{thres}. For each pair of functional responses, the following proportions are indicated for different X_r^{thres} values: different predator survival (existence of $\boldsymbol{x^{(2)}}$), predator survives and there is an only stable state with predator-prey fluctuations (stability of $\boldsymbol{x^{(2)}}$ when it exists). Note that the two proportion do not overlap with each other.

functional responses	X_r^{thres}	predator survival	predator oscillations
Holling - Ivlev	5	0.027	0.077
	10	0.016	0.040
	20	0.008	0.020
Holling - Tanh	5	0.035	0.115
	10	0.020	0.060
	20	0.010	0.030
Ivlev - Tanh	5	0.004	0.055
	10	0.002	0.027
	20	0.001	0.014

7.3 Predator-prey models without explicit reserves

7.3.1 Marr-Pirt model as a special case of the original DEB model

Explicit reserve dynamics is not required if it is assumed to be infinitely fast (i.e. instantaneous) in comparison to structure dynamics. Reserve dynamics is proportional to the energy conductance $\dot{k}_E^i$ (7.4). If $\dot{k}_E^i \to +\infty$, the scaled reserve density is always equal to the scaled functional response, i.e. $e_i = f_i(X_{i-1})$. Thus, the scaled reserve density is a function of the food available (resource or prey structure) at the same time. Infinitely fast reserve dynamics means that $\dot{k}_E^i, g_i \to +\infty$. At this limit, the growth rate of structure is:

$$\lim_{\dot{k}_E^i, g_i \to +\infty} \frac{\dot{k}_E^i e_i - \dot{k}_M^i g_i}{e_i + g_i} = \lim_{\dot{k}_E^i, g_i \to +\infty} \frac{\frac{\dot{k}_E^i}{g_i} e_i - \dot{k}_M^i}{\frac{e_i}{g_i} + 1} = \dot{\mu}_i f_i(X_{i-1}) - \dot{k}_M^i \text{ with } \dot{\mu}_i = \frac{\dot{k}_E^i}{g_i} \quad i = 1, 2. \tag{7.11}$$

The new parameter $\dot{\mu}_i$ is the maximum growth rate of the population. Using (7.11), the original DEB model (7.5) simplifies into the following three-dimensional system:

$$\dot{\boldsymbol{x}} = \boldsymbol{F}(\boldsymbol{x}) \Leftrightarrow \begin{cases} \dfrac{dX_0}{dt} &= \dot{h}(X_r - X_0) - f_1(X_0) j^1_{XAm} X_1 \\ \dfrac{dX_1}{dt} &= \left(\dot{\mu}_1 f_1(X_0) - \dot{k}^1_M - \dot{h}\right) X_1 - f_2(X_1) j^2_{XAm} X_2 \\ \dfrac{dX_2}{dt} &= \left(\dot{\mu}_2 f_2(X_1) - \dot{k}^2_M - \dot{h}\right) X_2, \end{cases} \tag{7.12}$$

where $\boldsymbol{x} = (X_0, X_1, X_2)^T$. Model (7.12) is Marr-Pirt model applied to a predator-prey system in chemostat. In this model, the ratio $\dot{\mu}_2 / j^2_{XAm}$ is the conversion efficiency of the predator. This conversion efficiency varies when we change the functional response formulation. Indeed, we re-estimate j^2_{XAm} but not $\dot{\mu}_2$, as its value is derived from metabolic parameters of the original DEB model. This assumption can be relaxed by varying $\dot{\mu}_2$ in order to keep a constant $\dot{\mu}_2 / j^2_{XAm}$ ratio between functional responses. Doing this does not affect our qualitative results (despite there are some quantitative changes, section 7.8 in Appendix) and the relevance of both assumptions will be discussed later.

7.3.2 Some generic results on equilibria and their bifurcations

Marr-Pirt model (7.12) has up to three equilibria. For each one, the right hand side of equations (7.12) vanishes. Function $F_3(\boldsymbol{x})$ vanishes if $X_2 = 0$ or if $X_1 = X_1^{(2)} := f_2^{-1}((\dot{k}^2_M + \dot{h})/\dot{\mu}_2)$. First, consider the case where $X_2 = 0$. Function $F_2(\boldsymbol{x})$ vanishes if $X_1 = 0$ or if $X_0 = X_0^{(1)} := f_1^{-1}((\dot{k}^1_M + \dot{h})/\dot{\mu}_1)$. Thus, there is a unique trivial equilibrium without prey and predator:

$$\boldsymbol{x^{(0)}} = (X_r, 0, 0)^T,$$

which exists for all parameter values. At $\boldsymbol{x^{(0)}}$, the resource concentration equals that of the feed.

Second, consider the case where $X_2 = 0$ and $X_0 = X_0^{(1)}$ from $F_2(\boldsymbol{x}) = F_3(\boldsymbol{x}) = 0$. There is a unique $X_0^{(1)}$, as f_1 is a strictly increasing function. Thus, there is a unique equilibrium with prey and without predator:

$$\boldsymbol{x^{(1)}} = \left(X_0^{(1)} := f_1^{-1}\left(\frac{\dot{k}^1_M + \dot{h}}{\dot{\mu}_1}\right), X_1^{(1)} := \frac{\dot{h}(X_r - X_0^{(1)})}{j^1_{Xam} f_1(X_0^{(1)})}, 0 \right)^T,$$

which exists if the conditions:

$$\dot{h} < \dot{\mu}_1 - \dot{k}_M^1,\ \dot{h} \leq \dot{h}^{(0,1)} := \dot{\mu}_1 f_1(X_r) - \dot{k}_M^1,$$

are fulfilled. The first condition is always fulfilled if $\dot{h} < \dot{h}^{(0,1)}$, which is both a necessary and sufficient condition for equilibrium existence. This condition means that prey growth rate is higher than the throughput rate of the chemostat if prey is rare (i.e. resource concentration is equal to that of the feed), and thus the prey can invade the system. If $\dot{h} = \dot{h}^{(0,1)}$, there is a double equilibrium $\boldsymbol{x^{(0)}} = \boldsymbol{x^{(1)}} := \boldsymbol{x^{(0,1)}}$. An increase of the resource concentration in the feed X_r increases the concentration of prey at equilibrium, but it does not affect the resource concentration in the chemostat.

Finally, consider the case where $X_1 = X_1^{(2)}$ from $F_2(\boldsymbol{x}) = 0$, $X_1^{(2)}$ being unique as f_2 is a strictly increasing function. Function $F_1(\boldsymbol{x})$ vanishes if $G(X_0) = 0$ where $G(X_0)$ is the same function as for the original DEB model (7.9-7.10). Thus, $G(X_0) = 0$ has one root $X_0^{(2)}$ and there is unique equilibrium with prey-predator coexistence:

$$\boldsymbol{x^{(2)}} = \left(X_0^{(2)}, X_1^{(2)} := f_1^{-1}\left(\frac{\dot{k}_M^2 + \dot{h}}{\dot{\mu}_2}\right), X_2^{(2)} := \frac{(\dot{\mu}_1 f_1(X_0^{(2)}) - \dot{k}_M^1 - \dot{h}) X_1^{(2)}}{j_{XAm}^2 f_2(X_1^{(2)})} \right)^T,$$

which exists if the condition

$$\dot{h} \leq \dot{h}^{(1,2)} := \min\left(\dot{\mu}_1 f_1(X_0^{(2)}) - \dot{k}_M^1, \dot{\mu}_2 - \dot{k}_M^2\right),$$

is satisfied. This condition means that (i) prey growth rate at equilibrium is higher than the throughput rate of the chemostat $\dot{h}$ and thus it can support losses through predation, (ii) predator growth rate is higher than $\dot{h}$ if prey concentration is high enough (i.e. $f_2(X_1) \to 1$), thus there is an intermediate prey concentration $X_1^{(2)}$ such that predator growth rate equals $\dot{h}$. If $\dot{h} = \dot{h}^{(1,2)}$, there is a double equilibrium $\boldsymbol{x^{(1)}} = \boldsymbol{x^{(2)}} := \boldsymbol{x^{(1,2)}}$. Note that $\dot{h}^{(1,2)}$ depends on $\dot{h}$ through $X_0^{(2)}$. An increase of resource concentration in the feed X_r does not increase the concentration of prey at equilibrium, which depends on the throughput rate of the chemostat and predator parameters. However, it increases both resource and predator concentrations. In addition, $X_0^{(2)} < X_r$ due to equation (7.9) and f_1 is a strictly increasing function, which means that $\dot{h}^{(1,2)} < \dot{h}^{(0,1)}$. This inequality implies that there is no predator-prey coexistence if the prey cannot survive without predator.

Results on stability and bifurcations of these equilibria are detailled in Appendix (section 7.7). They are qualitatively equivalent to those summarized in figure 7.4, despite the threshold values

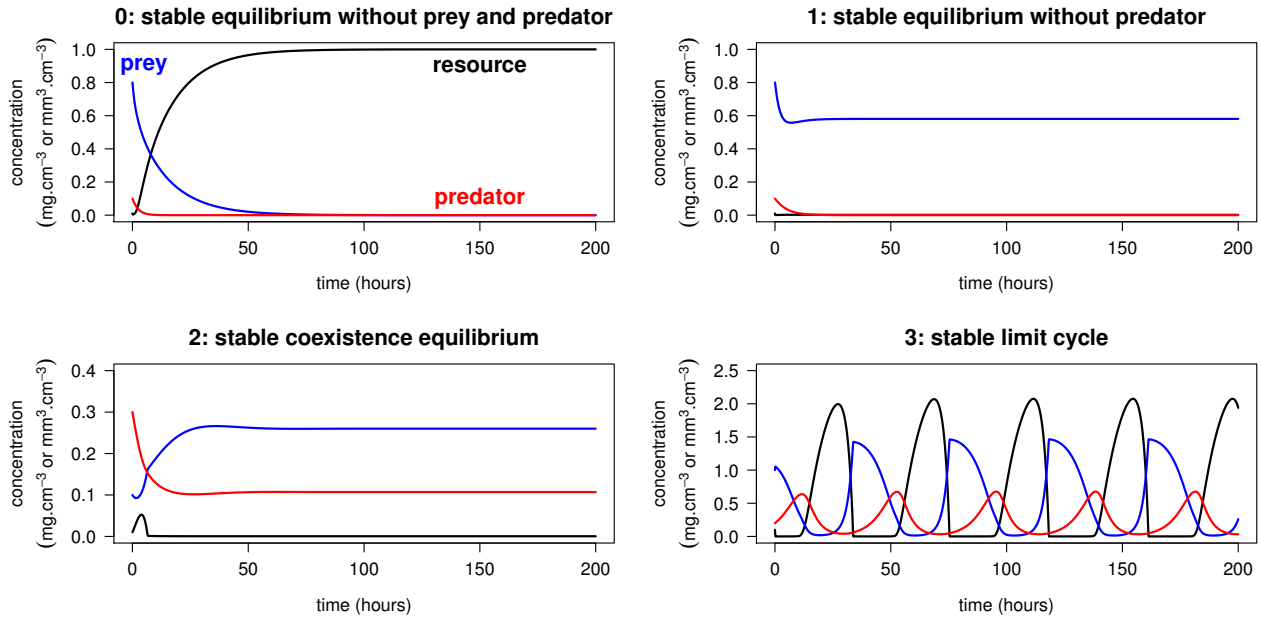

Figure 7.8. Simulations of the Marr-Pirt model showing all the qualitative dynamics found in this study. Different asymptotic dynamics with Holling's disc equation are obtained by changing environmental conditions: the throughput rate of the chemostat $\dot{h}$ and the resource concentration in the feed X_r. For panels 0 to 2: $X_r = 1$ and $\dot{h} = \{0.6, 0.4, 0.1\}$ respectively. For panel 3: $\dot{h} = 0.1$ and $X_r = 3$ respectively.

of $\dot{h}$ for bifurcations are those defined the current subsection. All the analytical results on the Marr-Pirt model presented in this subsection also hold for the Monod model. For this model, the only difference is that both somatic maintenance coefficients $\dot{k}_M^1$ and $\dot{k}_M^2$ are equal to zero (see table 7.2). Note that to study the asymptotic behaviour of the Monod model, it can be simplified into a model with two state variables (Thieme, 1994, Kooi & Boer, 2001, Cordoleani *et al.*, 2011). However, this simplification is not possible for the more generic Marr-Pirt model and is not presented for the sake of synthesis.

7.3.3 Numerical analysis of the Marr-Pirt model with different predator functional responses

Marr-Pirt model (7.12) with re-estimated parameter values (tables 7.2-7.3) can exhibit the same asymptotic dynamics (figure 7.8), bifurcations (figure 7.9) and enrichment paradox as the Droop model. The qualitative difference with the Droop model is that $\dot{h}$ needs to be high enough so that resource input overcomes maintenance costs and species can survive. Thus, the succession of species also occurs for increasing $\dot{h}$, as in the original DEB model.

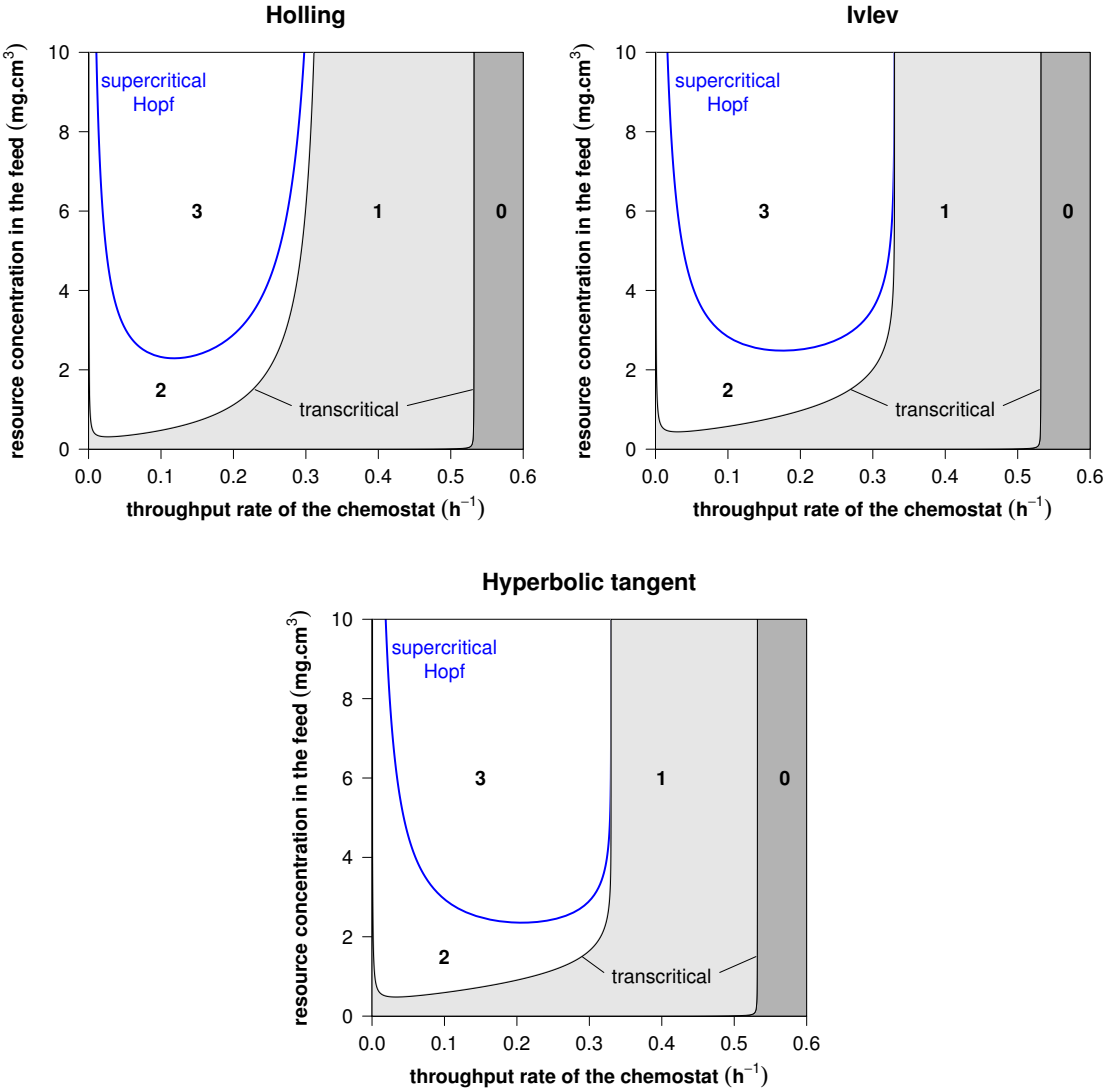

Figure 7.9. Bifurcation diagrams of the Marr-Pirt model with respect to environmental parameters, using different predator functional responses. The number in each region of the parameter space means that system dynamics is qualitatively equivalent to the corresponding panel in figure 7.8. In region 0, only the trivial equilibrium ($\boldsymbol{x^{(0)}}$) without prey and predator exists and is stable. It becomes unstable at the transcritical bifurcation between regions 0 and 1 ($\dot{h} = \dot{h}^{(0,1)}$), where the prey can invade at a stable prey-resource equilibrium ($\boldsymbol{x^{(1)}}$). This equilibrium becomes unstable at the transcritical bifurcation between regions 1 and 2 ($\dot{h} = \dot{h}^{(1,2)}$), where the predator starts can invade at a stable coexistence equilibrium ($\boldsymbol{x^{(2)}}$). This equilibrium becomes unstable at the supercritical Hopf bifurcation between regions 2 and 3 ($\dot{h} = \dot{h}^{(H)}$). In region 3, long-term coexistence occurs on a stable limit cycle. Note that all bifurcation curves might be very close, but they do not intersect with each others.

Table 7.6. Proportion of qualitatively different dynamics between functional responses in the Marr-Pirt model. The reference area corresponds to the parameter space where the prey can survive for resource concentration in the feed lower than an arbitrary value X_r^{thres}. For each pair of functional responses, the following proportions are indicated for different X_r^{thres} values: different predator survival (existence of $\boldsymbol{x^{(2)}}$), predator survives and there is an only stable state with predator-prey fluctuations (stability of $\boldsymbol{x^{(2)}}$ when it exists). Note that the two proportion do not overlap with each other.

functional responses	X_r^{thres}	predator survival	predator oscillations
Holling - Ivlev	5	0.068	0.075
	10	0.058	0.064
	20	0.041	0.044
Holling - Tanh	5	0.081	0.088
	10	0.065	0.074
	20	0.045	0.018
Ivlev - Tanh	5	0.014	0.028
	10	0.007	0.018
	20	0.003	0.010

In Marr-Pirt model, bifurcation diagrams obtained for the three functional responses are qualitatively similar. In addition, most quantitative differences between bifurcation diagrams occur for $X_r < 5$ (figure 7.9). Thus, an increase of X_r^{thres} value again decreases the proportions of different dynamics (table 7.6). As for previous models, differences concern more the stability of the coexistence equilibrium (from 1.0 % to 8.8 %) than its existence (i.e. predator survival, from 0.3 % to 8.1 %). The sorting of closest pairs of bifurcation diagrams is the same as for previous models. Based upon the same arguments as for the original DEB model, the structural sensitivity to the predator functional response is also low in Marr-Pirt model.

7.3.4 No somatic maintenance: the Monod model

As for Droop model, Monod model is a special case of the Marr-Pirt model (7.12), where somatic maintenance of organisms is not explicitely taken into account, i.e. $\dot{k}_M^i = 0$. However, some effects of somatic maintenance are indirectly taken into account by other parameter values, which are re-estimated in order to fit empirical data (tables 7.2-7.3).

Monod model can exhibit almost the same asymptotic dynamics, bifurcations (figure 7.10) and enrichment paradox as the Droop model. The only difference occurs in the bifurcation diagram based on the hyperbolic tangent. With this functional response, the supercritical Hopf bifurcation curve wraps at small $\dot{h}$ (like in models with somatic maintenance: original DEB and Marr-Pirt models) and becomes subcritical at a Bautin bifurcation point. From this point, a limit point of cycle bifurcation starts and stays between $\dot{h} = 0$ and the subcritical Hopf curve (due to continuity

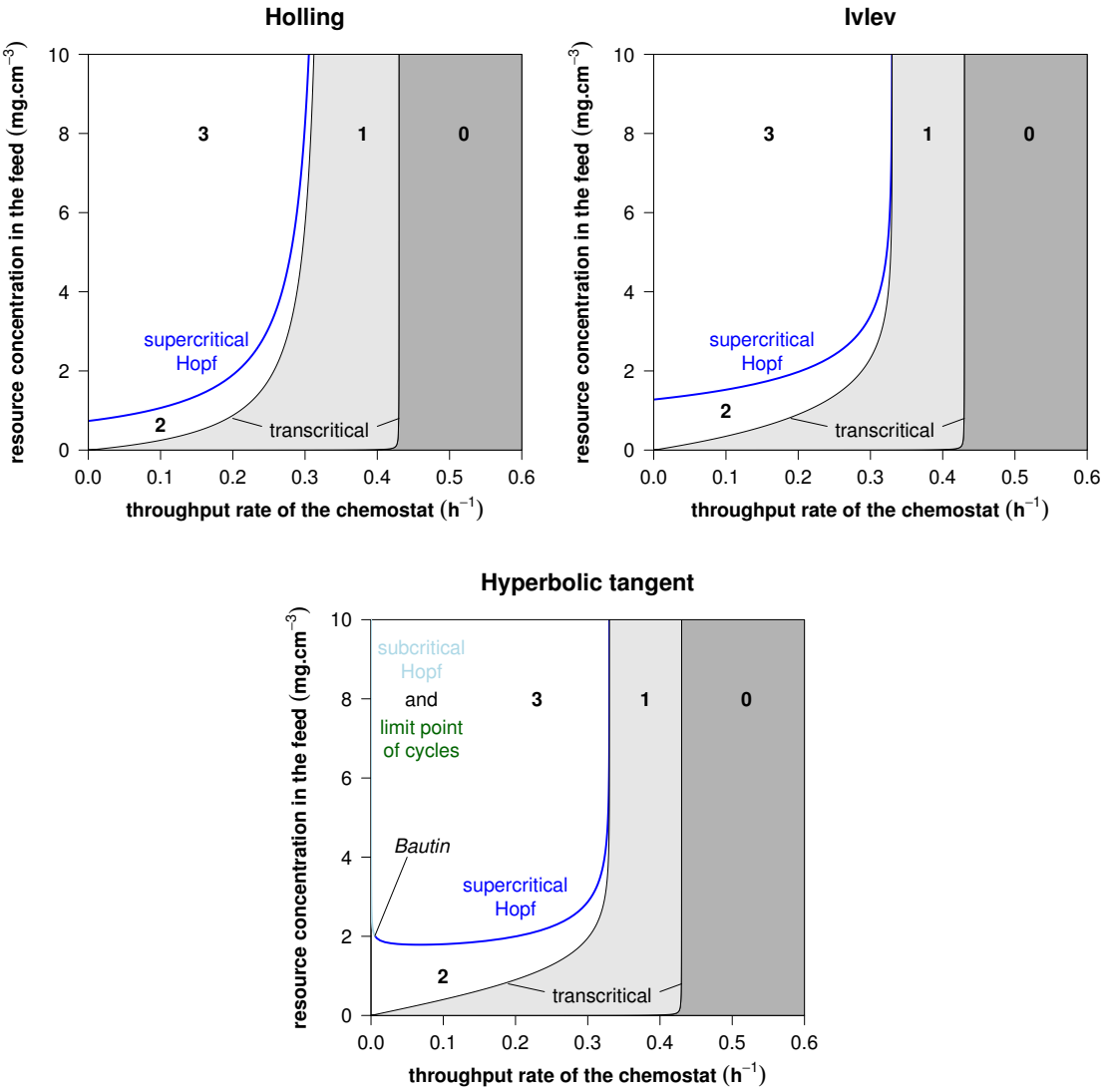

Figure 7.10. Bifurcation diagrams of the Monod model with respect to environmental parameters, using different predator functional responses. The number in each region of the parameter space means that system dynamics is qualitatively equivalent to the corresponding panel in figure 7.8. In region 0, only the trivial equilibrium ($\boldsymbol{x^{(0)}}$) without prey and predator exists and is stable. It becomes unstable at the transcritical bifurcation between regions 0 and 1 ($\dot{h} = \dot{h}^{(0,1)}$), where the prey can invade at a stable prey-resource equilibrium ($\boldsymbol{x^{(1)}}$). This equilibrium becomes unstable at the transcritical bifurcation between regions 1 and 2 ($\dot{h} = \dot{h}^{(1,2)}$), where the predator starts can invade at a stable coexistence equilibrium ($\boldsymbol{x^{(2)}}$). This equilibrium becomes unstable at the supercritical Hopf bifurcation between regions 2 and 3 ($\dot{h} = \dot{h}^{(H)}$). In region 3, long-term coexistence occurs on a stable limit cycle. With the hyperbolic tangent, the Hopf bifurcation can be either supercritical or subcritical, the two branches meet at a Bautin point. From this point, a limit point of cycles bifurcation curve starts and stays between $\dot{h} = 0$ and the subcritical Hopf bifurcation. In the tiny region between these two curves (curves are close to $\dot{h} = 0$), there are a stable limit cycle and a stable coexistence equilibrium.

of eigenvalues of the Jacobian matrix evaluated at the degenerated equilibrium $(0, 0, X_2 > 0)^T$ that exists for $\dot{h} = 0$). In this tiny region of the parameter space which cannot be precisely quantified, Monod model with the hyperbolic tangent has multiple stable states (an equilibrium and a stable limit cycle) like in the area 4 of the original DEB model (figure 7.5). Conversely to the original DEB model, this multistability occurs only for one functional response among the three tested.

This qualitative difference between functional responses is neglectible in term of proportion of the parameter space affected. Most quantitative differences between bifurcation diagrams occur for $X_r < 5$ (figure 7.9). Thus, an increase of X_r^{thres} value again decreases the proportions of different dynamics (table 7.7). As for previous models, differences concern more the stability of the coexistence equilibrium (from 1.5 % to 10.7 %) than its existence (i.e. predator survival, from 0.4 % to 7.4 %). The sorting of closest pairs of bifurcation diagrams is the same as for previous models.

Based upon the same arguments as for the original DEB model, the structural sensitivity to the predator functional response in Monod model can be considered as (i) important because there are qualitative differences in the bifurcations that occur, or (ii) low as these differences are quantitatively neglectible and other quantitative differences are small (relatively to the model studied in chapter 3). This second interpretation is based on quantitative results (proportions of the parameter space) that might depend on the parameter values used. A sensitivy analysis to all the biological parameters (table 7.2) would be computationally prohibitive due to the number of parameters and their range of values in empirical data (Kooijman, 2010, chapter 8). Furthermore, some parameter sets might no be realistic as many parameters covary in DEB theory. Instead of a sensitivity analysis, the next subsection presents results obtained for an example of parameter set derived from another chemostat experiment.

7.3.5 Monod model with parameter values from Canale et al. (1973)

Canale *et al.* (1973) investigated the dynamics of *Tetrahymena pyriformis* (ciliate) feeding on the bacterium *Aerobacter aerogenes* (which grows using carbohydrates) through a chemostat experiment. This experiment was coupled to a model in order to explain their results. These data and parameter values were used by Cordoleani *et al.* (2011) to study structural sensitivity (in term of location of the Hopf bifurcation) in a bitrophic Monod model. This model is written in a different (but equivalent) way than model (7.12) with $\dot{k}_M^i = 0$. Parameter values of model (7.12) presented in table 7.8 come from Cordoleani *et al.* (2011) and are estimated from Canale *et al.*'s experiment (1973). Note that in this case, the conversion efficiency of the predator $\dot{\mu}_2 / j_{Xam}^2$ is held constant between functional response formulations.

Table 7.7. Proportion of qualitatively different dynamics between functional responses in the Monod model. The reference area corresponds to the parameter space where the prey can survive for resource concentration in the feed lower than an arbitrary value X_r^{thres}. For each pair of functional responses, the following proportions are indicated for different X_r^{thres} values: different predator survival (existence of $\boldsymbol{x^{(2)}}$), predator survives and there is an only stable state with predator-prey fluctuations (stability of $\boldsymbol{x^{(2)}}$ when it exists). Note that the two proportion do not overlap with each other. Note that with the hyperbolic tangent, multistability occurs in a tiny region of the parameter space which is too small to be quantified precisely.

functional responses	X_r^{thres}	predator survival	predator oscillations
Holling - Ivlev	5	0.059	0.073
	10	0.057	0.049
	20	0.043	0.030
Holling - Tanh	5	0.074	0.107
	10	0.065	0.066
	20	0.047	0.038
Ivlev - Tanh	5	0.013	0.057
	10	0.007	0.030
	20	0.004	0.015

Table 7.8. Parameter values used in Cordoleani *et al.* (2011) based on data from an experiment by Canale *et al.* (1973). Only numerical values are shown. For the biological meaning of parameters, refer to table 7.2. Superscripts indicate the functional response used (H: Holling, I: Ivlev, t: hyperbolic tangent).

parameter	$\dot{j}_{XAm}^{1}$	K_1	$\dot{\mu}_1$	$\dot{j}_{XAm}^{2,H}$	K_2^H	$\dot{\mu}_2^H$
value	1.6	16	0.48	0.0789	5.26	0.0947
parameter	$\dot{j}_{XAm}^{2,I}$	K_2^I	$\dot{\mu}_2^I$	$\dot{j}_{XAm}^{2,t}$	K_2^t	$\dot{\mu}_2^t$
value	0.0733	6.67	0.088	0.0745	9.09	0.0895

Table 7.9. Proportion of qualitatively different dynamics between functional responses in the Monod model parameterized using data from Canale *et al.* (1973). The reference area corresponds to the parameter space where the prey can survive for resource concentration in the feed lower than an arbitrary value X_r^{thres}. For each pair of functional responses, the following proportions are indicated for different X_r^{thres} values: different predator survival (existence of $\boldsymbol{x^{(2)}}$), predator survives and there is an only stable state with predator-prey fluctuations (stability of $\boldsymbol{x^{(2)}}$ when it exists), existence of multiple stable states (stability of $\boldsymbol{x^{(2)}}$ when it exists and existence of a stable limit cycle). This classification is made to ease comparisons between models. Note that the first proportion does not overlap with the two others. Conversely, the latter two can overlap with each other.

functional responses	X_r^{thres}	predator survival	only oscillations	multi-stability
Holling - Ivlev	250	0.010	0.025	0
	500	0.007	0.011	0
Holling - Tanh	250	0.015	0.069	0.005
	500	0.008	0.048	0.004
Ivlev - Tanh	250	0.005	0.045	0.005
	500	0.004	0.027	0.004

With parameter values from Canale *et al.*'s experiment (1973), Monod model exhibits qualitatively the same dynamics, bifurcation diagrams and differences between functional responses as before (figure 7.11, table 7.9). However, the proportion of the parameter space where there is multistability with the hyperbolic tangent is not neglectible and can be quantified (0.4 % to 0.5 %). Proportions are hard to compare between the two chemostat experiments that were used to estimate parameter values. Indeed, the space of parameter investigated is arbitrarily (choice of X_r^{thres}) and the proportions we derived depend on the size of the parameter space where only the prey can survive (region 1). Nevertheless, as there is a qualitative difference between functional responses that is not quantitatively neglectible, one can say that structural sensitivity to the predator functional response is higher in Monod model than in the three other ones.

7.4 Discussion

7.4.1 Structural sensitivity and details in metabolism description

Monod model is significantely more sensitive to a change in predator functional response than the three other models. In these models, only bifurcations location varies with this change in model formulation, whereas it affects the type of bifurcations that occur in Monod model. In Monod model, a bifurcation of limit cycles that exists only with the hyperbolic tangent leads to multiple stable states (equilibrium and limit cycle). Similar results with the same functional responses has been observed for Rosenzweig & MacArthur's model (1963, Fussmann & Blasius, 2005). In the

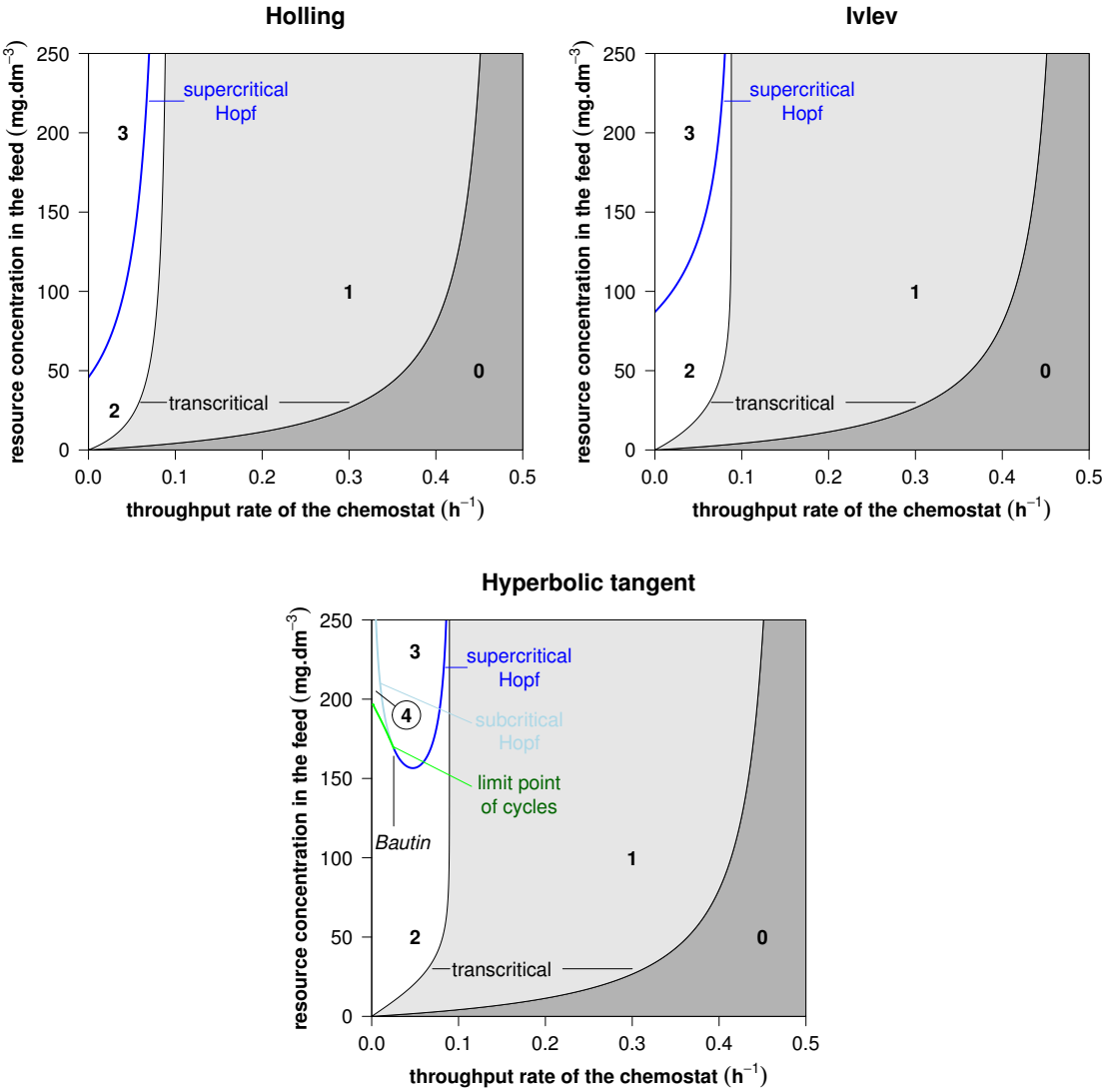

Figure 7.11. Bifurcation diagrams of the Monod model parameterized using data from Canale *et al.* (1973), with respect to environmental parameters, using different predator functional responses. The number in each region of the parameter space means that system dynamics is qualitatively equivalent to the corresponding panel in figure 7.8. In region 0, only the trivial equilibrium ($\boldsymbol{x^{(0)}}$) without prey and predator exists and is stable. It becomes unstable at the transcritical bifurcation between regions 0 and 1 ($\dot{h} = \dot{h}^{(0,1)}$), where the prey can invade at a stable prey-resource equilibrium ($\boldsymbol{x^{(1)}}$). This equilibrium becomes unstable at the transcritical bifurcation between regions 1 and 2 ($\dot{h} = \dot{h}^{(1,2)}$), where the predator starts can invade at a stable coexistence equilibrium ($\boldsymbol{x^{(2)}}$). This equilibrium becomes unstable at the supercritical Hopf bifurcation between regions 2 and 3 ($\dot{h} = \dot{h}^{(H)}$). In region 3, long-term coexistence occurs on a stable limit cycle. With the hyperbolic tangent, the Hopf bifurcation can be either supercritical or subcritical, the two branches meet at a Bautin point. From this point, a limit point of cycles bifurcation curve starts and stays between $\dot{h} = 0$ and the subcritical Hopf bifurcation. Between these two curves (region 4), there are a stable limit cycle and a stable coexistence equilibrium (panel 4 in figure 7.5, without reserve dynamics).

four models we tested, quantitative changes in bifurcation location are small in the sense that they mostly occur in a bounded part of the parameter space. In the parameter space investigated, the main difference concerns the prediction of equilibrium vs. fluctuating coexistence, i.e. changes in the Hopf bifurcation location. The amplitude of these changes may depend on the numerical values used for the biological parameters, as illustrated by the two parameter sets considered for the Monod model. However, these two parameter sets lead to qualitatively the same bifurcations. By extension, one can think that the qualitative shape of bifurcation diagrams for the three other models may remain the same if other parameter sets are used, despite this statement remains to be proved.

There is no buffer between feeding and population growth rate in Monod model, as it includes neither explicit reserve dynamics or maintenance costs. If at least one of these process is included, the resulting model is sensitive to functional response formulation in term of bifurcations location, but not in term of type of bifurcations that occur. By comparison with previous works, changes in the type of bifurcations seem to occur in predator-prey models without explicit reserve dynamics, and without either maintenance costs (or mortality rate) or explicit resource dynamics (table 7.10). Explicit resource dynamics are used in mass-balance models (here chemostat), whereas other models use a logistic growth equation for the prey. The logistic growth equation is phenomenological, so its use may be less justified in comparison to a mechanistic mass-balance equation of resource uptake. These two approaches can lead to very different dynamics in food chain models (Kooi *et al.*, 1997, 1998b). In addition to these limits of the logistic growth equation, we found that its use makes models more sensitive to changes in the mathematical representation of trophic interactions. We do not discuss which model features make a model more or less sensitive to predator functional response in term of bifurcations location, as these changes may be highly dependent to parameter values.

Only parameter values of predator functional response are re-estimated by fitting functional responses to Holling's disc equation. The latter is not parameterized from functional response data, but by optimizing all parameter values so that model dynamics fit empirical data (Kooi & Kooijman, 1994b). Using this method to re-estimate a complete parameter set for each functional response would take into account the covariation of some parameters (Lika *et al.*, 2011a,b). However, changes in other parameter values than those of the functional response would be small and might not affect our results on the type of bifurcations that occur. Furthermore, these results are robust to a re-estimation of the maximum growth rate of the predator in order to keep its conversion efficiency constant between functional response formulations (Appendix, section 7.8).

A limited number of functional response formulations are tested in this work. As in previous chapters, it is possible but not suitable to consider a family of unspecified functions using gen-

Table 7.10. Impact of functional response formulation on the presence/absence of bifurcations in predator-prey models including different processes. Resource representation is either: implicit through a logistic growth of the prey, or explicit using Holling's functional response for its uptake within a mass-balance chemostat. For all models, predator functional response is either: Holling's disc equation, Ivlev's functional response or the hyperbolic tangent (except for Bazykin's model, chapter 3). Note that for Monod and Rosenzweig-MacArthur models, the hyperbolic tangent leads to different bifurcations than the two other functional responses, whereas Ivlev's functional response and Holling's disc equation lead to different bifurcations in Bazykin's model.

model and reference	maintenance or mortality	reserve dynamics	explicit resource	pres./abs. of bifurcations
Bazykin (chapter 3)	linear mortality and competition	-	-	affected
Monod (chapter 7)	-	-	x	affected
Marr-Pirt (chapter 7)	maintenance	-	x	-
Droop (chapter 7)	-	x	x	-
original DEB (chapter 7)	maintenance	x	x	-
Rosenzweig-MacArthur (Fussmann & Blasius, 2005)	linear mortality	-	-	affected

eralized modelling (Gross & Feudel, 2006) or the method developped by Adamson & Morozov (2012, 2014). Indeed, these methods are local and cannot be used to study many properties of the models considered here. Such properties are the presence of bifurcations of limit cycles and some characteristics of local bifurcations that require a non-linear approximation of the model near bifurcation (type of Hopf bifurcation through the first Lyapunov coefficient). However, note that to estimate the DEB parameters of an organism from empirical data, some work has already been done with a partially specified DEB model where the function that links assimilation rate to body length is unspecified (Nisbet *et al.*, 2004).

7.4.2 Model dynamics and details in metabolism description

The most surprising result about the original DEB model is that multiple stable states can coexist with all tested functional responses. This feature is due to a global bifurcation that could not be found by the local analysis previously performed by Kooi & Kooijman (1994a). Kooi & Kooijman (1994b) argued that the original DEB model gives a better fit to data than the three simpler models because it includes both maintenance and reserve. Maintenance costs help to describe sharp population decreases, whereas reserve explains why population can grow at low food levels by including a delay between feeding and growth. These two effects can (i) dampen small perturbations near the coexistence equilibrium (i.e. it is stable), and (ii) amplify large perturbations leading to stable predator-prey oscillations.

Apart from the previous synergetic effect, reserve has a smaller impact on model predictions than maintenance. Maintenance costs imply that a species cannot survive if resource input (here the throughput rate of the chemostat) is not high enough to overcome these costs. This result was already known for models without reserve (Nisbet *et al.*, 1983, Kooi & Boer, 2001), and we extend it here to models with explicit reserve. Note that the four models predict very different thresholds of environmental parameters for species invasion (transcritical bifurcations). Indeed, biological parameter values are optimized from one data set corresponding to a single environmental condition. Thus, extrapolations from this reference condition are likely to vary between models. From a biological point of view, maintenance (or linear mortality in community models) is a basic process that should be taken into account even in simple models. Conversely, bifurcation locations are not strongly affected by the use of reserve. In addition, using explicit reserve without maintenance costs (Droop model) lead to the worst fit to empirical data (Kooi & Kooijman, 1994b). So, despite the use of reserve is relevant for many reasons (Kooijman, 2010, section 1.1.3), it is of lower importance than maintenance, at least for unicellular organisms with one limiting resource. Indeed, modelling n limiting resource requires n reserve compartments in DEB theory.

When multiple resources limit the growth of the prey, the way their colimited uptake is modelled deeply affect the predicted dynamics of a predator-prey system (Poggiale *et al.*, 2010). These dynamics also change if maintenance is explicitely taken into account or not, i.e. if we use a DEB or a Droop model. Moreover, it is not clear that Droop model is a special case of DEB model with multiple reserves. Modelling the uptake of multiple resources can be done in a mechanistic way through the concept of Synthetizing Units (SUs, Kooijman, 2010, chapter 3). SUs allow to represent different schemes of enzymatic reactions (like parallel or sequential uptake). The choice of a scheme depends on the reaction to model, and on modeller's choices about model complexity. This mechanistic background is useful to model the growth of phytoplankton for instance, as SUs describe processes at the intracellular level. Conversely, intracellular processes are only a part of predation, which also involves individual (like in Holling's disc equation) and collective behaviour, and sometimes digestion (like in Ivlev's functional response, note that gut contents are considered as being outside the organism in DEB theory). Thus, the SUs framework is not enough to fully describe predation. Here, we have found the predation formulation for the prey (i.e. resource uptake) has little effects on model dynamics with one limiting resource (data not shown). With multiple resources, the model would be sensitive to the formulation of both predation and colimited uptake, despite their relative importance remains to be assessed.

In addition to the number of limiting resources, the number of species in interaction also influences system dynamics (see chapter 5). Here, we have considered two species in interaction, but previous works showed that simple three-species food webs (tri-trophic food chain, omnivory)

can have far more complicated dynamics (including homoclinic and heteroclinic bifurcations) with Monod and Marr-Pirt models (Kooi & Boer, 2001). Thus, the original DEB model (7.5) applied to such food webs could lead to even more complicated bifurcation diagrams. Moreover, any changes of bifurcation diagrams with functional response formulation could be more complex to analyze for these models applied to simple food webs.

7.5 Conclusion

Our aim was to disentangle the respective effects of metabolism representation and feeding formulation on the predictions of a predator-prey model in chemostat. Four nested models including different level of metabolic details were analyzed for three type-II functional responses through a bifurcation analysis. Bifurcations location is quantitatively less affected by functional response formulation than in Bazykin's predator-prey model (chapter 3). In addition, new bifurcations appear when the functional response is changed only in very simple models. Models with a mass-balance equation for the resource (instead of a logistic growth of the prey) and maintenance costs exhibit qualitatively the same bifurcations for the three functional responses. For the three functional responses, adding explicit reserve dynamics to the previous model features allows the coexistence of two stable states (an equilibrium and a limit cycle). Multiple stable states has not been reported yet (from our knowledge) in DEB models for interacting populations. Including reserve (a key aspect of DEB theory) or not may depend of the trade-off between model simplicity and accuracy of the biological description.

This work highlights some features that are important to consider to make a model more robust to uncertainties in the mathematical description of other processes (here feeding). It turns out that these features (mass-balance resource uptake, maintenance) have already been spotted to be important in term of biological description. Thus, two main issues of model construction (mathematical robustness and biological relevance) can be tackled simultaneously by including these simple model features. However, the uncertainty on functional response formulation still has quantitative effects on bifurcations location and stable states value in all tested models. Identifying which model features can dampen these quantitative effects will require the use of methods to quantify structural sensitivity (chapter 6) with numerous parameter sets, i.e. a comparison between many organisms.

Appendices: Structural sensitivity in predator-prey models based on Dynamic Energy Budget theory: importance of metabolism

7.6 Bifurcations in models with reserves

All notations about model formulation and equilibria in this appendix refer to equations in section 7.2. We consider $\dot{h}$ as the bifurcation parameter, i.e. the vector function $\boldsymbol{F}(\boldsymbol{x})$ in model (7.5) is now a function of $\dot{h}$ and is written $\boldsymbol{F}(\boldsymbol{x}, \dot{h})$. For the criteria (detection, genericity) used to analyse transcritical bifurcations, the reader is refered to section 2.3.4.

7.6.1 Stability of the trivial equilibrium

System (7.5) has the following Jacobian matrix:

$$\boldsymbol{F}_{\boldsymbol{x}}(\boldsymbol{x}, \dot{h}) = \begin{pmatrix} -\dot{k}_E^1 & 0 & \dot{k}_E^1 f_1'(X_0) & 0 & 0 \\ 0 & -\dot{k}_E^2 & 0 & \dot{k}_E^2 f_2'(X_1) & 0 \\ 0 & 0 & J_{33} & -f_1(X_0) j_{XAm}^1 & 0 \\ \dfrac{\dot{k}_E^1 + \dot{k}_M^1}{(e_1+g_1)^2} g_1 X_1 & 0 & 0 & J_{44} & -f_2(X_1) j_{XAm}^2 \\ 0 & \dfrac{\dot{k}_E^2 + \dot{k}_M^2}{(e_2+g_2)^2} g_2 X_2 & 0 & 0 & J_{55} \end{pmatrix}, \tag{7.13}$$

with:

$$J_{33} = -\dot{h} - j_{XAm}^1 X_1 f_1'(X_0),$$

$$J_{44} = \frac{\dot{k}_E^1 e_1 - \dot{k}_M^1 g_1}{e_1 + g_1} - \dot{h} - j_{XAm}^2 X_2 f_2'(X_1),$$

$$J_{55} = \frac{\dot{k}_E^2 e_2 - \dot{k}_M^2 g_2}{e_2 + g_2} - \dot{h}.$$

This matrix evaluated at the trivial equilibrium $\boldsymbol{x^{(0)}}$ is upper triangular:

$$\boldsymbol{F_x}(\boldsymbol{x^{(0)}}, \dot{h}) = \begin{pmatrix} -\dot{k}_E^1 & 0 & \dot{k}_E^1 f_1'(X_r) & 0 & 0 \\ 0 & -\dot{k}_E^2 & 0 & \dot{k}_E^2 f_2'(0) & 0 \\ 0 & 0 & -\dot{h} & -f_1(X_r) j_{XAm}^1 & 0 \\ 0 & 0 & 0 & \dfrac{\dot{k}_E^1 f_1(X_r) - \dot{k}_M^1 g_1}{f_1(X_r) + g_1} - \dot{h} & 0 \\ 0 & 0 & 0 & 0 & -(\dot{h} + \dot{k}_M^2) \end{pmatrix},$$

so its diagonal elements are its eigenvalues. All eigenvalues are real and negative except:

$$\lambda_4^{(0)} = \frac{\dot{k}_E^1 f_1(X_r) - \dot{k}_M^1 g_1}{f_1(X_r) + g_1} - \dot{h} = \dot{h}^{(0,1)} - \dot{h},$$

which is negative if $\dot{h} > \dot{h}^{(0,1)}$. This condition is always violated when equilibrium $\boldsymbol{x^{(1)}}$ exists and is satisfied otherwise. Note that if $\dot{h} = \dot{h}^{(0,1)}$, i.e if $\boldsymbol{x^{(0)}} = \boldsymbol{x^{(0,1)}}$, then $\lambda_4^{(0)} = 0$ which indicates generally that system (7.5) exhibits a fold bifurcation. More precisely, calculations in the next subsection prove that it is a transcritical bifurcation, which is a degenerated fold bifurcation.

7.6.2 First transcritical bifurcation (prey invasion)

At the bifurcation $\dot{h} = \dot{h}^{(0,1)}$, Jacobian matrix (7.13) evaluated at equilibrium $\boldsymbol{x^{(0,1)}}$ is:

$$\boldsymbol{F_x}(\boldsymbol{x^{(0,1)}}, \dot{h}^{(0,1)}) = \begin{pmatrix} -\dot{k}_E^1 & 0 & \dot{k}_E^1 f_1'(X_r) & 0 & 0 \\ 0 & -\dot{k}_E^2 & 0 & \dot{k}_E^2 f_2'(0) & 0 \\ 0 & 0 & -\dot{h}^{(0,1)} & -f_1(X_r) j_{XAm}^1 & 0 \\ 0 & 0 & 0 & 0 & 0 \\ 0 & 0 & 0 & 0 & -(\dot{h}^{(0,1)} + \dot{k}_M^2) \end{pmatrix}. \quad (7.14)$$

This matrix has one zero eigenvalue associated to the left eigenvector $\boldsymbol{p^{(0,1)}} = (0,0,0,1,0)^T$ which satisfies ${\boldsymbol{p^{(0,1)}}}^T \boldsymbol{F_x}(\boldsymbol{x^{(0,1)}}, \dot{h}^{(0,1)}) = \boldsymbol{0}^T$. The condition for a transcritical bifurcation is:

$$\langle \boldsymbol{p^{(0,1)}}, \boldsymbol{F}_{\dot{h}}(\boldsymbol{x^{(0,1)}}, \dot{h}^{(0,1)}) \rangle = 0, \tag{7.15}$$

where

$$\boldsymbol{F}_{\dot{h}}(\boldsymbol{x}, \dot{h}) = (0, 0, X_r - X_0, -X_1, -X_2)^T, \tag{7.16}$$

from model (7.5). As $X_1^{(0,1)} = 0$, one can check that condition (7.15) for a transcritical bifurcation is fulfilled. Now, we have to check the two genericity conditions of this bifurcation.

First, the transversality condition for the transcritical bifurcation is:

$${\boldsymbol{p^{(0,1)}}}^T \boldsymbol{F}_{\dot{h}\boldsymbol{x}}(\boldsymbol{x^{(0,1)}}, \dot{h}^{(0,1)}) \boldsymbol{q^{(0,1)}} \neq 0, \tag{7.17}$$

where

$$\boldsymbol{q^{(0,1)}} = \left(f_1'(X_r), \frac{-\dot{h}}{f_1(X_r) j^1_{XAm}} f_2'(0), 1, \frac{-\dot{h}}{f_1(X_r) j^1_{XAm}}, 0 \right)^T$$

is the right eigenvector associated to the zero eigenvalue of the Jacobian matrix (7.14) which satisfies $\boldsymbol{F_x}(\boldsymbol{x^{(0,1)}}, \dot{h}^{(0,1)}) \boldsymbol{q^{(0,1)}} = \boldsymbol{0}$. The matrix of second-order partial derivatives of $\boldsymbol{F}$ with respect to $\boldsymbol{x}$ and $\dot{h}$ is:

$$\boldsymbol{F}_{\dot{h}\boldsymbol{x}}(\boldsymbol{x}, \dot{h}) = \begin{pmatrix} 0 & 0 & 0 & 0 & 0 \\ 0 & 0 & 0 & 0 & 0 \\ 0 & 0 & -1 & 0 & 0 \\ 0 & 0 & 0 & -1 & 0 \\ 0 & 0 & 0 & 0 & -1 \end{pmatrix}. \tag{7.18}$$

One can then check that the transversality condition (7.17) is fulfilled:

$${\boldsymbol{p^{(0,1)}}}^T \boldsymbol{F}_{\dot{h}\boldsymbol{x}}(\boldsymbol{x}, \dot{h}) \boldsymbol{q^{(0,1)}} = \frac{\dot{h}}{f_1(X_r) j^1_{XAm}} \neq 0.$$

Second, the non-degeneracy condition for a transcritical bifurcation is:

$$\langle \boldsymbol{p^{(0,1)}}, \boldsymbol{F_{xx}}(\boldsymbol{x^{(0,1)}}, \dot{h}^{(0,1)})(\boldsymbol{q^{(0,1)}}, \boldsymbol{q^{(0,1)}}) \rangle \neq 0.$$

The tensor $\boldsymbol{F_{xx}}(\boldsymbol{x^{(0,1)}}, \dot{h}^{(0,1)})$ is made of all second-order partial derivatives of $\boldsymbol{F}$ with respect to

$\boldsymbol{x}$. Its application to any vectors $\boldsymbol{u}, \boldsymbol{v} \in \mathbb{R}^5$ gives the vector of bilinear forms:

$$\boldsymbol{F_{xx}}(\boldsymbol{x^{(0,1)}}, \dot{h}^{(0,1)})(\boldsymbol{u}, \boldsymbol{v}) = \begin{pmatrix} \vdots \\ \sum_{j=1}^{5} \sum_{k=1}^{5} \dfrac{\partial^2 F_i(\boldsymbol{x^{(0,1)}}, \dot{h}^{(0,1)})}{\partial x_j \partial x_k} u_j v_k \\ \vdots \end{pmatrix}, \tag{7.19}$$

where x_j (resp. x_k) indicates the j-est (resp k-est) element of vector $\boldsymbol{x}$ to ease notation. One can check that the non-degeneracy condition is fulfilled:

$$\langle \boldsymbol{p^{(0,1)}}, \boldsymbol{F_{xx}}(\boldsymbol{x^{(0,1)}}, \dot{h}^{(0,1)})(\boldsymbol{q^{(0,1)}}, \boldsymbol{q^{(0,1)}}) \rangle = \frac{-2(\dot{k}_E^1 + \dot{k}_M^1)\dot{h} g_1}{(f_1(X_r) + g_1)^2 f_1(X_r) j_{XAm}^1} f_1'(X_r) \neq 0.$$

Thus the transcritical bifurcation where $\boldsymbol{x^{(0)}}$ and $\boldsymbol{x^{(1)}}$ collide at $\dot{h} = \dot{h}^{(0,1)}$ is generic.

7.6.3 Second transcritical bifurcation (predator invasion)

Let's do the same work with $\boldsymbol{x^{(1)}}$ and $\boldsymbol{x^{(2)}}$. The Jacobian matrix (7.13) evaluated at equilibrium $\boldsymbol{x^{(1,2)}}$ when $\dot{h} = \dot{h}^{(1,2)}$ is:

$$\boldsymbol{F_x}(\boldsymbol{x^{(1,2)}}, \dot{h}^{(1,2)}) = \begin{pmatrix} -\dot{k}_E^1 & 0 & \dot{k}_E^1 f_1'(X_0^{(1,2)}) & 0 & 0 \\ 0 & -\dot{k}_E^2 & 0 & \dot{k}_E^2 f_2'(X_1^{(1,2)}) & 0 \\ 0 & 0 & J_{33}^{(1,2)} & -f_1(X_0^{(1,2)}) j_{XAm}^1 & 0 \\ J_{41}^{(1,2)} & 0 & 0 & 0 & -f_2(X_1^{(1,2)}) j_{XAm}^2 \\ 0 & 0 & 0 & 0 & 0 \end{pmatrix}, \tag{7.20}$$

with:

$$J_{33}^{(1,2)} = -\dot{h} - j_{XAm}^1 X_1^{(1,2)} f_1'(X_0^{(1,2)}),$$

$$J_{41}^{(1,2)} = \frac{\dot{k}_E^1 + \dot{k}_M^1}{(e_1^{(1,2)} + g_1)^2} g_1 X_1^{(1,2)}$$

One can see that:

$$\det\left(\boldsymbol{F_x}(\boldsymbol{x^{(1,2)}}, \dot{h}^{(1,2)}) - \lambda I_5\right) = -\lambda P_4(\lambda),$$

where $P_4(\lambda)$ is a fourth-order polynom with respect to λ. Thus, Jacobian matrix $\boldsymbol{F_x}(\boldsymbol{x^{(1,2)}}, \dot{h}^{(1,2)})$ has at least one real zero eigenvalue, which indicates generally a fold bifurcation. This zero eigenvalue is associated to the left eigenvector $\boldsymbol{p^{(1,2)}} = (0, 0, 0, 0, 1)^T$. As $X_2^{(1,2)} = 0$, one can check

using (7.16) that the condition for a transcritical bifurcation:

$$\langle \boldsymbol{p^{(1,2)}}, \boldsymbol{F}_{\dot{h}}(\boldsymbol{x^{(1,2)}}, \dot{h}^{(1,2)}) \rangle = 0,$$

is fulfilled. Now, we have to check the genericity conditions of this bifurcation.

The right eigenvector of the Jacobian matrix (7.20) associated to the zero eigenvalue is:

$$\boldsymbol{q^{(1,2)}} = \begin{pmatrix} f_1'(X_0^{(1,2)}) \\ \left[-\dot{h} - j^1_{Xam} X_1^{(1,2)} f_1'(X_0^{(1,2)})\right] \dfrac{f_2'(X_1^{(1,2)})}{f_1(X_0^{(1,2)}) j^1_{XAm}} \\ 1 \\ \left[-\dot{h} - j^1_{Xam} X_1^{(1,2)} f_1'(X_0^{(1,2)})\right] \dfrac{1}{f_1(X_0^{(1,2)}) j^1_{XAm}} \\ \dfrac{(\dot{k}^1_E + \dot{k}^1_M) g_1 X_1^{(1,2)}}{(e_1^{(1,2)} + g_1)^2 j^2_{Xam} f_2(X_1^{(1,2)})} f_1'(X_0^{(1,2)}) \end{pmatrix}.$$

Thus, one can check using (7.18) that the transversality condition is fulfilled:

$$\boldsymbol{p^{(1,2)}}^T \boldsymbol{F}_{\dot{h}\boldsymbol{x}}(\boldsymbol{x^{(1,2)}}, \dot{h}^{(1,2)}) \boldsymbol{q^{(1,2)}} = \frac{-(\dot{k}^1_E + \dot{k}^1_M) g_1 X_1^{(1,2)}}{(e_1^{(1,2)} + g_1)^2 j^2_{Xam} f_2(X_1^{(1,2)})} f_1'(X_0^{(1,2)}) \neq 0.$$

Using (7.19), one can check that the non-degeneracy condition is also fulfilled:

$$\langle \boldsymbol{p^{(1,2)}}, \boldsymbol{F_{xx}}(\boldsymbol{x^{(1,2)}}, \dot{h}^{(1,2)})(\boldsymbol{q^{(1,2)}}, \boldsymbol{q^{(1,2)}}) \rangle = \frac{2(\dot{k}^2_E + \dot{k}^2_M) g_2}{(e_2^* + g_2)^2} q_2^{(1,2)} q_5^{(1,2)} \neq 0,$$

where $q_2^{(1,2)}$ and $q_5^{(1,2)}$ are the second and fifth elements of vector $\boldsymbol{q^{(1,2)}}$. Thus, the transcritical bifurcation where $\boldsymbol{x^{(1)}}$ and $\boldsymbol{x^{(2)}}$ collide at $\dot{h} = \dot{h}^{(1,2)}$ is generic.

7.6.4 Hopf bifurcation

Depending on parameter values, equilibrium $\boldsymbol{x^{(2)}}$ can have a pair of complex conjugate eigenvalues with zero real part, i.e. it crosses an Hopf bifurcation. This bifurcation can be located by solving the condition $\det(2J^{(2)} \odot I_5) = 0$, where $2J^{(2)} \odot I_5$ is a 10×10 matrix obtained using the bialternate product $\odot$ (see Kuznetsov, 2004, p527-528). This condition can be expressed analytically as $\dot{h} = \dot{h}^{(H)}$ where $\dot{h}^{(H)}$ depends on $\dot{h}$. However, the expression of $\dot{h}^{(H)}$ does not allow for a simple interpretation of the bifurcation condition. So, there is no interest of presenting this condition here.

Solving this condition for a given functional response formulation leads to the same results than numerical continuation methods. Using numerical methods, the type of Hopf bifurcation (subcritical vs. supercritical) is determined by computing the first Lyapunov coefficient. No analytical expression of this coefficient was derived as even the bifurcation condition cannot be interpreted in a simple way. A codimension-two Bautin bifurcation occurs when the first Lyapunov coefficient vanishes, so we have no analytical expression for this bifurcation.

7.7 Bifurcations in models without reserves

All notations about model formulation and equilibria in this appendix refer to equations in section 7.3. We consider $\dot{h}$ as the bifurcation parameter, i.e. the vector function $\boldsymbol{F}(\boldsymbol{x})$ in model (7.12) is now a function of $\dot{h}$ and is written $\boldsymbol{F}(\boldsymbol{x}, \dot{h})$. For the criteria (detection, genericity) used to analyse transcritical bifurcations, the reader is refered to section 2.3.4.

7.7.1 Stability of the trivial equilibrium

System (7.12) has the following Jacobian matrix:

$$\boldsymbol{F}_{\boldsymbol{x}}(\boldsymbol{x}, \dot{h}) = \begin{pmatrix} -\dot{h} - j^1_{XAm} X_1 f_1'(X_0) & -f_1 j^1_{XAm} & 0 \\ \dot{\mu}_1 X_1 f_1'(X_0) & \dot{\mu}_1 f_1 - \dot{k}^1_M - \dot{h} - j^2_{XAm} X_2 f_2'(X_1) & -f_2 j^2_{XAm} \\ 0 & \dot{\mu}_2 X_2 f_2'(X_1) & \dot{\mu}_2 f_2 - \dot{k}^2_M - \dot{h} \end{pmatrix}. \tag{7.21}$$

This matrix evaluated at the trivial equilibrium $\boldsymbol{x^{(0)}}$ is upper triangular:

$$\boldsymbol{F}_{\boldsymbol{x}}(\boldsymbol{x^{(0)}}, \dot{h}) = \begin{pmatrix} -\dot{h} & -f_1(X_r) j^1_{XAm} & 0 \\ 0 & \dot{\mu}_1 f_1(X_r) - \dot{k}^1_M - \dot{h} & 0 \\ 0 & 0 & -(\dot{k}^2_M + \dot{h}) \end{pmatrix},$$

so its diagonal elements are its eigenvalues. All eigenvalues are real and negative except:

$$\lambda_2^{(0)} = \dot{\mu}_1 f_1(X_r) - \dot{k}^1_M - \dot{h} = \dot{h}^{(0,1)} - \dot{h},$$

which is negative if $\dot{h} > \dot{h}^{(0,1)}$. This condition is always violated when equilibrium $\boldsymbol{x^{(1)}}$ exists and is satisfied otherwise. If $\dot{h} = \dot{h}^{(1,2)}$, i.e. if $\boldsymbol{x^{(0)}} = \boldsymbol{x^{(0,1)}}$, then $\lambda_2^{(0)} = 0$ which indicates generally that system (7.12) exhibits a fold bifurcation. As for the original DEB model, calculations in the next subsection prove that it is a transcritical bifurcation.

7.7.2 First transcritical bifurcation (prey invasion)

At the bifurcation $\dot{h} = \dot{h}^{(0,1)}$, Jacobian matrix (7.21) evaluated at equilibrium $\boldsymbol{x}^{(\mathbf{0,1})}$ is:

$$\boldsymbol{F}_{\boldsymbol{x}}(\boldsymbol{x}^{(\mathbf{0,1})}, \dot{h}^{(0,1)}) = \begin{pmatrix} -\dot{h} & -f_1(X_r) j^1_{XAm} & 0 \\ 0 & 0 & 0 \\ 0 & 0 & -(\dot{k}_M^2 + \dot{h}) \end{pmatrix}. \tag{7.22}$$

This matrix has one zero eigenvalue associated to the left eigenvector $\boldsymbol{p}^{(\mathbf{0,1})} = (0,1,0)^T$ which satisfies $\boldsymbol{p}^{(\mathbf{0,1})^T} \boldsymbol{F}_{\boldsymbol{x}}(\boldsymbol{x}^{(\mathbf{0,1})}, \dot{h}^{(0,1)}) = \mathbf{0}^T$. The condition for a transcritical bifurcation is that:

$$\langle \boldsymbol{p}^{(\mathbf{0,1})}, \boldsymbol{F}_{\dot{h}}(\boldsymbol{x}^{(\mathbf{0,1})}, \dot{h}^{(0,1)}) \rangle = 0,$$

where

$$\boldsymbol{F}_{\dot{h}}(\boldsymbol{x}, \dot{h}) = (X_r - X_0, -X_1, -X_2)^T,$$

from model (7.12). As $X_1^{(0,1)} = 0$, one can check that condition (7.7.2) for a transcritical bifurcation is fulfilled. Now, we have to check the two genericity conditions of this bifurcation.

First, the transversality condition for the transcritical bifurcation is:

$$\boldsymbol{p}^{(\mathbf{0,1})^T} \boldsymbol{F}_{\dot{h}\boldsymbol{x}}(\boldsymbol{x}^{(\mathbf{0,1})}, \dot{h}^{(0,1)}) \boldsymbol{q}^{(\mathbf{0,1})} \neq 0,$$

where

$$\boldsymbol{q}^{(\mathbf{0,1})} = \begin{pmatrix} \dfrac{-f_1(X_r) j^1_{XAm}}{\dot{h}} \\ 1 \\ 0 \end{pmatrix}.$$

is the right eigenvector associated to the zero eigenvalue of the Jacobian matrix (7.22) which satisfies $\boldsymbol{F}_{\boldsymbol{x}}(\boldsymbol{x}^{(\mathbf{0,1})}, \dot{h}^{(0,1)}) \boldsymbol{q}^{(\mathbf{0,1})} = \mathbf{0}$. The matrix of second-order partial derivatives of $\boldsymbol{F}$ with respect to $\boldsymbol{x}$ and $\dot{h}$ is:

$$\boldsymbol{F}_{\dot{h}\boldsymbol{x}}(\boldsymbol{x}, \dot{h}) = \begin{pmatrix} -1 & 0 & 0 \\ 0 & -1 & 0 \\ 0 & 0 & -1 \end{pmatrix}. \tag{7.23}$$

One can then check that the transversality condition is fulfilled:

$$\boldsymbol{p}^{(\mathbf{0,1})^T} \boldsymbol{F}_{\dot{h}\boldsymbol{x}}(\boldsymbol{x}^{(\mathbf{0,1})}, \dot{h}^{(0,1)}) \boldsymbol{q}^{(\mathbf{0,1})} = -1 \neq 0.$$

Second, the non-degeneracy condition for a transcritical bifurcation is:

$$\langle \boldsymbol{p^{(0,1)}}, \boldsymbol{F_{xx}}(\boldsymbol{x^{(0,1)}}, \dot{h}^{(0,1)})(\boldsymbol{q^{(0,1)}}, \boldsymbol{q^{(0,1)}})\rangle \neq 0.$$

The tensor $\boldsymbol{F_{xx}}(\boldsymbol{x^{(0,1)}}, \dot{h}^{(0,1)})$ is made of all second-order partial derivatives of $\boldsymbol{F}$ with respect to $\boldsymbol{x}$. Its application to any vectors $\boldsymbol{u}, \boldsymbol{v} \in \mathbb{R}^3$ gives the vector of bilinear forms:

$$\boldsymbol{F_{xx}}(\boldsymbol{x^{(0,1)}}, \dot{h}^{(0,1)})(\boldsymbol{u}, \boldsymbol{v}) = \begin{pmatrix} \vdots \\ \sum_{j=1}^{3}\sum_{k=1}^{3} \dfrac{\partial^2 F_i(\boldsymbol{x^{(0,1)}}, \dot{h}^{(0,1)})}{\partial X_{j-1}\partial X_{k-1}} u_j v_k \\ \vdots \end{pmatrix}, \tag{7.24}$$

One can check that the non-degeneracy condition is fulfilled:

$$\langle \boldsymbol{p^{(0,1)}}, \boldsymbol{F_{xx}}(\boldsymbol{x^{(0,1)}}, \dot{h}^{(0,1)})(\boldsymbol{q^{(0,1)}}, \boldsymbol{q^{(0,1)}})\rangle = \frac{-2\dot{\mu}_1 f_1(X_r) j^1_{XAm}}{\dot{h}} f_1'(X_r) \neq 0,$$

Thus the transcritical bifurcation where $\boldsymbol{x^{(0)}}$ and $\boldsymbol{x^{(1)}}$ collide at $\dot{h} = \dot{h}^{(0,1)}$ is generic.

7.7.3 Second transcritical bifurcation (predator invasion)

Let's do the same work with $\boldsymbol{x^{(1)}}$ and $\boldsymbol{x^{(2)}}$. The Jacobian matrix (7.21) evaluated at equilibrium $\boldsymbol{x^{(1,2)}}$ when $\dot{h} = \dot{h}^{(1,2)}$ is:

$$\boldsymbol{F_x}(\boldsymbol{x^{(1,2)}}, \dot{h}^{(1,2)}) = \begin{pmatrix} -\dot{h} - j^1_{XAm} X_1^{1,2} f_1'(X_0^{(1,2)}) & -f_1(X_0^{(1,2)}) j^1_{XAm} & 0 \\ \dot{\mu}_1 X_1^{(1,2)} f_1'(X_0^{(1,2)}) & \dot{\mu}_1 f_1(X_0^{(1,2)}) - \dot{k}^1_M - \dot{h} & -f_2(X_1^{(1,2)}) j^2_{XAm} \\ 0 & 0 & 0 \end{pmatrix}. \tag{7.25}$$

One can see that:

$$\det\left(\boldsymbol{F_x}(\boldsymbol{x^{(1,2)}}, \dot{h}^{(1,2)}) - \lambda \boldsymbol{I}\right) = -\lambda P_2(\lambda),$$

where $P_2(\lambda)$ is a second-order polynom with respect to λ. Thus, Jacobian matrix $\boldsymbol{F_x}(\boldsymbol{x^{(1,2)}}, \dot{h}^{(1,2)})$ has at least one real zero eigenvalue, which indicates generally a fold bifurcation. This zero eigenvalue is associated to the left eigenvector $\boldsymbol{p^{(1,2)}} = (0, 0, 1)^T$. As $X_2^{(1,2)} = 0$, one can check using (7.7.2) that the condition for a transcritical bifurcation:

$$\langle \boldsymbol{p^{(1,2)}}, \boldsymbol{F_x}(\boldsymbol{x^{(1,2)}}, \dot{h}^{(1,2)})\rangle = 0,$$

is fulfilled. Now, we have to check the genericity conditions of this bifurcation.

The right eigenvector of the Jacobian matrix (7.25) associated to the zero eigenvalue is:

$$\boldsymbol{q}^{(\mathbf{1,2})} = \begin{pmatrix} 1 \\ -\dot{h} \\ \overline{f_1(X_r) j^1_{XAm}} \\ \dfrac{\dot{\mu}_1 X_1^{(1,2)}}{j^2_{Xam} f_2(X_1^{(1,2)})} f_1'(X_0^{(1,2)}) \end{pmatrix}.$$

Thus, one can check using (7.23) that the transversality condition is fulfilled:

$$\boldsymbol{p}^{(\mathbf{1,2})^T} \boldsymbol{F}_{\dot{h}\boldsymbol{x}}(\boldsymbol{x}^{(\mathbf{1,2})}, \dot{h}^{(1,2)}) \boldsymbol{q}^{(\mathbf{1,2})} = \frac{-\dot{\mu}_1 X_1^{(1,2)}}{j^2_{Xam} f_2(X_1^{(1,2)})} f_1'(X_0^{(1,2)}) \neq 0.$$

Using (7.24), one can check that the non-degeneracy condition is also fulfilled:

$$\langle \boldsymbol{p}^{(\mathbf{1,2})}, \boldsymbol{F}_{\boldsymbol{xx}}(\boldsymbol{x}^{(\mathbf{0,1})}, \dot{h}^{(0,1)})(\boldsymbol{q}^{(\mathbf{1,2})}, \boldsymbol{q}^{(\mathbf{1,2})}) \rangle = \frac{-2\dot{h}\dot{\mu}_1\dot{\mu}_2 X_1^{(1,2)} f_1'(X_0^{(1,2)}) f_2'(X_1^{(1,2)})}{j^1_{XAm} j^2_{XAm} f_1(X_0^{(1,2)}) f_2(X_1^{(1,2)})} \neq 0,$$

thus the transcritical bifurcation where $\boldsymbol{x}^{(\mathbf{1})}$ and $\boldsymbol{x}^{(\mathbf{2})}$ collide at $\dot{h} = \dot{h}^{(1,2)}$ is generic.

7.7.4 Hopf bifurcation

Depending on parameter values, equilibrium $\boldsymbol{x}^{(\mathbf{2})}$ can have a pair of complex conjugate eigenvalues with zero real part, i.e. it crosses an Hopf bifurcation. This bifurcation can be located by solving the condition $\det(2J^{(2)} \odot I_3) = 0$, where $2J^{(2)} \odot I_3$ is a 3×3 matrix obtained using the bialternate product $\odot$ (see Kuznetsov, 2004, p527-528). This condition can be expressed analytically as $\dot{h} = \dot{h}^{(H)}$ where $\dot{h}^{(H)}$ depends on $\dot{h}$. However, as for the original DEB model, the expression of $\dot{h}^{(H)}$ does not allow for a simple interpretation of the bifurcation condition. So, there is no interest of presenting this condition here. Solving this condition for a given functional response formulation leads to the same results than numerical continuation methods. Using numerical methods, the type of Hopf bifurcation (subcritical vs. supercritical) is determined by computing the first Lyapunov coefficient. No analytical expression of this coefficient was derived as even the bifurcation condition cannot be interpreted in a simple way. A codimension-two Bautin bifurcation occurs when the first Lyapunov coefficient vanishes, so we have no analytical expression for this bifurcation.

Table 7.11. Maximum growth rate of the predator is a fixed fraction of its maximum assimilation rate: parameter values for each functional response in models without explicit reserve. Ivlev's functional response and the hyperbolic tangent are parameterized in order to mimize their Euclidean distance with Holling's disc equation.

model	parameter	Holling	Ivlev	Hyperbolic tangent
Marr-Pirt	$j_{XAm}^{2,\phi}$	0.55	0.523	0.521
	K_2^ϕ	0.23	0.416	0.550
	$\dot{\mu}_2^\phi$	0.49	0.466	0.464
Monod	$j_{XAm}^{2,\phi}$	0.49	0.459	0.456
	K_2^ϕ	0.34	0.578	0.767
	$\dot{\mu}_2^\phi$	0.33	0.309	0.307

7.8 Maximum growth rate of the predator in models without explicit reserve

Varying the maximum growth rate of the predator between functional response formulation (table 7.11) in order to keep a constant conversion efficiency has only a small quantitative impact on the results for Marr-Pirt and Monod models (tables 7.12-7.13).

Table 7.12. Proportion of qualitatively different dynamics between functional responses in the Marr-Pirt model when the maximum growth rate of the predator is a fixed fraction of its maximum assimilation rate. The reference area corresponds to the parameter space where the prey can survive for resource concentration in the feed lower than an arbitrary value X_r^{thres}. For each pair of functional responses, the following proportions are indicated for different X_r^{thres} values: different predator survival (existence of $\boldsymbol{x^{(2)}}$), predator survives and there is an only stable state with predator-prey fluctuations (stability of $\boldsymbol{x^{(2)}}$ when it exists). Note that the two proportion do not overlap with each other.

functional responses	X_r^{thres}	predator survival	predator oscillations
Holling - Ivlev	5	0.034	0.073
	10	0.021	0.065
	20	0.021	0.037
Holling - Tanh	5	0.043	0.088
	10	0.025	0.073
	20	0.025	0.043
Ivlev - Tanh	5	0.015	0.024
	10	0.009	0.016
	20	0.007	0.011

Table 7.13. Proportion of qualitatively different dynamics between functional responses in the Monod model when the maximum growth rate of the predator is a fixed fraction of its maximum assimilation rate. The reference area corresponds to the parameter space where the prey can survive for resource concentration in the feed lower than an arbitrary value X_r^{thres}. For each pair of functional responses, the following proportions are indicated for different X_r^{thres} values: different predator survival (existence of $\boldsymbol{x^{(2)}}$), predator survives and there is an only stable state with predator-prey fluctuations (stability of $\boldsymbol{x^{(2)}}$ when it exists). Note that the two proportion do not overlap with each other.

functional responses	X_r^{thres}	predator survival	predator oscillations
Holling - Ivlev	5	0.025	0.077
	10	0.017	0.052
	20	0.018	0.026
Holling - Tanh	5	0.035	0.114
	10	0.022	0.066
	20	0.023	0.033
Ivlev - Tanh	5	0.001	0.048
	10	0.003	0.024
	20	0.004	0.012

CHAPTER 8

Concluding remarks and perspectives

"The field of ecology is distinguished by the complexity of the processes and interactions that are its primary focus and also the primary excuse for ecologists' failure"

Michael A. Huston,
"Hidden treatments in ecological experiments:
re-evaluating the ecosystem function of biodiversity" (Huston, 1997).

8.1 Summary of the thesis

The general question that guides the research presented in this thesis is: *how far choices in model construction can affect the predicted dynamics of ecological systems and the information they provide on their resilience?* The original research performed to answer this question is summarized in figure 8.1. Chapter 3 shows that a quantitatively minor change in model formulation can affect the qualitative dynamics predicted by the model (structural sensitivity). Uncertainties in the predicted type and number of stable states arise from changes in bifurcations type and location, which propagate into uncertainties in predicted system resilience in case of external disturbances. These changes in model dynamics can be explained in the context of bifurcation theory by turning the problem of model formulation into a problem of model parameterization (chapter 4). Going beyond this qualitative analysis, chapter 6 suggests new methods to quantify model sensitivity when multiple stable states coexist. These generic questions (chapters 3, 4 and 6) are illustrated through an example of predator-prey model with density-dependent mortality. In parallel to these mathematical developments (left side of figure 8.1), ecological questions on the complexity of ecological systems and its integration into mathematical models are also tackled (right side of figure 8.1). Chapter 5 disentangles the respective effects of structural sensitivity and trophic complexity (number of species and interactions) in food web models. This holistic approach goes toward the integration of more system components (species). Conversely, the reductionist approach used in chapter 7 goes toward more details on individual metabolism. If a minimum level of biological details is included, models are less structurally sensitive (no effect on the number of stable states). This provide a clue to deal with structural sensitivity in biological models, despite more details about metabolism also means more potential sources of uncertainty in model construction. Uncertainty in model construction (formulation and parameterization of a process, complexity of the network of interactions, metabolism and other assumptions) comes from the fact that in ecology we are dealing with complex systems (chapter 1).

In comparison to the complex systems we are dealing with, all the work presented in this thesis is simple. First, it is simple in mathematical terms: the same work can be done on ecological models with more complex dynamics and bifurcations. In addition, many biological systems can be modelled using slow-fast systems (state variables have different time scale dynamics, e.g. predator-prey dynamics in Rinaldi & Muratori, 1992, Kooi *et al.*, 1998a, 2002) or discontinuous piecewise systems (Filippov systems, model formulation changes over the state space, e.g. harvested population in Kuznetsov *et al.*, 2003). Including explicit space or considering structured populations may also require the use of partial differential equations. One can easily imagine many way to

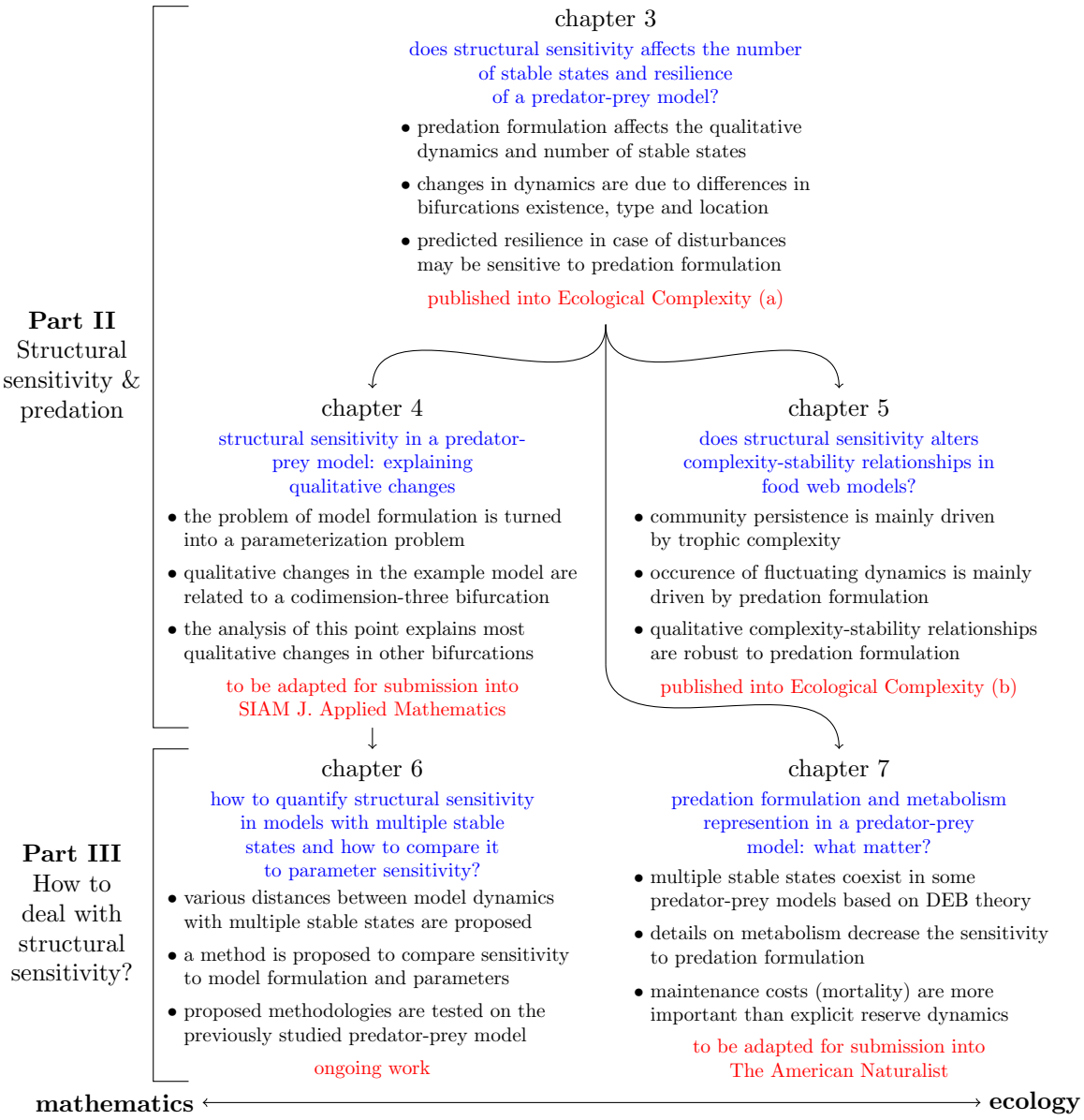

Figure 8.1. Synthesis of the original research presented in this thesis. For each chapter, the corresponding question (blue), main answers found (black) and the current state of my research about it (red) are provided. As in figure 1.4, chapters are presented according to their relative (and subjective) location between the sciences of ecology and mathematics.

build complex models by considering more and more aspects of an ecosystem. Secondly, the work presented in this thesis is simple in biological terms. Individual variability is neglected at the population scale in whole models. These models do not consider an explicit spatial repartition of organisms, as well as many other processes (e.g. nutrient recycling, evolution) and interactions (e.g. mutualism, parasitism). Indeed, we attempted to keep things as simple as possible regarding the scope of this thesis and the infinite number of studies that are possible using mathematical models.

8.2 Some general perspectives: toward more accurate predictions

The problem with mathematical modelling is that we can study model sensitivity to almost everything: its scope (e.g. number of species, limiting resources, explicit space), included processes (e.g. mortality, competition, explicit reserves), processes formulation and parameterization. Each side of model sensitivity contains numerous underlying questions, as highlighted throughout this thesis. This infinite aspect of modelling is nicely illustrated by a question I got from SALM Kooijman during the 8th international course on Dynamic Energy Budget theory: *"You told us that you compared the dynamics predicted by two different functions. Then, you said that now you are doing this with three. But you can also do it with four and five, and my question is: are you going to do this all your life?"*[1]. Of course my answer is no. I used a few functions as examples among the most used ones in order to answer the questions I was asking.

Years ago in "kindergarden" (let's say when I was an undergraduate student), I was in that rush where I wanted to know everything. At this time, I though that science was about getting the right answers. Now, I think that science is more about asking the right questions. As an infinite number of questions can be asked, we can find an infinite number of answers and gather an infinite amount of knowledge. Most knowledge is made of specific informations (e.g. "species A grows at a rate X"), whereas the most interesting one in my opinion gives an understanding that explains these specific informations (e.g. "the growth rate of species A is a function of factors B and C") or use them to answer more general questions (e.g. "all species doing process A have to interact with a species doing process B to grow") (chapter 19 in Schimel, 2012).

This is this last type of knowledge that this thesis aims to provide. For example, chapters 3 and 4 are not about the sensitivity of a given model to the formulation of a given process. These chapters present the first (as far as I know) example of ecological model where a given type of

[1] Due to my human memory, this quote is not rigorously exact, but its spirit is here.

uncertainty in model formulation (quantitatively close functions with the same general properties) leads to a given type of uncertainty in model predictions (number of stable states, resilience) that is relevant for applied predictions and managing issues. Now, I am not saying that we should test this sensitivity in all known models. Most modellers cannot test it in their own model (there is an infinite amount of other questions to answer) but may want to know if this sensibility is likely to be important in their model. Thus, one may ask if this sensitivity also occur in other classes of ecological models (e.g. food webs in chapter 5) or if there are counter-examples where this sensitivity does not occur (e.g. chapter 7 with models based on Dynamic Energy Budget theory). If one wants to assess the structural sensitivity of a model, appropriate mathematical tools are required (e.g. chapter 6).

All the perspectives for future research mentioned in the previous paragraph and chapters can be gathered under the goal of improving model predictions. This idea links theoretical and applied research in modelling. Theoretical studies are made to tackle general questions (e.g. *"Will a large complex system be stable?"*, May, 1972) and attempt to get general results. These results should not be sensitive to any small change in model construction in order to provide significant knowledge and interesting theory. In addition, theoretical research is also oriented toward the improvement of model predictions for applied (i.e. operational) modelling (figure 8.2). This improvement goes through the development of model formulations derived from a mechanistic representation of underlying processes (e.g. Poggiale *et al.*, 2010, Cordoleani *et al.*, 2013, Accolla, 2015). These formulations might be more appropriate in some situations than classical ones, as they include processes that are important in some systems (e.g. co-limitation, space, schooling). However, they still remain an approximation of a complex biological system. Thus, general studies on model sensitivity are still required. Such studies would investigate the effect of structural sensitivity on the number of stable states in complex food webs (perspectives of chapters 3 to 5) or the interplay between trophic complexity and metabolic details in small food webs (perspectives of chapters 5 and 7). These analysis can be strengthened by the use of quantitative methods to estimate model sensitivity (perspectives of chapter 6). These quantitative methods may be useful to design experiments coupled with modelling and oriented toward a decrease of uncertainties in model predictions.

8.3 Personal comments about modelling

Errare humanum est.

The first comment I would like to make is more about research on modelling rather than

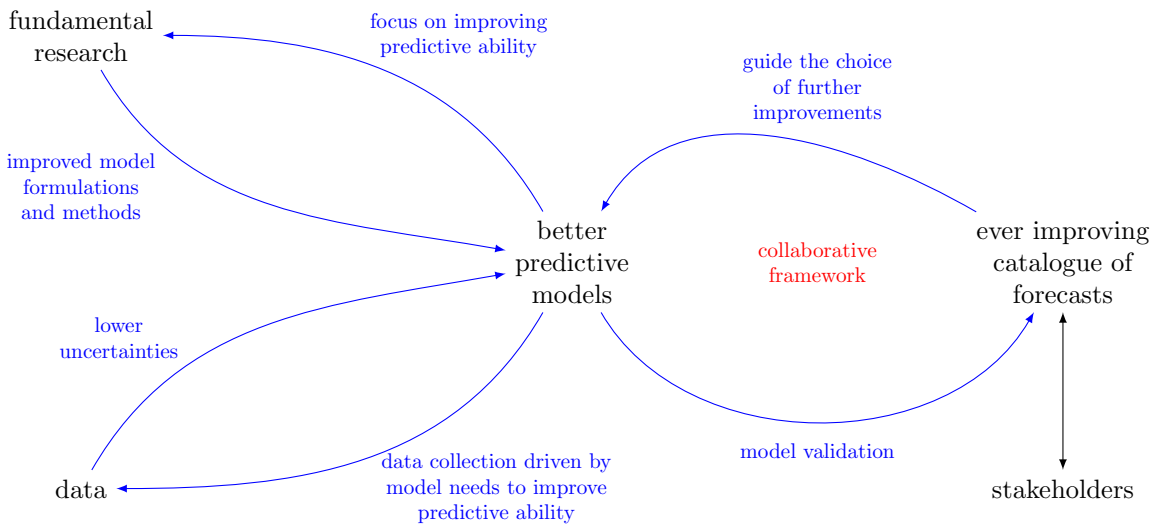

Figure 8.2. Road map for advancing research on ecological predictability proposed by Petchey *et al.* (2015, modified). Interactions between "fundamental research" and "data" are not explicitely represented as they occur through "better predictive models".

about modelling itself. Recent reviews still highlight the lack of validation, sensitivity analysis and report of model assumptions in most modelling studies (Corley *et al.*, 2014, Gregr & Chan, 2014). Thus, conclusions from these studies might be uncertain and we have no idea of their robustness. Assessing the robustness of model results is time-consuming and is at most briefly mentioned in a paper. Publishing a detailed description of model construction and robustness is not appealing for most readers. Indeed, the citation rate of papers in biology is negatively correlated with their content in equations (Fawcett & Higginson, 2012). This paradox was described as *"the incompatibility between the inherent complexity of social-ecological systems and the focus of scientific publishing on concise, interesting results"* (Gregr & Chan, 2014). This focus on concise and interesting results is the spirit of science (the so-called Occam's razor, see section 2 in Jusup *et al.*, in press, for an introduction in biology) and of human mind, which always struggle to summarize a huge amount of information. Such summary is necessary to share information among scientists. However, a detailed description of the model and of the robustness of its results is required (at least in appendices, where number of equations has no influence on readership, Fawcett & Higginson, 2012) to avoid an accumulation of papers making punchy conclusions that cannot be objectively discussed. Such precautions are important for the purpose of scientific rigor, but also to assess the likelihood of forecasts used to help stakeholders that have to manage complex social-ecological systems.

Complex systems do not necessarily need to be understood to make accurate projections of

their future state (Breiman, 2001). However, while making predictions we are often trying to understand the system itself (Schmueli, 2010). The same observation can be explained by different mathematical arguments (i.e. different models) because of the "unreasonnable effectiveness of mathematics" (Wigner, 1960). Thus, complex models need to be used together with simpler models in order to have a better understanding of the model as a mathematical object. A mathematical model cannot make unequivocal predictions "à la Newton". Studies like this thesis highlight how far predictions of complex ecological systems are uncertain. However, uncertain predictions do not mean that we should stop using mathematical models. Indeed, models can still predict the qualitative state of a natural system (e.g. Benincà *et al.*, 2015). In addition, simple models are sometimes enough to deal with important socio-ecological issues such as species invasion (Hastings *et al.*, 2006, Hall & Hastings, 2007) or epidemics (May, 2004). Finally, quantitative predictions remain valid for short-term forecasting, the "short-term" being for example defined by the forecast horizon (Petchey *et al.*, 2015). This quantitative measure of model ability to predict dynamics that are sensitive to initial conditions is an example of tools that might help both theoretical and operational modelling research to move toward more accurate predictions (figure 8.2).

To conclude this thesis about modelling complex ecological systems, I want to recall that any model of a system is not the system. The model is how a human mind see the system in a given context (figure 1.1a). As the model is built by a human mind, the only limit is our own ability to conceptualize and understand the system we want to model. When modelling the system, both holistic and reductionist approaches are missing some properties of the system. Thus, in a Newtonian perspective, every modelling attempt will fail. This is not a failure of modelling and mathematics themself, but a failure of human mind which cannot understand everything as a whole in its surrounding environment. Indeed, human mind is based on human brain, which has its own "carrying capacity" because of its finite size. This brain simplifies the information it receives by always making conceptual and statistical models. A few of these models are formalized in mathematical terms by the scientist who want to answer a given question. Indeed, in modelling like in the known history of life on the Earth, everything is a matter of needs and purposes.

CHAPTER 9

Résumé détaillé de la thèse (Detailed French summary)

Ce résumé détaillé en français est composé de la traduction (texte et figures):

- du chapitre 1: état de l'art et présentation des thématiques abordées dans la thèse, stratégie suivie lors de la thèse et plan du manuscrit,
- du chapitre 8: synthèse des travaux réalisés dans le cadre de la thèse, perspectives générales et réflexions personnelles sur la modélisation en écologie.

Préambule: tout le monde fait des modèles

"Il y a de petites rides sur l'eau à la pointe Est de l'île, donc il y a du courant d'Est et les poissons sont concentrés entre 10 et 20 mètres de fond le long du tombant Sud."[1] Cette phrase est un exemple parmi les nombreux autres ques nous avons tous entendu de la part de "personnes expérimentées". Par "personnes expérimentées", je parle des personnes qui (pour n'importe qu'elle raison) ont appris de leur environnement, la mer, la montagne, ou les bois autour d'elles, durant des anées ou des décennies. Grâce à cette longue période d'observation, ces personnes sont capables de faire des prédictions heuristiques sur leur environnement ou la météo. Cette capacité est ce que nous appelons habituellement "l'expérience" ou "l'intuition". Au-delà de cette approche statistique, on peut avoir certaines idées sur comment les choses interagissent (*"Les courants sont importants pour les poissons."*). Ces interactions peuvent être en partie comprises comme un phénomène (*"Un courant plus fort implique plus de poissons."*) ou à travers leurs méchanismes sous-jacents (*"Le courant transporte de la nourriture pour les organismes par advection."*). Toutes ces visions sont basées sur des modèles, i.e une représentation simplifiée d'un système complexe. Un système complexe ne peut pas être compris simplement en le décomposant en composants plus petits comme pour une horloge. Ainsi, il n'y a pas de modèle unique pour représenter un système complexe. Pour chaque situation, définir quel est le modéle le plus appropré restera toujours un débat ouvert. Mais comme nous avons tous nos propres idées sur comment le monde fonctionne, **nous faisons tous des modèles**.

9.1 Prédire le futur: de l'intuition aux mathématiques

9.1.1 L'expérience personnelle comme modèles statistiques et conceptuels

L'expérience personnelle est une forme d'apprentissage basée sur la mémoire d'évènements répétés. Ainsi, l'expérience est un modèle statistique. Un modèle statistique fait des prédictions à partir d'observations préalables. La répétitions des observations donne une fréquence d'évènements pour estimer leur probabilitée d'avoir lieu. Cette estimation devient en général plus précise lorsque le nombre d'observations augmente. En observant le monde autour d'eux durant des années, les "personnes expérimentées" peuvent faire des prédictions heuristiques. Des prédictions heuristiques peuvent être justes, mais quand elles ne le sont pas nous ne pouvons pas expliquer pourquoi (Mouquet *et al.*, 2015). En effet, il n'y a aucune explication des processus dans un modèle statistique.

[1] J'ai écrit cette citation fictive (et les autres du paragraphe) pour cette introduction, à partir de phrases similaires que j'ai entendu de nombreuses "personnes expérimentées", marins, pêcheurs, plongeurs, et autres.

Ce modèle est uniquement basé sur les corrélations entre de nombreuses variables explicatives, mais leurs interactions menant à ces corrélations sont inconnues *a priori* (Breiman, 2001)

Une approche statistique peut être utilse pour faire des prédictions opérationnelles (pour des exemples en océanographie, voir Nerini & Ghattas, 2007, Nerini *et al.*, 2010, Bayle *et al.*, 2015). Cependant, seules des situations appartenant à la gamme de celle qui ont déjà été observées peuvent être prédites. Prédire des évènements en dehors du cadre initial du modèle (extrapolation) est trs risqué, car il n'y a aucune contraintes (données ou hypothèses sur les processus) sur les prédictions du modèle. Cette situation pourrait être la règle plutôt que l'exception, car les évènements uniques au sens strict sont dominants. En effet, seuls 75 évènements se produisant indépendemment les uns aprs les autres mènent à $75! \approx 10^{106}$ séquences possibles, ce qui est plus que le nombre d'évènements simples qui ont eu lieu depuis le début (il y a ≈ 15 milliards d'années) de l'Univers connu (Elsasser, 1969 *in* Planque, 2015). Même si les évènements ne sont pas indépendants l'un de l'autre, toutes les situations possibles ne peuvent pas avoir eu lieu dans le passé. Un argument simple est que les organismes vivants évoluent, donc des gènes et des espèces inconnus peuvent apparaitre pendant que d'autres disparaissent.

Les modèles conceptuels vont au-delà des modèles statistiques au sens qu'ils spécifient des interactions entre des compartiments d'intérêt. (pour un exemple en océanographie, voir Legendre & Le Fèvre, 1989). Cette approche permet de faire des prévisions qualitatives ou semi-quantitative comme un avis d'expert (encore, nous faisons tous des modèles). Par exemple, estimer l'état d'un écosystème pour aider à la décision de politiques environmentales est possible à l'aide d'un modèle conceptuel (Personnic *et al.*, 2014). A partir de ce modèle, un indicateur semi-quantitatif de l'état de l'écosystème est déduit de l'état de chaque compartiment. Ce dernier est estimer avec plus ou moins de confiance selon l'information disponible (de pas d'information à données récentes, ou encore un jugement d'experts).

9.1.2 Décrire les processus: complexité et approches multiples

L'idée de décrire des processus avec des mathématiques semblent commencer avec Pythagore (580-495 BC), et s'est répandu durant la Renaissance avec de célèbres découvertes en astronomie (Israel, 1996). L'astronome Johannes Kepler (1571-1630) a découvertt le mouvement elliptique des planètes et a proposé une vision géométrique de l'Univers. Dans une approche plus quantitative basée sur les nombres, Galileo Galilei (1564-1642) a suggéré que le monde ne pouvait être compris que si on connait son langage, les mathématiques. Une grande avancée en mathématiques fut l'invention du calcul infinitésimal (dérivées et intégrales) par Pierre de Fermat (début 1600's-1665), Gottfried Leibniz (1646-1716) et Isaac Newton (1642-1727). Newton a lancé un courant de pensée basé sur

une vision mécaniste des sciences, renforcée plus tard par Pierre-Simon Laplace (1749-1827) qui argumentat que tous les phénomènes suivent une équation. Cette équation est une loi gouvernant le phénomème, d'après la vision Newtonienne.

L'approche précédente peut réussir à décrire un système compliqué, comme une horloge. Un système compliqué peut être simplifié en composants plus petits dont la compréhension permet de comprendre le système complet. A l'inverse, un système complexe ne peut pas être simplifié en sous-composants sans perte d'information, à cause de ses propriétés émergentes (Le Moigne, 1999). De plus, un système complexe es fait de tellement de composants (e.g. le nombre d'Avogadro's, 6.022×10^{23} atomes dans 12 g de carbone ^{12}C) et d'interactions qu'il ne peut pas être décrit en entier. En conséquence, il doit être modélisé, le modèle étant une représentation simplifiée du système complexe. La recherche sur les systèmes complexes en écologie a commencé avec le travail fondateur de von Bertalanffy (1968). Maintenant, la plupart des sciences font appel à l'analyse de systèmes complexes (Israel, 1996).

Comme un système complexe sera toujours représenté de façon incomplète, tout acte de modélisation nécessite de faire des choix. Le choix des caractéristiques du système (composants, interactions) à prendre en compte dépend du cadre de létude. Ainsi, la modélisation est passé d'une approche objective (Newtonienne) à une approche projective (figure 9.1a). Dans l'approche projective, il n'y a pas un seul modèle pour un système donné, mais une variété de modèles selon les intérêts du modélisateur. Par exemple, un animal peut être vu comme un système émergent fait de nombreuses cellules et molécules, ou comme un composant d'une population consitutée de nombreux individus.

Les différents modèles d'un système peuvent être définis de façon relative en modèles mécanistes, phénoménologiques et empiriques (figure 9.1b). Dans les modèles empiriques, la formulation d'un phénomène n'a pas de justification théorique, mais cette fonction mathématique reproduitles données empiriques. Par exemple, des données sur la photosynthèse par le phytoplancton P en fonction de l'irradiance lumineuse L peuvent être décritent de façon satisfaisante par une fonction tangente hyperbolique (avec des paramètres a et b):

$$P(L) = a \tanh(bL), \tag{9.1}$$

qui n'a aucune justification théorique (Jassby & Platt, 1976).

Dans des modèles phénoménologiques, la formulation d'un phénomène décrit ses propriétés

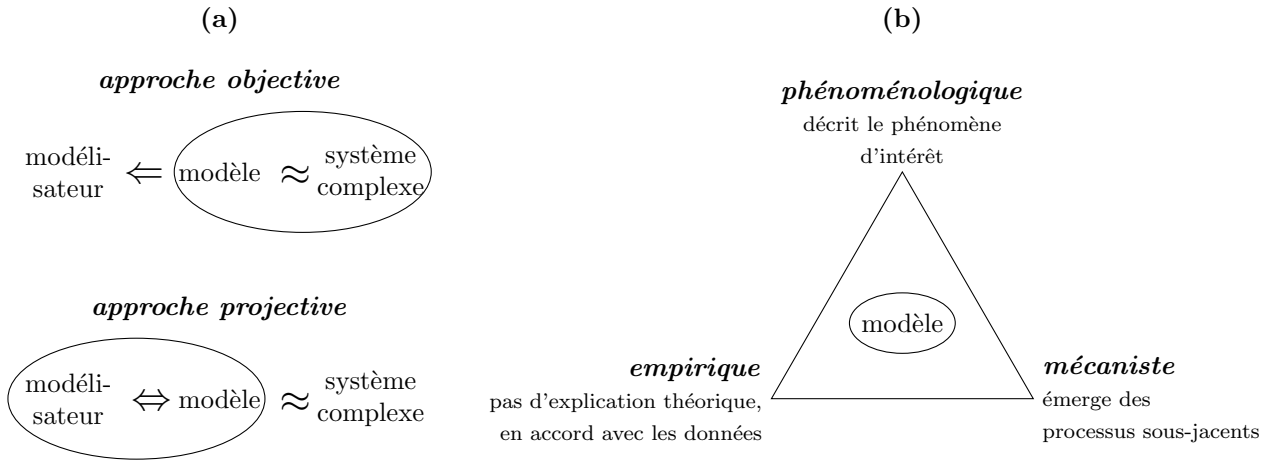

Figure 9.1. La modélisation des systèmes complexes: approche objective vs. projective (a, redessiné d'après Le Moigne, 1999) et différents types de modèles (b). Dans l'approche objective, le modèle est attaché au système et est utilisé par le modélisateur (le modélisateur est en dehors du couple modèle-système). Dans l'approche projective, le modélisateur interagit avec le modèle (choix dans sa construction) afin de représenter le système en fonction de ses intérêts (le système est à l'extérieur du couple modélisateur-modèle). Les différents types de modèles sont définis de façon relative. Certaines parties d'un modèle peuvent être d'un type, et d'autres parties peuvent être d'un autre type.

émergents. Par exemple, l'équation de croissance logistique:

$$\frac{dx}{dt} = xR(x) = xr\left(1 - \frac{x}{K}\right), \tag{9.2}$$

est une équation différentielle ordinaire qui décrit la croissance d'une population x au cours du temps t (Verhulst, 1838). Le modèle suppose que le taux de croissance net de la population $R(x)$ est une fonction décroissante de x, donnée par $r(1 - x/K)$. Cette décroissance n'est pas expliquée par ses processus sous-jacents (e.g. compétition entre individus, ressources limitées, maladies). Elle est uniquement décrite par un taux de croissance maximal r et une taille maximale de population qui peut être maintenue par l'environnement K (capacité limite).

Enfin, les modèles mécanistes représentent un phénomène à partir de ses processus sous-jacents. Si ces processus satisfont certaines hypothèses, ces hypothèses mènent à la formulation du phénomène. Par exemple, la réponse fonctionnelle $f(x)$ (quantité de proies x consommées par unité de prédateur et par unité de temps) peut être modélisée par l'équation du disque de Holling (1959b):

$$f(x) = \frac{ax}{b + x}, \tag{9.3}$$

qui est obtenue en supposant que (i) la répartition spatiale des individus est homogène, et (ii) que le prédateur sépare sont temps d'activité entre la recherche de proies et la gestion (e.g. tuer, manger) d'une proie capturée (et quelques hypothèses supplémentaires). Des explications mécanistes d'un modèle empirique ou phénoménologique peuvent être trouvées après que le modèle ait été proposé (pour l'équation de croissance logistique, voir Kooi *et al.*, 1998b, Poggiale, 1998, Loreau, 2010).

Le modèle de croissance logistique (9.2) utilisé comme exemple est un modèle déterministe. Dans les modèles déterministes, une condition initiale (e.g taille de population) va toujours prédire la même dynamique temporelle des système pour des valeurs de paramètre fixées. A l'inverse, un modèle stochastique peut prédire des résultats différents à partir d'une même condition initiale. Celà signifie que le modèle dépend de variables aléatoires (la productivité d'une espèce par exemple dans Yachi & Loreau, 1999). Ces variables aléatoires peuvent être vues comme une représentation phénoménologique de nombreux processus sous-jacents qui ne sont pas représentés dans le modèle.

Les modèles déterministes et stochastiques peuvent être reliés à l'aide de la théorie du chaos déterministe (for quelques exemples, voir chapitre 2 dans Guckenheimer & Holmes, 1983). Le chaos déterministe émerge dans des systèmes déquations non-linéaires. A cause des non-linéarités, des trajectoires du système initialement proches vont diverger au cours du temps, un phénomème appelé sensibilité aux conditions initiales. Ce phénomène a été d'abord décrit dans un modèle hydrodynamique par Lorenz (1963), puis dans des modèles écologiques simples par May (1974, 1976). Hastings *et al.* (1993) argumentent qu'il n'y a ps de dichotomie entre la stochasticité et le chaos déterministe. En effet, le chaos déterministe amplifie une incertitude sur l'état initiale du système qui devient une incertitude sur la dynamique du système. A une échelle supérieure, cette incertitude déterministe peut être vue comme de la stochasticité. Par exemple, si tout était parfaitement connu, nous connaitrions le résultat de n'importe quel lancer de dés, bien que ce résultat soit sensible à des changements infimes dans notre geste.

Pour conclure cette première section nommée *Prédire le futur*, je veux souligner qu'elle concerne aussi bien les prédictions opérationnelles d'un système donné (modélisation prédictive) que la modélisation conceptuelle (*sensu* Petrovskii & Petrovskaya, 2012). Dans la modélisation conceptuelle, le but d'un modèle est de capturer les caractéristiques qualitatives d'une classe de système (e.g. une especèce dont l'abondance dépend d'une ressource limitante) pour tester des hypothèses théoriques, comme la conséquence de prendre un processus en compte ou non. Celà nous mène à une propriété importante d'un modèle, qui est sa capacité d'abstraction et de généralité. La généralité veut dire qu'un même modèle peut représenter différents systèmes ayant des propriétés communes. Ces propriétés peuvent être prises en compte de façon abstraite (e.g. non-spécifique à un organisme). Ainsi, des hypothèses générales peuvent être faites sur le fonctionnement de ce type de systèmes.

9.2 Ecologie et complexité

9.2.1 Une histoire d'échelle, de frontières et d'approches

L'écologie[2] est la science qui étudie les interactions des organismes vivants entre eux et avec leur environnement. Ainsi, même si l'écologie est souvent vue comme une partie de la biologie, elle interagit avec la physique (e.g. advection et diffusion dans l'eau), la chimie (e.g. composition de la matière organique, contaminants), la géologie (e.g. composition des sols, relargage de composés chimiques) et la climatologie. De plus, l'écologie s'intéresse aux niveaux d'organisation des systèmes vivants. Ces niveaux sont imbriqués et couvre une large échelle spatio-temporelle (figure 9.2 et définitions associées). L'échelle d'un seul niveau d'organisation comme l'individu peut couvrir de nombreux ordres de grandeur (le volume et la durée de vie des organismes connus couvrent respectivement plus de 20 et plus de 6 ordres de grandeurs, Kooijman, 2010, chapitre 8). Cette imbrication d'échelles implique que le nombre de composants (molécules, cellules, individus) empêche toute description du système dans son ensemble, même si tous les composants et toutes les interactions étaient connus. Ceci est un premier aspect de la complexité des écosystèmes.

Un autre aspect de la complexité en écologie est que tous les niveaux d'organisations ont des frontières vagues (figure 9.2). Des frontières vagues caractérisent également les système d'un même niveau. A tous les niveaux d'organisation, les systèmes vivants sont ouverts d'un point de vue thermodynamique, car de l'énergie et de la matière sont échangés. En conséquence, délimiter un écosystème déprendra fortement de l'échelle et du cadre de l'étude. De même, les organismes eux-mêmes sont difficiles à classifier (voir Ragan, 2009, pour un historique des arbres du vivant). Les classifications évoluent en permanence, la plus commune étant la classification taxonomique (voir Baldauf, 2003, 2008, pour les eucaryotes). D'autres classifications se basent sur le rôle fonctionnel des organismes ou leur métabolisme. En effet, même des souches de la même espèce de bactérie peuvent présenter de grandes diffŕences phénotypiques (comme la cyanobactérie *Crocosphaera watsonii*, Webb *et al.*, 2009).

Deux grands courants de recherche en écologie sont l'écologie des populations et l'écologie des écosystèmes (Odum, 1964). La première se focalise sur les populations et leurs interactions, à travers les changements d'abondance de populations. A l'inverse, la seconde se focalise sur les interactions entre les populations et leur environnement, à travers les flux de matière et dénergie. Ces deux approches ne sont pas opposées, et les recherches les plus récentes essayent de concilier les deux (Loreau, 2010, et les références associées).

De façon similaire, les systèmes complexes comme les systèmes vivants peuvent être étudiés

[2]Le mot *écologie* vient du grec ancien *oikos* et *logos* qui signifient *maison* et *science*.

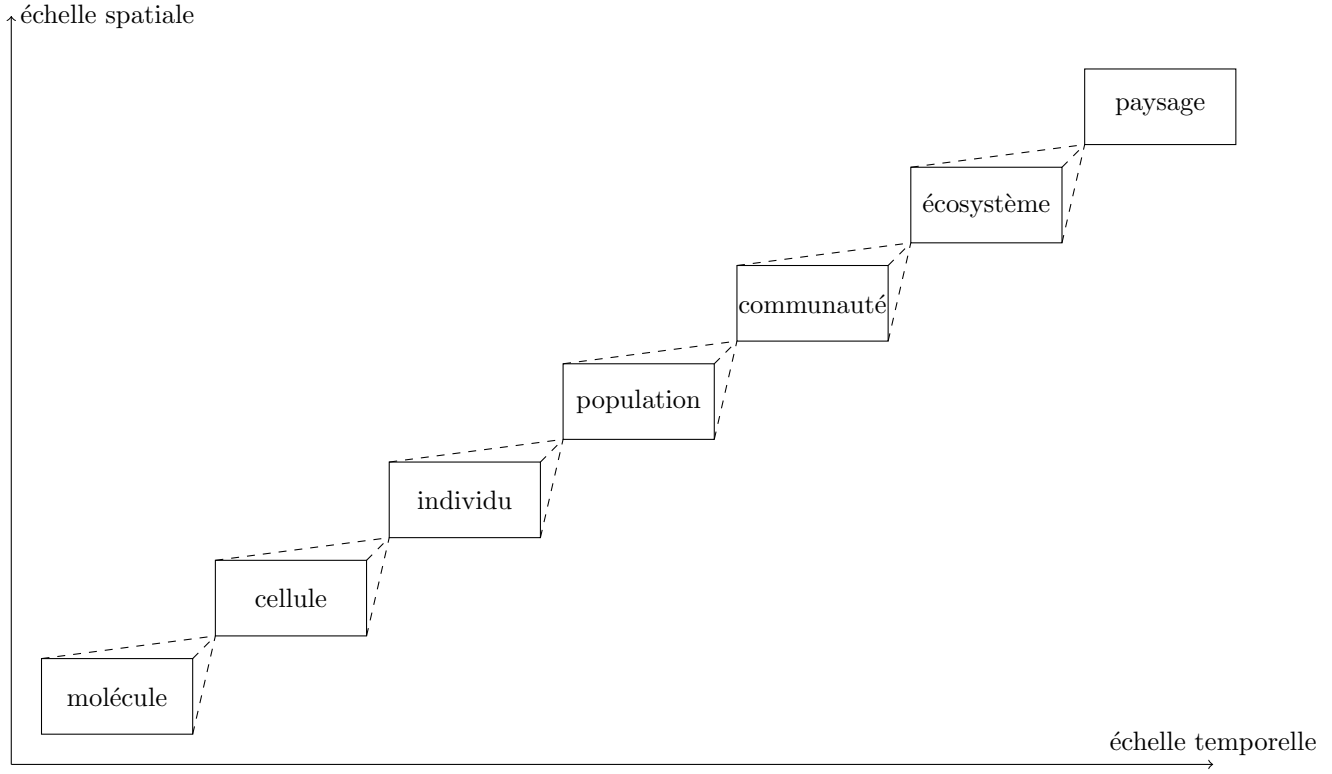

Figure 9.2. Imbrication des niveaux d'organistation des systèmes vivants, en fonction de leurs échelles relatives. Les molécules (et les atomes) sont les constituants de la matière, et donc des cellules. Une cellule peut être un individu (unicellulaire) ou une partie d'un individu (multicellulaire). Un ensemble d'individu d'une même espeèce est une population. Les frontières de la cellule à la population peuvent être vagues et arbitraires (voir Kooijman, 2010, section 1.1.2). Un ensemble de populations d'espèces différentes est une communauté. Cette communauté est appelée biocénose si elle regroupe toutes les espèces présentes dans un écosysteme donné. L'écosystème est composé de la biocénose, son environnement biotique et abiotique (habitat), et toutes les interactions entre les organismes et l'environnement. A travers l'environnement, l'organisation spatiale de plusieurs écosystèmes (avec leurs interactions biotiques et abiotiques) est appelée un paysage. De la population au paysage, les niveaux d'organisations sont définis pour un temps et un endroit donné, mais aussi en fonction de l'échelle et du cadre de l'étude. Par exemple, un paysage du point de vue du microbiologiste est seulement une infime partie d'un écosystème du point de vue de l'ichtyologue. De plus, un inidividu (comme un arbre) peut être un paysage pour des organismes plus petits (micro-organismes, insectes). Modifié d'après Lévêque (2003).

de deux points de vue, holisme et réductionisme. L'approche holiste considère qu'à cause de ses propriétés émergentes, le système complexe ne peut qu'être considéré en entier en modélisant ses propriétés émergentes. Un exemple en écologie est la théorie intégrative pour les écosystèmes (Jørgensen *et al.*, 2007) qui essayent de modéliser les écosystèmes d'un point de vue thermodynamique, à travers les flux d'énergie. A l'inverse, l'approche réductionistese focalise sur certains composants *a priori* importants du système à l'aide de modèles mécanistes. Un exemple en écologie est la théorie des Budgets d'Energie Dynamique (Kooijman, 2010) qui se focalise sur les individus et propose un cadre général pour représenter leur métabolisme (également à travers l'énergie).

9.2.2 Interactions entre organismes

Les interactions entre deux organismes peuvent être classifiées selon leur impact respectif sur chaque organisme (tableau 9.1). Les trois principales interactions sont l'exploitation, la compétition et le mutualisme. L'exploitation concerne les proies tuées par un prédateur ou mangées par un brouteur (la proie survie), ainsi que les hôtes infectés par un parasite. La compétition concerne les organismes qui partagent un même facteur limitant. Un facteur limitant peut être n'importe quelle forme de ressource (proie, nutriment, lumière), son abondance spatio-temporelle (i.e. pics, fluctuations, hétérogénéité), un prédateur auquel échapper, l'espace et beaucoup d'autres (Loreau, 2010). Les organismes mutualistes sont dans une interaction mutuellement bénéfique, comme la production et le partage d'une ressource limitante de l'autre (e.g. coraux, Eynaud *et al.*, 2011, rhizobium, Akçay & Roughgarden, 2007). Cette classification des interactions est individu-centrée. A l'échelle de la population, de l'exploitation peut par exemple devenir du mutualisme indirect car la population de proies est régulée (e.g. évite une consommation excessive de sa ressource par la proie, Loreau, 2010) par la population de prédateurs.

Table 9.1. Différents types d'interactions entre deux organismes A et B, selon leur impact respectif (positif, negatif or neutre) sur l'autre. D'après CF Boudouresque (pers. comm).

$A \to B$	$A \leftarrow B$	$A \leftrightarrow B$
$+$	$-$	exploitation
$-$	$-$	compétition
$+$	$+$	mutualisme
$=$	$-$	antagonisme
$=$	$+$	commensalisme
$=$	$=$	indépendance

Les interactions entre de nombreux organismes sont organisées en réseaux, les plus étudiés étants les réseaux trophiques (prédation, Cohen *et al.*, 1990) et les réseaux mutualistes (Bascompte, 2008). Ces réseaux sont souvent caractérisés par leur complexité structurelle (nombre d'espèces[3] et d'interactions entre elles). La même complexité structurelle peut être observée pour de très nombreux réseaux. Par exemple, considérons 30 espèces qui peuvent toutes interagir avec toutes les autres (y compris elle-même par cannibalisme). Supposons qu'il y a 135 interactions entre ces espèces (15 % du nombre d'interactions possibles $30 \times 30 = 900$, une valeur courante pour les réseaux trophiques, Williams & Martinez, 2000), celà nous donne $C_{900}^{135} = 900!/(135!865!) \approx 6.2\ 10^{163}$ réseaux différents possibles. La racine carrée de ce nombre est plus grande que 10^{80},

[3]Sauf mention explicite, le mot *espèce* est maintenant utilisé dans son sens large pour faire référence à des organismes appartenant au même taxon ou groupe fonctionnel et qui on ́té regroupés pour le but de l'étude.

le nombre estimé d'atomes dans l'Univers observable (Wikipedia Free Encyclopedia, 2016). Ce nombre ne prend pas en compte le fait que certaines interactions ne peuvent pas avoir lieu càuse de contraintes physiologique (e.g. taille respoective de la proie et du prédateur, capacité à produire un composé chimique donné). Mais l'idée derrière ce calcul de coin de table eqt que là encore, toutes les situations possibles (ici les réseaux) ne peuvent pas être explorées à cause de leur nombre.

9.3 Quelques problématiques actuelles de la modélisation en écologie

Les quatres problématiques détaillées dans cette section peuvent regrouper autour de la question suivante: *Quel est l'impact des choix faits lors de la construction du modèle sur les prédictions de la dynamique des systèmes écologiques et les informations qu'elles fournissent sur la résilience de ces systèmes?* Cette question est le fil conducteur de cette thèse (dont le cadre est défini dans la section suivante) et elle fait le lien entre les problématiques suivantes.

9.3.1 Emergence de la "computational ecology" et "efficacité déraisonnable des mathématiques"

Un aspect des modèles mathématiques que nous n'avons pas encore abordé est notre capacité à analyser et utiliser un modèle. Par exemple, il est très simple d'écrire un système d'équations différentielles ordinaires. Mais il est souvent impossible de résoudre ce système (i.e. connaître la dynamique qu'il prédit) ou d'en trouver les propriétés générales (i.e. équilibres, bifurcations) de façon analytique. Des résultats analytiques sont génériques car ils sont exprimés sous forme de fonctions des paramètres. A l'inverse, des résultats numériques peuvent être obtenus plus facilement pour des valeurs spécifiques de paramètres mais ce sont principalement des approximations numériques. Leur précision dépend des méthodes d'approximation numérique utilisées. Ces méthodes numériques étaient initialement utilisées "à la main" (e.g. les méthodes de Runge-Kutta pour résoudre des équations différentielles ordinaires ont été proposées en 1901) et leur utilisation croit fortement depuis le développement des ordinateurs.

L'utilisation des ordinateurs en modélisation en écologie a atteint un point où certains auteurs parlent de "computational ecology" comme une science émergente (Petrovskii & Petrovskaya, 2012). L'émergence de "computational ecology" concerne à la fois la modélisation prédictive et conceptuelle. En modélisation conceptuelle, de nouvelles voies de recherches ont été ouvertes grâce aux simulations numériques. Un exemple est l'émergence des modèles (stochastiques) individus-

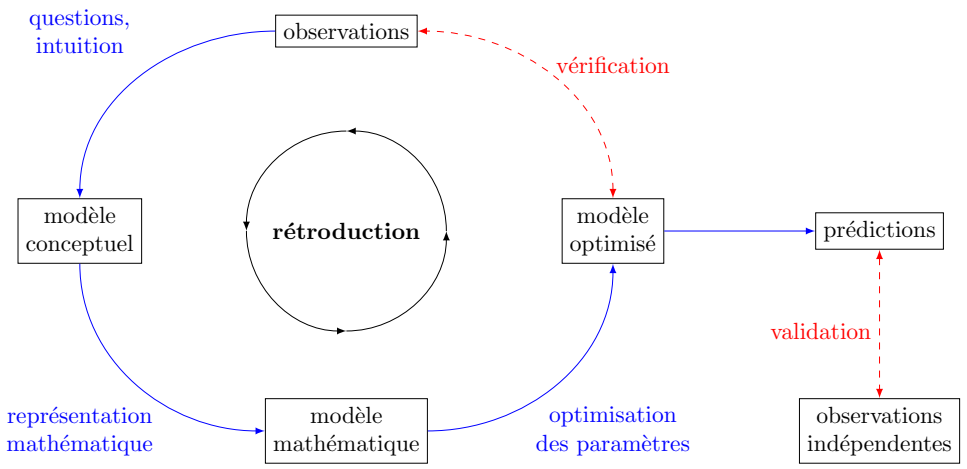

Figure 9.3. Méthode de modélisation prédictive selon Anderson (2010, modifié). Les étapes en bleu correspondent au chemin classique de constuction et d'utilisation d'un modèle. Les étapes en rouge correspondent à la comparaison du modèle aux données.

centrés (DeAngelis & Grimm, 2014) qui prennent en compte un très grand nombre d'individus en interaction (pour un exemple sur la formation des bancs de poissons, voir Accolla *et al.*, 2015). Un autre exemple est la possibilité d'étudier un nombre significatif (plusieurs milliards) de réseaux d'interaction possibles entre des dizaines d'espèces (pour les réseaux trophiques, voir Gross *et al.*, 2009).

L'utilisation massive de simulations numériques augmente le risque pour le modélisateur d'être induit en erreur par "l'efficacité déraisonnable des mathématique" (Wigner, 1960, Anderson, 2005, 2010). Les objets mathématiques (e.g. modèles, fonctions) ne sont pas les objets (e.g. organismes, interactions biotiques) qu'ils visent à représenter. Ce point critique doit être gardé à l'esprit à chaque fois que les résultats du modèles sont reliés aves le système modélisé (interpretation, validation, figure 9.3). En effet, un modèle peut être une description précise d'un jeu de données pour des raisons purement statistiques, i.e. la complexité du modèle (nombre de variables et de paramètres) lui permet de reproduire n'importe quel jeu de données après estimation des paramètres. Le risque est de croire que le modèle est un description appropriée du système (il prend en compte tous ses processus clés) alors qu'on observe juste un artéfact de sur-paramétrisation. Ainsi, le choix de la complexité d'un modèle est un point toujours sujet à débat (Evans *et al.*, 2013). Un autre point de débat est sur la façon de faire collaborer des chercheurs de différents domaines scientifiques (biologie et mathématiques) et avec des approches différentes (tendance vers une description détaillée vs. vers la simplicité) doivent interagir lors de la construction du modèle (Flynn, 2005).

La méthode de modélisation prédictive décrite par la figure 9.3 met en valeur l'importance de la

vérification et de la validation du modèle avec des données empiriques. Une étape supplémentaire est l'analyse mathématique du modèle lui-même, afin de mieux comprendre pourquoi il reproduit ou non les données et quelles seraient ses prédictions en dehors de sa gamme de validation. Cependante, une méta-analyse de 153 modèles aquatiques mécanistes indique que la majorité de ces modèles opérationnels n'ont pas été validés, et qu'aucune analyse de sensibilité de leur prédictions n'a été faite (Arhonditsis & Brett, 2004). En effet, une analyse de sensibilité numérique (comme la robustesse à des changements de valeurs de paramètres) peut être très coûteuse en temps de calcul pour des modèles opérationnels complexes. De plus, ces modèles ne peuvent pas être étudiés mathématiquement comme les modèles simples. Celà souligne l'intérêt des petits modèles théoriques simples. A partir de leurs propriétés mathématiques et de leurs résulats génériques, on peut avoir des indices pour comprendre les prédictions de modèles plus complexes (Baklouti *et al.*, 2006b,a).

9.3.2 La formulation mathématique d'un processus

Comme ce sont des systèmes complexes, même l'environnement physique et chimique est représenté de façon simplifiée dans un modèle. Cependant, comme souligné par Flynn (2005): *"The description of the physical environment is also simplistic, but physics and chemistry are sciences blessed with laws so at least implications can be more carefully considered."*. La notion de "lois" est utilisée ici en comparaison avec la biologie où il n'existe rien comme les lois du mouvement de Newton en mécanique classique. Celà veut dire que le problème avec la physique et la chimie est principalement due au nombre de composants (atomes) du système et à la résolution utilisée dans les simulations numériques (comme pour les prédictions météo). A l'inverse, les systèmes biologiques sont trop complexes à nos échelles d'intérêt (individu, population) pour être décrits par des lois. Ainsi, de multiples modèles peuvent décrire un même phénomène.

La prédation par exemple, peut être modéliser par de nombreuses formulations de la réponse fonctionnelle (pour une synthèse, voir Jeschke *et al.*, 2002, Gentleman *et al.*, 2003). Le concept de réponse fonctionnelle a été d'abord introduit par Solomon (1949). Holling (1965) a proposé une classification pour les réponses fonctionnelles qui dépendent uniquement de l'abondance de proies, mais des réponses fonctionnelles prédateur-dépendentes et ratio-dépendentes existent également (Ivlev, 1955, Beddington, 1975, DeAngelis *et al.*, 1975, Arditi & Ginzburg, 1989, DeAngelis, 2013). Ces différents types de réponses fonctionnelles correspondent à des hypothèses différentes sur le phénomène de prédation. Il n'est donc pas contre-intuitif qu'elles prédisent des dynamiques différentes dans un modèle (Oaten & Murdoch, 1975, Scheffer & de Boer, 1995, Cantrell & Cosner, 2001).

Etonnement, des prédictions différentes peuvent également être obtenues à partir de fonctions qui ont les même propriétés (e.g. pour la prédation, ce sont des réponses fonctionnelles du même type) et qui décrivent les données empiriques avec la même précision. Ce phénomème est appelé sensibilité structurelle (Fussmann & Blasius, 2005, Cordoleani *et al.*, 2011). La sensibilité structurelle concerne à la fois des changements qualitatifs (stabilité structurelle, *sensu* Kuznetsov, 2004) et quantitatifs (e.g. valeurs d'équilibre) dans les prédictions du modèle. La sensibilité structurelle a été étudiée dans des modèles simples avec quelques variables d'états, principalement dans le contexte des interactions prédateur-proie (Myerscough *et al.*, 1996, Wood & Thomas, 1999, Gross *et al.*, 2004, Fussmann & Blasius, 2005, Poggiale *et al.*, 2010, Cordoleani *et al.*, 2011, Adamson & Morozov, 2012, 2014). D'un point de vue opérationnel, la sensibilité structurelle pose des problèmes car des prédictions différentes sont obtenues à partir de modèles basés sur des hypothèses similaires (propriétés mathématiques communes) et qui peuvent être considérés *a priori* comme proches (ils décrivent les mêmes données). De plus, la sensibilité structurelle peut avoir un impact plus important sur les dynamiques du modèle que la sensibilité aux paramètres (Cordoleani *et al.*, 2011). Cependant, la sensibilité aux paramètres est plus souvent étudiée dans les analyses de sensibilité de modèles (Arhonditsis & Brett, 2004).

9.3.3 Diversité, réseaux d'interaction et fonctionnement des écosystèmes

La diversité des espèces et des traits fonctionnels dans un écosystème influence l'intensité de processus comme la fixation de carbone, ainsi que la taille et la variabilité temporelle des populations. Afin d'estimer ces relations diversité-fonctionnement, différentes expérience de biodiversité ont été réalisées sur des plantes terrestres (Hector *et al.*, 1999, Tilman *et al.*, 1997, 2001, 2006) ou dans des microcosmes controlés (Naeem *et al.*, 1994, Naeem & Li, 1997, McGrady-Steed *et al.*, 1997). Jiang & Pu (2009) ont fait une synthèse des récentes études empiriques sur le sujets. Dans ces études, de nombreux biais (Huston, 1997) et facteurs de confusion altèrent souvent l'interprétation des résultats (Hector, 1998, Loreau, 1998, Loreau & Hector, 2001). Bengtsson (1998) argumente que ces difficultés vienne du fait que la biodiversité est une propriété abstraite et aggégée du système.

En parallèle de ces études empiriques, des recherches théoriques ont également été réalisées sur le lien entre la diversité et le fonctionnement des écosystèmes. L'hypothèse d'assurance suggère qu'une diversité élevée diminue la variabilité de la productivité de l'écosystème en augmentant la probabilité d'avoir une espèce performante dans n'importe quelle condition environnementale (Yachi & Loreau, 1999). Cependant, un maximum de n expèces peuvent coexister avec n ressources limitantes dans un environnement homogène (principe d'exclusion competitive, Loreau, 2010), ce qui empècherait un accroissement infini de la diversité.

Allant au-delà de la diversité, d'autres études ont étudié comment le fonctionnement des écosystèmes est influencé par la complexité du réseau d'interactions (nombre d'espèces et nombre d'interactions). Cette complexité était d'abord considérée comme stabilisant les communautés écologiques (MacArthur, 1955). L'opposé a ensuite était défendu par May (1972, 1973). Le travail pionnier de May a conduit à un long débat sur est-ce qu'un système complexe sera plus ou moins stable qu'un système plus simple. Ce débat est toujours ouvert (May, 1999, McCann, 2000, Loreau, 2010), principalement parce qu'il y a de nombreuses définitions de la stabilité et de la complexité en écologie (Holling, 1973, Pimm, 1984, Grimm & Wissel, 1997). Un autre aspect de la complexité des réseaux d'interactions est l'existence de clusters de communautés avec beaucoup d'interactions. Ces clusters sont connus pour affecter la dynamique des réseaux trophiques (Stouffer & Bascompte, 2010, 2011). Cependant, la définition mathématique formelle et la détection de ces communautés d'interactions sont toujours le sujet de recherches en cours (Fortunato, 2010).

Les travaux mentionnés dans cette sous-section sont motivés par des questions sur le rôle de la diversité (complexité) en écologie. En conséquence, si la diversité a un impact important sur la dynamique du système, elle devrait être prise en compte dans un modèle. Ne pas le faire créerait le risque de négliger des propriétés importantes du système écologique qui est étudié. Cependant, étudier des modèles écologiques complexes posent certains problèmes soulignés dans les sous-sections précédentes. De plus, la dynamique de réseaux complexes d'interactions peut être presque impossible à étudier, car même des modèles simples peuvent prédire des dynamiques complexes (Kuznetsov & Rinaldi, 1996, Kooi & Boer, 2001), y compris du chaos déterministe (Hastings & Powell, 1991, Rinaldi & De Feo, 1999).

9.3.4 Résilience et états stables multiples

La résilience a d'abord été définie par Holling (1973): *"Resilience determines the persistence of relationships within a system and is a measure of the ability of these systems to absorb changes of state variables, driving variables, and parameters, and still persist."*. Cette définition reste un concept abstrait, car dans un contexte opérationnel la plupart des points de la définition ("changements", "variables", "paramètres", "persistence") peuvent être définis et quantifiés d'une infinité de façons. Cependant, le concept de résilience est utilisé pour faire référence à la capacité d'un système à se maintenir et à retrouver son état initial après une perturbation. L'étude de la résilience des écosystème est en pleine croissance, en raison de son importance pour les prises de décisions et les politiques environnementales (Scheffer *et al.*, 2009, 2012).

Certaines propriétés d'un système rattachées au concept de résilience sont bien définies d'un point de vue mathématique. Un modèle mathématique peut être charactérisé par le comportement

asymptotique des dynamiques su'il prédit. Ces dynamiques peuvent converger sur des états stables (e.g. équilibres, oscillations) que le système va maintenir au cours du temps. Un modèle peut avoir plusieurs états stables, une situation appelée états stables multiples (ou alternatifs) en écologie (Beisner *et al.*, 2003, Knowlton, 2004). L'existence de ces états stables multiples dans un système subissant une perturbation peut mener au phénomène d'hystéresis. L'hystéresis signifie que la quantité de changement requise pour remetter le système dans son état original est de plus grande amplitude que la perturbation initiale. Cette situation a lieu quand le système s'est déplacé d'un état stable vers un autre à cause de la perturbation (e.g. Ludwig *et al.*, 1978).

9.4 Cadre de la thèse

Le travail de recherche présenté dans cette thèse lie les quatre problématiques détaillées dans la section précédente. Ces différentes problématiques peuvent être regroupées par la question suivante: *Quel est l'impact des choix faits lors de la construction du modèle sur les prédictions de la dynamique des systèmes écologiques et les informations qu'elles fournissent sur la résilience de ces systèmes?*

Le fil conducteur de cette thèse est l'étude de la sensibilité structurelle à travers l'exemple de la formulation de la prédation dans différents modèles écologiques. Les études précédentes sur la sensibilité structurelle se sont focalisées par simplicité sur des modèles qui: (i) ont un seul état stable, (ii) ont quelques variables d'états, et (iii) font des hypothèses simples sur le métabolisme des individus (Myerscough *et al.*, 1996, Gross *et al.*, 2004, Fussmann & Blasius, 2005, Poggiale *et al.*, 2010, Cordoleani *et al.*, 2011, Adamson & Morozov, 2012). Ces trois simplifications sont relaxées durant cette thèse, afin de voir si la sensibilité structurelle est un problème spécifique à des modèles théoriques simples ou si elle peut affecter également des modèles écologiques complexes. Les modèles étudiés dans cette thèse sont plus ou moins complexes, ce qui permet une compréhension mathématique plus ou moins profonde de leur dynamique. De plus, ces modèles couvrent différents aspects de la complexité en écologie: la complexité des réseaux d'interactions (approche holiste, dizaines de variables d'états) et la complexité du métabolisme interne des organismes (approche réductioniste, à travers la théorie des Budgets d'Energie Dynamiques). Enfin, ces modèles peuvent présenter des dynamiques complexes, y compris la coexistence de plusieurs états stables.

Le prochain chapitre introduit certains outils mathématiques pour étudier des modèles de populations à travers des exemples d'application (figure 9.4). Il se termine par une analyse de jeux de données publiés qui montrent pourquoi la représentation mathématique d'un processus comme la prédation reste incertaine. La seconde partie de cette thèse présente une étude détaillée de

la sensibilité structurelle. Cette étude commence par l'impact de la sensibilité structurelle sur la dynamique et la résilience d'un modèle prédateur-proie. Les résultats sont expliqués par une analyse mathématique plus détaillée dans le contexte de la théorie des bifurcations (chapitre 4). Ensuite, le modèle prédateur-proie est étendu pour modéliser des réseaux trophiques complexes. La dynamique de ces réseaux est analysée en fonction de la formulation du modèle et de la complexité du réseau d'interactions (chapitre 5). La troisième partie de la thèse explore des façons de gérer la sensibilité structurelle. Le chapitre 6 propose des méthodes pour quantifier la sensibilité structurelle dans des modèles avec des dynamiques complexes comme des états stables multiples et le phénomène d'hystéresis. En plus de cette approche mathématique, le chapitre 7 teste si l'incorporation de certains détails appropriés dans la représentation du métabolisme des individus peut atténuer l'effet de la sensibilité structurelle. Les conclusions et implications de tous les chapitres sont résumés dans le dernier chapitre, qui se termine avec des perpectives pour des recherches futures et des réflexions personnelles sur la modélisation en écologie.

9.5 Résumé de la thèse

La question générale qui guide le travail présenté dans cette thèse est: *Quel est l'impact des choix faits lors de la construction du modèle sur les prédictions de la dynamique des systèmes écologiques et les informations qu'elles fournissent sur la résilience de ces systèmes?* Le travail de recherche effectué pour répondre à cette question est résumé dans la figure 9.5. Le chapitre 3 montre qu'un changement quantitativement mineur dans la formulation d'un modèle peut affecter les dynamiques qualitatives qu'il prédit (sensibilité structurelle). Des incertitudes sur le type et le nombre d'états stables apparaissent à cause de changements de type et de localisation des bifurcations, qui se propagent en une incertitude dans la résilience prédite du système en cas de perturbations externes. Ces changements de dynamiques du modèle peuvent être expliqués dans le contexte de la théorie des bifurcations en tournant le problème de formulation du modèle en un problème de paramétrisation du modèle (chapitre 4). Pour aller au-delà de cette analyse qualitative, le chapitre 6 propose de nouvelles méthodes pour quantifier la sensibilité d'un modèle quand plusieurs états stables coexistent. Ces questions génériques (chapitres 3, 4 et 6) sont illustrées à travers un exemple de modèle prédateur-proie avec mortalité densité-dépendante. En parallèle de ces développements mathématiques (côté gauche de la figure 9.5), des questions écologiques sur la complexité des systèmes écologiques et son intégration dans les modèles mathématiques sont également abordées (côté droit de la figure 9.5). Le chapitre 5 décompose les effets respectifs de la sensibilité structurelle et de la complexité trophique (nombre d'espèces et d'interactions) dans des modèles de réseaux

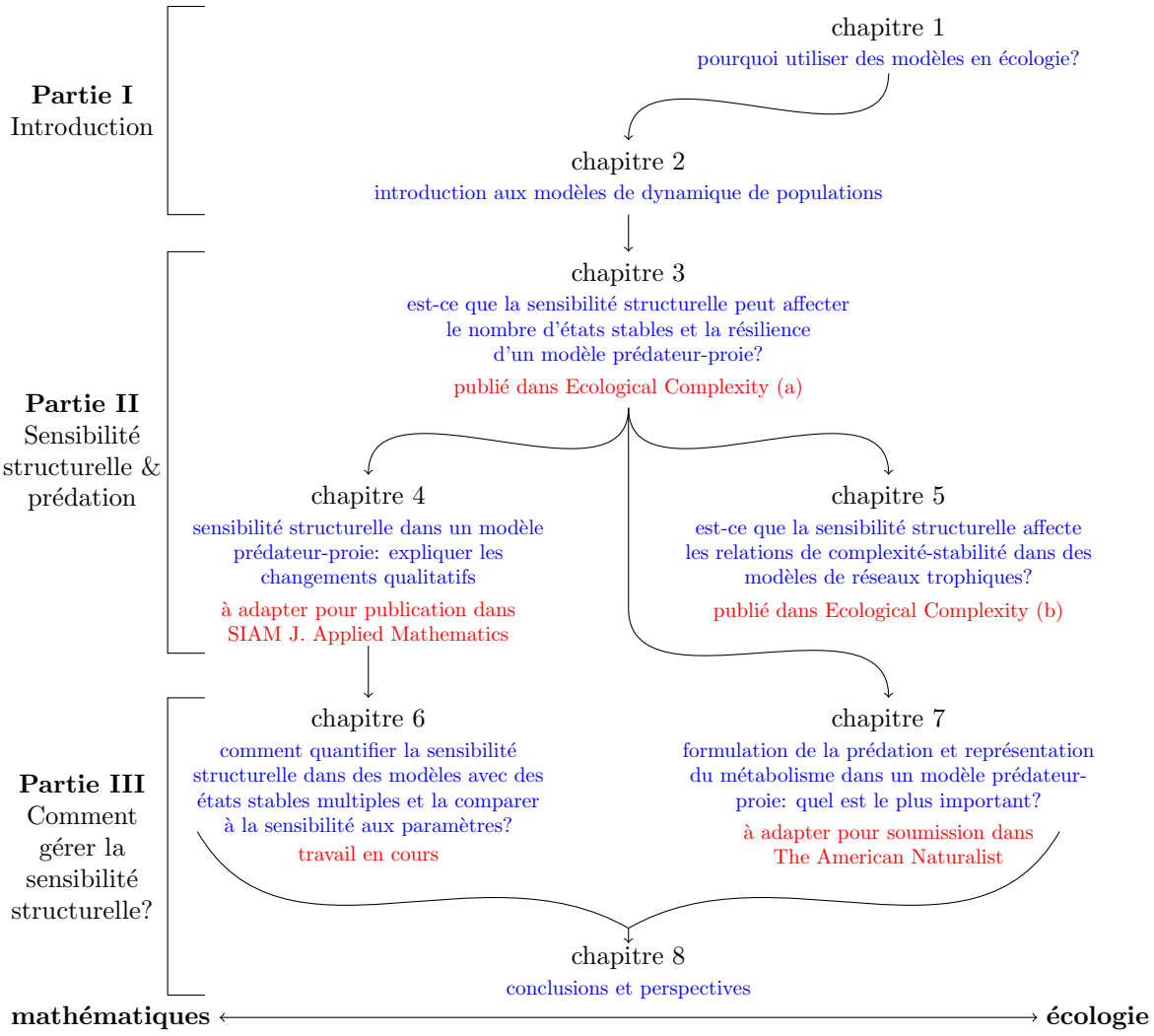

Figure 9.4. Cadre de la thèse. Pour chaque chapitre, la question associée (bleu) et l'état actuel de ma recherche sur le sujet (rouge) sont indiqués. Les chapitres sont présentés en fonction de leur position relative entre les mathématiques (gauche) et l'écologie (droite). Cette localisation est purement subjective et personnelle: tous les chapitres peuvent être des mathématiques du point de vue du biologiste expérimental, alors qu'ils peuvent tous être de l'écologie du point de vue du mathématicien. Voir section 9.4 pour plus d'informations.
Conseils pour lire cette thèse (flèches): à travers des exemples en écologie, le chapitre 2 résume les conceptsde systèmes dynamiques et de bifurcations requis pour la suite. Le lecteur familier avec ces notions peut passer rapidement sur ce chapitre. A l'inverse, le lecteur intéressé par les applications de ces notions en écologie peut comprendre la plupart d'entre elles à l'aide des figures. Le travail présenté dans le chapitre 3 est la base de tous les sujets explorés dans les chapitres suivants. Les chapitres 4 et 6 sont orientés vers des aspects mathématiques et leur lecture n'est pas nécessaire pour le lecteur principalement intéressé par les applications en écologie. Concernant les applications en écologie, les chapitres 3 à 5 présentent une analyse détaillée de la sensibilité structurelle dans des modèles de complexité variable (partie II), et les chapitres 6 et 7 explorent des possibilités pour gérer cette sensibilité structurelle en modélisation en écologie (partie III). Les conclusions et implications de tous les chapitres sont résumées dans le dernier chapitre, qui se termine avec des réflexions personnelles et des perspectives pour les recherches futures.

trophiques. Cette approche holiste va vers une intégration de plus de composantes du système (espèces). A l'inverse, l'approche réductionniste utilisée dans le chapitre 7 va vers plus détails sur le métabolisme individuel. Si un minimum de détails biologiques sont inclus, les modèles semblent être moins structurellement sensibles (pas d'effet sur le nombre d'états stables). Ceci nous donne des indications pour gérer la sensibilité structurelle dans les modèles biologiques, bien que plus de détails sur le métabolisme signifie également plus de sources possibles d'incertitudes dans la construction des modèles. Ces incertitudes dans la construction des modèles (formulation et paramétrisation d'un processus, complexité du réseau d'interactions, métabolisme et autres hyothèses) viennent du fait qu'en écologie nous traitons avec des systèmes complexes (chapitre 1).

Comme nous traitons avec des systèmes complexes, tout le travail présenté dans cette thèse est simple. Premièrement, il est simple d'un point de vue mathématique: le même travail peut-être réalisé sur des modèles écologiques avec des dynamiques et des bifurcations plus complexes. De plus, beaucoup de systèmes biologiques peuvent être modélisé avec des systèmes lents-rapides (les dynamiques des variables détats ont différentes échelles de temps, e.g. dynamiques prédateur-proie dans Rinaldi & Muratori, 1992, Kooi *et al.*, 1998a, 2002) ou des systèmes par morceaux discontinus (systèmes de Filippov, le formulation du modèle change à travers l'espace des phases, e.g. population exploitée dans Kuznetsov *et al.*, 2003). Incorporer explicitement l'espace ou considérer des populations structurées peut également nécessiter l'utilisation d'équations différentielles aux dérivés partielles. On peut imaginer facilement beaucoup de façon de construire des modèles complexes en considérant de plus en plus d'aspects d'un écosystème. Secondement, le travail présenté dans cette thèse est simple en termes biologiques. La variabilité individuelle est négligée à l'échelle de la population dans tous les modèles considérés. Ces modèles n'incluent aucune répartition spatiale explicite des organismes, ainsi qu'un grand nombre d'autres processus (e.g. recyclege de la matière, évolution) et d'interactions (e.g. mutualisme, parasitisme). En effet, nous avons essayé de garder les choses aussi simples que possibles par rapport au cadre de la thèse et au nombre infini de questions différentes que l'on peut aborder à l'aide de modèles mathématiques.

9.6 Quelques perspectives générales: vers des prédictions plus précises

Le problème avec la modélisation mathématique est que nous pouvons étudier la sensibilité d'un modèle à presque tout: son cadre (e.g. nombre d'espèces, ressources limitantes, espace explicite), les processus inclus (e.g. mortalité, compétition, réserves explicites), leur formulation et leur paramétrisation. Chaque aspect de la sensibilité d'un modèle contient de nombreuses questions

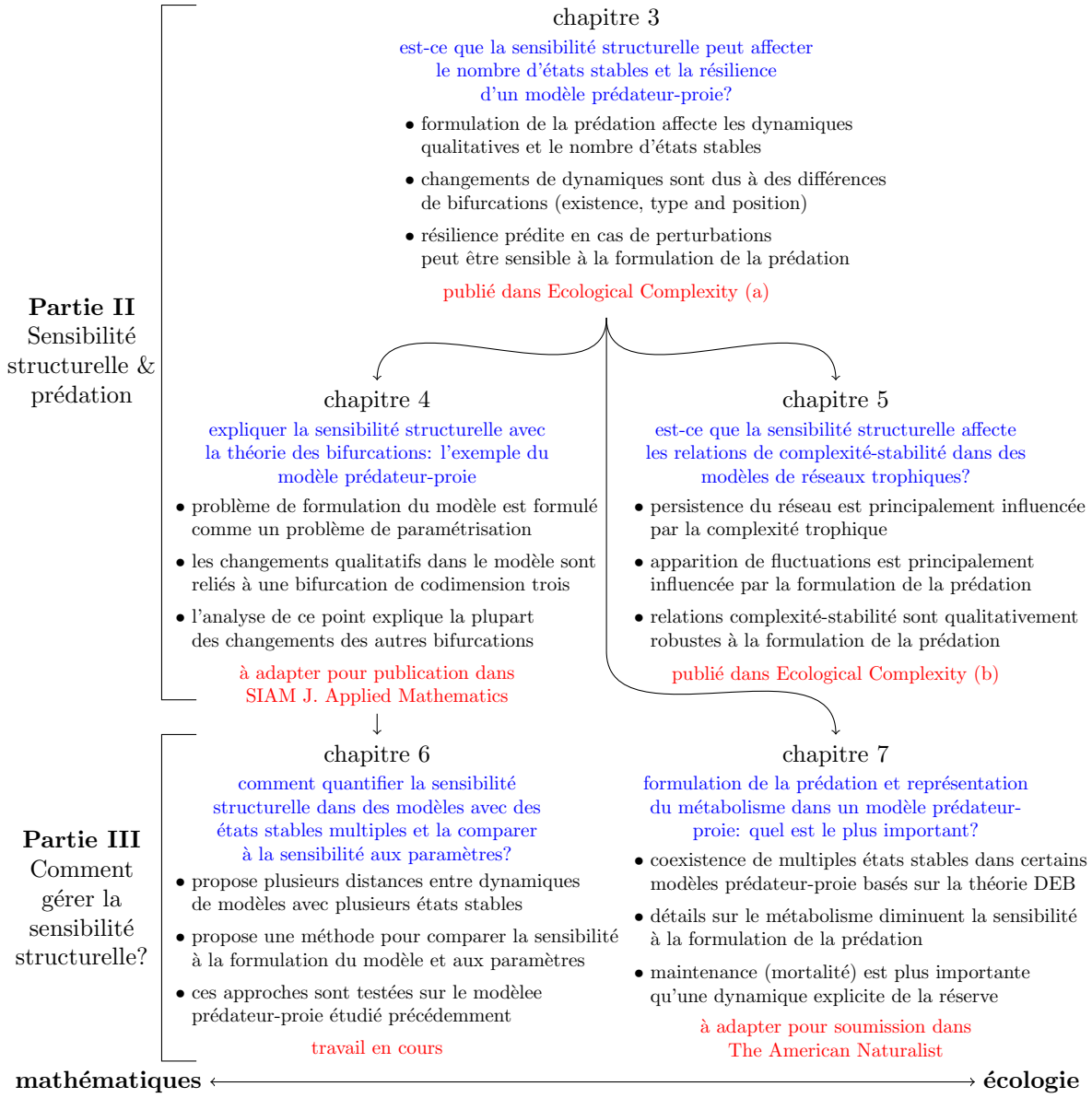

Figure 9.5. Synthèse du travail de recherche présenté dans cette thèse. Pour chaque chapitre, la question abordée (bleu), les réponses principales trouvées (noir) et l'état actuel de ma recherche sur le sujet (rouge) sont indiqués. Comme dans la figure 9.4, les chapitres sont présentés selon leur localisation relative (et subjective) entre l'écologie et les mathématiques.

sous-jacentes, comme souligné tout au long de cette thèse. Cet aspect infini de la modélisation est élégamment illustré par une question que m'a posée SALM Kooijman durant le 8ème cours international sur la théorie des Budgets d'Energie Dynamiques: *"You told us that you compared the dynamics predicted by two different functions. Then, you said that now you are doing this with three. But you can also do it with four and five, and my question is: are you going to do this all your life?"*[4]. Bien sûr ma réponse est non. J'ai utilisé quelques fonctions comme exemples parmi les plus utilisées afin de répondre aux questions que je me posais.

Il y a plusieurs années au "jardin d'enfants" (disons quand j'étais étudiant en Licence), j'étais dans cette frénésie où je voulais tout savoir. A cette époque, je pensais que la science cétais trouver les bonnes réponses. Maintenant, je pense que la science c'est plutôt poser les bonnes questions. Comme une infinité de questions peuvent être posées, on peut trouver une infinité de réponses et accumuler une quantité infinie de savoir. La plupart du savoir est fait d'informations spécifiques (e.g. "l'espèces A croit à un taux X"), alors que le savoir le plus intéressant à mon opinion nous donne une explication à ces informations spécifiques (e.g. "le taux de croissance de l'espèce A est une fonction des facteurs B et C") ou les utilise pour répondre à des questions plus générales (e.g. "toutes les espèces faisant le processus A doivent intéragir avec une espèce faisant le processus B pour croître") (chapitre 19 dans Schimel, 2012).

C'est ce dernier type de savoir que cette thèse essaye de fournir. Par exemple, les chapitres 3 et 4 ne traitent pas de la sensibilité d'un modèle donné à un processus donné. Ces chapitres présentent le premier (aussi loin que je sache) exemple de modèle en écologie où un certain type d'incertitude dans la formulation d'un modèle (des fonctions quantitativement proches et ayant les mêmes propiétés générales) se répercute en un certain type d'incertitude sur les prédictions du modèle (nombre d'états stables, résilience) qui est important pour les prédiction opérationnelles et des problèmes de gestion. Maintenant, je ne suis pas en train de dire que nous devrions tester cette sensibilité dans tous les modèles connus. La plupart des modélisateurs ne peuvent pas le faire dans leur propre modèle (il y a une infinité d'autres questions à traiter) mais souhaiteraient probablement savoir si cette sensibilité à des chances d'être importante dans leur modèle. Ainsi, on peut se demander si cette sensibilité se retrouve dans d'autres types de modèles (e.g. réseaux trophiques dans le chapitre 5) ou si il y a des contre-exemples où on ne retrouve pas cette sensibilité (e.g. chapitre 7 avec des modèles basés sur la théorie des Budgets d'Energie Dynamiques). Si quelqu'un souhaite quantifier la sensibilité structurelle dans un modèle, les outils mathématiques appropriés sont nécessaires (e.g. chapitre 6).

Toutes les perspectives de recherches futures mentionnées dans le paragraphe et les chapitres

[4] A cause de mémoire humaine, la citation n'est pas rigoureusement exacte mais son esprit est là.

précédents peuvent être regroupés sous l'objectif d'améliorer les prédictions des modèles. Cette idée lie la recherche théorique et appliquée en modélisation. Les études théoriques sont faites pour aborder des questions générales (e.g. *"Will a large complex system be stable?"*, May, 1972) et essayer d'obtenir des résultats génériques. Ces résultats ne doivent pas être sensible à un petit changement dans la construction d'un modèle afin de fournir un savoir significatif et une théorie intéressante. De plus, la recherche théorique est aussi orientée vers l'amélioration des prédictions de modèles pour la modélisation appliquée (i.e. opérationnelle) (figure 9.6). Cette amélioration passe par le développement de formulations de modèle dérivées d'une représentation mécaniste des processus sous-jacents (e.g. Poggiale *et al.*, 2010, Cordoleani *et al.*, 2013, Accolla, 2015). Ces formulations peuvent être plus appropriées dans certaintes situations que des formulations plus classiques, car elles incluent des processus qui sont importants dans certains systèmes (e.g. co-limitation, espace, formation de bancs). Cependant, ces formulations restent une approximation d'un système biologique complexe. Ainsi, des études générales sur la sensibilité des modèles sont toujours requises. De telles études pourraient explorer l'effet de la sensibilié structurelle sur le nombre d'états stables dans des réseaux trophiques complexes (perspectives des chapitres 3 à 5) ou sur l'interaction entre la complexité trophique et les détails sur le métabolisme (perspectives des chapitres 5 et 7). Ces analyses peuvent être renforcées par l'utilisation de méthodes quantitatives pour estimer la sensibilité des modèles (perspectives du chapitre 6). Ces méthodes quantitatives pourraient être utiles pour concevoir des expérimentations couplées avec de la modélisation et orientées vers une diminution des incertitudes dans les prédictions des modèles.

9.7 Réflexions personnelles sur la modélisation

Errare humanum est.

La première réflexion que je souhaite présenter est plus sur la recherche en modélisation que la modélisation elle-même. De récentes synthèses bibliographiques soulignent toujours le manque de validation, d'analyses de sensibilité et de description des hypothèses dans la plupart des études de modélisation (Corley *et al.*, 2014, Gregr & Chan, 2014). Ainsi, les conclusions de ces études pourraient être incertaines et nous n'avons aucune idée de leur robustesse. Estimer la robustesse des résultats d'un modèle prend du temps et est au mieux brièvement mentionnée dans un article. Publier une description détaillée de la construction d'un modèle et de sa robustesse n'est pas attirant pour la plupart des lecteurs. En effet, le taux de citation des articles en biologie est corrélé négativement avec leur contenu en équations (Fawcett & Higginson, 2012). Ce paradox a été décrit comme *"the incompatibility between the inherent complexity of social-ecological systems*

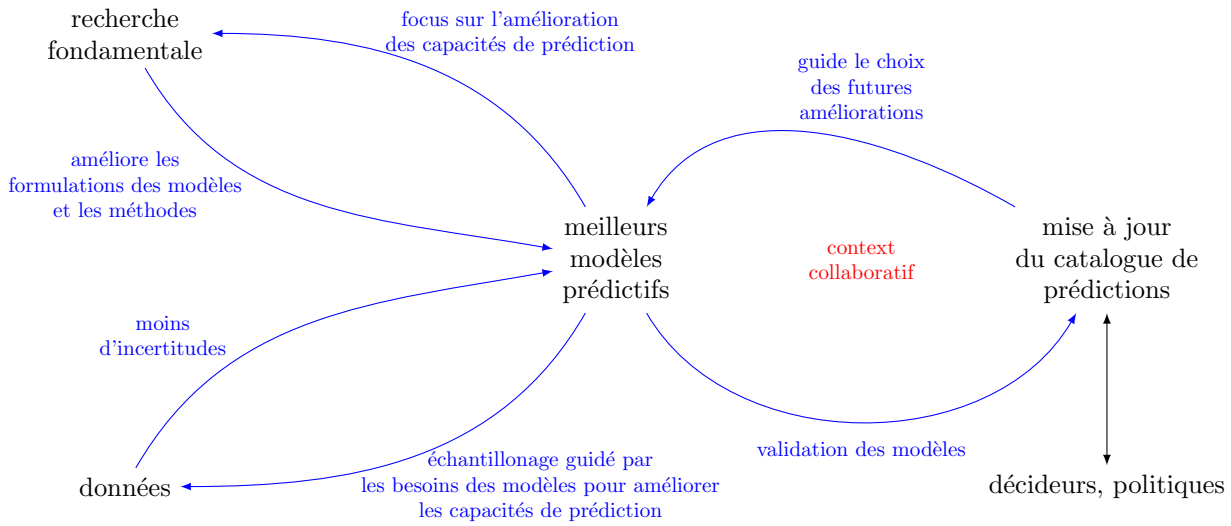

Figure 9.6. Stratégie pour améliorer la recherche sur la prédictabilité en écologie proposée par Petchey *et al.* (2015, modifiée). Les interactions entre "recherche fondamentale" et "données" ne sont pas explicitement représentées et sont lieu via de "meilleurs modèles prédictifs".

and the focus of scientific publishing on concise, interesting results" (Gregr & Chan, 2014). Cet intérêt pour des résulats concis et intéressants est l'esprit même de la science (le principe du rasoir d'Occam, voir la section 2 dans Jusup *et al.*, in press, pour une introduction en biologie) et de l'esprit humain, qui lutte en permanence pour résumer une énorme quantité d'information. Un tel résumé est nécessaire pour partager les informations entre scientifiques. Cependant, une description détaillée d'un modèle et de la robustesse de ses résultats est nécessaire (au moins en annexes, où le nombre d'équations n'a pas d'influence sur la lecture par des non-spécialistes, Fawcett & Higginson, 2012) afin d'éviter une accumulation d'articles faisant des conclusions attirantes qui ne peuvent pas être objectivement discutées. De telles précautions sont importantes dans un but de rigueur scientifique, mais aussi pour estimer la vraisemblance des prédictions utilisées pour aider les décideurs qui doivent gérer des systèmes socio-écologiques complexes.

Des systèmes complexes n'ont pas forcément besoin d'être compris pour faire des prédictions précises de leur état futur (Breiman, 2001). Cependant, en faisant des prédictions nous essayons souvent de comprendre le système lui-même (Schmueli, 2010). La même observation peut être expliquée par différents arguments mathématiques (i.e. différents modèles) en raison de l'"efficacité déraisonnable des mathématiques" (Wigner, 1960). Ainsi, des modèles complexes doivent être utilisés en même temps que des modèles plus simples afin d'avoir une meilleure compréhension du modèle en tant qu'objet mathématique. Un modèle mathématique ne peut pas faire de prédiction univoque "à la Newton". Des études comme cette thèse souligne à quel point les prédictions

de systèmes écologiques complexes sont incertaines. Cependant, des prédiction incertaines ne signifient pas que nous devrions arrêter d'utiliser des modèles mathématiques. En effet, les modèles peuvent toujours prédire l'état qualitatif d'un système naturel (e.g. Benincà *et al.*, 2015). De plus, des modèles simples sont parfois suffisant pour gérer d'importants problèmes socio-écologiques comme des invasions d'espèces (Hastings *et al.*, 2006, Hall & Hastings, 2007) ou des épidémies (May, 2004). Enfin, des prédictions quantitatives restent valablent pour des prédiction à court term, le "court terme" étant défini par exemple par l'horizon de prédiction (Petchey *et al.*, 2015). Cette mesure quantitative de la capacité d'un modèle à prédire des dynamiques qui sont pourtant sensibles aux conditions initiales est un exemple des outils qui pourraient aider la recherche en modélisation théorique et opérationnelle à aller vers des prédictions plus précises (figure 9.6).

Pour conclure cette thèse sur la modélisation de systèmes écologiques complexes, je souhaite rappeler que n'importe quel modèle d'un système n'est pas le système. Le modèle est une vision que l'esprit humain a du système dans un contexte donné (figure 1.1a). Comme le modèle est construit par un esprit humain, la seule limite est notre capacité à conceptualiser et comprendre le système que nous voulons modéliser. En modélisant le système, les deux approches holiste et réductionniste négligent certaines propriété du système. Ainsi, dans une perspective Newtonienne, chaque tentative de modélisation va échouer. Ceci n'est pas un échec de la modélisation et des mathématiques eux-mêmes, mais un échec de l'esprit humain qui ne peut pas comprendre tout son environnement dans sa globalité. En effet, l'esprit humain est basé sur le cerveau humain, qui a sa propre "capacité limite" en raison de sa dimension finie. Ce cerveau simplifie l'information qu'il reçoit en faisant en permanence des modèles conceptuels et statistiques. Une petite partie de ces modèles sont formalisés en des termes mathématiques par le scientifique qui veut répondre à une question donnée. En effet, en modélisation comme dans l'histoire connue de la vie sur Terre, tout est une question de besoins et d'objectifs.

Bibliography

Accolla, C. 2015. *Modélisation de la formation des bancs de poissons : Évaluation des conséquences de l'agrégation des individus dans un système proies-prédateurs à différentes échelles*. Ph.D. thesis. Aix-Marseille Université, 132 pp.

Accolla, C, Nerini, D, Maury, O, Poggiale, JC. 2015. Analysis of functional response in presence of schooling phenomena: An IBM approach. *Progress in Oceanography*, **134**, 232–243.

Adamson, MW, Morozov, AY. 2012. When can we trust our model predictions? Unearthing structural sensitivity in biological systems. *Proceedings of the Royal Society of London A*, **469**(2149).

Adamson, MW, Morozov, AY. 2014. Defining and detecting structural sensitivity in biological models: developing a new framework. *Journal of Mathematical Biology*, **69**, 1815–1848.

Akçay, E, Roughgarden, J. 2007. Negociation of mutualism: rhizobia and legumes. *Proceedings of the Royal Society of London B*, **274**, 25–32.

Aldebert, C, Nerini, D, Gauduchon, M, Poggiale, JC. 2016a. Does structural sensitivity alter complexity-stability relationships? *Ecological Complexity*, **28**, 104–112. doi:10.1016/j.ecocom.2016.07.004.

Aldebert, C, Nerini, D, Gauduchon, M, Poggiale, JC. 2016b. Structural sensitivity and resilience in a predator-prey model with density-dependent mortality. *Ecological Complexity*, **28**, 163–173. doi:10.1016/j.ecocom.2016.05.004.

Allesina, S, Alonso, D, Pascual, M. 2008. A general model for food web structure. *Science*, **320**, 658–661.

Anderson, TR. 2005. Plankton functional type modelling: running before we can walk? *Journal of Plankton Research*, **27**(11), 1073–1081.

Anderson, TR. 2010. Progress in marine ecosystem modelling and the "unreasonable effectiveness of mathematics". *Journal of Marine Systems*, **81**, 4–11.

Anderson, TR, Gentleman, WC, Sinha, B. 2010. Influence of grazing formulations on the emergent properties of a complex ecosystem model in a global ocean general circulation model. *Progress in Oceanography*, **87**, 201–213.

Arditi, R, Ginzburg, LR. 1989. Coupling in predator-prey dynamics: ratio-dependence. *Journal of Theoretical Biology*, **139**, 311–326.

Arhonditsis, GB, Brett, MT. 2004. Evaluation of the current state of mechanistic aquatic biogeochemical modeling. *Marine Ecology Progress Series*, **271**, 13–26.

Arnold, V. 1974. *Equations différentielles ordinaires (Ordinary differential equations, in French).* Mir, Moscow. 268 pp.

Baer, SM, Kooi, BW, Kuznetsov, YuA, Thieme, HR. 2006. Multiparametric bifurcation analysis of a basic two-stage population model. *SIAM Journal on Applied Mathematics*, **66**(4), 1339–1365.

Baklouti, M, Faure, V, Pawlowski, L, Sciandra, A. 2006a. Investigation and sensitivity analysis of a mechanistic phytoplankton model implemented in a new modular numerical tool (Eco3M) dedicated to biogeochemical modelling. *Progress in Oceanography*, **71**(1), 34–58.

Baklouti, M, Diaz, F, Pinazo, C, Faure, V, Quéguiner, B. 2006b. Investigation of mechanistic formulations depicting phytoplankton dynamics for models of marine pelagic ecosystems and description of a new model. *Progress in Oceanography*, **71**(1), 1–33.

Baldauf, SL. 2003. The deep roots of eukaryotes. *Science*, **300**, 1703–1706.

Baldauf, SL. 2008. An overview of the phylogeny and diversity of eukaryotes. *Journal of Systematics and Evolution*, **46**(3), 263–273.

Bascompte, J. 2008. Mutualistic networks. *Frontiers in Ecology and the Environment*, **7**(8), 429–436.

Bayle, S, Monestiez, P, Guinet, C, Nerini, D. 2015. Moving toward finer scales in oceanography: Predictive linear functional model of Chlorophyll *a* profile from light data. *Progress in oceanography*, **134**, 221–231.

Bazykin, AD. 1998. *Nonlinear dynamics of interacting populations*. World Scientific, Singapore. 193 pp.

Bazykin, AD, Kuznetsov, YuA, Khibnik, AI. 1985. *Bifurcation diagrams of planar dynamical systems*. Research Computing Center, USSR Academy of Sciences, Pushchino, Moscow Region. *in Russian*.

Becks, L, Hilker, FM, Malchow, H, Jürgens, K, Arndt, H. 2005. Experimental demonstration of chaos in a microbial food chain. *Nature*, **435**(30), 1226–1229.

Beddington, JR. 1975. Mutual interference between parasites or predators and its effect on searching efficiency. *Journal of Animal Ecology*, **44**(1), 331–340.

Beisner, BE, Haydon, DT, Cuddington, K. 2003. Alternative stable states in ecology. *Frontiers in Ecology*, **1**(7), 376–382.

Bengtsson, J. 1998. Which species? What kind of diversity? Which ecosystem function? Some problems in studies of relations between biodiversity and ecosystem function. *Applied Soil Ecology*, **10**, 191–199.

Benincà, E, Huisman, J, Heerkloss, R, Jöhnk, KD, Branco, P, Van Nes, EH, Scheffer, M, Ellner, SP. 2008. Chaos in a long-term experiment with a plankton community. *Nature Letters*, **451**(14), 822–825.

Benincà, E, Ballantine, B, Ellner, SP, Huisman, J. 2015. Species fluctuations sustained by a cyclic succession at the edge of chaos. *Proceedings of the National Academy of Sciences of the United States of America*, **112**(20), 6389–6394.

von Bertalanffy, L. 1968. *General system theory*. Braziller, New-York. 289 pp.

Bjørnstad, ON. 2015. Nonlinearity and chaos in ecological dynamics revisited. *Proceedings of the National Academy of Sciences of the United States of America*, **112**(20), 6252–6253.

Brauer, F, Castillo-Chávez, C. 2001. *Mathematical models in population biology and epidemiology*. Springer-Verlag, New York. 416 pp.

Breiman, L. 2001. Statistical modeling: the two cultures. *Statistical Science*, **16**(3), 199–231.

ten Broeke, GA, van Voom, GAK, Kooi, BW, Molenaar, J. 2016. Detecting tipping points in ecological models with sensitivity analysis. *Mathematical Modelling of Natural Phenomena*, **11**(4), 47–72.

Brose, U, Williams, RJ, Martinez, ND. 2006. Allometric scaling enhances stability in complex food webs. *Ecology Letters*, **9**, 1228–1236.

Brown, JH, Gillooly, JF, Allen, AP, Savage, VM, West, GB. 2004. Toward a metabolic theory of ecology. *Ecology*, **85**, 1771–1789.

Canale, RP, Lustig, TD, Kehrberger, PM, Salo, JE. 1973. Experimental and mathematical modeling studies of protozoan predation on bacteria. *Biotechnology and Bioengineering*, **15**, 707–728.

Cantrell, RS, Cosner, C. 2001. On the dynamics of predator-prey models with the Beddington-DeAngelis functional response. *Journal of Mathematical Analysis and Applications*, **257**, 206–222.

Cattin, MF, Bersier, LF, Banasek-Richter, C, Baltensperger, R, Gabriel, JP. 2004. Phylogenetic constraints and adaptation explain food-web structure. *Nature*, **427**, 835–839.

Cohen, JE, Newman, CM. 1985. A stochastic theory of community food webs: I. Models and aggregated data. *Proceedings of the Royal Society of London B*, **224**, 421–448.

Cohen, JE, Briand, F, Newman, CM. 1990. *Community food webs: data and theory*. Springer-Verlag, Berlin Heidelberg. 459 pp.

Cordoleani, F, Nerini, D, Gauduchon, M, Morozov, A, Poggiale, JC. 2011. Structural sensitivity of biological models revisited. *Journal of Theoretical Biology*, **283**, 82–91.

Cordoleani, F, Nerini, D, Morozov, A, Gauduchon, M, Poggiale, JC. 2013. Scaling up the predator functional response in heterogeneous environment: When Holling type III can emerge? *Journal of Theoretical Biology*, **336**, 200–208.

Corley, CD, Pullum, LL, Hartley, DM, Benedum, C, Noonan, C, Rabinowitz, PM, Lancaster, MJ. 2014. Disease prediction models and operational readiness. *PlosOne*, **9**(3), e91989.

DeAngelis, DL. 2013. The case for ratio-dependence in trophic ecology. *Trends in Ecology and Evolution*, **28**, 259–260.

DeAngelis, DL, Grimm, V. 2014. Individual-based models in ecology after four decades. *F1000Prime Reports*, **6**(39). doi:10.12703/P6-39.

DeAngelis, DL, Goldstein, RA, O'Neill, RV. 1975. A model for trophic interaction. *Ecology*, **56**, 881–892.

Dent, VE, Bazin, MJ, Saunders, PT. 1976. Behaviour of *Dictyostelium discoideum* Amoebae and *Escherichia coli* grown together in chemostat culture. *Archives in Microbiology*, **109**, 187–194.

Dhooge, A, Govaerts, W, Kuznetsov, YuA, Mestrom, W, Riet, AM, Sautois, B. 2006. *MATCONT and CL MATCONT: Continuation toolboxes in matlab*. `http://matcont.ugent.be/`.

Diestel, R. 2010. *Graph theory*. 4th edn. Springer. 436 pp.

Doedel, EJ, Champneys, AR, Fairgrieve, TF, Kuznetsov, YA, Sandstede, B, Wang, X. 1997. *Auto 97: Continuation and bifurcationn software for ordinary differential equations*. Concordia University, Montreal, Canada.

Droop, MR. 1973. Some thoughs on nutrient limitation in algae. *Journal of Phycology*, **9**, 264–272.

Droop, MR. 1983. 25 years of algal growth kinetics. *Botanica Marina*, **26**, 99–112.

Drossel, B, Higgs, PG, McKane, AJ. 2001. The influence of predator-prey population dynamics on the long-term evolution of food web structure. *Journal of Theoretical Biology*, **208**, 91–107.

Dumortier, F, Roussarie, R, Sotomayor, J, Żoladek, H. 1991. *Bifurcations of planar vector fields. Nilpotent singularities and Abelian integrals*. Springer-Verlag, Berlin. 226 pp.

Elsasser, WM. 1969. Acausal phenomena in physics and biology: A case for reconstruction. *American Scientist*, **57**, 502–516.

Evans, MR, Grimm, V, Johst, K, Knuuttila, T, de Langhe, R, Lessells, CM, Merz, M, O'Malley, MA, Orzack, SH, Weisberg, M, *et al.* 2013. Do simple models lead to generality in ecology? *Trends in Ecology and Evolution*, **28**(10), 578–583.

Eynaud, Y, Nisbet, RM, Muller, EB. 2011. Impact of excess and harmful radiation on energy budgets in scleratinian corals. *Ecological Modelling*, **222**, 1315–1322.

Fawcett, TW, Higginson, AD. 2012. Heavy use of equations impedes communication among biologists. *Proceedings of the National Academy of Science of the United States of America*, **109**(29), 11735–11739.

Fenchel, T. 1980. Suspension feeding in ciliated protozoa: functional response and particle size selection. *Microbial Ecology*, **6**, 1–11.

Flynn, KJ. 2005. Castles built on sand: dysfunctionality in plankton models and the inadequacy of dialogue between biologists and modellers. *Journal of Plankton Research*, **27**(12), 1205–1210.

Fortunato, S. 2010. Community detection in graphs. *arXiv*, 0906.0612v2.

Frost, BW. 1972. Effects of size and concentration of food particles on the feeding behaviour of the marine planktonic copepod *Calanus pacificus*. *Limnology and Oceanography*, **17**(6), 805–815.

Fulton, EA, Smith, ADM, Johnson, CR. 2003a. Effect of complexity on marine ecosystem models. *Marine Ecology Progress Series*, **253**, 1–16.

Fulton, EA, Smith, ADM, Johnson, CR. 2003b. Mortality and predation in ecosystem models: is it important how these are expressed? *Ecological Modelling*, **169**, 157–178.

Fussmann, GF, Blasius, B. 2005. Community response to enrichment is highly sensitive to model structure. *Biology Letters*, **1**(1), 9–12.

Fussmann, GF, Ellner, SP, Shertzer, KW, Hairston Jr, NG. 2000. Crossing the Hopf bifurcation in a live predator-prey system. *Science*, **290**, 1358–1360.

Galassi, M, Davies, J, Theiler, J, Gough, B, Jungman, G, Alken, P, Booth, M, Rossi, F, Ulerich, R. 2013. *GNU Scientific Library Reference Manual (3rd eds), version 1.16*. ISBN 0954612078, `http://www.gnu.org/software/gsl/`.

Gentleman, W, Leising, A, Frost, B, Strom, S, Murray, J. 2003. Functional responses for zooplankton feeding on multiple resources: a review of assumptions and biological dynamics. *Deep-Sea Research II*, **50**, 2847–2875.

Gregr, EJ, Chan, KMA. 2014. Leaps of faith: how implicit assumptions compromise the utility of ecosystem models for decision-making. *Bioscience*, **65**, 43–54.

Grimm, V, Wissel, C. 1997. Babel, or the ecological stability discussions: an inventory and analysis of terminology and a guide for avoiding confusion. *Oecologia*, **109**, 323–334.

Gross, T, Feudel, U. 2006. Generalized models as a universal approach to the analysis of nonlinear dynamical systems. *Physical Review E*, **73**(1), 016205.

Gross, T, Ebenhöh, W, Feudel, U. 2004. Enrichment and foodchain stability: the impact of different forms of predator-prey interaction. *Journal of Theoretical Biology*, **227**, 349–358.

Gross, T, Rudolf, L, Levin, SA, Dieckmann, U. 2009. Generalized models reveal stabilizing factors in food webs. *Science*, **325**, 747–750.

Guckenheimer, J, Holmes, P. 1983. *Nonlinear oscillations, dynamical systems, and bifurcations of vector fields*. Springer. 459 pp.

Hall, RJ, Hastings, A. 2007. Minimizing invader impacts: striking the right balance between removal and restoration. *Journal of Theoretical Biology*, **249**, 437–444.

Hastings, A, Powell, T. 1991. Chaos in a three-species food chain. *Ecology*, **72**(3), 896–903.

Hastings, A, Hom, CL, Ellner, S, Turchin, P, Godfray, HCJ. 1993. Chaos in ecology: is Mother Nature a stange attractor? *Annual Review of Ecology and Systematics*, **24**, 1–33.

Hastings, A, Hall, RJ, Taylor, CM. 2006. A simple approach to optimal control of invasive species. *Theoretical Population Biology*, **70**, 431–435.

Heckmann, L, Drossel, B, Brose, U, Guill, C. 2012. Interactive effects of body-size structure and adaptative foraging on food-web stability. *Ecology Letters*, **15**, 243–250.

Hector, A. 1998. The effect of diversity on productivity: detecting the role of species complementarity. *Oikos*, **82**(3), 597–599.

Hector, A, Schmid, B, Beierkuhnlein, C, Caldeira, MC, Diemer, M, Dimitrakopoulos, PG, Finn, JA, Freitas, H, Giller, PS, Good, J, *et al.* 1999. Plant diversity and productivity experiments in European grasslands. *Science*, **286**, 1123–1127.

Holling, CS. 1959a. The components of predation as revealed by a study of small-mammal predation of the European pine sawfly. *The Canadian Entomologist*, **91**(7), 293–320.

Holling, CS. 1959b. Some characteristics of simple types of predation and parasitism. *The Canadian Entomologist*, **91**(7), 385–398.

Holling, CS. 1965. The functional response of predators to prey density and its role in mimicry and population regulation. *Memoirs of the Entomological Society of Canada*, **45**, 3–60.

Holling, CS. 1973. Resilience and stability of ecological systems. *Annual Review of Ecology and Systematics*, **4**, 1–23.

Hsu, SB. 1977. On global stability of a predator-prey system. *Mathematical Biosciences*, **39**, 1–10.

Huston, MA. 1997. Hidden treatments in ecological experiments: re-evaluating the ecosystem function of biodiversity. *Oecologia*, **110**, 449–460.

Hutchinson, GE. 1957. *Concluding remarks.* Cold Spring Harbor symposium on quantitative biology. **22**, 415-427.

Israel, G. 1996. *La mathématisation du réel (Mathematics and reality, in French).* Seuil, Paris. 366 pp.

Ivlev, VS. 1955. *Experimental ecology of the feeding of fishes.* Pischepromizdat, Moscow. 302 pp. (translated from Russian by D. Scott, Yale University Press, New Haven, 1961).

Jassby, AD, Platt, T. 1976. Mathematical formulation of the relationship between photosynthesis and light for phytoplankton. *Limnology and Oceanography*, **21**(4), 540–547.

Jeschke, JM, Kopp, M, Tollrian, R. 2002. Predator functional response: discriminating between handling and digesting prey. *Ecological Monographs*, **72**(1), 95–112.

Jiang, L, Pu, Z. 2009. Different effects of species diversity on temporal stability in single-trophic and multitrophic communities. *The American Naturalist*, **174**(5), 651–659.

Jørgensen, SE, Fath, BD, Bastianoni, S, Marques, JC, Müller, F, Nielsen, SN, Patten, BC, Tiezzi, E, Ulanowicz, RE. 2007. *A new ecology systems perspective.* Elsevier, Oxford. 275 pp.

Jusup, M, Sousa, T, Domingos, T, Labinac, V, Marn, N, Wang, Z, Klanjišček, T. in press. Physics of metabolic organization. *Physiucs of Life Reviews.* doi:10.1016/j.plrev.2016.09.001.

Kartascheff, B, Guill, C, Drossel, B. 2009. Positive complexity-stability relations in food web models without foraging adaptation. *Journal of Theoretical Biology*, **259**, 12–23.

Kartascheff, B, Heckmann, L, Drossel, B, Guill, C. 2010. Why allometric scaling enhances stability in food web models. *Theoretical Ecology*, **3**, 195–208.

Knowlton, N. 2004. Multiple "stable" states and the conservation of marine ecosystems. *Progress in Oceanography*, **60**, 387–396.

Kooi, BW, Boer, MP. 2001. Bifurcations in ecosystem models and their biological interpretation. *Applicable Analysis*, **77**, 29–59.

Kooi, BW, Kooijman, SALM. 1994a. Existence and stability of microbial prey-predator systems. *Journal of Theoretical Biology*, **170**, 75–85.

Kooi, BW, Kooijman, SALM. 1994b. The transient behaviour of food chains in chemostat. *Journal of Theoretical Biology*, **170**, 87–94.

Kooi, BW, Boer, MP, Kooijman, SALM. 1997. Mass balance equation versus logistic equation in food chains. *Journal of Biological Systems*, **5**(1), 77–85.

Kooi, BW, Poggiale, JC, Auger, P. 1998a. Aggregation methods in food chains. *Mathematical and Computer Modelling*, **27**(4), 109–120.

Kooi, BW, Boer, MP, Kooijman, SALM. 1998b. On the use of the logistic equation in models of food chains. *Bulletin of Mathematical Biology*, **60**, 231–246.

Kooi, BW, Auger, P, Poggiale, JC, Kooijman, SALM. 2002. Aggregation methods in food chains with nutrient recycling. *Ecological Modelling*, **157**, 69–86.

Kooijman, SALM. 2010. *Dynamic energy budget theory for metabolic organisation*. 3rd edn. Cambridge University Press, Cambridge. 514 pp.

Kooijman, SALM. 2015. DEB theory: where fascination meets profession. In: Kooijman, SALM, *Trilogy on a case study in theoretical biology*, Farewell adress VU University, Amsterdam, pp 13-30.

Kuehn, C, Gross, T. 2011. Nonlocal generalized models of predator-prey systems. *arXiv preprint*, 1105.3662.

Kuznetsov, YuA. 2004. *Elements of applied bifurcation theory*. 3rd edn. Springer, New York. 361 pp.

Kuznetsov, YuA, Rinaldi, S. 1996. Remarks on food chain dynamics. *Mathematical Biosciences*, **134**, 1–33.

Kuznetsov, YuA, Rinaldi, S, Gragnani, A. 2003. One-parameter bifurcations in planar Filippov systems. *International Journal of Bifurcation and Chaos*, **13**(8), 2157–2188.

Le Moigne, JL. 1999. *La modélisation des systèmes complexes (Modelling complex systems, in French)*. Dunot, Paris. 178 pp.

Legendre, L, Le Fèvre, J. 1989. Hydrodynamic singularities as controls of recycled versus export production in oceans. *in* Berger, WH, Smetacek, VS, Wefer, G (éds) *Productivity of the ocean: present and past*, Wiley, Chichester, pp 49-63.

Lévêque, C. 2003. *Ecology: from ecosystem to biosphere*. Science Publishers. 477 pp.

Lika, K, Kearney, MR, Freitas, V, van der Veer, HW, van der Meer, J, Wijsman, JWM, Pecquerie, L, Kooijman, SALM. 2011a. The "covariation method" for estimating the parameters of the standard Dynamic Energy Budget model I: Philosophy and approach. *Journal of Sea Research*, **66**, 270–277.

Lika, K, Kearney, MR, Kooijman, SALM. 2011b. The "covariation method" for estimating the parameters of the standard Dynamic Energy Budget model II: Properties and preliminary patterns. *Journal of Sea Research*, **66**, 278–288.

Loeuille, N, Loreau, M. 2005. Evolutionary emergence of size-structure food webs. *Proceedings of the National Academy of Sciences of the United States of America*, **102**(16), 5761–5766.

Loreau, M. 1998. Separating sampling and other effects in biodiversity experiments. *Oikos*, **82**(3), 600–602.

Loreau, M. 2010. *From populations to ecosystems: theoretical foundations for a new ecological synthesis*. Princeton University Press, Princeton. 297 pp.

Loreau, M, Hector, A. 2001. Partitioning selection and complementarity in biodiversity experiments. *Nature*, **412**, 72–76.

Lorenz, EN. 1963. Deterministic nonperiodic flow. *Journal of the Atmospheric Sciences*, **20**, 130–141.

Lotka, AJ. 1925. *Elements of physical biology*. Williams & Wilkins, Baltimore.

Ludwig, D, Jones, DD, Holling, CS. 1978. Qualitative analysis of insect outbreak systems: the spruce budworm and forest. *Journal of Animal Ecology*, **47**, 315–332.

MacArthur, R. 1955. Fluctuations of animal populations and a measure of commmunity stability. *Ecology*, **36**(3), 533–536.

Malthus, T. 1798. *An essay on the principle of population*. J Johnson, London. 126 pp.

Marr, AG, Nilson, EH, Clark, DJ. 1963. The maintenance requirement of *Escherichia coli*. *Annals New York Academy of Sciences*, **102**, 536–548.

Martinez, ND. 1991. Artifacts or attributes? Effects of resolution on the Little Rock Lake food web. *Ecological Monographs*, **61**(4), 367–392.

May, RM. 1972. Will a large complex system be stable? *Nature*, **238**, 413–414.

May, RM. 1973. Qualitative stability in model ecosystems. *Ecology*, **54**(3), 638–641.

May, RM. 1974. Biological populations with nonoverlapping generations: stable points, stable cycles, and chaos. *Science*, **186**(4164), 645–647.

May, RM. 1976. Simple dynamical models with very complicated dynamics. *Nature*, **261**, 459–467.

May, RM. 1999. Unanswered questions in ecology. *Philosophical Transactions of the Royal Society of London B*, **354**, 1951–1959.

May, RM. 2004. Uses and abuses of mathematics in biology. *Science*, **303**, 790–793.

McCann, K, Hastings, A, Huxel, GR. 1998. Weak trophic interaction and the balance of nature. *Nature*, **395**, 794–798.

McCann, KS. 2000. The diversity-stability debate. *Nature*, **405**, 228–233.

McGrady-Steed, J, Harris, PM, Morin, PJ. 1997. Biodiversity regulates ecosystem predictability. *Nature*, **390**, 162–165.

McMahon, JW, Rigler, FH. 1965. Feeding rate of *Daphnia magna* Straus in different foods labeled with radioactive phosphorus. *Limnology and Oceanography*, **10**, 105–113.

Metzler, W, Wischniewsky, W. 1985. Bifurcations of equilibria in Bazykin's predator-prey model. *Mathematical Modelling*, **6**, 111–123.

Monod, J. 1942. *Recherches sur la croissance des cultures bactériennes (Researches on the growth of bacterial cultures, in French)*. 2nd edn. Hermann, Paris. 459 pp.

Mouquet, N, Lagadeuc, Y, Devictor, V, Doyen, L, Duputie, A, Eveillard, D, Faure, D, Garnier, E, Gimenez, O, *et al.*, P Huneman. 2015. Predictive ecology in a changing world. *Journal of Applied Ecology*, **52**, 1293–1310.

Mullin, MM, Stewart, EF, Fuglister, FJ. 1975. Ingestion by planktonic grazers as a function of food concentration. *Limnology and Oceanography*, **20**(2), 259–262.

Myerscough, MR, Darwen, MJ, Hogarth, WL. 1996. Stability, persistence and structural stability in a classical predator-prey model. *Ecological Modelling*, **89**, 31–42.

Naeem, S, Li, S. 1997. Biodiversity enhances ecosystem reliability. *Nature*, **390**, 507–509.

Naeem, S, Thompson, LJ, Lawler, SP, Lawton, JH, Woodfin, RM. 1994. Declining the biodiversity can alter the performance of ecosystems. *Nature*, **368**, 734–737.

Nelder, JA, Mead, R. 1965. A simplex method for function minimization. *Computer journal*, **7**(4), 308–313.

Nerini, D, Ghattas, B. 2007. Classifying densities using functional regression trees: Applications in oceanology. *Computational Statistics & Data Analysis*, **51**, 4984–4993.

Nerini, D, Monestiez, P, Mante, C. 2010. Cokriging for spatial functional data. *Journal of Multivariate Analysis*, **101**, 409–418.

Nisbet, RM, Cunningham, A, Gurney, WSC. 1983. Endogenous metabolism and the stability of microbial prey-predator systems. *Biotechnology and Bioengineering*, **25**, 301–306.

Nisbet, RM, McCauley, E, Murdoch, WSC Gurney WW, Wood, SN. 2004. Formulating and testing a partially specified Dynamic Energy Budget model. *Ecology*, **85**(11), 3132–3139.

Nozdracheva, VP. 1982. Bifurcation of structurally unstable separatrix loop. *Differentsial'nyye Uravneiya*, **18**, 1551–1558.

Oaten, OA, Murdoch, WW. 1975. Functional response and stability in predator-prey systems. *The American Naturalist*, **109**, 289–298.

Odum, EP. 1964. The new ecology. *BioScience*, **17**(7), 14–16.

Perko, L. 1996. *Differential equations and dynamical systems*. 2nd edn. Springer, New York. 525 pp.

Personnic, S, Boudouresque, CF, Astruch, P, Ballesteros, E, Blouet, S, Bellan-Santini, D, Bonhomme, P, Thibault-Botha, D, Feunteun, E, Harmelin-Vivien, M, Pergent, G, Pergent-Martini, C, Pastor, J, Poggiale, JC, Renaud, F, Thibaut, T, Ruitton, S. 2014. An ecosystem-based

approach to assess the status of a Mediterranean ecosystem, the *Posidonia oceanica* seagrass meadow. *PloS ONE*, **9**(6), e98994.

Petchey, OL, Pontarp, M, Massie, TM, Kéfi, S, Ozgul, A, Weilenmann, M, Palamara, GM, Altermatt, F, Matthews, B, Levine, JM, *et al.* 2015. The ecological forecast horizon, and examples of its uses and determinants. *Ecology Letters*, **18**, 597–611.

Petrovskii, S, Petrovskaya, N. 2012. Computational ecology as an emerging science. *Interface Focus*, **2**(2), 241–254.

Pimm, SL. 1984. The complexity and stability of ecosystems. *Nature*, **307**, 321–326.

Pirt, SJ. 1965. The maintenance energy of bacteria in growing cultures. *Proceedings of the Royal Society of London B*, **163**, 224–231.

Planque, B. 2015. Projecting the future state of marine ecosystems,"la grande illusion". *ICES Journal of Marine Sciences*, **73**(2), 204–208.

Plitzko, SJ, Drossel, B, Guill, C. 2012. Complexity-stability relations in generalized food-web models with realistic parameters. *Journal of Theoretical Biology*, **306**, 7–14.

Poggiale, JC. 1998. From behavioural to population level: growth and competition. *Mathematical and Computer Modelling*, **27**(4), 41–49.

Poggiale, JC, Baklouti, M, Queguiner, B, Kooijman, SALM. 2010. How far details are important in ecosystem modelling: the case of multi-limiting nutrients in phytoplankton-zooplankton interactions. *Philosophical Transactions of the Royal Society of London B*, **365**, 3495–3507.

R Core Team. 2013. *R: A Language and Environment for Statistical Computing*. R Foundation for Statistical Computing, Vienna, Austria. `http://www.R-project.org/`.

Ragan, MA. 2009. Trees and networks before and after Darwin. *Biology Direct*, **4**, 43.

Rinaldi, S, De Feo, O. 1999. Top-predator abundance and chaos in tritrophic food chains. *Ecology Letters*, **2**, 6–10.

Rinaldi, S, Muratori, S. 1992. Slow-fast limit cycles in predator-prey models. *Ecological Modelling*, **61**, 287–308.

Rosenzweig, ML. 1971. Paradox of enrichment: destablilization of exploitation ecosystems in ecological time. *Science*, **171**(3969), 385–387.

Rosenzweig, ML, MacArthur, RH. 1963. Graphical representation and stability conditions of predator-prey interaction. *The American Naturalist*, **97**(895), 209–223.

Rossberg, AG, Matsuda, H, Amemiya, T, Itoh, K. 2006. Food webs: experts consuming families of experts. *Journal of Theoretical Biology*, **241**, 552–563.

Scheffer, M, de Boer, RJ. 1995. Implications of spatial heterogeneity for the paradox of enrichment. *Ecology*, **76**(7), 2270–2277.

Scheffer, M, Bascompte, J, Brock, WA, Brokvin, V, Carpenter, SR, Dakos, V, Held, H, van Nes, EH, Rietkerk, M, Sugihara, G. 2009. Early-warning signals for critical transitions. *Nature*, **461**, 53–59.

Scheffer, M, Carpenter, SR, Lenton, TM, Bascompte, J, Brock, WA, Dakos, V, van de Koppel, J, van de Leemput, IA, Levin, SA, van Nes, EH, Pascual, M, Vandermeer, J. 2012. Anticipating critical transitions. *Science*, **338**, 344–348.

Schimel, J. 2012. *Writing science: how to write papers that get cited and proposals that get funded*. Oxford University Press, New York. 221 pp.

Schmueli, G. 2010. To explain or to predict. *Statistical Science*, **25**(3), 289–310.

Simonoff, JS. 1996. *Smoothing methods in statistics*. Springer, New York. 338 pp.

Solomon, ME. 1949. The natural control of animal populations. *Journal of Animal Ecology*, **18**(1), 1–35.

Solow, AR, Beet, AR. 1998. On lumping species in food webs. *Ecology*, **79**(6), 2013–2018.

Stouffer, DB, Bascompte, J. 2010. Understanding food-web persistence from local to global scales. *Ecology Letters*, **13**, 154–161.

Stouffer, DB, Bascompte, J. 2011. Compartmentalization increases food-web persistence. *Proceedings of the National Academy of Sciences of the United States of America*, **108**(9), 3648–3652.

Stouffer, DB, Camacho, J, Guimera, R, Ng, CA, Amaral, LA Nunes. 2005. Quantitative patterns in the structure of model and empirical food webs. *Ecology*, **86**(5), 1301–1311.

Takeuchi, Y. 1996. *Global dynamical properties of Lotka-Volterra systems*. World Scientific Publishing Company, Singapour. 302 pp.

Thieme, HR. 1994. Asymptotically autonomous differential equations in the plane. *Rocky Mountain Journal of Mathematics*, **24**, 351–380.

Tilman, D, Knops, J, Wedin, D, Reich, P, Ritchie, M, Siemann, E. 1997. The influence of functional diversity and composition on ecosystem processes. *Science*, **227**, 1300–1302.

Tilman, D, Reich, PB, Knops, J, Wedin, D, Mielke, T, Lehman, C. 2001. Diversity and productivity in a long-term grassland experiment. *Science*, **294**, 843–845.

Tilman, D, Reich, PB, Knops, JMH. 2006. Biodiversity and ecosystem stability in a decade-long grassland experiment. *Nature*, **441**, 629–632.

Uchida, S, Drossel, B. 2007. Relation between complexity and stability in food webs with adaptive behavior. *Journal of Theoretical Biology*, **247**, 713–722.

Verhulst, PF. 1838. Notice sur la loi que la population poursuit dans son accroissement (Note on the law of population growth, in French). *Correspondance Mathématique et Physique*, **10**, 113–121.

Volterra, V. 1926. Fluctuations in the abundance of a species considered mathematically. *Nature*, **118**, 558–560.

Webb, EA, Ehrenreich, IM, Brown, SL, Valois, FW, Waterbury, JB. 2009. Phenotypic and genotypic characterization of multiple strains of the diazotrophic cyanobacterium, *Crocosphaera watsonii*, isolated from the open ocean. *Environmental Microbiology*, **11**(2), 338–348.

Wigner, EP. 1960. The unreasonable effectiveness of mathematics in the natural sciences. *Communications in Pure and Applied Mathematics*, **13**, 1–14.

Wikipedia Free Encyclopedia. 2016. *en.wikipedia.org/wiki/Observable_universe*. accessed the 8th June 2016.

Williams, RJ. 2008. Effects of network and dynamical model structure on species persistence in large model food webs. *Theoretical Ecology*, **1**(3), 141–151.

Williams, RJ, Martinez, ND. 2000. Simple rules yield complex food webs. *Nature*, **404**, 180–183.

Williams, RJ, Martinez, ND. 2004. Stabilization of chaotic and non-permanent food-web dynamics. *The European Physical Journal B*, **38**, 297–303.

Wilmshurst, JF, Fryxell, JM, Colucci, PE. 1999. What constraints daily intake in Thomson's gazelles. *Ecology*, **80**(7), 2338–2347.

Wood, SN, Thomas, MB. 1999. Super–sensitivity to structure in biological models. *Proceedings of the Royal Society of London B*, **266**, 565–570.

Yachi, S, Loreau, M. 1999. Biodiversity and ecosystem productivity in a fluctuating environment: the insurance hypothesis. *Proceedings of the National Academy of Sciences of the United States of America*, **96**, 1463–1468.

Yeakel, JD, Stiefs, D, Novak, M, Gross, T. 2011. Generalized modeling of ecological population dynamics. *Theoretical Ecology*, **4**, 179–194.

Yodzis, P, Innes, S. 1992. Body size and consumer-resource dynamics. *The American Naturalist*, **139**(6), 1151–1175.

Abstract

Ecological systems are complex systems which cannot be described by a single mathematical model. Multiple models of a same system can be built, depending on modeller's interests and on its choices during model construction. *How far these choices in model construction can affect the predicted dynamics of ecological systems and the information they provide on their resilience?* is the general question that leads the research presented in this thesis. This thesis focuses on a choice between model formulations that are based on biological mechanisms and describe empirical data with the same accuracy. These models are close to each other, so they are expected to predict similar system dynamics. However, we show through a generic example of predator-prey model that similar formulations of the predation process can predict qualitatively different system dynamics in term of: (i) number and type of stable states, and (ii) system response to external disturbance and its potential for recovery. These differences in model predictions are explained by a detailed mathematical analysis of the predator-prey model. Next, this model is extended to complex food webs made of tens of species. The complexity of these networks (number of species and interactions) drives their persistence, whereas their temporal dynamics is strongly affected by the function used to model predation. Methods to quantify model sensitivity are also proposed. Finally, we show that if a minimum level of biological details is included, predator-prey models are less sensitive to predation formulation. This provide a clue to deal with uncertainties in model construction, which are intrinsic to the complexity of natural systems.

Keywords: modelling · resilience · structural sensitivity · bifurcations · food webs · Dynamic Energy Budget

Résumé

Les systèmes écologiques sont des systèmes complexes qui ne peuvent pas être décrits par un unique modèle mathématique. De nombreux modèles peuvent être construits pour un même système, selon les intérêts du modélisateur et ses choix dans la construction du modèle. *Quel est l'impact de ces choix dans la construction du modèle sur les prédictions de la dynamique des systèmes écologiques et les informations qu'elles fournissent sur la résilience de ces systèmes?* est la question générale qui guide le travail présenté dans cette thèse. Cette thèse se focalise sur un choix entre formulations de modèle basées sur des méchanismes biologiques et qui décrivent les données empiriques avec la même efficacité. Ces modèles sont proches l'un de l'autre, donc on s'attendrait à ce que leurs prédictions soient similaires. Cependant, nous montrons avec un exemple générique de modèle prédateur-proie que des formulations similaires du processus de prédation peuvent prédire des dynamiques qualitativement différentes en terme de: (i) nombre et type d'états stables, et (ii) réponse et résilience du système face à une perturbation extérieure. Ces différences dans les prédictions du modèle sont expliquées par une analyse mathématique détaillée du modèle prédateur-proie. Ensuite, ce modèle est étendu à des réseaux trophiques composés de dizaines d'espèces. La complexité de ces réseaux (nombre d'espèces et d'interactions) explique leur persistence, alors que leur dynamique temporelle est fortement affectée par la fonction utilisée pour modéliser la prédation. Des méthodes sont également proposées pour quantifier la sensibilité d'un modèle. Finalement, nous montrons que si un minimum de détails biologiques sont pris en compte, des modèles prédateurs-proies sont moins sensibles à la formulation de la prédation. Ceci nous donne des pistes pour gérer les incertitudes dans la construction d'un modèle, qui sont intrinsèques à la complexité des systèmes naturels.

Mots-clés: modélisation · résilience · sensibilité structurelle · bifurcations · réseaux trophiques · Budgets d'Énergie Dynamiques